FROM MOLECULAR OLIGOMERS TO SUPRAMOLECULAR GELS: PHOTOPHYSICS OF CONJUGATED METAL-ORGANIC SYSTEMS

By

THOMAS CARDOLACCIA

A DISSERTATION PRESENTED TO THE GRADUATE SCHOOL
OF THE UNIVERSITY OF FLORIDA IN PARTIAL FULFILLMENT
OF THE REQUIREMENTS FOR THE DEGREE OF
DOCTOR OF PHILOSOPHY

UNIVERSITY OF FLORIDA

2005

Dedicated to my parents for their support
Dedicated to my wife for her love
And vice versa….

ACKNOWLEDGMENTS

These years as a graduate student have been without a doubt the most stimulating and rewarding years of my life. Many people have contributed to make this journey a positive and gratifying adventure and they are hereby acknowledged. Some many things to say, so little space . . .

First I would like to thank my advisor, Dr. Kirk S. Schanze, for his guidance and support throughout those years. His constant encouragements and motivation have been an incredible source of strength in many occasions. His genuine care for the intellectual development of his students is evidenced in the time he often took to explain new concepts to me or demonstrate the operation of some instruments. Dr. Schanze has always been willing to let me go my way, giving me a significant degree of freedom on my research. More importantly, he never made me feel bad for mistakes and failed experiments. Through these times of failure and success, I have grown as a scientist and a person, inspired by his creativity and approach to sciences.

I would like to thank my committee members, Dr. John Reynolds, Dr. William Dolbier, Dr. Michael Scott and Dr. Bruce Carroll. Special gratitude goes to Dr. Dolbier for organizing and managing the Thursday night Bull Sessions, where I have been exposed to some aspects of organic chemistry I would have never encountered otherwise.

Many people have been involved with my research and I would like to thank Dr. Xiaoming Zhao for synthesizing polymers faster than I could characterize them spectroscopically, Dr. Alison M. Funston and Dr. John R. Miller for carrying out the

pulse radiolysis in Brookhaven National Laboratory, Dr. Stephen Hagen for the use of his CD spectrometer, and Dr. Richard Weiss for carrying out the polarizing microscopy experiments.

My experience in the laboratory has been particularly enriching due to several exceptional individuals willing to share their knowledge and time. Thanks go to Dr. Ben Harrison, Dr. Yiting Li, Dr. Mauricio R. Pinto, Dr. Yao Liu, Dr. Ksenija Haskins-Glusac, Dr. Eric Silverman and all present members of the Schanze's group.

I thank my parents for making me what I am today and my family for the love I was always surrounded with.

TABLE OF CONTENTS

LIST OF TABLES

LIST OF FIGURES

Abstract of Dissertation Presented to the Graduate School
of the University of Florida in Partial Fulfillment of the
Requirements for the Degree of Doctor of Philosophy

FROM MOLECULAR OLIGOMERS TO SUPRAMOLECULAR GELS:
PHOTOPHYSICS OF CONJUGATED METAL-ORGANIC SYSTEMS

By

Thomas Cardolaccia

August, 2005

Chair: Kirk S. Schanze
Major Department: Chemistry

In this dissertation, several series of platinum acetylide oligomers have been prepared and studied by photophysical methods. The motivation for the research stems from direct opto-electronic applications that platinum acetylide materials may be used for, as well as from a more fundamental need to gain a better understanding on the triplet excited state in conjugated systems.

First, platinum acetylide oligomers containing energy traps were prepared in order to investigate their effect on the triplet excited state. Second, the delocalization of charge carriers (radical anions and cations) was studied to determine the charge transport properties of these materials and the effect of platinum on the charge carriers. Third, a series of platinum acetylide oligomer was designed to self-assemble in solution with the goal of determining the consequences of aggregation on the triplet excited state. The goal of this work was to gain an insight into the dynamics of the triplet excited state in conjugated systems.

The most significant findings of the study are as follows: (i) although more localized than the singlet exciton, the triplet exciton is also sensitive to the presence of energy traps, which can have a significant impact on the photophysical properties of the materials; (ii) charge carriers are relatively localized on the oligomer chain and the estimated delocalization of the radical cation is no more than two repeat units; (iii) the consequences of aggregation on the triplet excited state may be very limited or relatively important, depending on the mode of aggregation.

CHAPTER 1
INTRODUCTION

The interaction of light with matter is an elementary process in nature responsible for the life of plants and many other species. Absorption of light is the source of energy for plants, of heat for some animals. It is the process by which humans and many other animals see their environment and are able to interact with it and with each other. In the next chapter, some concepts relying on the interaction of light with molecules will be presented. It is therefore important to review several fundamental photophysical processes before. This introductory chapter is divided into two parts. The first part reviews several important concepts for photophysical studies such as absorption and emission of light. Then a closer look is taken of the general structure and photophysical properties of platinum acetylide polymers and oligomers.

Introduction to Photophysics

Absorption of Light

The understanding of the interaction of light with matter has been considerably changed with the notion of the dual nature of light and the non-classical description of atomic structure. Maxwell's theory of electromagnetism in 1860 and the development of quantum mechanics started by Schödinger in 1928 have provided scientists with mathematical equations describing these phenomena.[1] Light is often referred to as an elementary particle called a photon but can also be thought of as an electromagnetic wave. Electrons also possess this dual nature and can be visualized as an elementary

particle or a wave. The energy of the photon and the frequency of its electromagnetic wave are related by the following equation:

$$E = h\nu = \frac{hc}{\lambda} \quad (1)$$

where E is the energy in Joules (J), ν is the frequency (Hz or s^{-1}), h is Planck's constant (6.63×10^{-34} J.s), c is the speed of light (3.00×10^{8} $m.s^{-1}$ in a vacuum) and λ is the wavelength (m).

When a molecule interacts with an optical field, the outer valence electrons of the molecule interact with the light and can be promoted to higher energy levels. For this to occur, the light, or the photon, must have the appropriate energy (or quantum) that corresponds to the difference in energy between the two energy levels involved. This is because the energy levels of the electrons in an atom or a molecule are not continuous but discrete. Therefore the wavelength of the light absorbed provides the energy difference between these energy levels. For many conditions, the absorption of radiation follows Beer's law

$$A = -\log T = \varepsilon l C \quad (2)$$

where A is the absorbance, T is the transmittance, l is the pathlength of absorption (cm), ε is the molar absorptivity ($L.mol^{-1}.cm^{-1}$), and C is the concentration of the absorbing species ($mol.L^{-1}$). The molar absorptivity represents the probability of the transition to occur and is related to the transition dipole moments between the initial and final states.

The molar absorptivity is a function of the radiation frequency and is usually reported for λ_{max} as ε_{max}. However, a better measure of the transition intensity is obtained by integrating ε over the whole absorption spectrum,[2] which gives the integrated absorption coefficient α:

$$\alpha = \int_{band} \varepsilon(\tilde{\upsilon}) d\tilde{\upsilon} \tag{3}$$

The integrated absorption coefficient provides a connection between the experimental spectrum and a theoretical quantity known as the oscillator strength, f_{nm}. This latter is a measure of the strength of an electric dipole transition between electronic states n and m compared to that of a free electron oscillating in three dimensions. It is given by

$$f_{nm} = \left(\frac{4\varepsilon_0 m_e c^2 \ln(10)}{N_A e^2} \right) \alpha \tag{4}$$

where ε_0 is the permittivity of vacuum, m_e is the mass of the electron, c is the speed of light in vacuum, N_A is the Avogadro's number and e is the elementary charge. The collection of fundamental constant has a value of 4.319 x 10^{-9} mol.L^{-3}.cm^2.

Assuming a Lorentzian band profile for the absorption band, the integrated absorption coefficient can be calculated from the experimental absorption spectrum using

$$\alpha = \frac{1}{2} \pi \varepsilon_{\max} \Gamma \tag{5}$$

where Γ is the full width at half maximum (FWHM). The oscillator strength equation then becomes

$$f_{nm} = 4.319 \times 10^{-9} \frac{\pi \varepsilon_{\max} \Gamma}{2} = 6.784 \times 10^{-9} \varepsilon_{\max} \Gamma \tag{6}$$

Moreover, the oscillator strength can also be related to the transition dipole moment μ_{nm}

$$f_{nm} = \left(\frac{8\pi^2 m_e c}{3e^2 h} \right) \tilde{\nu} \left| \mu_{nm} \right|^2 = 4.702 \times 10^{-7} \tilde{\nu} \left| \mu_{nm} \right|^2 \tag{7}$$

where h is Planck's constant and the collection of fundamental constant has a value of 4.226 x10^{52} C^{-2}.m^{-2}.cm, or 4.702 x 10^{-7} D^{-2}.cm.

Even though the energy involved in an electronic transition is discrete, absorption bands in molecules do not appear as sharp lines, but usually as more or less broad bands. The reason for this is that electronic transitions are usually accompanied by vibrational transitions. The explanation for this lies in the fact that electronic transitions occur very rapidly (10^{-15} s) with respect to the re-adjustement time of the inter-atomic distance (10^{-13} s) and this is referred to as the Franck Condon principle. This can be illustrated by representing the potential energy curves of the ground and excited states as a function of their respective equilibrium geometry, as shown in Figure 1-1. Electronic transitions are termed "vertical" with respect to the equilibrium geometry, conveying the idea that the electron is excited to the upper state before the nuclei have had the time to re-equilibrate.

Nature of the Excited State

Following excitation and creation of an electronic excited state, the molecule will first relax to the lowest vibrational level by thermal (emission of heat) or collisional (collision with solvent or solute molecules) relaxation. When the initial state is a ground neutral state, the electrons are paired and of opposite spin, according to Hund's rule. Due to spin restrictions imposed by quantum mechanics, the electron promoted to a higher energy level does not change its spin during excitation and the excited state formed is called a singlet excited state (S_1). In certain cases, however, the spin of the promoted electron can flip and the resulting overall spin momentum of this excited state becomes equal to three. This process is called intersystem crossing (ISC) and the resulting state is called a triplet excited state (T_1).[3] Similarly to the excitation into a singlet excited state, the triplet excited state formed is first vibrationnally excited and then relaxes to its lowest vibrational level. In organic molecules, the rate of ISC is slow and consequently the yield of the triplet excited state is usually low. Certain factors can greatly increase the ISC rate

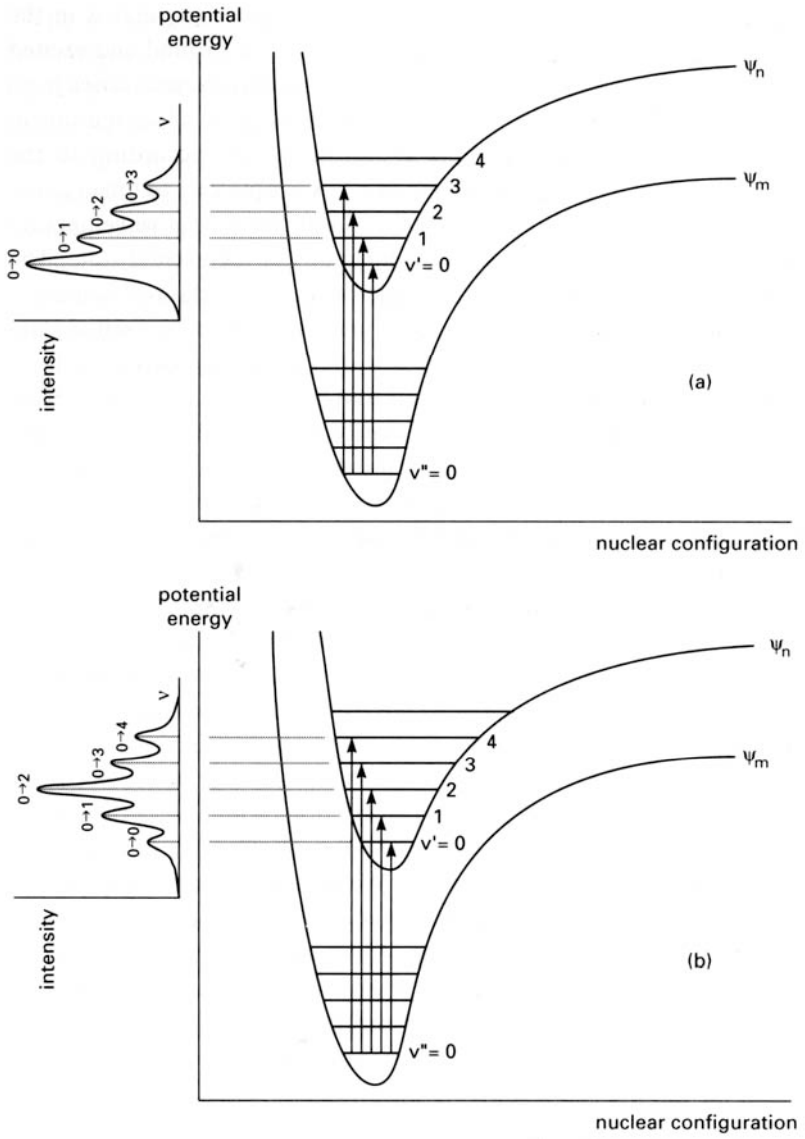

Figure 1-1. Potential energy curves for electronic transitions. (a) Transition between states of similar equilibrium nuclear geometry. (b) Transition between states of different equilibrium nuclear geometry. The figure was adopted from Gilbert and Baggot.[2]

and the yield of the triplet excited state is then increased. The process of ISC relies on spin-orbit coupling and it is facilitated through the heavy-atom effect (internal via valence bond or external via solvent). In heavy atoms, the spin angular momentum and the orbital angular momentum of the electron can interact and are not separately

conserved. Therefore as long as the total orbital momentum is conserved, the spin of the electron can be changed. Rapid intersystem crossing and efficient creation of triplet excited states are thus common in inorganic or organometallic molecules, and the platinum acetylide systems that are the focus of this study are among them.

Another important feature of excited states is the singlet-triplet splitting energy (E_{S-T}). The first singlet excited state is always higher in energy than the first triplet excited state and the reasoning for this is as follows: In the singlet excited state, the electrons are of opposite spin and are therefore not prevented by quantum mechanics to be in the same region of space. In the triplet excited state, the electrons are of the same spin and are therefore forbidden from being in the same region. This leads to a higher coulombic repulsion energy in the case of the singlet excited state compared to the triplet excited state. In a small molecule, this repulsive energy is large and the E_{S-T} is therefore also large. In large molecules such as a conjugated polymer, the repulsive energy may not be as large and thus E_{S-T} may not be large either.

Relaxation of Excited States

The excited state is metastable and the electrons will return to their initial configuration (ground state) by one of two self-relaxation mechanisms: radiative decay and nonradiative decay.

Radiative decay. In radiative decay, the excited electron will relax to the ground state by emission of a photon. This photon will carry a quantum of energy corresponding to the energy difference between the geometrically relaxed excited state and ground state, similar to the absorption process. If the excited state is a singlet, this emission of light is called fluorescence whereas it is called phosphorescence if the excited state is a triplet. Since fluorescence is a transition between states of same spins, it is allowed by quantum

mechanics and the radiative rate of the singlet excited state is fast (~10^8 s^{-1}).[4] Phosphorescence on the other hand is a transition between states of opposite spin and although facilitated by the presence of heavy atoms in the molecules, it is not as fast as fluorescence and the radiative rate of triplet excited states is typically much slower (~10^5 – 10^2 s^{-1}). Fluorescence caused by direct excitation to S_1 is called more precisely prompt fluorescence. Delayed fluorescence has a longer lifetime than prompt fluorescence because S_1 is populated by indirect mechanisms. This alternate S_1 population can proceed through a thermally-assisted ISC back to S_1 from T_1 ($T_1 \rightarrow S_1$, E-type delayed fluorescence) or through a bimolecular triplet-triplet annihilation ($T_1 + T_1 \rightarrow S_0 + S_1$, P-type delayed fluorescence).

Before the radiative decay, the electron has relaxed to the v = 0 vibrational level so the energy of this transition will be less than that of the absorption. This results in fluorescence bands appearing at a longer wavelength than the absorption and this is called the Stokes shift. The extent of the Stokes shift is then a representation of the structural differences between the ground and excited states. If the excited state is largely distorted, a large Stokes shift will be observed.

Nonradiative decay. Another type of relaxation mechanism is nonradiative decay. In this case, energy is released to the system as heat and does not involve a photon. This process, as well as the vibrational relaxation, is also referred to as internal conversion. The relative rate of non-radiative decay is governed by the energy gap law, which states that as the energy of the excited state decreases, the rate of non-radiative decays will increase exponentially.[5-7] The triplet excited state being lower in energy than the singlet

for the reason provided above, it is therefore sometimes difficult to observe phosphorescence, even though the triplet excited state was formed.

It is helpful to look at all these transitions in a representative Jablonski diagram, as shown in Figure 1-2 below.

There are two characteristics of the excited state that will be encountered in the next chapters that are worth mentioning at this stage: the photoluminescence quantum yield Φ and the lifetime τ. The fluorescence quantum yield is the ratio of the number of emitted photons to the number of photons absorbed[4] and it is given by

$$\Phi_F = \frac{k_f}{k_f + k_{nr}} \tag{8}$$

where Φ_F is the quantum yield of fluorescence, k_f is rate constant of fluorescence and k_{nr}

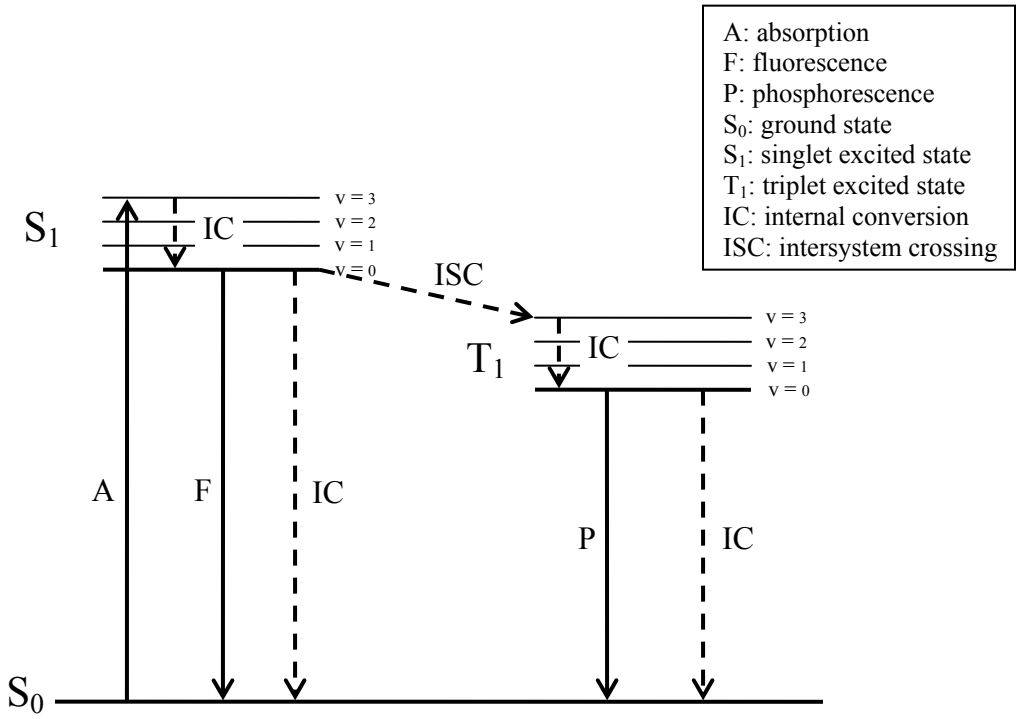

Figure 1-2. Jablonski diagram representing the possible transitions after absorption.

is the rate constant of non-radiative decay for S_1. In the case of phosphorescence, the quantum yield is given by

$$\Phi_P = \left(\frac{k_{ISC}}{k_F + k_{nr}} \right) \left(\frac{k_P}{k_P + k'_{nr}} \right) \tag{9}$$

where Φ_P is the quantum yield of phosphorescence, k_{ISC} is the rate constant of inter-system crossing, k_P is the rate constant of phosphorescence and k'_{nr} is the rate constant of non-radiative decay for T_1.

The luminescence lifetime τ is defined as the time for the luminescence signal to decay to $1/e$ of its initial value.[4] The lifetimes for fluorescence τ_F and phosphorescence τ_P are related to the rate constants for deactivation with the following equations

$$\tau_F = \frac{1}{k_F + k_{nr}} \tag{10}$$

$$\tau_P = \frac{1}{k_P + k'_{nr}} \tag{11}$$

Energy Transfer

Other than by self-relaxation, excited states may relax to the ground state by transferring the excitation to other molecules present in the system by a bimolecular process as in equation 12 below.

$$D^* + A \rightarrow D + A^* \tag{12}$$

where D is the energy donor, A is the energy acceptor and * denotes an excited state. Different mechanisms for energy transfer can occur, depending on the environment, but some conditions require (1) that the energy of D* is higher than the energy of A*; (2) that the energy transfer rate is more rapid than the decay rate of D*. Two mechanisms for energy transfer can be distinguished: exchange and Coulombic energy transfer.

Exchange energy transfer. Also called collisional or Dexter energy transfer,[8] this mechanism requires contact or a short separation (6-10 Å) between the donor and the acceptor. The rate of energy transfer is therefore diffusion controlled and depends on the temperature and the viscosity of the solvent. It also requires an overlap between the orbitals of the donor and the acceptor. Both S-S and T-T energy transfer processes are allowed and this is in fact the dominant mechanism in triplet-triplet energy transfer. The mechanism can be represented schematically as in Figure 1-3 below. The transfer rate constant k_{ET} is given by

$$k_{ET} \propto [h/(2\pi]P^2 J \exp(-2r/L) \tag{13}$$

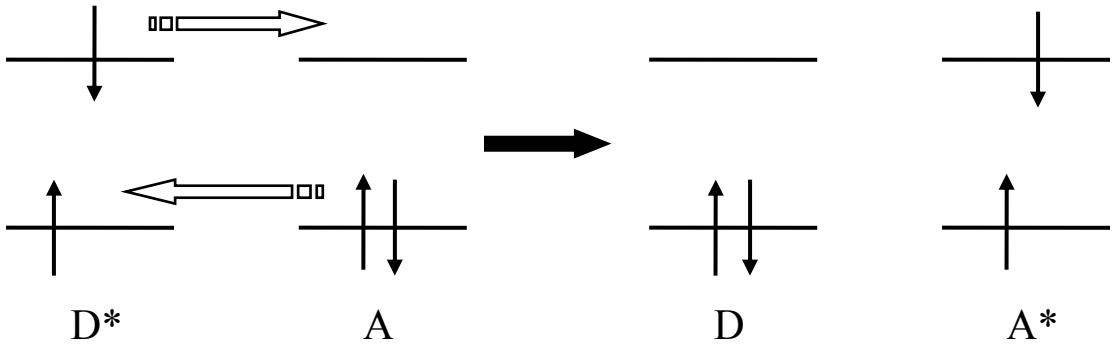

Figure 1-3. Diagram for the exchange energy transfer mechanism.

where r is the distance between D and A, L and P are constant not easily related to experimentally determinable quantities and J is the spectral overlap integral.

The decrease in emission intensity due to collisional quenching[9] is described by the Stern-Volmer equation

$$\frac{F_0}{F} = \frac{\Phi_0}{\Phi} = 1 + K_q[Q] = 1 + k_q\tau_0[Q] \tag{14}$$

where F and F_0 are the fluorescence intensities in the presence and in the absence of the quencher (or acceptor), respectively, Φ and Φ_0 are the quantum yields of fluorescence in the presence and in the absence of quencher, respectively, K_q is the Stern-Volmer quenching constant, k_q is the bimolecular quenching constant, τ_0 is the lifetime in the absence of quencher, and [Q] is the quencher (or acceptor) concentration. A similar Stern-Volmer equation can be written in the case of phosphorescence. However, as can be seen from equation 9, excited species with long lifetimes (such as triplet excited states) are more prone to quenching than species with short lifetimes (such as singlet excited states). Oxygen is an efficient quencher of triplet excited states and for this reason, phosphorescence measurements are usually carried out in deoxygenated solutions or frozen matrix.

Coulombic energy transfer. Also called the dipole-dipole or Förster energy transfer mechanism,[10] this long-range interaction does not require contact between the donor and the acceptor. Efficient long-range energy transfer is favored in situations where the emission spectrum of the donor and the absorption spectrum of the acceptor overlap. It is important to note that no photon is involved. As opposed to the exchange energy transfer, only S-S energy transfer is allowed. This type of energy transfer can be considered to be due to dipole-dipole coupling between the donor and the acceptor and can be represented as in Figure 1-4 below.

The rate of energy transfer[11] in this case is given by

$$k_{ET} = \left(\frac{1}{\tau_D}\right)\left(\frac{R_0}{R}\right)^6 \qquad (15)$$

where τ_D is the lifetime of the donor, R is the average distance between donor and acceptor and R_0 is the Förster distance (which is a measure of the spectral overlap).

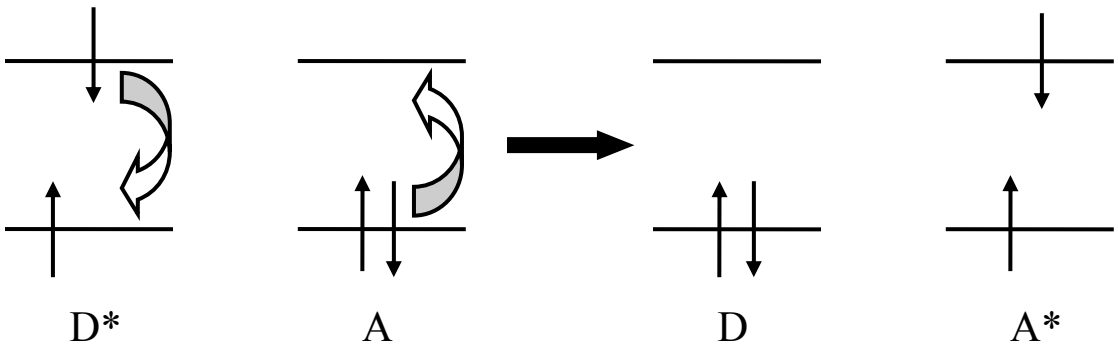

Figure 1-4. Diagram for the Coulombic energy transfer mechanism.

Förster distances are in the range of 20 to 50 Å and can be as large as 100 Å for efficient acceptors. This is comparable in size to biological macromolecules and for this reason energy transfer has been used as a "spectroscopic ruler" for measurements of distances between sites on proteins.[12-14]

Singlet and Triplet Excimers

Under certain conditions, there is another possible fate for the excited state, which is to form an excited complex, either with a different analyte (to form an exciplex) or with another like molecule (to form an excimer, or exited state dimer).[15] The excimer formation mechanism can be represented by

$$^{1,3}M^* + {}^1M \rightarrow {}^{1,3}E^* \qquad (16)$$

where the excimer E* can be a singlet or a triplet depending on the spin multiplicity of the excited molecule M* from which it is formed. The concentration of the analyte must be relatively high for excimer formation to be likely. Alternatively, a poor solvent or a restricted environment may induce the formation of excimers. A very-well known example of a molecule that can form an excimer is pyrene (first discovered by Förster and Kasper in 1954) and its fluorescence spectrum is shown in Figure 1-5 below.

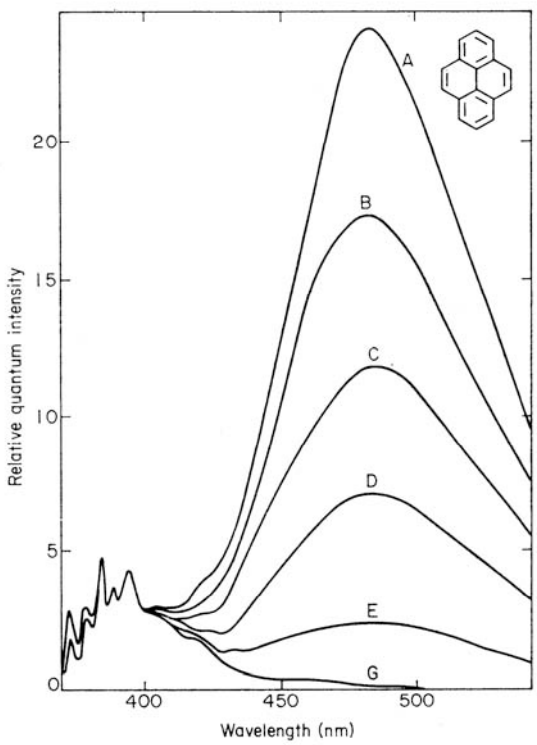

Figure 1-5. Fluorescence spectra of pyrene solutions in cyclohexane. Intensities are normalized to a common value of Φ_{FM}. Concentrations decrease from A (10^{-2} M) to G (10^{-4} M). Figure was adopted from Birks.[15]

At low concentration, pyrene displays a highly structured emission. At higher concentrations, a broad structureless band appears at longer wavelengths, due to the excimer luminescence. This is a general characteristic of excimer luminescence which is usually broader and red-shifted from the monomeric emission. This is due to the fact that the ground state of the excimer is unstable and therefore the potential energy of the ground state dimer increases with decreasing intermolecular distance. Another consequence of the absence of a bound dimer in the ground state is that a longer lifetime is usually observed for excimer emission compared to monomer emission. This is illustrated in Figure 1-6. Studies of fluorescence in crystals,[16] sandwich dimers[17] and diarylalkanes[18] all indicate that the preferred conformation of singlet excimers is close to a symmetrical sandwich structure with a separation of 3-4 Å. The binding energy in the

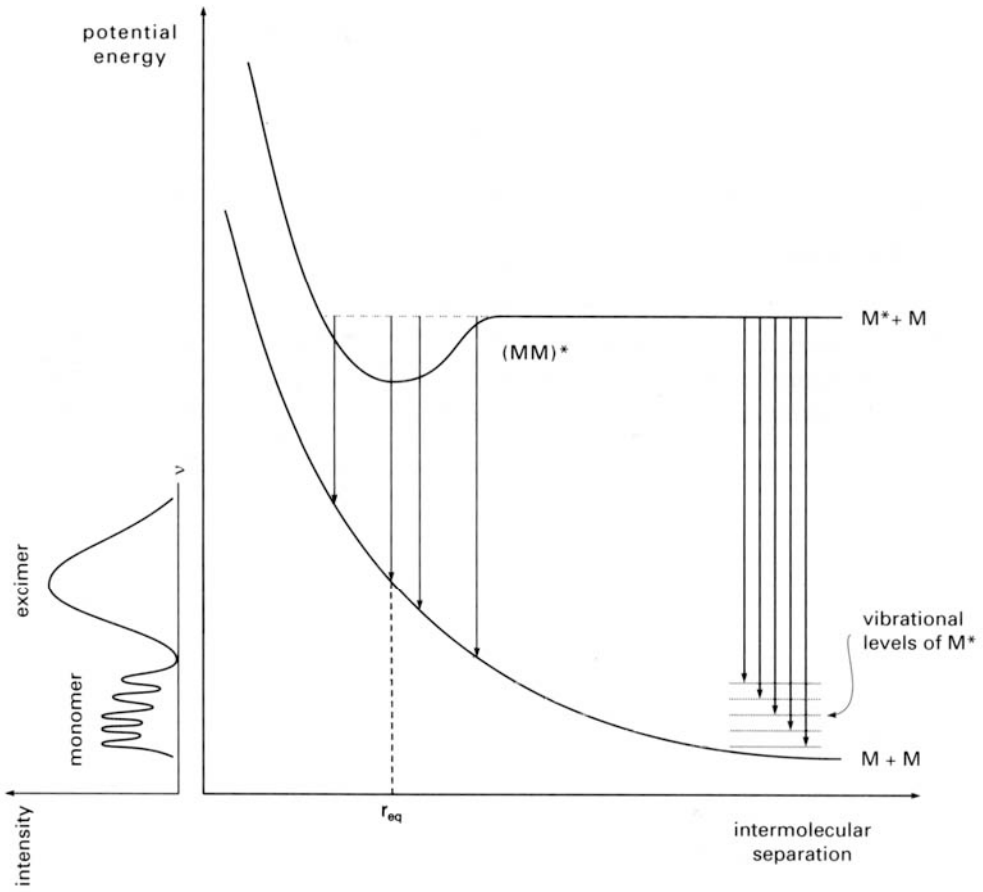

Figure 1-6. Potential energy curves for monomer and excimer. This figure was adapted from Gilbert and Baggot.[2]

singlet excimer comes mainly from the exciton resonance and to a lesser extent from charge resonance.

Triplet excimers, which are more related to this study, have been less studied due to the experimental difficulties associated with their detection. In fact there has been much debate on their existence and identification.[19,20] But an extensive and pioneering work by Lim[21] greatly contributed to establish triplet excimers as physical species.

Experimental evidences point towards a different structure for the triplet excimer than for the singlet. In a spectroscopic study on a series of 1,n-di-α-naphtylalkanes (n=1-4), Subudhi and Lim[22] have concluded that the triplet excimer adopts a skewed

conformation, where the short axis of the naphthalene are highly nonparallel while the long axes are parallel. The angle between the short axes was found to be 100-120°. As a result, the activation energy of triplet excimer formation is higher than for singlet excimer and the rate constant of formation of triplet excimer is smaller than for a singlet excimer.

More recently, triplet excimers have also been observed in polymers[23] and fullerenes[24] and have been used as the main source of white light emission in electrophosphorescent organic light emitting devices.[25] However, they remain rather elusive and more work is needed to fully comprehend their photophysical properties.

Exciton Coupling in Molecular Aggregates

In 1962, the molecular exciton model was developed by Davydov[26] to provide a theory describing the effects induced by the strong coupling of the collective excited states in organic crystals. Later, Kasha and co-workers[27,28] provided chemists with a model derived from the molecular exciton model that would provide simple tools to predict some of the photophysical properties of non-crystalline molecular aggregates. In particular, the molecular exciton model has proven useful in explaining the photophysical properties of porphyrins[29,30] and different dyes[31,32] in aggregates.

One of the important features of this model is the ability to explain the spectral shift of the absorption band observed in aggregates. This spectral shift is due to the splitting of the monomer excited state into two excitonic levels. The exciton band splitting can be derived from detailed quantum calculations but an approximation of the excited state interaction can be made by considering the electrostatic interaction of the transition dipole moments. This is illustrated in Figure 1-7 for co-planar dimers arranged in a parallel and head-to-tail geometry. In the case of parallel geometry, the out-of-phase arrangement corresponds to a lowering of energy, so E' lies lower than E (excited state of

monomer), whereas the in-phase dipole interaction gives repulsion, so E'' lies higher than E. Since the transition dipole moment is given by the vector sum of the individual transition dipole moments, transitions from ground-state to exciton state E' are forbidden whereas those from ground-state to E'' are allowed. The spectroscopic consequence of the exciton splitting will therefore be observed as blue-shift of the absorption in the aggregate in parallel arrangement compared to the monomer. For the head-to-tail geometry, the situation is opposite. The in-phase arrangement of individual dipole moments leads to an electrostatic attraction, whereas the out-of-phase arrangement causes electrostatic repulsion. However, transitions to E' are allowed whereas transitions to E'' are forbidden. In this case, the spectroscopic consequence of the exciton splitting will be observed as a red-shift of the absorption in the head-to-tail aggregate compared to the monomer. In the literature, aggregates in parallel arrangement are often referred to as J-aggregate, and the head-to-tail as H-aggregates.

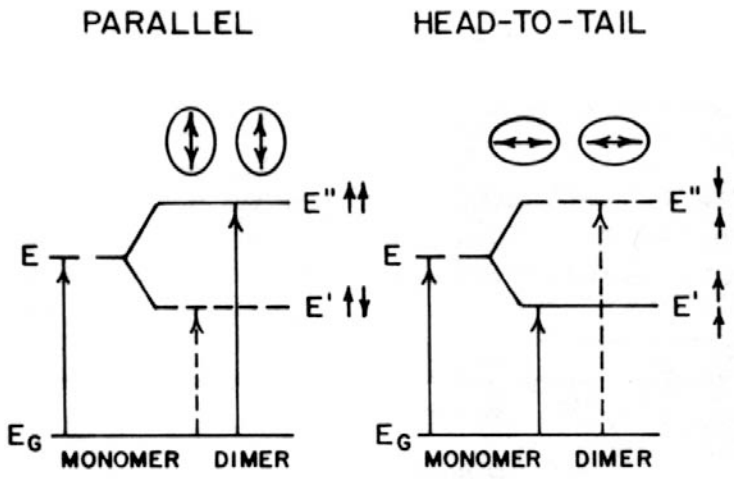

Figure 1-7. Schematic representation of the energy levels of the excited state of the monomer and of aggregates in parallel (left) and head-to-tail (right) geometry. Solid arrows and dashed arrows represent allowed transitions and forbidden transitions, respectively. This figure was adopted from Kasha.[33]

For planar aggregates composed of N monomers and in the point-dipole approximation, the exciton splitting energy ΔE is given by

$$\Delta E = 4\left(\frac{N-1}{N}\right)\frac{1}{4\pi\varepsilon_0}\left(\frac{\mu^2}{R^3}\right)\left(1-3\cos^2\theta\right) \qquad (17)$$

where ΔE is in joules, μ is the electronic transition moment of the monomer in Coulomb meter, R is the point-dipole—point-dipole distance in meter and θ is the angle between the long axis of the molecule and the line of molecular centers. This equation shows that the exciton splitting energy depends on the number of aggregates, that it is proportional to the square of the transition moment of the monomer and proportional to the inverse cube of the distance between monomers. The theory also predicts that for an angle θ = arcos(1/√3) = 54.7°, the exciton splitting energy is equal to zero and therefore no spectral shift may be observed in the absorption spectrum. This is the angle for which the aggregate will shift from J-aggregate to H-aggregate, as shown in Figure 1-8 below.

While the spectroscopic consequence of aggregation can be easily identified in the absorption spectrum, there is also a consequence on the photoluminescence. In the case of H-aggregates, where the excited state is the higher excited state E'', there is usually a quenching of fluorescence observed in the emission spectrum of aggregates. After excitation to E'', there is a rapid internal conversion to the lower exciton level E'. Since the transition from E' to the ground-state is not allowed, the system goes back to ground-state via nonradiative decay or intersystem crossing through the triplet excited state. Experimentally, the fluorescence detected is red-shifted (as it originates from the lower excitonic level E') and longer lived (as the transition from E' to ground state is forbidden) compared to the fluorescence of the monomer. A phosphorescence enhancement was observed by several authors[34,35] in the 1950s and was later rationalized

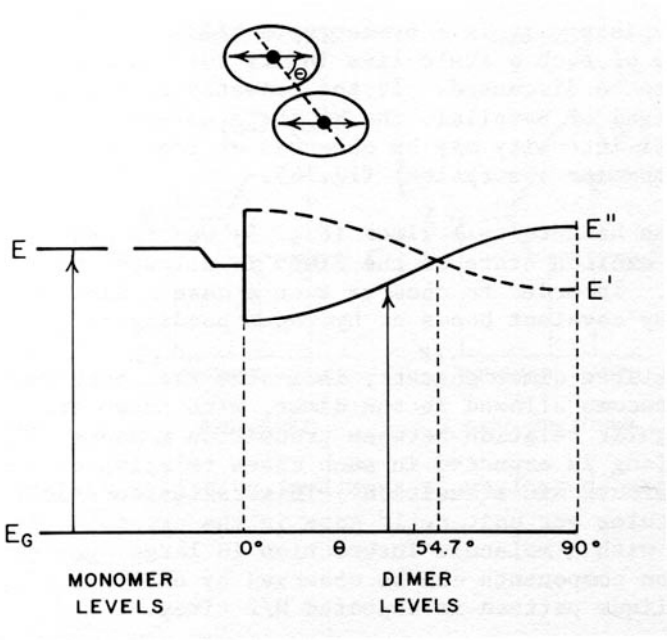

Figure 1-8. Exciton band splitting energy diagram for a co-planar molecular dimer as a function of the angle θ. This figure was adopted from Kasha.[33]

by Kasha using the molecular exciton model.[28,36] In the case of J-aggregates, emission occurs from the lowest exciton level E', at lower energy than the corresponding monomer emission. The emission from J-aggregates may be enhanced compared to the emission from the monomer although the interplay of inter- and intramolecular effects are often difficult to discern.[37] Note that in this model and in the dipole-dipole approximation, the triplet excited state is considered to remain degenerate since the oscillator strength (and hence the transition dipole moment) for singlet-triplet transition is zero.

More recently, J- and H-aggregates have been observed in many different systems, some of them closely related to the molecules studied in the next chapters. Whitten has studied fatty-acid derivatives of *trans*-stilbene in Langmuir-Blodget films, in order to study the effect of aggregation on the photophysical properties of stilbene.[38,39] The absorption and fluorescence spectra of a *trans*-stilbene derivative in solution and in multilayers in shown in Figure 1-9. The consequences of the aggregate formation are

found in both spectra. The absorption spectrum shows a hypsochromic shift compared to the monomer while the fluorescence spectrum shows a bathochromic shift compared to the monomer. This is consistent with the presence of H-aggregates in the supported multilayers system. In this case, fluorescence is observed from the lower excitonic state E' even though it is a forbidden process. But the lifetime of the fluorescence band in the multilayers is four times longer (3.3 ns) than the fluorescence lifetime of *trans*-stilbene (0.8 ns), consistent with a forbidden radiative decay.[38]

Examples of J-aggregates are found in a recent study of carbocyanine dyes by Pawlik *et al.*[40] Cyanines are strongly aggregating systems and the absorption spectrum (Figure 1-10) shows the presence of aggregates even in dilute solution. However, it is dependent on the concentration and increases with concentration. The absorption band for the aggregate is sharp and red-shifted from the absorption band of the monomer, consistent with a J-aggregate.

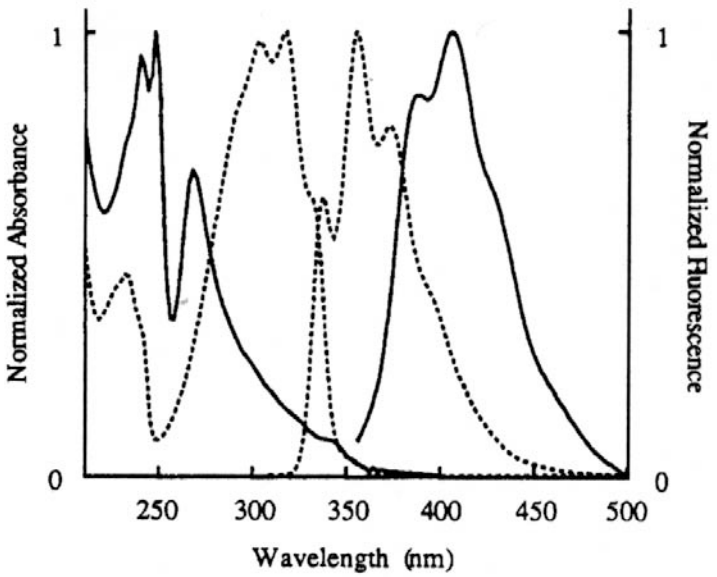

Figure 1-9. Absorption and fluorescence spectra for cyclohexane solution (dotted line) and multilayers of fatty acid derivative of *trans*-stilbene (solid line). Figure was adopted from Whitten.[39]

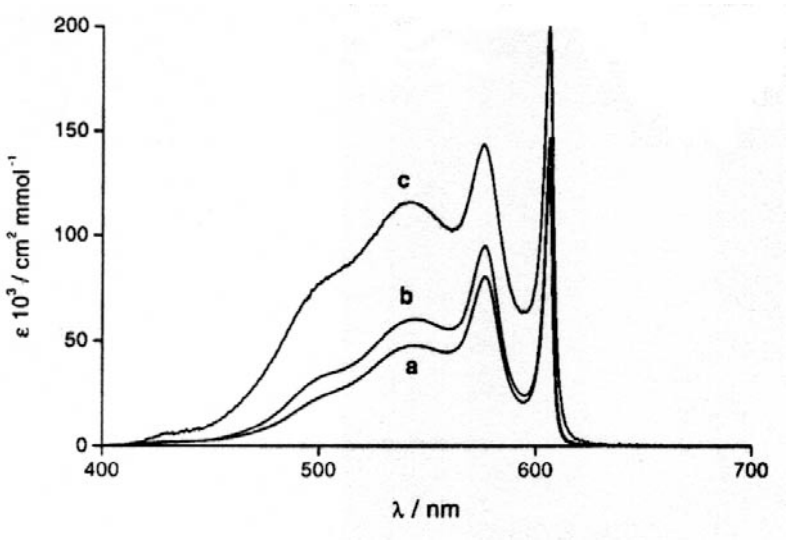

Figure 1-10. Absorption spectra of a carbocyanine derivative in 10^{-2} M aqueous sodium hydroxide solution at different concentrations and room temperature. (a) 1.7 x 10^{-5} M; (b) 2.2 x 10^{-5} M; (c) 4.4 x 10^{-4} M. Figure was adopted from Pawlik *et al*.[40]

Triplet Excited States in Conjugated Systems

While their presence usually goes undetected in organic conjugated polymers (CPs) for reasons mentioned previously (slow ISC), triplet excited states are still important in these systems. This is particularly true for organic light-emitting devices (OLEDs) where electroluminescence is generated by the recombination of electrons and holes injected from the electrodes. If conventional spin statistics were applied, only 25% of all recombination events would lead to potentially emissive singlet states, and 75% would lead to non-emissive triplet states. However, a number of recent experimental[41] and theoretical[42] studies point to the existence of a chain-length dependence on the exciton spin formation. It is therefore critical for the optimization of OLEDs to understand the factors controlling the formation of triplet excited states.

The quantum yield of ISC in some representative organic CPs has been measured by Burrows *et al.*[43] using photoacoustic calorimetry and the values varied from 0.50-0.80

for some polythiophenes to 0.01-0.04 for poly(p-phenylene vinylene)s. The higher value of ISC obtained for the polythiophene are attributed to the efficient spin-orbit coupling induced by the sulfur atom.

Monkman and Burrows have also carried out an extensive study on a broad range of organic conjugated polymers and measured their singlet and triplet energies by pulse radiolysis and energy transfer.[44] The polymers studied are presented in Figure 1-11 and a plot of triplet energy gap against singlet energy gap is shown in Figure 1-12. As can be seen, there is a linear correlation between the triplet and the singlet energy gaps for the very different polymers studied. Above the trend line are polymers with rigid and planar backbone structures while twisted polymers lie below the trend line. From this, it appears that while planarity enhances the delocalization of singlet excited state, triplets do not

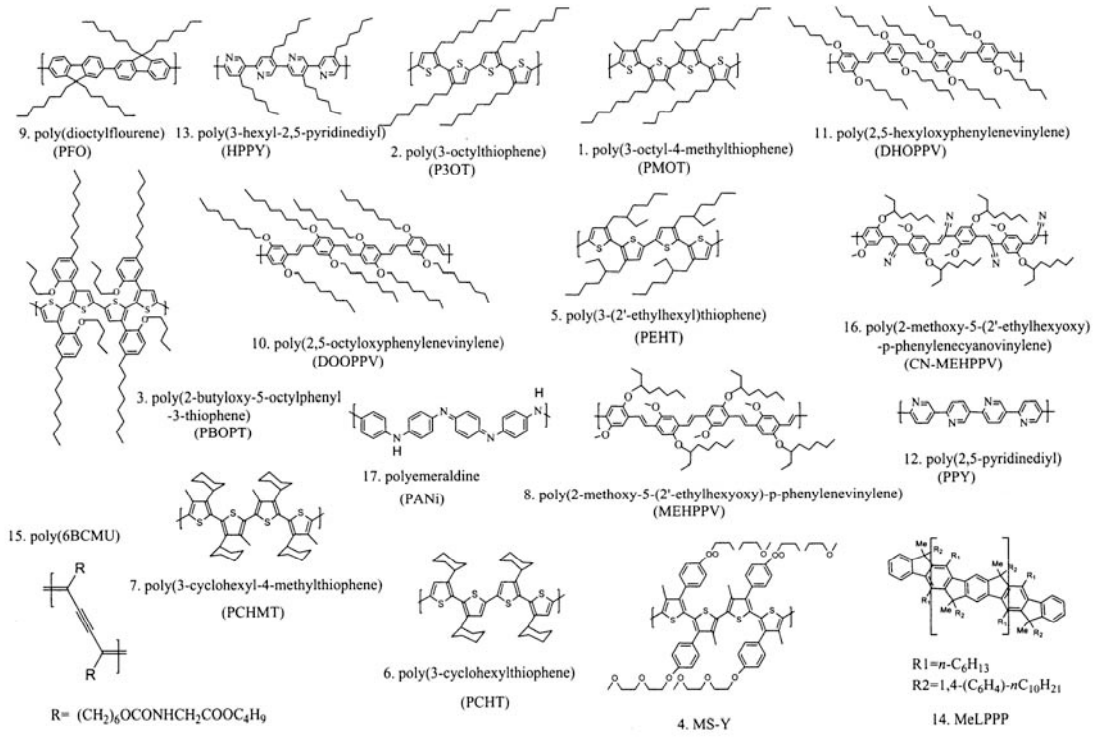

Figure 1-11. Schematic pictures of conjugated polymers studied by Monkman and Burrows.[44]

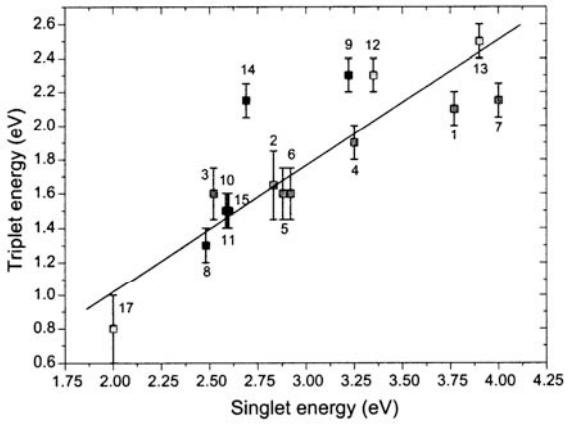

Figure 1-12. Plot of triplet energy against singlet energy for the conjugated polymers studied by Monkman and Burrows. Figure was adopted from Monkman *et al*.[44]

benefit as much from delocalization enhancements and while torsion angles tend to localize singlet excited states, this has les impact on the localization of triplet excited states. It follows then that triplet excitons must be more localized than singlet excitons, for which it is commonly agreed that their delocalization extends over 7-8 repeat units. Köhler *et al.*[45] have carried out a systematic study of singlet-triplet splitting energy (E_{S-T}) in organic poly(phenylene ethynylene) polymers, varying the optical bandgap by changing the nature of the spacer. They found that the E_{S-T} was always 0.7±0.1 eV and this is similar to what has been reported in other organic CPs.[46,47] Monomers, oligomers and twisted polymers have higher E_{S-T} because of the exciton confinement, which impacts the singlet more than the triplet exciton.[48]

Platinum Acetylides

Structure and Synthesis

Platinum acetylide materials are a class of compounds which have recently attracted significant attention due to their non-linear optical properties and potential application in optical limiting. The general structure of a platinum acetylide polymer is

presented in Figure 1-13. The aryl group (Ar) is usually a phenyl or a thienyl group, while the R is typically a short to medium alkyl chain (1 to 8 carbons) or even a phenyl group.

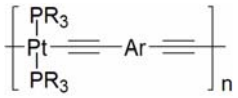

Figure 1-13. General structure of a platinum acetylide polymer.

The synthesis of the first Pt-acetylide complex was accomplished by Hagihara and co-workers[49] in 1978 and it involves the coupling of a platinum chloride complex with acetylene. The reaction is carried out in the presence of a base such as an alkylamine needed for the deprotonation of the arylacetylene while a catalyst such as copper iodide(I) is used to activate the acetylene function towards deprotonation. To avoid unwanted oxidation of the catalyst and of the platinum complex, the reaction is best carried out under inert atmosphere. Recently, it has been found that a *trans*-platinum complex is not necessary to obtain *trans*-platinum acetylide products, as the *cis*-platinum complex rapidly isomerizes in the presence of an amine. The two isomers can be identified by ^{31}P NMR, from the coupling constant between the phosphorous and one of the NMR active platinum isotope (^{195}Pt, I = ½, 33.8% natural abundance). While a trans isomer will typically have a $J_{Pt\text{-}P}$ below 2500 Hz, the $J_{Pt\text{-}P}$ for the cis isomer is usually higher than 2500 Hz.[50-52]

Due to their attractive non-linear optical properties, first reported by Davy and Staromlynska[53,54] in 1994, different architectures of platinum acetylide have been prepared in the last few years. These include dendrimers[55-57] (one of them containing up to 189 platinum atoms), liquid-forming oligomers,[58] and metallamacrocycles.[59]

Excited State

The photophysics of transition metal complexes involve the electrons in the d-orbitals, which are split into different energy levels depending on the electronic environment provided by the ligands. In the case of Pt(II) with four ligands, a d^8 complex, the ligand field stabilizes the d_{yz}, d_{xz}, d_z^2 and d_{xy} oriented away from the ligands and destabilizes the $d_{x^2-y^2}$ pointing towards the ligands. The resulting orbital diagram is shown in Figure 1-14. As can be seen, the HOMO orbital is the d_{xy} and the LUMO is the $d_{x^2-y^2}$ so the photophysics of Pt(II) are expected to involve those two orbitals. Optical transitions encountered in organometallic complexes may be purely metallic (d-d transitions) or metal-to-ligand charge-transfer (MLCT). When the ligands have a π-system, π-π* transitions localized on the ligand may also be observed.

In platinum acetylide oligomers and polymers there is a mixing between the platinum d-orbitals and the π-system and the optical transitions do not clearly fall in one or the other category. The extent of mixing depends on the overlap between the ligand and metal orbitals, the size of the spacer and the extent of conjugation in the ligand. The emission of platinum acetylide complexes typically shows vibronic bands, which is consistent with a MLCT or π-π* excited state, but not with a d-d transition. Also, phosphorescence lifetimes of are often found to be intermediate between a typical ^{3}π-π* or ^{3}MLCT. Theoretical work[60-62] has shown that the HOMO of platinum acetylide complexes is composed mostly of the π orbitals of the acetylide ligands with some contribution from the d_{xy} metal orbital, while the LUMO consists only of the ligand π* orbitals. Therefore the phosphorescence in platinum acetylide complexes is best thought of as originating from a ^{3}π-π*/^{3}MLCT manifold with predominantly intraligand character. Platinum acetylide complexes and polymers absorb light into the S_1 state between 300

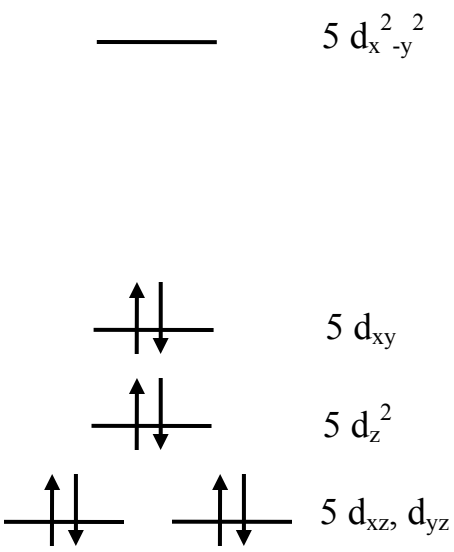

Figure 1-14. Splitting of d orbital levels in square-planar Pt(II) complexes.

and 400 nm. Rapid and efficient intersystem crossing (with close to unite quantum efficiency) converts the singlet excited state into triplets, so that their emission spectrum may show some fluorescence (decay of S_1) between 370 and 450 nm and phosphorescence (decay of T_1) between 500 and 600 nm. The triplet excited state absorbs light into higher triplet excited states (T_n) between 600 and 800 nm.

Several groups, including ours, are actively working on the photophysics of platinum acetylide complexes and in the next section, the state of the research on these materials is described.

Chawdhury *et al.*[63] have studied the evolution of the singlet and triplet excited states with the number of thienyl rings in platinum-acetylide dimers and polymers (shown in Figure 1-15). From absorption measurements of the polymers and dimers and comparison with the 2,5-diethynyl-oligothiophenes, they observed that the introduction of platinum lowers the energy of the $S_0 \rightarrow S_1$ transition. This shows that conjugation is

preserved through the platinum centers and that they do not confine the singlet exciton. The photoluminescence spectra of the polymers show a phosphorescence band between 650 and 740 nm, however phosphorescence was not observed for the terthienyl-containing polymer. They attributed the absence of phosphorescence to the reduced influence of the heavy-metal center responsible for ISC when increasing the number of thiophene rings.

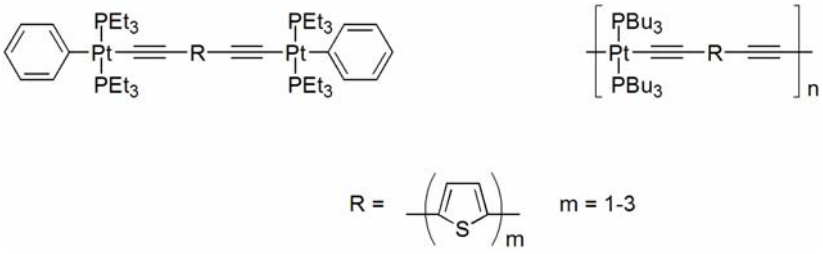

Figure 1-15. Structures of platinum acetylide dimers and polymers studied by Chawdhury *et al.*[63]

From a closer inspection of the fluorescence bands in the polymers, they observed increasing intensity in the vibronic bands as the number of thiophene rings increased. This is an indication that that the excited state geometry differs more from the ground state geometry and that the excited state takes more of a π-π* thiophene-based character with increasing thiophene rings. They also observed a constant S_1-T_1 splitting energy of 0.7 eV across the polymer series.

This constant S_1-T_1 gap of 0.7 eV was also exhibited in a larger range of platinum acetylide polymers (shown in Figure 1-16) studied by Wilson *et al.*[64] The polymers were chosen so that the triplet energy level would be tuned between 2.5 and 1.3 eV and this trend could be related to changes in nonradiative decay rates. Indeed, shorter lifetimes and lower quantum yields of phosphorescence were observed as the triplet energy level decreased, as illustrated in Figure 1-17. Calculations of the radiative and nonradiative

rates showed that as the triplet energy level decreases, the rate of nonradiative decay rates increases exponentially. This is the consequence of the energy gap law, which relates the rate of nonradiative decay rate of a transition rate to the energy gap between the states involved.

In simple terms, the energy gap law can be written as

$$k_{nr} \propto \exp\left(\frac{-\gamma \Delta E}{\hbar \omega_M}\right) \tag{18}$$

where ΔE is the energy gap between the states involved, γ is a term expressed in terms of molecular parameters and ω_M is the maximum and dominant vibrational frequency available in the system.[65] Plots of $\ln(k_{nr})$ against $\Delta E(T_1\text{-}S_0)$ gave straight lines for the monomers and the polymers studied, implying that platinum acetylide polymers and monomers follow the energy gap law. Another finding of this study is that radiative decay rates will be large enough to compete with nonradiative decay rates for materials with $T_1\text{-}S_0$ gaps of 2.4 eV or above.

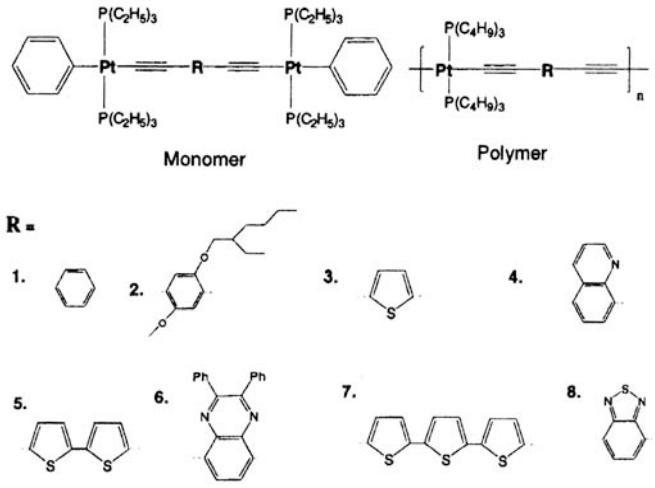

Figure 1-16. Platinum acetylide dimers and polymers studied by Wilson *et al.*[64] from which figure was adopted.

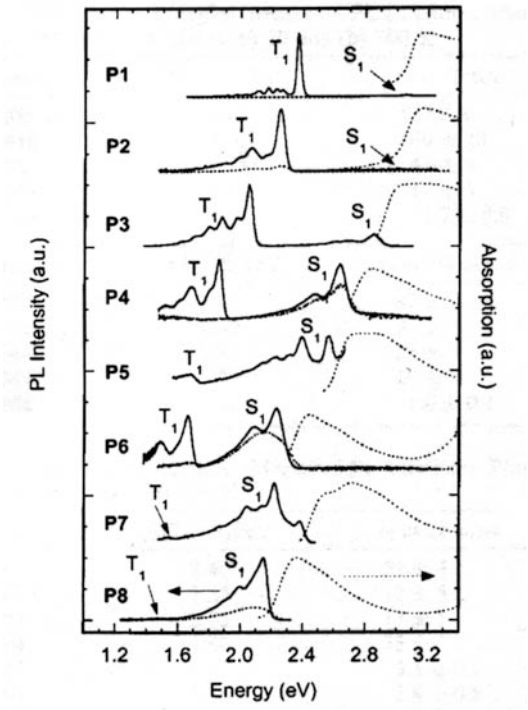

Figure 1-17. Absorption spectra (high energy dotted lines) and photoluminescence spectra (at 300 K dotted lines, at 20 K solid lines) of films of polymers **P1**-**P8**. Figure was adopted from Wilson *et al*.[64]

Extending the series of platinum-containing polymers studied and comparing them with their respective organic counterparts, Köhler *et al.*[45] proved that conclusions drawn on the triplet excited state in platinum acetylide polymers could be carried to the corresponding organic polymers. In a series of 15 platinum-containing and organic polymers with various optical bandgaps, a constant singlet-triplet energy gap of 0.7 ± 0.1 eV was found in both series (Figure 1-18).

In a study concerned with the influence of the size of the ligand in platinum acetylide complexes (shown in Figure 1-19), Rogers *et al.*[66] have also greatly contributed to the field. The study found that the effect of increased conjugation is a red-shift and an increase in the molar absorption coefficient of S_0-S_1 and T_1-T_n absorption bands and an

increase in the singlet-triplet energy gap. The authors concluded that as the conjugation increased, the S_0-S_1 transition is more localized on the ligand with less metal character

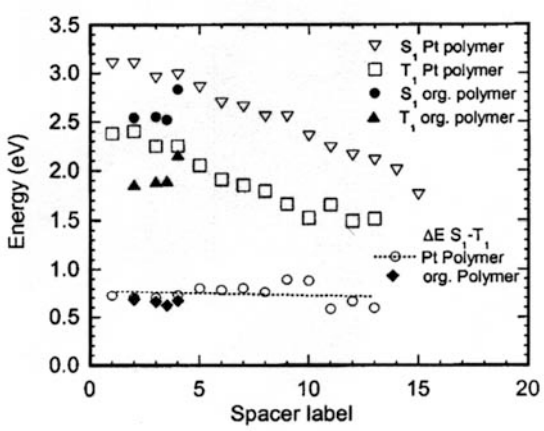

Figure 1-18. Energy levels of the S_1 and T_1 excited states and singlet-triplet energy gap for the Pt-containing and organic polymers. Figure was adopted from Köhler *et al*.[45]

and therefore slower intersystem crossing occurs. This was supported by the longer lifetimes of T_1 and lower quantum yield of phosphorescence observed.

Finally, our group carried out a systematic study of the delocalization of the singlet and triplet excited state in a series of mono-disperse platinum acetylide oligomers[67] (Figure 1-20). While the previous studies had some indications that the triplet exciton

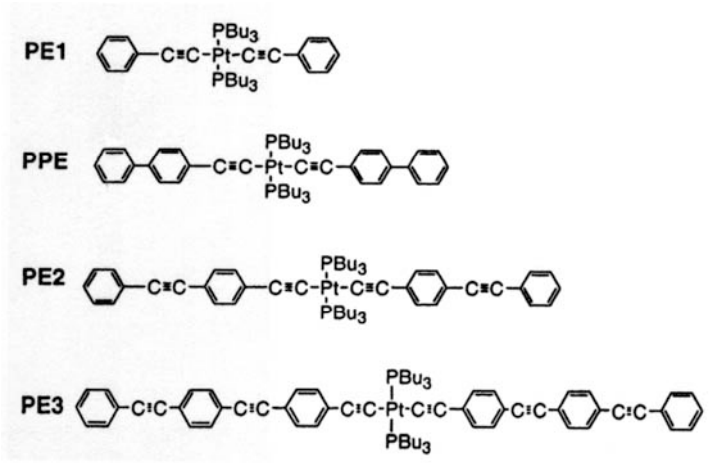

Figure 1-19. Platinum acetylide oligomers studied by Rogers *et al.*[66] from which figure was adopted.

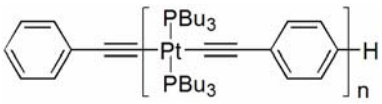

Figure 1-20. Platinum oligomers Pt-n (n = 1-5,7) studied by Liu *et al.*[67]

may be more localized than the singlet exciton, no definite conclusions could be drawn by comparing long conjugated polymers and short monomers. Polymers have a distribution of chain lengths and it is therefore not possible to relate the molecular weight of the polymers to the optical properties. The absorption and emission spectra measured for this series of oligomers is shown in Figure 1-21. The main absorption band found between 320 and 370 nm red-shifts across the series but the change is small between **Pt-5** and **Pt-7**, indicating that the effective and maximum conjugation length of the S_1 state is approximately 6 repeat units. The emission spectra of the oligomers displayed weak fluorescence between 370 and 390 nm and was dominated by a strong phosphorescence band at λ = 518 nm. The fluorescence red-shifted as the oligomer size increased but leveled off between **Pt-5** and **Pt-7**, consistent with the absorption data. However, the phosphorescence was found to be independent of oligomer length and this clearly showed that the triplet exciton is only delocalized over one or two repeat units. Figure 1-22 shows the estimated size of the triplet exciton based on these experiments. Consistent with this idea and the observations made in previous studies, the singlet-triplet energy gap was not constant in this oligomer series and varied from 0.91 to 0.78 eV as the oligomers length increased.

Objective of Present Study

Platinum acetylide oligomers offer a unique framework to study triplet excited state in conjugated system. Their monodisperse length and precise chemical structure allows structure-property relationship to be established by the synthesis of different derivatives.

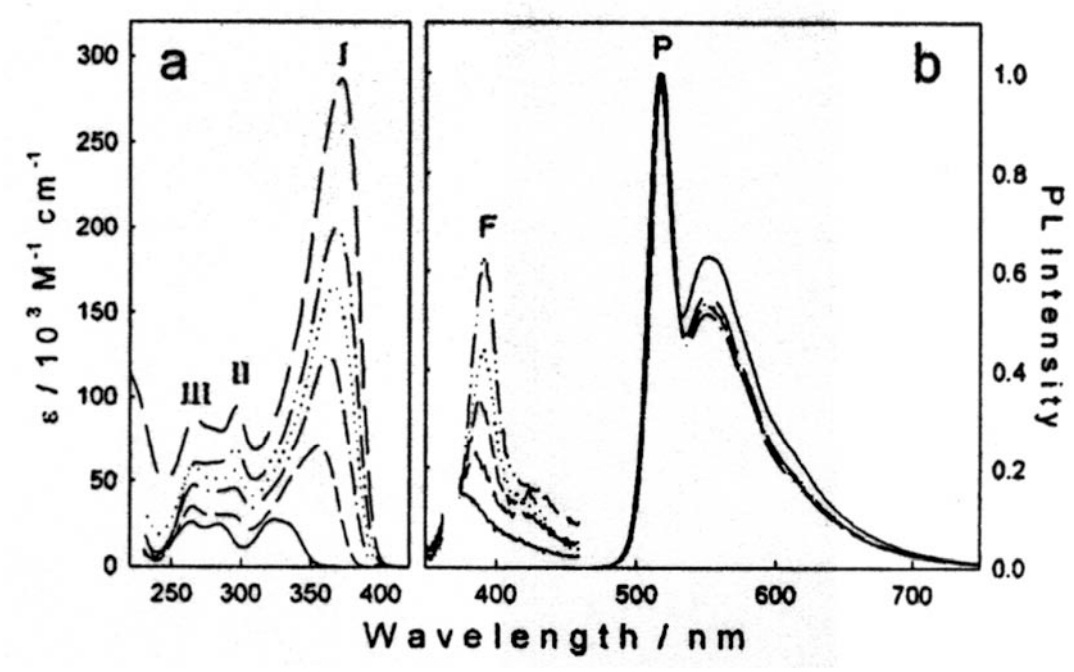

Figure 1-21. Absorption (a) and photoluminescence (b) spectra of Pt-n oligomers. Fluorescence (F) intensity scale is magnified 100X compared to phosphorescence (P). Figure was adopted from Liu *et al*.[67]

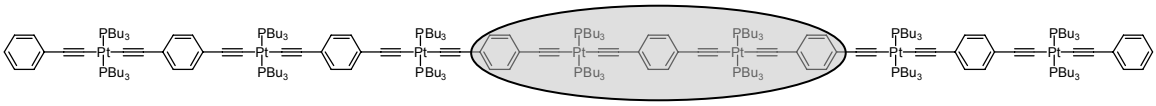

Figure 1-22. Triplet exciton confinement in platinum acetylide oligomers. Location of exciton is arbitrary.

The information gained from the study of platinum acetylide oligomers can be extrapolated to metal-organic[68] and even all-organic[45] polymers, where the triplet excited state is just as crucial as the singlet excited state. The need for more research on these unique molecules is therefore at a fundamental level.

There is also a direct motivation as platinum acetylide oligomers are promising candidates for optical limiting applications. McKay and co-workers[53,69] have found evidence that platinum acetylide oligomers could be used as the active component of a broadband, frequency agile optical limiter. This is a crucially important technology for

protection against intrusive, possibly damaging, laser radiations that have become increasingly present.

While the study of platinum acetylide oligomers and polymers carried thus far have significantly improved general knowledge on triplet excited states in these systems and related conjugated systems, much work remain to be done. In particular, several questions still need to be addressed in platinum acetylide materials:

What is effect of a low energy site on triplet excitons? While these effects are known in the case of the singlet exciton,[70,71] the situation may be different given the relative localization of the triplet excited state compared to the delocalized singlet excited state. For this, a series of platinum acetylide oligomers Pt4Tn with triplet energy traps were synthesized. The traps consisted of oligothiophenes (n = 1-3), which are known to have a lower triplet excited than benzene. The effect of these traps on the photophysical properties of platinum acetylide oligomer was probed and compared to a "trap-free" oligomer.

What is the extent of delocalization of charge carriers? In all-organic conjugated polymers, the charge carriers are believed to extend over several repeat units[72] but the effect of a metal center on the delocalization of charge carriers remains unknown. In order to determine the extent of delocalization of charge carriers, oligomer series Ptn and oligomer series P4Ttn were studied with electrochemistry and pulse radiolysis. The first series of oligomers Ptn (n = 1-5) provided a system to study the delocalization of charge carriers as a function of conjugation length while the second series of oligomers Pt4Tn probed the effect of low energy sites on charge carriers.

What are the consequences of aggregation? While these consequences can have a dramatic effect on the singlet exciton and are now fairly well understood,[73,74] almost no information is available for the triplet exciton in conjugated systems. A parallel to organic crystals has to be made and it remains unclear whether this is reasonable or not. With the concepts of supramolecular chemistry, complex conjugated systems have appeared in the literature in the past few years[75] and it appeared that platinum acetylide oligomers could be easily modified and designed to self-assemble. A series of short platinum acetylide oligomers where the phenylene end-group was tri-substituted with dodecanoxy chains were synthesized and their photophysical properties in molecular aggregates studied by steady-state and time-resolved spectroscopy using standard solution techniques.

CHAPTER 2
TRIPLET EXCITED STATES IN BICHROMOPHORIC PLATINUM ACETYLIDE OLIGOMERS

Introduction

Conjugated systems have received tremendous attention in the past fifteen years. Conjugated polymers in particular have been the subject of an enormous research effort, as they combine attractive photophysical and mechanical properties. Much of the research efforts are aimed towards understanding the dynamics of the different photophysical processes involved in an opto-electronic devices. For example in a light emitting diode, an exciton is formed following recombination of an electron and a hole.[76-78] The radiative decay of this exciton will give rise to luminescence. But the exciton may encounter a defect or low-energy site within the time of its lifetime, which will usually lead to nonradiative decay and a reduction of the device luminescence and performance.[79-84] It is therefore important to understand the susceptibility of the exciton to these low-energy traps, which are almost inevitable in polymer systems.

Most of the conjugated polymers studied are all-organic polymers, the photophysics of which are dominated by singlet excited states and fluorescence. The extent of delocalizaton of the singlet exciton[85,86] and its migration ability[70,87] are now fairly well understood. The triplet excited state on the other hand, being elusive and not directly active in all-organic conjugated polymers, has been less studied and is therefore less understood. Our group has a special interest in platinum acetylide polymers and oligomers. The introduction of the platinum center in the conjugated backbone increases

the ISC yield by spin-orbit coupling due to the heavy atom effect induced by platinum. The photophysics of these platinum oligomers and polymers are therefore dominated by the triplet excited state and intense phosphorescence emission. These systems provide access to the triplet excited state and allow its study through standard photophysical techniques. Using a series of platinum acetylide oligomers of increasing length, our group has successfully determined the extent of delocalization of the triplet excited state.[67] While the singlet excited state is sensitive to changes in conjugation length, the triplet excited state proved to be rather insensitive to the changes in conjugation length, implying that it is rather localized. The study points out to a triplet excited state localized between two platinum centers with some electronic density on the "outer" ligands as well.

Since the triplet excited state is believed to be much more localized than the singlet excited state, we wondered whether it would also be sensitive to the presence of low-energy traps in the conjugated backbone. For this we prepared the series of platinum acetylide oligomer Pt4Tn containing oligothienyl units in the center. Oligothiophenes are known to have lower triplet energies than benzene.[88,89] It is therefore anticipated that the oligothiophenes would act as low-energy traps. Thus their influence on the platinum acetylide photophysics could be observed and compared to a "trap-free" oligomer **Pt4**. The structures of the oligomers are shown in Figure 2-1 below. Each oligomer contains four platinum centers spaced out by phenyleneethynylenes linkages. **Pt4** is the "trap-free" reference oligomer and **Pt4T1** to **Pt4T3** are the oligomers with an oligothienyl unit energy trap of decreasing singlet and triplet energy. In the present study, we will first briefly look at the synthetic pathway to the oligomer series. We will then examine their

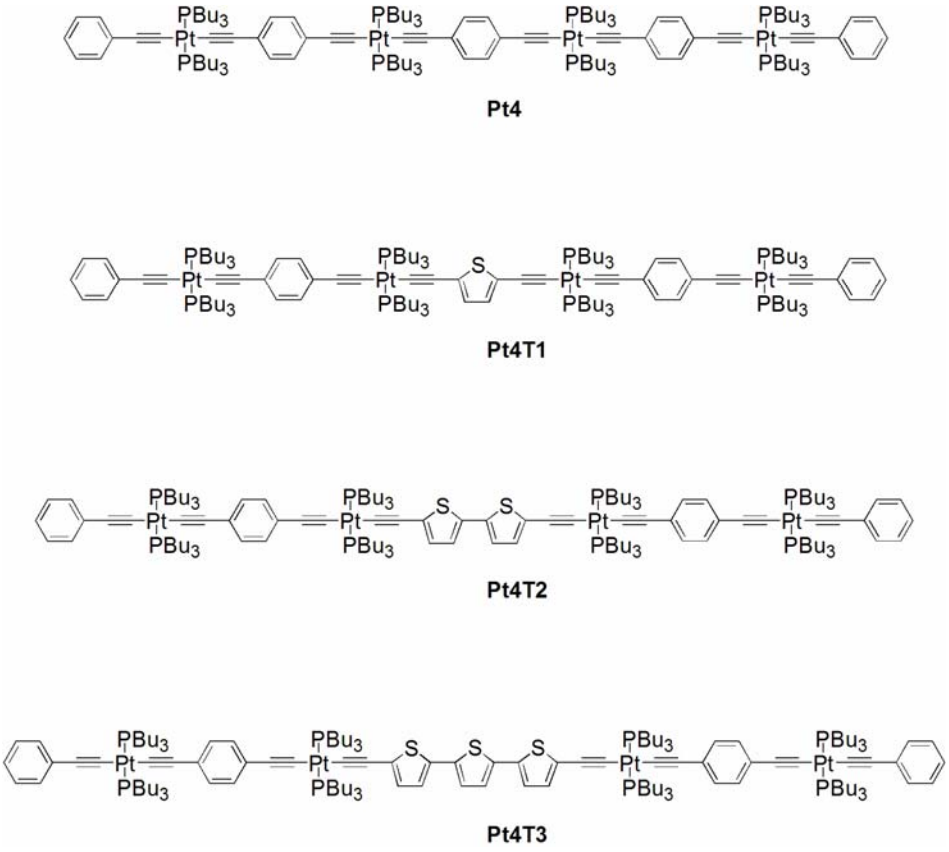

Figure 2-1. The structures of platinum acetylide oligomers **Pt4** and Pt4Tn (n = 1-3).

photophysical properties measured by steady-state and time-resolved techniques. Finally a discussion will provide some explanations for the results observed and what has been learned on the dynamics of triplet exciton in these metal-organic conjugated systems.

Synthesis

The synthetic strategy chosen for this series of oligomers is convergent, which allows the same platinum acetylide complex intermediate to be used for the synthesis of all four oligomers. The synthesis of the different platinum acetylide complexes **5a-d** is shown in Figure 2-2 below. It started with the iodination of oligothiophenes with N-iodosuccimide, in the presence of acetic acid and a co-solvent. The diiodo-oligothiophenes **2b-d** were then reacted with 2.1 equivalents of trimethylsilylacetylene under Sonogashira coupling conditions[90] to give the protected diacetylene-

oligothiophenes **3b-d** in good yields. After deprotection of the acetylenes under basic conditions, the diacetylene-oligothiophene **4b-d** are reacted with 3 equivalents of *cis*-dichloro-bis-(tri-*n*-butylphosphine)platinum(II) in the presence of diethylamine to give the four different platinum acetylide complexes **5a-d** in moderate to good yields.

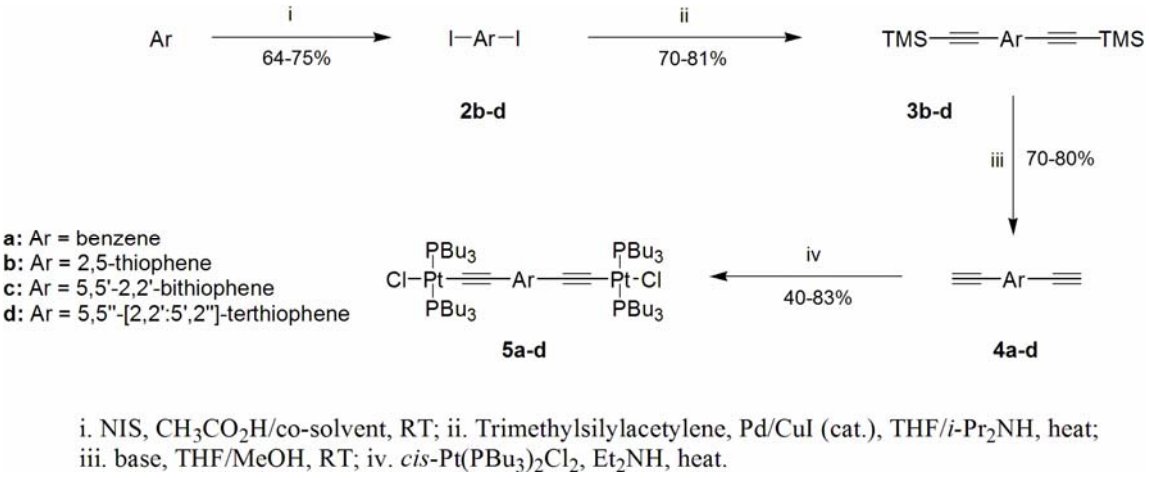

i. NIS, CH_3CO_2H/co-solvent, RT; ii. Trimethylsilylacetylene, Pd/CuI (cat.), THF/*i*-Pr_2NH, heat; iii. base, THF/MeOH, RT; iv. *cis*-$Pt(PBu_3)_2Cl_2$, Et_2NH, heat.

Figure 2-2. Synthesis of platinum acetylide complexes **5a-d**.

The synthesis of the common platinum acetylide complex intermediate **11** is shown in Figure 2-3 below. This was achieved by subjecting 1,4-diiodobenzene to a one-pot double Sonogashira coupling reaction with tri-*iso*-propylsilylacetylene and propargyl alcohol to give the unsymmetrically protected bis-acetylenebenzene **7**. Selective deprotection of one acetylene function with manganese oxide and potassium hydroxide gave the unsymmetrically protected bis-acetylene compound **8**. In parallel, phenylacetylene was reacted with *cis*-dichloro-bis-(tri-*n*-butylphosphine)platinum(II) to give platinum complex **9** in excellent yield. This latter was then reacted with compound **8,** affording the platinum complex intermediate **10** in very good yield, which after deprotection with TBAF, gave the desired platinum acetylide complex intermediate **11** in good yield.

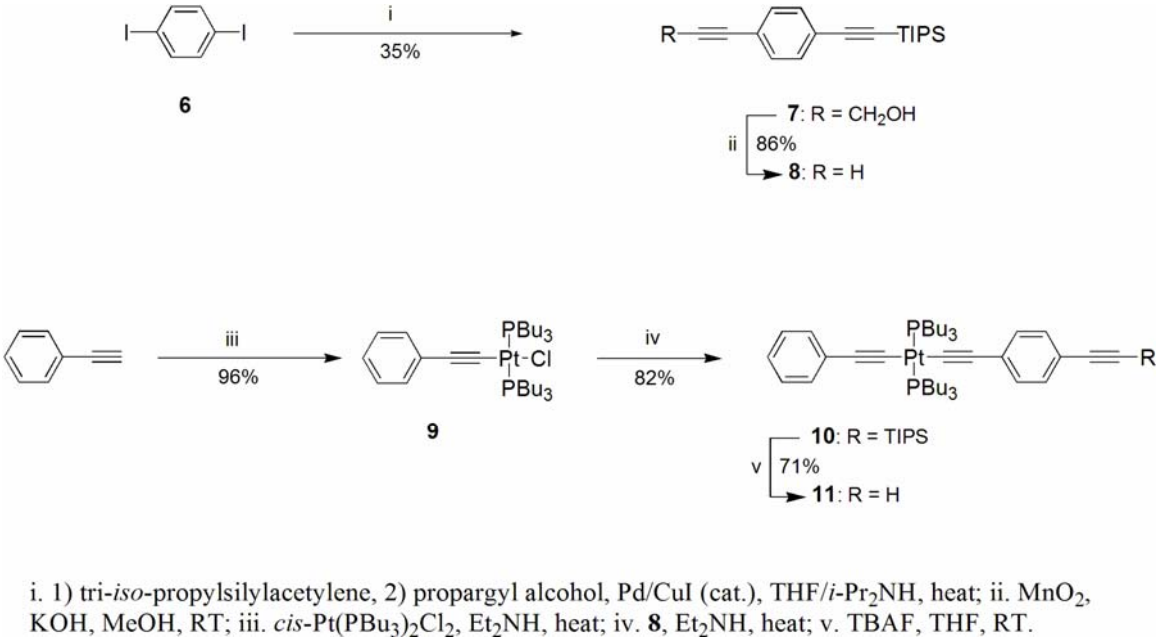

i. 1) tri-*iso*-propylsilylacetylene, 2) propargyl alcohol, Pd/CuI (cat.), THF/*i*-Pr_2NH, heat; ii. MnO_2, KOH, MeOH, RT; iii. *cis*-$Pt(PBu_3)_2Cl_2$, Et_2NH, heat; iv. **8**, Et_2NH, heat; v. TBAF, THF, RT.

Figure 2-3. Synthesis of platinum acetylide complex intermediate **11**.

The synthesis of the oligomers was finally achieved by reacting 2 equivalents of the platinum complex **11** and one equivalent of the required platinum acetylide complex **5a-d** in diethylamine under mild reflux. The oligomers were obtained in moderate to good yields. The reaction is illustrated in Figure 2-4 below.

The oligomers were characterized by ^1H and ^{31}P NMR, MALDI-DIOS and elemental analysis. The ^1H NMR allows the identification of the oligothiophene unit in each oligomer, their protons appearing downfield compared to the phenylene protons. The ^{31}P NMR shows two peaks, due to the two different magnetic environments of the phosphorus atoms in the oligomers. The value of the $J_{Pt\text{-}P}$ coupling constant (2340-2360 Hz) indicates that all platinum centers have a trans geometry in all oligomers.

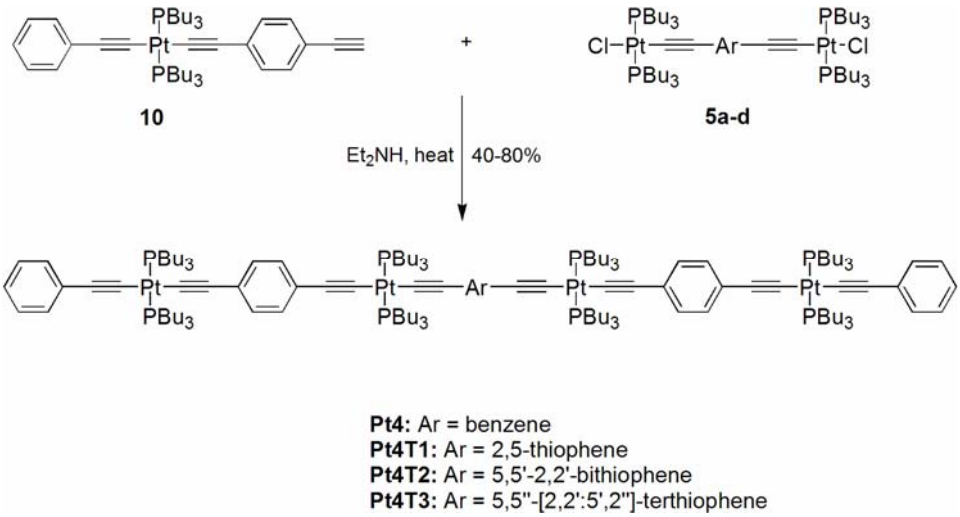

Figure 2-4. Synthesis of oligomers **Pt4** and Pt4Tn (n = 1-3).

Results

UV-Vis Absorption

The absorption spectra of the oligomers were recorded in THF and the results are presented in Figure 2-5 below. **Pt4** displays a strong absorption band at λ_{max} = 352 nm and some weaker bands at higher energy. The strong band is believed to arise from the long-axis polarized π,π^* transition, whereas the weaker low-energy bands arise from short-axis polarized transitions.[67,91] These transitions are comonly agreed to be mostly ligand-based and have only little metal-based character. The influence of the low energy thiophene in **Pt4T1** can be observed from the broadening of the main absorption band in this oligomer. The effect is more pronounced in **Pt4T2** and **Pt4T3** which both exhibit an extra thienyl-based band at λ_{max} = 410 nm and λ_{max} = 440 nm in addition to the phenyl-based absorption. The red-shifting of the thienyl-based absorption is consistent with the idea that the increasing size and conjugation length of the oligothienyl leads to greater stabilization of the singlet excited state. From these spectra, it appears that while the phenyl-based and thienyl-based chromophores are too close in energy to be give two

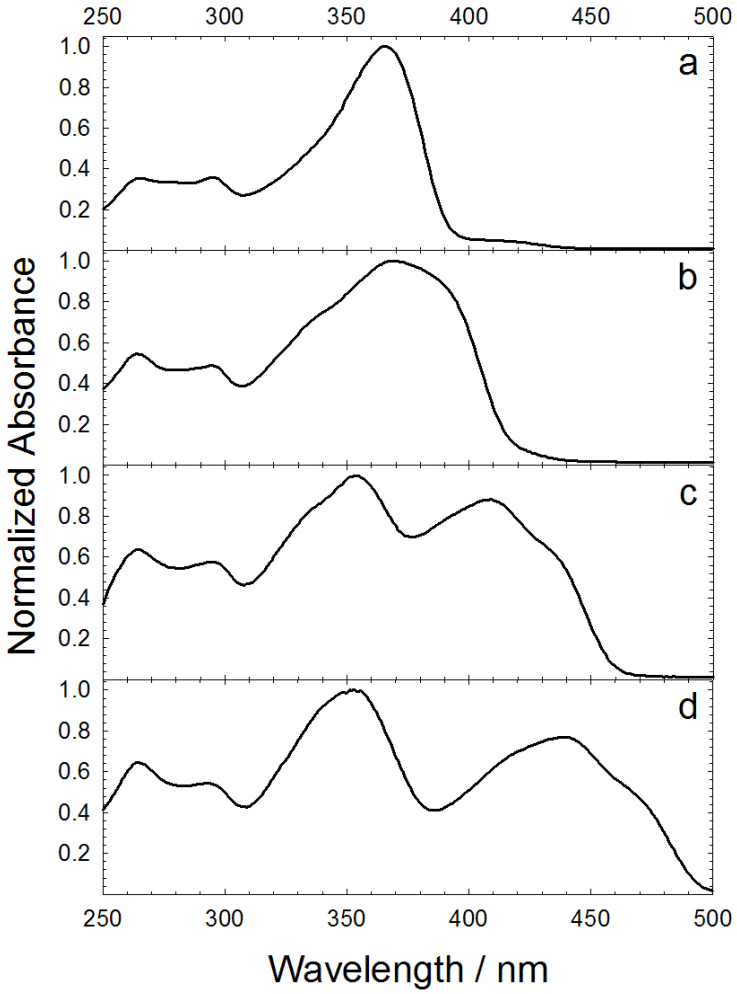

Figure 2-5. Absorption spectra of oligomers in THF. (a) **Pt4**; (b) **Pt4T1**; (c) **Pt4T2**; (d) **Pt4T3**.

distinct states in **Pt4T1**, the corresponding larger difference in energy in **Pt4T2** and **Pt4T3** allows the identification of two distinctly localized phenyl-based and oligothienyl-based excited states.

However, the thienyl singlet exciton is not experiencing its optimum delocalization and stabilization in these oligomers. In a series of thienyl-containing platinum acetylide polymers, Chawdhury *et al.*[63] reported absorption bands at lower energy (λ_{max} = 457 nm and λ_{max} = 469 nm for the bithienyl and terthienyl-containing platinum polymers, respectively) than the thienyl-based absorption here. This is probably due to the

confinement of the singlet exciton and to the presence of the higher-energy phenyl chromophores. Interestingly, the corresponding thienyl-containing platinum acetylide monomers end-capped with phenylacetylene were found to have absorption bands at λ_{max} = 406 nm and λ_{max} = 433 nm, very similar in energy to the thienyl-based absorption in **Pt4T2** and **Pt4T3**. This would imply that the singlet confinement is not the largest contribution to the difference in stability between the Pt4Tn oligomers series and the thienyl-containing platinum acetylide polymers.

Steady-State Photoluminescence

The photoluminescence of the oligomers was recorded in deoxygenated THF solutions with an excitation wavelength λ = 352 nm for all oligomers and the spectra are shown in Figure 2-6. The excitation wavelength was chosen on the blue edge of the absorption band of **Pt4** to minimize direct excitation of the thienyl units in the Pt4Tn oligomers. The dotted line across the spectra identifies the position of the main emission band observed in **Pt4**. This band is centered at λ = 520 nm and it arises from the relaxation of a well-studied triplet excited state.[45,66,67] The delocalization of the triplet exciton is believed to be 1-2 repeat units, based on a previous study.[67] Very little fluorescence is seen in the spectrum, implying that intersystem crossing is very efficient in **Pt4**. The emission spectrum of **Pt4T1** appears very different from that of **Pt4**. The spectrum is dominated by a broad band with a maximum at λ = 604 nm, while the phosphorescence band at λ =520 nm observed in **Pt4** is relatively weak. This broad band is believed to be originating from a thienyl-based triplet excited state. This assignment is made by comparison with the broad phosphorescence observed around λ = 604 nm in a platinum acetylide polymer with a thiophene unit as a spacer.[63] Some fluorescence is also

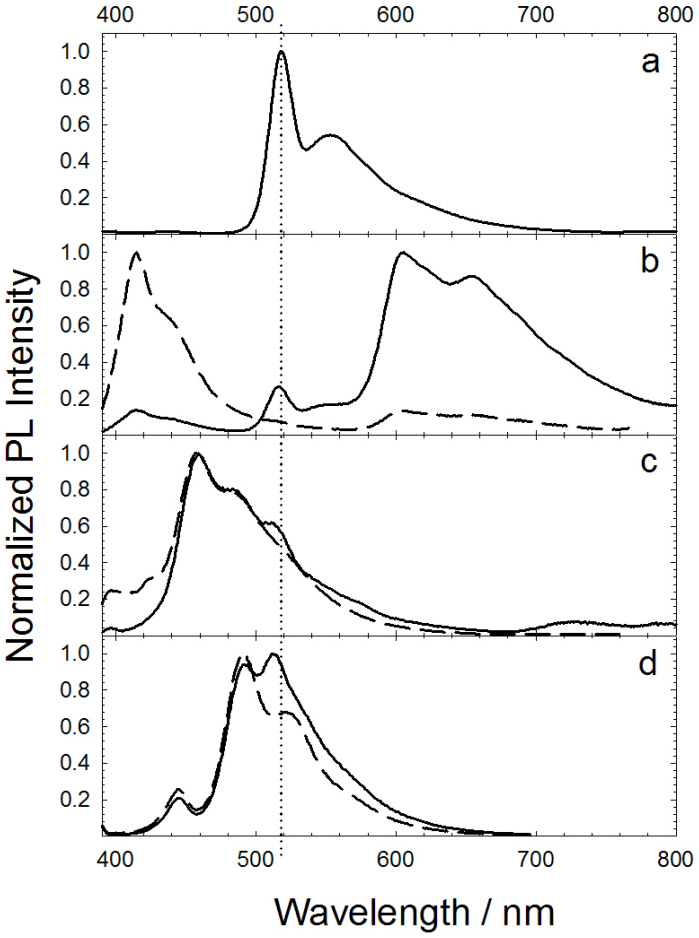

Figure 2-6. Photoluminescence spectra of oligomers in deoxygenated THF with an excitation λ = 352 nm. (a) **Pt4**; (b) **Pt4T1**; (c) **Pt4T2**; (d) **Pt4T3**. Dotted line indicates the position of main emission band in **Pt4**. Solid and dashed lines are for deoxygenated and air-saturated solutions, respectively.

seen in this spectrum (λ = 415 nm) and it is believed to be originating from the thienyl-localized singlet excited state, as it is not phenyl-based[67] and it corresponds to a slightly less stable singlet excited state than in the thiophene-containing platinum acetylide polymer reported by Köhler and Beljonne[48] (λ = 435 nm). This is consistent with the idea that the singlet excited state in these oligomers will experience a destabilizing confinement effect not found in polymers and thus will be found at higher energy than in the corresponding polymers. The observed maximum delocalization of the singlet excited

state in platinum acetylide oligomers was found to be about six repeat units by Liu *et al*.[67] In the present oligomers series, there are only four repeat units, so that the singlet excited state is confined and experiencing a destabilization compared to the corresponding polymers.

The emission spectra of **Pt4T2** and **Pt4T3** are similar. The emission is dominated by strong fluorescence (λ = 457 nm and λ = 491 nm for **Pt4T2** and **Pt4T3**, respectively) arising from a thienyl-based singlet excited state. The fluorescence peak shifts to lower energies from **Pt4T1** to **Pt4T3**, consistent with the bathochromic shift of the thienyl-based absorption band in the absorption spectra. The singlet excited state energies of **Pt4T2** and **Pt4T3** are again found at higher energies than those found in platinum acetylide polymers with the same oligothienyl unit spacing units.[48] Some phenyl-localized phosphorescence is also observed buried under the fluorescence emission. The phenyl-based phosphorescence can be identified by comparison with the air-saturated emission spectrum from which it is not observed. In addition, **Pt4T2** displays a very weak band around λ = 728 nm which arises from the bithienyl-based triplet excited state. This is consistent with the phosphorescence observed around λ = 746 nm for a platinum acetylide polymer with a bithiophene spacer.[48,63] No terthienyl-based phosphorescence emission was observed at room temperature in **Pt4T3**, even in the near-IR up to 1600 nm. It is interesting to note that Chawdhury *et al.*[63] did not observed phosphorescence from the terthiophene-containing platinum acetylide polymer at room temperature. They did however observe this phosphorescence at λ = 816 nm when photoluminescence was measured at T = 10 K.

The overall quantum yields of photoluminescence (fluorescence and phosphorescence) were measured for **Pt4** (Φ = 6.8%), **Pt4T1** (Φ = 1.8%) and **Pt4T3** (Φ = 0.9%). These values are an important characteristic of this series and will be discussed further in the discussion. But it is important to notice the decreasing trend of the quantum yield of photoluminescence as the triplet exciton energy decreases. This trend is in fact expected as it is a prediction of the energy gap law.[64]

The effect of the excitation wavelength was studied in order to determine if direct excitation of the oligothienyl moieties contributes to their observed luminescence (Figure 2-7). We therefore examined the photoluminescence spectrum in THF solutions of each oligomer at two excitation wavelengths: one is the phenylene-based chromophore absorption wavelength (λ = 352 nm) and the other is the oligothienyl-based chromophore absorption wavelength (λ = 369, 409 and 438 nm for **Pt4T1**, **Pt4T2** and **Pt4T3**, respectively). The dependence of the photoluminescence on the excitation wavelength is not dramatic but significant nonetheless. When exciting the oligothienyl units directly, the phosphorescence observed at λ = 518 nm decreases (in **Pt4T1**) or disappears (in **Pt4T2** and **Pt4T3**). It is not entirely unexpected to observe phenyl-based phosphorescence in **Pt4T1** even when exciting at λ = 369 nm since the chromophores are not resolved in the absorption spectrum due to the proximity of their energy levels. The absorption spectrum of **Pt4** shows that absorption is possible even at λ = 369 nm (see Figure 2-5) given that $\varepsilon^{367} \approx 160{,}000\ M^{-1}.cm^{-1}$.[67] More importantly, the phosphorescence arising from the oligothienyl group in **Pt4T1** (λ = 604 nm) and **Pt4T2** (λ = 723 nm) does not increase significantly upon direct excitation of the thienyl-based chromophore. While it could be argued that the same amount of thienyl chromophores could be directly

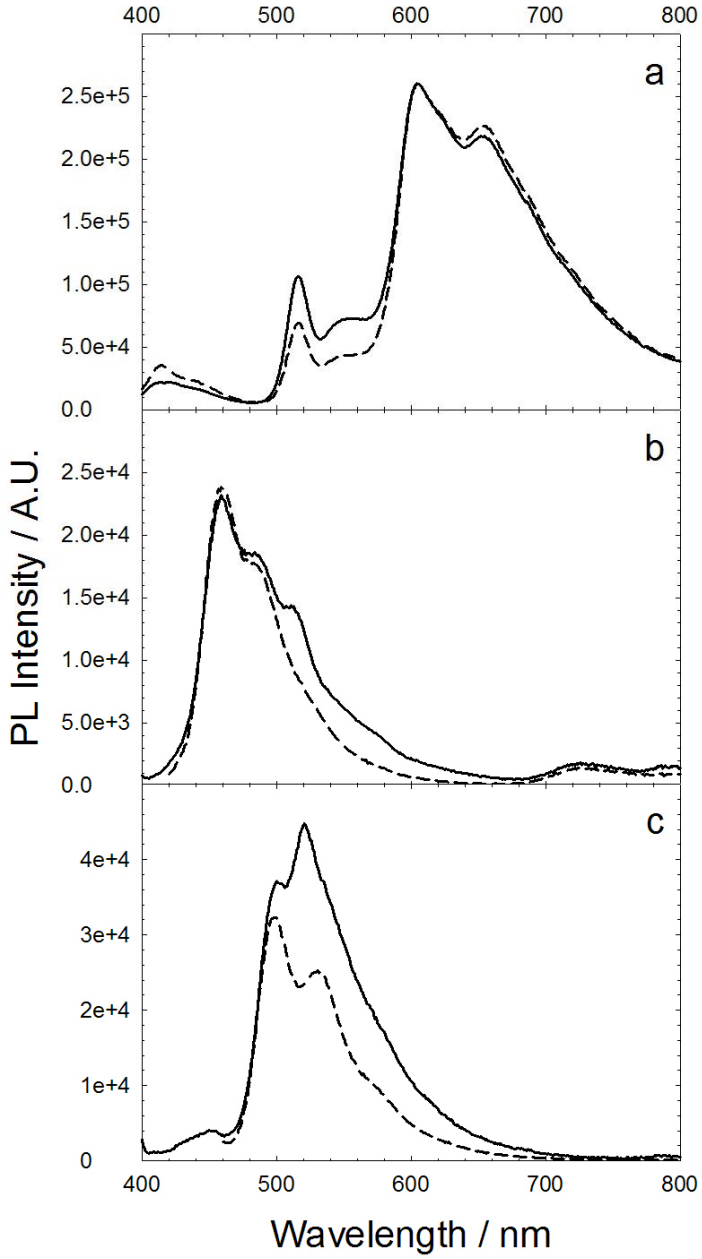

Figure 2-7. Photoluminescence spectra of oligomers Pt4Tn in deoxygenated THF. (a) **Pt4T1**, λ_{ex} = 352 nm (—), λ_{ex} = 369 nm (– –); (b) **Pt4T2** λ_{ex} = 352 nm (—), λ_{ex} = 369 nm (– –); (c) **Pt4T3** λ_{ex} = 352 nm (—), λ_{ex} = 369 nm (– –).

excited at λ = 352 nm and λ = 369 nm in **Pt4T1**, it does not hold for **Pt4T2**, where the absorption bands of both chromophores are resolved in the absorption spectrum. This implies that the phosphorescence of the bithienyl units is limited by other factors. One possible reason is that the nonradiative decay is much faster than the radiative decay of

the bithienyl-based triplet excited state and inherently limits the luminescence. Another reason could be that an equilibrium exists between the phenyl-based and the bithienyl-based excited state. In this case, no matter how many more bithienyl excited states are produced by direct excitation, the equilibrium will effectively balance the excitation on both chromophores.

In order to clarify the exact origin of the bands observed in the emission spectra of the oligomers, we now turn to the excitation spectra of the Pt4Tn series measured in THF solutions (Figure 2-8). The oligothienyl fluorescence bands (λ = 415, 457 and 491 nm for **Pt4T1**, **Pt4T**2 and **Pt4T3**, respectively), the phenyl-based phosphorescence (λ =520 nm) and oligothienyl phosphorescence bands (λ = 604 and 723 nm for **Pt4T1** and **Pt4T2**, respectively) are monitored while scanning for excitation and the results are very revealing. It is not surprising to see some of the phenyl-based absorption in the fluorescence of the oligothienyl since the oligothienyl-based singlet excited state is lower in energy than the phenyl-based and excitation transfer is therefore downhill. It is however striking that some of the thienyl-based absorption is seen in the phenyl-based phosphorescence, as this is uphill and therefore not energetically favorable. This supports the idea of an equilibrium between the excited states located on the phenylene and the thienyl, whereby a thienyl-based excited state can transfer some of the excitation back to the phenyl-based chromophore. The dynamics of the excited state in these oligomers is therefore more complex than it may have appeared until now and this will be discussed further in the discussion.

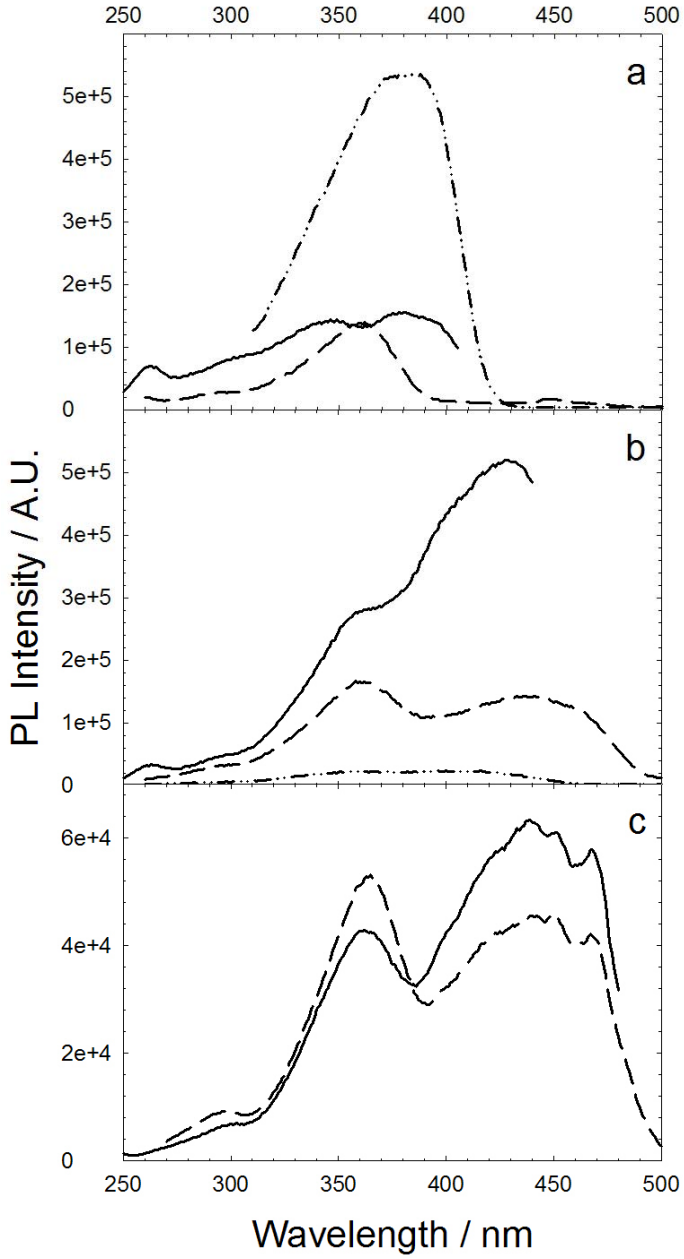

Figure 2-8. Excitation spectra of oligomers Pt4Tn in deoxygenated THF. (a) **Pt4T1** excitation for λ_{em} = 425 nm (—), λ_{em} = 520 nm (– –) and λ_{em} = 604 nm (– • • –); (b) **Pt4T2** excitation for λ_{em} = 457 nm (—), λ_{em} = 520 nm (– –) and λ_{em} = 723 nm (– • • –); (c) **Pt4T3** excitation for λ_{em} = 500 nm (—), λ_{em} = 520 nm (– –).

If an equilibrium is indeed present between the phenyl and thienyl-based excited state, it may be possible to influence it by changing the temperature. Moreover, lowering the temperature may reveal the terthienyl phosphorescence that has been elusive so far.

Therefore, the photoluminescence spectrum of **Pt4T1** was recorded in deoxygenated MeTHF at low temperature (Figure 2-9). As the temperature decreases, the phenyl-based emission intensity increases relative to the thienyl-based emission. The change levels off at 220 K and only an overall intensity change is observed at lower temperatures. This is consistent with the previously proposed equilibrium concept between the phenyl and thienyl-based triplet excited state. The thienyl-based triplet excited being lower in energy

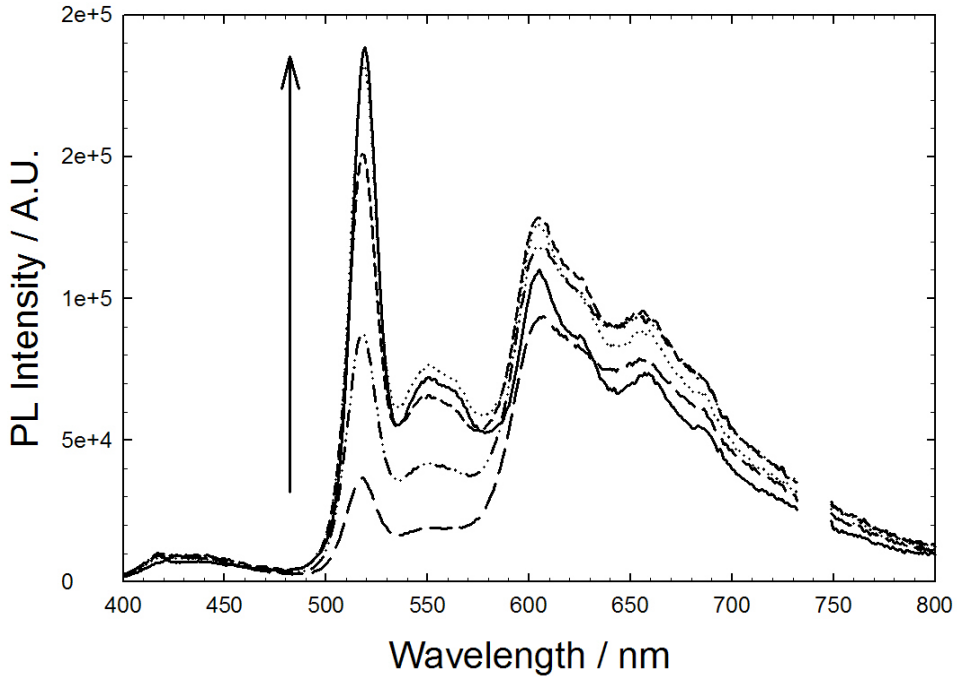

Figure 2-9. Low-temperature photoluminescence spectrum of **Pt4T1** in deoxygenated MeTHF with an excitation λ = 352 nm. Direction of arrow indicates effect of decreasing temperature from 300 K to 220 K. Region between 730 and 750 nm is removed because a strong scattering peak appears at this wavelength.

than the phenyl-based, the energy transfer to the phenyl-based is energetically not favorable and is slowed down at lower temperature. However, this could also be due to an activation energy associated with the energy transfer from the phenyl to the thienyl-based triplet excited state.

Photoluminescence of **Pt4T2** and **Pt4T3** (Figure 2-10) were recorded under similar conditions and the emission at 90 K and 300 K are shown only. The effect of temperature appears to be the same as the one observed in **Pt4T1**. Compared to the emission spectrum at room temperature, the phenyl-based phosphorescence is stronger and dominates the emission in **Pt4T2** and **Pt4T3** at T = 90 K. In fact, the phenyl-based phosphorescence band at λ = 520 nm in **Pt4T3** is almost identical to the phosphorescence of **Pt4** at room temperature (see Figure 2-6). No terthienyl-based phosphorescence was detected at T = 90 K in **Pt4T3**, even in the near-IR region up to 1600 cm (not shown).

Transient Absorption

In order to better understand the nature of the excited state present following the excitation of the oligomers, their transient absorption spectrum was recorded in deoxygenated THF (Figure 2-11). All oligomers feature a strong triplet-triplet (T_1-T_n) absorption band between 600 and 700 nm, and the lifetimes extracted from the decay of this band are presented in Table 2-1. The lifetime of the triplet excited state present is longest for **Pt4** (17.3 μs) and decreases from **Pt4T1** (9.4 μs) to **Pt4T2** and **Pt4T3** (4.4 and 4.6 μs, respectively), which have a similar lifetime. All oligomers also feature a bleaching band between 360 and 440 nm, where the singlet ground state absorbs. The red-shift and the narrowing of the T_1-T_n band from **Pt4T1** to **Pt4T3** is a clear indication of a thienyl-based triplet excited state. This is particularly significant for **Pt4T3**, where no terthienyl-based phosphorescence was observed in the steady-state photoluminescence study. The red-shift of the triplet-triplet absorption band is consistent with a more stable triplet exciton as the size of the oligothienyl increases. The narrowing of the band implies that the triplet exciton is also better defined as the size of the oligothienyl increases.

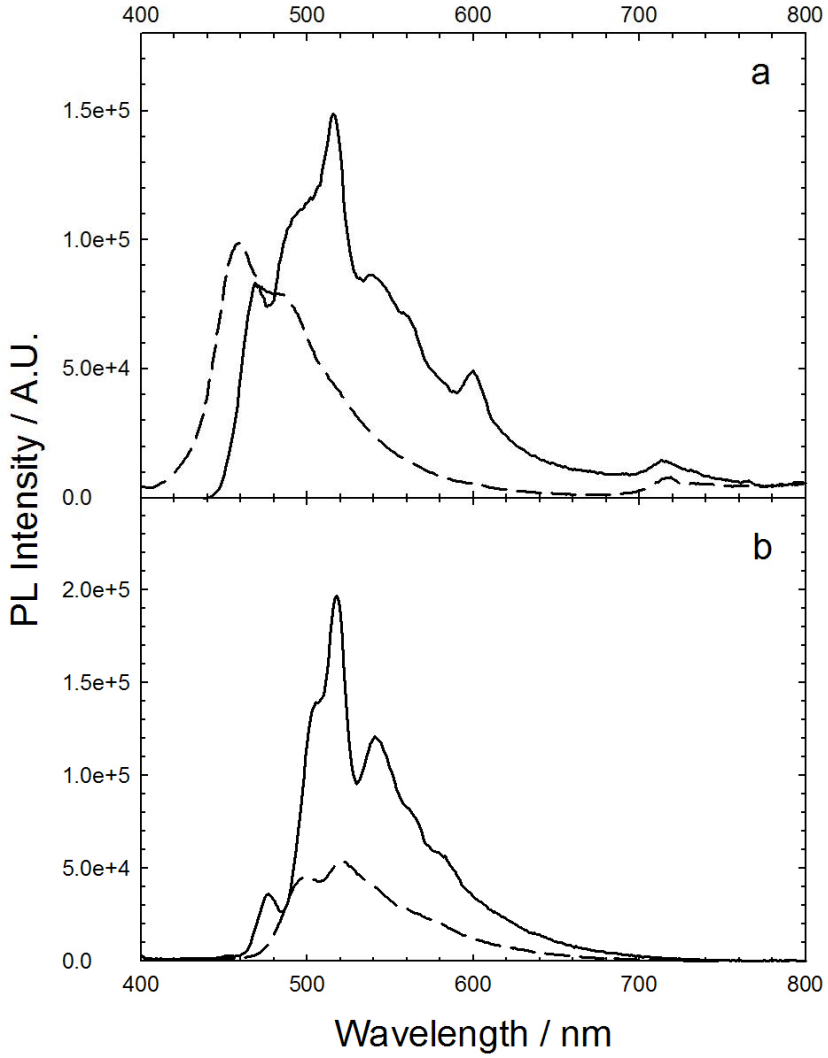

Figure 2-10. Low-temperature photoluminescence spectrum in deoxygenated MeTHF with an excitation λ = 352 nm at T = 90 K (—) and T = 300 K (– –). (a) **Pt4T2**; (b) **Pt4T3**.

Time-Resolved Photoluminescence

In order to gain insight into the dynamics and decays of the triplet excited states, time-resolved emission measurements were carried out in deoxygenated THF on the three oligothienyl-containing oligomers (Figure 2-12). The lifetimes extracted from these measurements, as well as other relevant data for the platinum acetylide oligomers are presented in Table 2-1. The lifetimes are on the order of microseconds in support of our

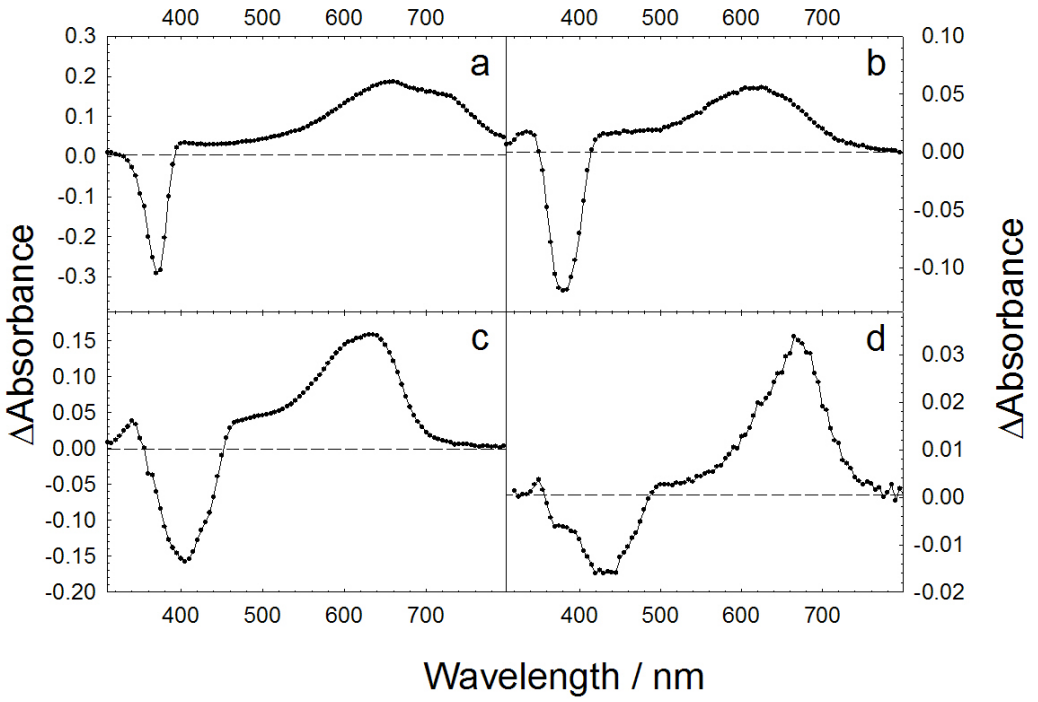

Figure 2-11. Transient absorption spectra of oligomers in deoxygenated THF following 355 nm excitation. (a) **Pt4**, 4 μs delay; (b) **Pt4T1**, 1.6 μs; (c) **Pt4T2**, 1.6 μs delay; (d) **Pt4T3**, 1.6 μs delay.

assignment as emission from a triplet excited state for the emission bands at λ = 606 nm and λ = 723 nm for **Pt4T1** and **Pt4T2**, respectively. It also supports the assignment as fluorescence for the emission bands observed between λ = 415 and 491 nm in **Pt4T1** to **Pt4T3**. These bands decayed within ~ 200 ns and are typical of a singlet excited state lifetime. Since any prompt fluorescence has been gated out in these experiments, the phenyl-based phosphorescence is now clearly identified in **Pt4T2** and **Pt4T3**. However once again, no phosphorescence from the terthienyl was detected by time-resolved measurements. All emission decays were found to give better fit with a bi-exponential function than with a mono-exponential function. Therefore, the lifetimes extracted from this sets of measurements shown in Table 2-1 give the lifetime and the corresponding contribution of each exponential decay.

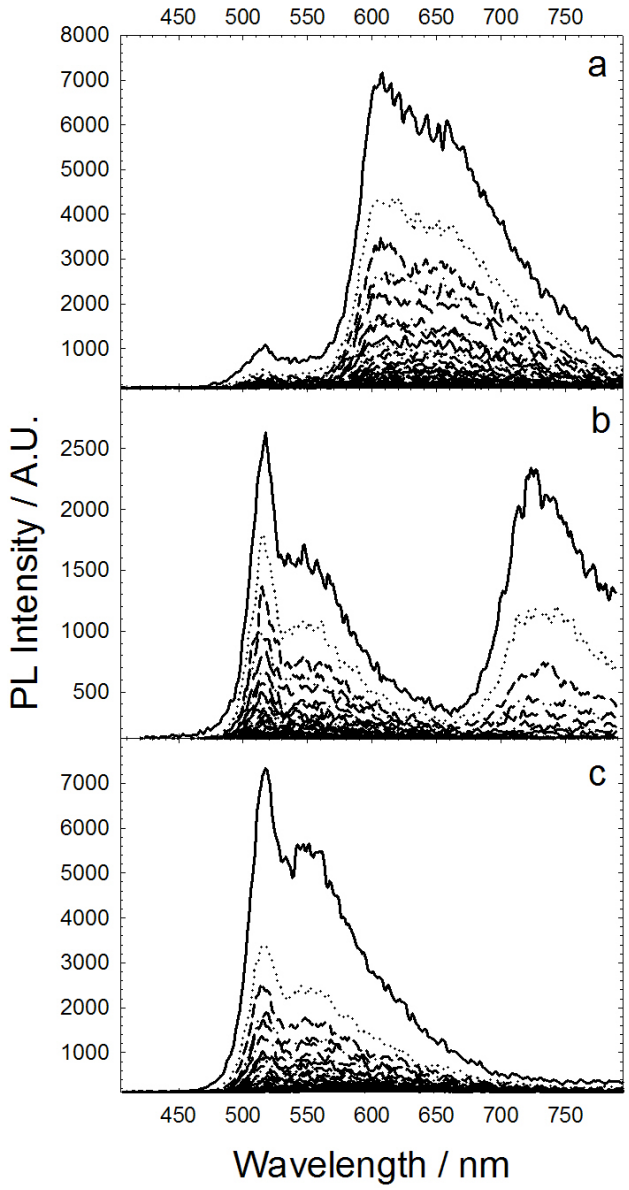

Figure 2-12. Time-resolved photoluminescence spectra of oligomers Pt4Tn in deoxygenated THF following 355 nm excitation. (a) **Pt4T1**, camera delay 0.4 μs, delay increment 1.3 μs; (b) **Pt4T2**, camera delay 0.5 μs, delay increment 2.0 μs; (c) **Pt4T3**, camera delay 0.4 μs, delay increment 2.5 μs.

The presence of the oligothienyl units is reflected in the lower lifetimes for the phenylene emission in all Pt4Tn oligomers compared to **Pt4**. The oligothienyl units act as energy acceptors and provide an alternate relaxation pathway for the phenyl-based triplet excited state, resulting in a shorter phenyl-based triplet excited state lifetime in all Pt4Tn

oligomers. For the phenylene emission decay, it is difficult to make a prediction on what should be observed. If energy transfer takes place through an exchange mechanism, which depends on the orbital spectral overlap between donor and acceptor, the rate of energy transfer and thus the phenylene emission lifetime should not change across the Pt4Tn oligomers series. Indeed, the orbital overlap between the donor (phenyl-based triplet excited state) and the acceptor (oligothienyl-based triplet state) should not change across the Pt4Tn oligomers series, as the same orbitals are most likely involved in all cases ($^3\pi,\pi$ with some metal character). However, other unidentified effects may also have an influence on the energy transfer rate. As can be seen from Table 2-1, while the phenylene lifetime drops from **Pt4** to **Pt4T1**, it is slightly longer for **Pt4T2** and about the same for **Pt4T3**. For the thienyl emission decay, for which one would expect the lifetime to get shorter as the thienyl-based triplet excited state energy level decreases, the lifetimes for **Pt4T2** and **Pt4T3** seem to follow the prediction based on the energy gap law. However it is difficult to interpret this as an energy gap law effect since only two decay lifetimes are available. These results only seem to indicate that the dynamics of the triplet exciton are not well-behaved and do not involve only forward energy transfer from a phenyl-based to a thienyl-based triplet excited state.

Discussion

Energy of the Triplet Excited State in Pt4T3.

It is possible to estimate the energy of the terthienyl-based triplet excited state present in **Pt4T3**. As discussed in the first chapter, the singlet-triplet splitting energy is constant in a family of platinum acetylide polymers, regardless of the energy of the singlet excited state. In monomers and oligomers, the S_1-T_1 gap is larger than for the

Table 2-1. Photophysical data for oligomers **Pt4** and **Pt4Tn**.

	UV-vis λ_{max} / nm	PL λ_{max} / nm		ϕ[f] / %	τ TA[g] / μs	τ PL[h] / μs	
		F[d]	P[e]			P[i]	Tn[j]
Pt4	366	389	517	6.8	17.3	18.6	[b]
Pt4T1	369	415	516, 606	1.8	9.4	0.8 (64%) 8.4 (36%)	1.1 (43%) 7.4 (57%)
Pt4T2	354, 409	457	515, 723	[a]	4.4	2.7 (51%) 11.8 (49%)	1.6 (51%) 4.7 (49%)
Pt4T3	353, 438	491	511	0.9	4.6	1.4 (56%) 12.7 (44%)	[b]

[a] Not measured; [b] Not applicable; [c] From ref.[67]; [d] F: fluorescence; [e] P: phosphorescence; [f] Total quantum yield of photoluminescence (F+P); [g] Transient absorption decay lifetime; [h] Photoluminescence decay lifetime (number in parentheses indicates relative amplitude of component); [i] P: decay at 517 nm; [j] Tn: decay at 606 nm for **Pt4T1**, decay at 723 nm for **Pt4T2**.

corresponding polymer. This difference has been attributed to the fact that the triplet exciton is more localized than the singlet exciton and is therefore less sensitive to the confinement effect experienced by the singlet exciton in monomers and oligomers. Polymers with either thiophene, bithiophene or terthiophene as the spacer in platinum acetylide polymers have been studied by Köhler *et al.*[45] and a constant S_1-T_1 energy gap of 0.7 ± 0.1 eV was found for these three polymers. It is therefore expected that the S_1-T_1 gap should be close but higher than this in our oligomers series.

From the steady-state emission fluorescence and phosphorescence of the mono- and bithienyl chromophores in **Pt4T1** and **Pt4T2**, the S_1-T_1 energy gap can be calculated:

Pt4T1: $E_{S\text{-}T} = E_S - E_T = 0.94$ eV

Pt4T2: $E_{S\text{-}T} = E_S - E_T = 1.00$ eV

As can be seen, these values of S_1-T_1 are very close. If we assume a value of 1.0 ± 0.1 eV for the series of Pt4Tn oligomers, the energy of the terthienyl-based triplet excited state should be:

Pt4T3: $E_T = E_S - E_{S-T} = 1.52$ eV

This value is similar to the S-T splitting energy found in a platinum acetylide polymer based on the terthienyl spacer.[64] This means that a terthienyl-based phosphorescence would appear at $\lambda = 816$ nm and that it should have been detected in our measurements if this state was sufficiently emissive. In fact this emission has been detected by Chawdhury *et al.* at a temperature T =10 K at the exact same position $\lambda = 816$ nm in a terthiophene-containing platinum acetylide polymer.[63]

The Absence of Phosphorescence in Pt4T3

Now that the energy of the terthienyl-based triplet excited state and the wavelength at which it should have appeared have been determined, some possible explanations for the absence of phosphorescence from this excited state will be provided.

While phosphorescence from the terthienyl chromophore in **Pt4T3** was not successfully detected, it is important to bear in mind that such a state exists in this molecule. Evidence for this lies in its transient absorption spectrum which clearly identifies a triplet excited state fitting the trend started in **Pt4T1** and **Pt4T2**. The red-shifting and the narrowing of the T_1-T_n band is consistent with a terthienyl-based triplet excited state. As seen in Chapter 1, radiative decays are always in competition with nonradiative decay processes and the observation of light emission only means that the radiative rate is fast enough to compete with the nonradiative decay rate. In the case of **Pt4T3**, the absence of terthienyl-based phosphorescence only means that for this excited state, the radiative rate is too slow and that the relaxation of the terthienyl-based triplet

excited state occurs only through nonradiative channels. One reason for that is that as we move from **Pt4T1** to **Pt4T3**, the organic content of the oligothienyl chromophore increases and the metal content decreases. Therefore the spin-orbit coupling must be less efficient so ISC should be slower. The consequences are a slower rate of radiative decay for the T_1-S_0 transition and a lower quantum yield of phosphorescence. Cryogenic temperatures in a frozen solvent matrix are often used to detect phosphorescence too weak at room temperature. However, the photoluminescence spectrum of **Pt4T3** recorded under these conditions (although T = 70 K was the lowest temperature where the measurement was carried) did not reveal the terthienyl-based phosphorescence. Looking at the low-temperature photoluminescence of **Pt4T1** at low-temperature, it appears that lowering the temperature favors the phenyl-based emission more than the thienyl-based. Therefore, the same effect can be expected in **Pt4T3** and it should not be surprising that the low-temperature emission spectrum did not display any terthienyl-based phosphorescence.

While a slower ISC is probably partly responsible for the absence of phosphorescence from the terthienyl-based triplet excited state, there is almost certainly another factor playing a part. As already discussed in Chapter 1, the energy gap law has been shown to apply to platinum acetylide polymers and monomers.[64] It had previously been shown to apply to metal complexes[7,92]. Simply stated, the energy gap law predicts that as the energy of the triplet excited state decreases, the rate of nonradiative decay increases exponentially. In fact, the calculated radiative and nonradiative rates for the terthiophene platinum acetylide polymer[64] were found to be $k_r = 3 \times 10^3\ s^{-1}$ and $k_{nr} = 4.2 \times 10^6\ s^{-1}$ at 300 K. At 20 K, they were $k_r = 0.4 \times 10^3\ s^{-1}$ and $k_{nr} = 6 \times 10^5\ s^{-1}$. These values

mean that at room temperature, the rate of radiative decay is too small to compete with nonradiative decay for a terthienyl-based triplet excited state. The authors concluded from their study that rates of nonradiative decay are only small enough for materials with a triplet energy level of 2.4 eV and more, which is well above our estimate of the energy level of terthienyl-based triplet excited state (1.52 eV).

Excited State Dynamics

So far, it has been shown that the presence of a low-energy trap can have a dramatic effect on the photophysical properties of platinum acetylide oligomers. Introduction of a thiophene unit results in a bathochromic shift of 90 nm with lower quantum yield of photoluminescence. Introduction of even lower energy trap such as bithiophene and terthiophene results in an emission spectrum dominated by fluorescence from the trap and the long-lived phosphorescence is lost. This could potentially be very problematic for optical applications relying on the triplet excited state of this type of compound.[53,69]

It is therefore critical to understand the dynamics of the triplet excited state in these systems and the interplay of low-energy sites. The photophysical study of this series of oligomers with energy traps of decreasing energy has shown that the dynamics of the triplet exciton in these systems is rather complicated. There appears to be more than just a simple energy migration to the low-energy traps and subsequent decay from those traps. Several experiments seem to indicate the presence of an equilibrium between the phenylene and thienyl-localized excited states. Evidence for the equilibrium lies in the excitation spectra of the Pt4Tn oligomers which shows that the phenylene emission is arising from excited states localized both on the phenylene and on the oligothienyl moieties, with equal contributions. This can be explained by an equilibrium between the

phenyl-based and thienyl-based excited state. Also, the photoluminescence collected upon direct excitation of the oligothienyl fragment did not show a significant increase in thienyl luminescence, either from the singlet or the triplet excited state localized on the oligothiophenes. This is also consistent with an equilibrium effectively balancing the proportion of excited states and their respective luminescence, which is shown to be quite independent of the location of the initially formed excited state. The low-temperature photoluminescence of **Pt4T1** revealed that the energy transfer is slowed down at lower temperature and relatively more phosphorescence from the phenyl-based triplet excited state is observed. This is also consistent with an equilibrium where the least energetically favorable process (back energy transfer to higher excited state is endothermic) is slowed down at lower temperature. However, this could also be explained by a simple thermally-activated energy transfer from the phenyl-based to the thienyl-based triplet excited state. The lifetime data extracted from the emission decays are not easily interpreted and rationalized. While the thienyl-based phosphorescence seems to be in agreement with the expected decreasing trend with the decrease in triplet energy level, the phenylene-based phosphorescence does not really follow any trend. Although this does not support the presence of an equilibrium, it does not disprove it either.

To illustrate this equilibrium, the photophysical processes involved in the oligomers series is presented in Figure 2-13 below. The equilibrium would be brought in by relatively efficient processes **11** or **9**, in addition to the forward processes **10** and **8**. The experiments carried out in this study do not allow distinguishing whether the forward energy transfer takes place between the singlets (process **8**) or the triplets (process **10**). In fact both the singlet and the triplet energy transfer could be operating in this system.

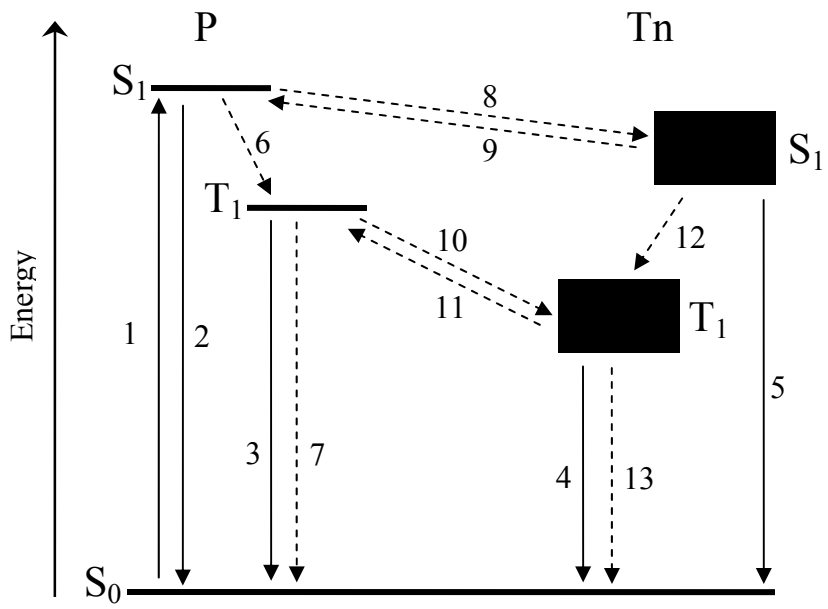

Figure 2-13. Energy diagram representing the photophysical processes involved in the Pt4Tn oligomers.

For the singlets to be in equilibrium, this would require singlet energy transfer (processes **8** and **9**) to be faster than ISC (processes **5** and **12**). Both of these processes have been shown to be fast[93,94], therefore it is not possible to rule out the singlet or the triplet energy transfer without exact calculations of the rate constants for the processes involved.

Although not commonly observed and studied, the presence of an excited state equilibrium is not unprecedented. In fact such a dynamic equilibrium has been observed recently in related metal-organic oligomers[95-97]. The absence of a clear trend in the lifetimes of emission suggests that while the equilibrium might be operating in **Pt4T1**, it does not seem to be the case in **Pt4T2** and **Pt4T3**. Indeed, it appears that in **Pt4T1**, the phenyl-based and the thienyl-based triplet excited states decay at similar rates (7-8 μs), close to the lifetime extracted from transient absorption (9 μs). However, in **Pt4T2**, the phenyl-based and the bithienyl-based triplet excited states do not decay at the same rate.

The lifetime of the phenyl-based triplet excited state increases (12 μs), closer to the lifetime observed in **Pt4** (18 μs), while the lifetime of the bithienyl-based triplet excited state decreases further (5 μs). It is however in accordance with the lifetime of triplet excited state detected by transient absorption, supporting the idea that this latter is localized on the bithiophene. Therefore if there are strong evidences for an excited state equilibrium in **Pt4T1**, it appears to be dependent on the energy gap and does not operate in the other oligomers of the series.

Conclusion

In this chapter, a series of platinum acetylide oligomers has been synthesized and their photophyisical properties studied. The oligomers incorporated oligothiophene units in the main chain to act as energy traps. The increasing length the oligothiophenes provided a series of oligomers with decreasing energy trap.

The photophysics of these oligomers have shown that the presence of an energy trap can have dramatic consequence on the photophysical properties of the oligomers. Efficient energy transfer creates excited state on the low energy sites. From there, radiative decay can occur and red-shifted emission can be observed. Alternatively, the radiative decay rate may become too small to compete with nonradiative decay as the energy of the trap decreases and the excited state created by energy transfer will relax by nonradiative decay processes. It has been shown that the energy of the trap can determine the dominant relaxation mechanism, due to the energy gap law. Finally, the presence of an excited state equilibrium has been suggested to explain the photophysical data collected on this oligomer series. However, the equilibrium seems to depend upon in the energy gap between the excited states and may be shut down by large energy gaps between excited states.

Experimental

Photophysical Measurements

Steady-state absorption spectra were recorded on a Varian Cary 100 dual-beam spectrophotometer. Corrected steady-state emission measurements were conducted on a SPEX F-112 fluorescence spectrometer. Samples were degassed by argon purging for 30 min and concentrations were adjusted to produce "optically dilute" solutions (i.e., $A_{max} < 0.20$). Low-temperature fluorescence measurements were made by cooling the samples in a LN_2 cooled Oxford Instruments DN-1704 optical cryostat connected to an Omega CYC3200 temperature controller. Samples were degassed by 4 repeated cycles of freeze-pump-thaw on a high vacuum line.

Photoluminescence quantum yields were determined according to the "optically dilute" method described by Demas and Crosby, with the quantum yield being computed according to eq. 14 in their paper.[98] *fac*-Ir(2-phenylpyridine)$_3$ was used as an actinometer ($\Phi_F = 0.40$ in THF) .

Transient absorption measurements were conducted on a home-built apparatus, which has been described elsewhere.[99] Samples were contained in a cell holding a total volume of 10 mL and the contents were continuously circulated through the pump-probe region of the cell. Samples were degassed by argon purging for 30 mn. Excitation was provided by the 3rd harmonic output of a Nd:YAG laser (355 nm, Spectra Physics, GCR-14). Typical pulse energies were 5 mJ/pulse which corresponds to an irradiance in the pump-probe region of 20 mJ/cm. Sample concentration were adjusted so that $A \approx 0.8$.

Time-resolved emission measurements were recorded on a home-built apparatus consisting of a Quanta Ray GCR Series Nd:YAG laser as a source ($\lambda = 355$nm, 10 ns fwhm), with time-resolved detection provided by an intensified CCD detector (Princeton

Instruments, PI-MAX iCCD) coupled to an Acton SpectraPro 150 spectrograph. Optically dilute solutions were used.

Mass Spectrometry of Pt Oligomers

The samples were analyzed using a Bruker Reflex II time-of-flight mass spectrometer equipped with delayed extraction (Bruker Daltonics, Billerica, MA). The analysis mode was desorption ionization on silicon (DIOS).[100] The samples were dissolved in dichloromethane at 1-10 μM and 1 μL was spotted on a DIOS plate that had been electrochemically etched with HF under tungsten light illumination.[101] Desorption was achieved using a nitrogen laser at 337 nm.

Synthesis

General. All chemicals used for synthesis were of reagent grade and used without purification unless noted. Reactions were carried out under an argon atmosphere with freshly distilled solvents, unless otherwise noted. ^{1}H, ^{13}C and ^{31}P NMR spectra were recorded on a Varian Gemini 300, VXR 300 or Mercury 300 spectrometer and chemical shifts are reported in ppm relative to TMS. *cis*-Dichloro-bis(tri-*n*-butylphosphine)-platinum(II)[102] and 1,4-diethynylbenzene[67] were prepared by literature methods.

2,5-diiodothiophene (2b). Thiophene (1.0 g, 11.9 mmol) and N-iodosuccinimide (5.48 g, 24.4 mmol) were dissolved in acetic acid (6 mL) and chloroform (8 mL). The flask was covered with aluminum foil and the mixture was stirred at room temperature overnight. The mixture was then washed with 10% sodium thiosulfate and water, the organic phase was dried on $MgSO_4$, filtered and the solvent was removed. The dark red oil obtained was further purified by column chromatography (silica gel, hexane) giving the desired product **2b** as a yellow oil (3.0 g, 75%). ^{1}H NMR (C_6D_6, 300 MHz) δ 7.23 (s, 2H); ^{13}C NMR (C_6D_6, 75 MHz) δ 77.0, 139.3.

5,5'-diiodo-2,2'-bithiophene (2c). 2,2'-Bithiophene (0.5 g, 3 mmol) and N-iodosuccinimide (1.67 g, 7.5 mmol) were dissolved in methanol (45 mL). To this solution, acetic acid (0.5 mL) was added. After stirring for 2 hours, a precipitate had formed and the flask was placed in freezer overnight to ensure complete precipitation of product. The white solid was then filtered by suction filtration and washed with cold methanol. After drying under vacuum, product **2c** was obtained as a white solid (0.80 g, 64 %). ^{1}H NMR ($CDCl_3$, 300 MHz) δ 6.80 (d, 2H), 7.18 (d, 2H).

5,5''-diiodo-[2,2'-5',2'']-terthiophene (2d). [2,2'-5',2'']-terthiophene (0.1 g, 0.4 mmol) and N-iodosuccinimide (0.199 g, 0.89 mmol) were dissolved in dichloromethane (6 mL) and acetic acid (0.05 mL) and flask was purged with nitrogen. The mixture was stirred in a water/ice bath for 2 hours after which time a yellow solid had precipitated. The solid was collected by suction filtration, washed with cold methanol and dried under vacuum giving product **2d** as a yellow solid (0.15 g, 73 %). ^{1}H NMR (C_6D_6, 300 MHz) δ 6.39 (d, 2H), 6.58 (s, 2H), 6.74 (d, 2H).

2,5-Bis-[(trimethylsilyl)-ethynyl]-thiophene (3b). 2,5-diiodothiophene **2b** (2.0 g, 5.96 mmol) and trimethylsilylacetylene (1.22 g, 12.5 mmol) were dissolved in Et_2NH (8 mL) and the solution was degassed with argon for 30 min. Then, $Pd(PPh_3)_2Cl_2$ (0.21 g, 5% eq., 0.298 mmol) and CuI (0.114 g, 10 % eq., 0.596 mmol) were added and mixture was stirred at room temperature for 12 hours. The mixture was then passed through a bed of Celite, washed with 10 % ammonium hydroxide, water, the organic phase dried on $MgSO_4$, filtered and the solvent was removed. Chromatography (silica gel, hexane) gave the desired product **3b** as a yellow solid (1.15 g, 70 %). ^{1}H NMR ($CDCl_3$, 300 MHz) δ

0.22 (s, 18H), 7.05 (s, 2H); ^{13}C NMR ($CDCl_3$, 75 MHz) δ 0.01, 97.1, 100.1, 124.7, 132.5, 169.0.

5,5'-Bis-[(trimethylsilyl)-ethynyl]-2,2'-bithiophene (3c). This compound was synthesized according to the same procedure used for 2,5-bis-[(trimethylsilyl)-ethynyl]-thiophene **3b** except 5,5'-diiodo-2,2'-bithiophene **2c** (0.2 g, 0.48 mmol) was used and the reaction was completed in 4 hours. The desired product **3c** was obtained as a yellow solid (0.129 g, 75 %). ^{1}H NMR ($CDCl_3$, 300 MHz) δ 0.22 (s, 18H), 7.00 (d, 2H), 7.10 (d, 2H); ^{13}C NMR ($CDCl_3$, 75 MHz) δ 0.1, 97.4, 100.7, 122.7, 123.9, 133.6, 138.2.

5,5''-Bis-[trimethylsilyl)ethynyl]-[2,2',5'2'']-terthiophene (3d). This compound was synthesized according to the same procedure used for 2,5-bis-[(trimethylsilyl)-ethynyl]-thiophene **3b** except 5,5''-diiodo-[2,2'-5',2'']-terthiophene **2d** (0.135 g, 0.27 mmol) was used and the reaction was stirred at 45˚C for 2 hours. The desired product **3d** was obtained as a bright yellow solid (0.096 g, 81 %). ^{1}H NMR ($CDCl_3$, 300 MHz) δ 0.24 (s, 18H), 7.01 (d, 2H), 7.08 (s, 2H), 7.14 (d, 2H).

2,5-Diethynyl-thiophene (4b). 2,5-bis-[(Trimethylsilyl)-ethynyl]-thiophene **3b** (0.392 g, 1.42 mmol) was dissolved in methanol (24 mL) and the solution was degassed with nitrogen. To this solution, 0.1 mL of a 0.5 M KOH solution was added and the mixture was stirred at room temperature for 2 hours. After this time, water (50 mL) was added and the mixture was extracted with pentane, the organic phase dried on Na_2SO_4, filtered, and the solvent was removed under reduced pressure at room temperature. The desired product **4b** was obtained as a colorless oil (0.15 g, 80 %). ^{1}H NMR ($CDCl_3$, 300 MHz) δ 3.5 (s, 2H), 7.22 (s, 2H); ^{13}C NMR ($CDCl_3$, 75 MHz) δ 76.4, 82.3, 123.8, 132.8.

5,5'-Diethynyl-2,2'-bithiophene (4c). 5,5'-bis-[(Trimethylsilyl)-ethynyl]-2,2'-bithiophene **3c** (30.7 mg, 0.086 mmol) was dissolved in THF (2 mL) and the solution was degassed with nitrogen. Then, tetrabutylammonium fluoride (0.35 mL of a 1 M THF solution, 0.35 mmol) was added via a syringe and the mixture was stirred at room temperature protected from light for 3 hours. After this time, the solvent was removed and chromatography (silica gel, hexane) gave the desired product **4c** as a yellow solid (14.4 mg, 78 %). ^{1}H NMR ($CDCl_3$, 300 MHz) δ 3.4 (s, 2H), 7.04 (d, 2H), 7.19 (d, 2H); ^{13}C NMR ($CDCl_3$, 75 MHz) δ 82.9, 121.6, 124.1, 134.2, 138.3.

5,5''-Diethynyl-[2,2',5',5'']-terthiophene (4d). 5,5''-Bis-[trimethylsilyl)ethynyl]-[2,2',5'2'']-terthiophene **3d** (93 mg, 0.21 mmol) and K_2CO_3 (29 mg, 0.21 mmol) were dissolved in MeOH (9 mL) and THF (4 mL) and solution degassed with argon. The mixture was stirred at room temperature overnight after which time the solvent was removed. The brown residue obtained was dissolved in CH_2Cl_2, washed with 10% HCl, water, the organic phase dried on $MgSO_4$, filtered and the solvent was removed. Chromatography (silica gel, hexane) gave the desired product **4d** as a yellow solid (43.5 mg, 70 %). ^{1}H NMR ($CDCl_3$, 300 MHz) δ 3.42 (s, 2H), 7.02 (d, 2H), 7.10 (s, 2H), 7.20 (d, 2H).

Complex 5a. 1,4-diethynylbenzene (46.2 mg, 0.373 mmol) and *cis*-dichloro-bis-(tri-*n*-butylphosphine)platinum(II) were dissolved in Et_2NH (15 mL) and the solution was degassed with nitrogen. The mixture was stirred under reflux for 8 hours. The solvent was removed and the crude product purified by flash chromatography (silica gel, hexane then 7:3 hexane/CH_2Cl_2) giving the desired product **5a** as a yellow solid (210 mg, 40 %). ^{1}H NMR ($CDCl_3$, 300 MHz) δ 0.85-1.0 (t, 36H), 1.40-1.63 (m, 48H), 1.9-2.0 (m, 24H),

7.05 (s, 4H); ^{13}C NMR ($CDCl_3$, 75 MHz) δ 14.0, 22.1, 24.5, 26.3, 101.6, 125.3, 130.5; ^{31}P NMR ($CDCl_3$, 121 MHz) δ 7.89 (J_{Pt-P} = 2390.8 Hz).

Complex 5b. This compound was synthesized according to the same procedure used for complex **5a**, except 2,5-diethynyl-thiophene **4b** (64 mg, 0.483 mmol) and *cis*-dichloro-bis(tri-*n*-butylphosphine)platinum(II) (0.648 g, 0.967 mmol) were used. Flash chromatography (silica gel, hexane then 7:3 hexane/CH_2Cl_2) gave the desired product **5b** as a dark orange oil (288 mg, 43 %). ^{1}H NMR ($CDCl_3$, 300 MHz) δ 0.85-1.0 (t, 36H), 1.40-1.60 (m, 48H), 1.9-2.0 (m, 24H), 6.6 (s, 2H); ^{13}C NMR ($CDCl_3$, 75 MHz) δ 13.9, 22.1, 24.4, 26.2, 53.5, 88.5, 93.9, 127.0; ^{31}P NMR ($CDCl_3$, 121 MHz) δ 8.03 (J_{Pt-P} = 2364.0 Hz).

Complex 5c. This compound was synthesized according to the same procedure used for complex **5a**, except 5,5'-diethynyl-2,2'-bithiophene **4c** (14.4 mg, 0.067 mmol) and *cis*-dichloro-bis(tri-*n*-butylphosphine)platinum(II) (134.1 mg, 0.2 mmol) were used. Flash chromatography (silica gel, hexane then 9:1 hexane/CH_2Cl_2) gave the desired product **5c** as a yellow film-forming oil (82.8 mg, 83 %). ^{1}H NMR ($CDCl_3$, 300 MHz) δ 0.9-1.0 (t, 36H), 1.40-1.65 (m, 48H), 1.9-2.0 (m, 24H), 6.70 (d, 2H), 6.85 (d, 2H); ^{13}C NMR ($CDCl_3$, 75 MHz) δ 14.0, 22.2, 24.5, 26.2, 91.5, 93.7, 122.6, 128.2, 128.4, 134.9; ^{31}P NMR ($CDCl_3$, 121 MHz) δ 8.15 (J_{Pt-P} = 2364.6 Hz).

Complex 5d. This compound was synthesized according to the same procedure used for complex **5a**, except 5,5''-diethynyl-[2,2',5',5'']-terthiophene **4d** (43.5 mg, 0.15 mmol) and *cis*-dichloro-bis(tri-*n*-butylphosphine)platinum(II) (201.2 mg, 0.30 mmol) were used. Flash chromatography (silica gel, hexane then 7:3 hexane/CH_2Cl_2) gave the desired product **5d** as a yellow film-forming oil (135 mg, 57 %). ^{1}H NMR ($CDCl_3$, 300

MHz) δ 0.8-1.0 (t, 36H), 1.4-1.6 (m, 48H), 1.9-2.0 (m, 24H), 6.75 (d, 2H), 6.94 (d, 2H), 6.98 (s, 2H); ^{13}C NMR ($CDCl_3$, 75 MHz) δ 14.0, 22.2, 24.5, 26.3, 92.5, 93.8, 123.2, 123.7, 128.3, 129.1, 134.1, 136.2; ^{31}P NMR ($CDCl_3$, 121 MHz) δ 8.19 (J_{Pt-P} = 2347.6 Hz).

3-{4-[(Triisopropylsilyl)-ethynyl]-phenyl}-prop-2-yn-1-ol (7). 1,4-Diiodobenzene (5.0 g, 15.16 mmol) was dissolved in THF (60 mL) and *i*-Pr_2NH (40 mL) in a Schlenk flask and the solution was degassed with argon for 30 min. Then, tri-*iso*-propylsilylacetylene (2.76 g, 15.16 mmol), $Pd(PPh_3)_2Cl_2$ (0.642g, 0.9 mmol) and CuI (0.346 g, 1.8 mmol) were added. The mixture was stirred at 70˚C for 3 hours, after which time prop-2-yn-1-ol was added dropwise via a syringe. The mixture was stirred overnight at 70˚C. After cooling down, the mixture was passed through a bed of Celite, washed with 10% NH_4OH (3 x 50 mL) and water (3 x 50 mL), the organic phase dried on $MgSO_4$, filtered and the solvents were removed. Chromatography on silica (hexane first, then 9:1 hexane/CH_2Cl_2) gave the desired product **7** as a red oil (1.65 g, 35 %). ^{1}H NMR ($CDCl_3$, 300 MHz) δ 1.20 (s, 21H), 4.40 (br, 1H), 4.58 (s, 2H), 7.40 (m, 4H); ^{13}C NMR ($CDCl_3$, 75 MHz) δ 11.4, 18.7, 51.1, 85.1, 89.3, 92.5, 106.7, 122.7, 123.6, 131.5, 131.9.

1-Ethynyl-4-(tri-iso-propylsilylethynyl)-benzene (8). 3-{4-[(Tri-*iso*-propylsilyl)-ethynyl]-phenyl}-prop-2-yn-1-ol (1.43 g, 4.58 mmol) was dissolved in Et_2O (80 mL) and degassed with nitrogen for 15min. Then, activated MnO_2 (6.37 g, 73.3 mmol) and KOH (2.05 g, 36.6 mmol) were added in four fractions every hour and mixture was stirred at room temperature for 4 hours protected from light. After this time, mixture was washed with 5% HCl (3 x 50 mL), water (3 x 50 mL), dried on MgSO4, filtered and the solvent was removed. Chromatography (silica gel, hexane) gave the desired product **8** as a red oil

(0.99 g, 86 %). ^{1}H NMR ($CDCl_3$, 300 MHz) δ 0.98 (s, 21H), 2.98 (s, 1H), 7.22 (s, 4H); ^{13}C NMR ($CDCl_3$, 75 MHz) δ 11.3, 18.6, 78.8, 83.2, 92.9, 106.4, 121.9, 124.0, 131.9.

Complex 9. *cis*-dichloro-bis(tri-*n*-butylphosphine)platinum(II) (0.500 g, 0.74 mmol) and phenylacetylene (76.5 mg, 0.75 mmol) were dissolved in Et_2NH (20 mL) and degassed with nitrogen for 15 min. The mixture was then stirred under gentle reflux for 8 hours after which time all phenylacetylene has been consumed. Mixture was allowed to cool down, solvents removed and crude product was purified by flash chromatography (silica gel, hexane) giving the desired product **9** as yellow solid (522.0 mg, 96 %). ^{1}H NMR ($CDCl_3$, 300 MHz) δ 0.95 (t, 18H), 1.45 (m, 12H), 1.60 (m ,12H), 2.03 (m, 12H), 7.21 (m, 5H); ^{13}C NMR ($CDCl_3$, 75 MHz) δ 14.02, 21.94, 22.16, 22.38, 24.08, 24.43, 24.52, 24.61, 26.01, 26.29, 26.42, 26.56, 31.79, 125.27, 128.03, 128.01, 130.97, 130.99; ^{31}P NMR ($CDCl_3$, 121 MHz) δ 7.95 ($J_{Pt\text{-}P}$ = 2395.2 Hz).

Complex 10. Platinum complex **9** (0.235 mg, 0.32 mmol) and 1-ethynyl-4-(tri-*iso*-propylsilylethynyl)-benzene (100.0 mg, 0.35 mmol) were placed in Et_2NH (6 mL) and the solution was degassed with nitrogen for 15 min. Mixture was stirred under gentle reflux for 8h. After cooling down, the solvents were removed and the crude product was purified by flash chromatography (silica gel, hexane then 4:1 hexane/CH_2Cl_2) giving the desired product as yellow solid (258.0 mg, 82%). ^{1}H NMR (300 MHz, CDCl3) δ 0.98 (t, 18H), 1.18 (s, 21H), 1.50 (m, 12H), 1.64 (m,12H), 2.19 (m, 12H), 7.25 (m, 9H); ^{13}C NMR (75 MHz, $CDCl_3$) δ 11.56, 14.01, 14.32, 15.57, 18.88, 22.86, 23.88, 24.11, 24.34, 24.51, 24.61, 24.69, 24.48, 25.48, 26.56, 31.80, 34.87, 90.67, 107.97, 119.68, 125.03, 128.03, 130.68, 130.95, 130.95, 131.82; 31P NMR (121 MHz, CDCl2) δ 4.21 ($J_{Pt\text{-}P}$ = 2395.4 Hz).

Complex 11. Platinum complex **10** (340.0 mg, 0.35 mmol) was dissolved in THF (6 mL) and the solution was degassed with nitrogen for 15 min. Then, TBAF (0.70 mL of a 1M solution in THF, 0.70 mmol) was added and the mixture was stirred at room temperature protected from light for 4 hours. Then the mixture was diluted to 50 mL with CH_2Cl_2 , washed with brine (2 x 30 mL) and water (2 x 30 mL), dried on MgSO4, filtered and the solvents removed. The crude oil was purified by flash chromatography (silica gel, hexane then 4:1 hexane/CH_2Cl_2) giving the desired product as a yellow solid (240.0 mg, 83%). ^{1}H NMR ($CDCl_3$, 300 MHz) δ 0.98 (t, 18H), 1.47 (m, 12H), 1.63 (m, 12H), 2.18 (12H), 7.22 (m, 9H); ^{13}C NMR ($CDCl_3$, 75 MHz) δ 14.07, 23.90, 24.13, 24.35, 24.56, 24.65, 24.74, 26.44, 26.59, 26.74, 84.49, 107.86, 109.16, 109.34, 112.59, 112.79, 123.64, 125.03, 125.11, 128.10, 129.22, 129.98, 130.83, 131.02, 131.96; ^{31}P NMR ($CDCl_3$, 121 MHz) δ 4.22 (J_{Pt-P} = 2357.0 Hz).

Pt4. Complex **5a** (67.5 mg, 0.048 mmol) and complex **10** (0.08 g, 0.097 mmol) were dissolved in Et_2NH (9 mL) and the solution was degassed with nitrogen for 15 min. The mixture was stirred under reflux overnight. After cooling down, solvents were removed and crude product purified by flash chromatography (silica gel, hexane then 7:3 hexane/CH_2Cl_2) gave **Pt4** as a yellow solid (65 mg, 46 %). ^{1}H NMR ($CDCl_3$, 300 MHz) δ 0.95 (t, 72H), 1.47 (m, 48H), 1.65 (m, 48H), 2.15 (m ,48H), 7.20 (m, 22H); ^{31}P NMR ($CDCl_3$, 121 MHz) δ 3.98, 4.05 (J_{Pt-P} = 2363.2 Hz).

Pt4T1. This compound was synthesized according to the same procedure used for **Pt4**, except complex **5b** (87 mg, 0.062 mmol) and complex **10** (0.103 mg, 0.125 mmol) were used. Flash chromatography (silica gel, hexane then 7:3 hexane/CH_2Cl_2) gave **Pt4T1** as a yellow solid (110 mg, 59 %). ^{1}H NMR ($CDCl_3$, 300 MHz) δ 0.95 (t, 72H),

1.35 (m ,48H), 1.62 (m, 48H), 2.12 (m, 48H), 6.66 (s, 2H), 7.27 (m, 18H); ^{31}P NMR ($CDCl_3$, 121 MHz) δ 4.05, 4.08 (J_{Pt-P} = 2365.5 Hz); Mass spec. (MALDI-TOF) calc'd for $C_{140}H_{236}P_8Pt_4S$ 2979.54, found 2978; Elemental anal. calc'd C 56.43, H 7.98, found C 56.58, H 8.06.

Pt4T2. This compound was synthesized according to the same procedure used for **Pt4**, except complex **5c** (82.8 mg, 0.056 mmol) and complex **10** (101.5 mg, 0.123 mmol) were used. Flash chromatography (silica gel, hexane then 7:3 hexane/CH_2Cl_2) gave **Pt4T2** as a yellow solid (98.4 mg, 57 %). ^{1}H NMR ($CDCl_3$, 300 MHz) δ 1.0 (m, 72H), 1.55 (m, 96H), 2.12 (m, 48H), 6.7 (d, 2H), 6.9 (d, 2H), 7.22 (m, 18H); ^{31}P NMR ($CDCl_3$, 121 MHz) δ 4.07, 4.21 (J_{Pt-P} = 2356.2 Hz); Mass spec. (MALDI-TOF) calc'd for $C_{144}H_{238}P_8Pt_4S_2$ 3061.66, found 3058; Elemental anal. calc'd C 56.49, H 7.84, found C 56.45, H 8.10.

Pt4T3. This compound was synthesized according to the same procedure used for **Pt4**, except complex **5d** (102 mg, 0.065 mmol) and complex **10** (107.4 mg, 0.13 mmol) were used. Chromatography on silica (hexane first, 7:3 hexane/CH_2Cl_2) gave **Pt4T3** as a red film-forming solid (106 mg, 51 %). ^{1}H NMR ($CDCl_3$, 300 MHz) δ 0.95 (m, 72H), 1.48 (m, 48H), 1.65 (m, 48H), 2.13 (m, 48H), 6.74 (d, 2H), 6.94 (s, 2H), 6.97 (s, 2H), 7.25 (m, 18H); ^{31}P NMR ($CDCl_3$, 121 MHz) δ 4.07, 4.25 (J_{Pt-P} = 2362.8 Hz); Mass spec. (MALDI-TOF) calc'd for $C_{148}H_{240}P_8P_4S_3$ 3143.79, found 3141; Elemental anal. calc'd C 56.54, H 7.69, found C 56.43, H 8.00.

CHAPTER 3
DELOCALIZATION OF CHARGE CARRIERS IN PLATINUM ACETYLIDE OLIGOMERS

Introduction

Conjugated polymers are promising active materials for use in light-emitting diodes (LEDs),[76-78,103] field-effect transistors[104,105] and photovoltaic devices.[106,107] All of these applications rely on charge carriers for charge transport.[108] Much debate arose over the last twenty years concerning the exact nature of these charge carriers, and whether they were solitons,[109] polarons[110] or bipolarons.[111] It is now believed that the charge carriers in most nondegenerate conjugated polymers such as poly(thiophene), poly(*p*-phenylene) and poly(*p*-phenylenevinylene)[112] are polarons, essentially radical ions. These charge carriers and the charge transport properties of conjugated polymers have therefore received a lot of attention in order to determine structure property-relationships[113,114] and improve the performance of devices based on conjugated polymers.[115]

In organic light-emitting diodes (OLEDs), the internal electroluminescent quantum efficiency is limited by the proportion singlet excitons formed after recombination of an electron and a hole on the polymer chain[78] (a negative and a positive polaron). Based on spin statistics and assuming electron-hole recombination is spin-independent, the electron-hole recombination should give 25% of singlet excitons and 75% of triplet excitons. Since the triplet exciton is usually not emissive in organic molecules, this would mean that the maximum efficiency of OLEDs would be 25%. However, several groups have now independently demonstrated that the exciton formation is spin-dependent and

internal quantum efficiencies up to 63% have been reported.[116-119] The reason for this is currently under strong theoretical and experimental investigation.[42,120]

However, it is likely that triplet formation will always limit the efficiency of OLEDs so other groups have proposed and successfully demonstrated different strategies, such as using transition metal complexes.[121-123] The idea is that due to the heavy atoms inducing mixing of singlet and triplet excitons, all excitons formed will luminescence through rapid radiative decay of the triplet exciton and thus all electron-hole recombination leads to an emissive exciton. In fact, there are examples of singlet-harvesting platinum(II) complexes used in light-emitting devices with external efficiency up to 11%.[124-126] There is therefore clearly a technological need for a better understanding of the dynamics of charge carriers in metal-organic systems such as platinum acetylide and this is one of the motivations for the work presented in this chapter.

On a more fundamental level, our group also has an interest in conjugation through metal. After having successfully demonstrated the difference in delocalization of singlet and triplet excited states in platinum acetylide oligomers,[67] it appeared that this platinum oligomer series of increasing length would provide an interesting system to study the effect of chain length on the delocalization of charge carriers. Moreover, the oligothiophene-containing platinum acetylide oligomers studied in Chapter 2 would provide a system to study the effects of low-energy sites on charge carriers in platinum acetylide oligomers.

Therefore the conjugation and delocalization effects of charge carriers have been explored through electrochemistry and pulse radiolysis. These techniques[93,113,127,128] and other time-of-flight techniques[129-131] have been used extensively and successfully to study

charge transport in organic conjugated oligomers and polymers. Among them, thiophene-based oligomers[132,133] and polymers[134,135] in particular have received considerable attention due to their rich and promising electrochemical properties. Conjugated metal-organic systems are less common than all-organic conjugated systems but are gaining increasing attention due to the unique electrochemical properties of transition metal complexes.[136-139]

The oligomers studied here are presented in Figure 3-1 and Figure 3-2 below. The first series (Ptn), consists of platinum acetylide oligomers containing one to five platinum centers in the conjugated phenyleneethynylene backbone. Their synthesis has been described elsewhere[67] and their NMR spectra were identical to the oligomers prepared previously. The second series (PT4Tn) consists of platinum acetylide oligomers containing four platinum centers where the central benzene ring is replaced by thiophene, bithiophene or terthiophene. Their synthesis and characterization has been described in Chapter 2.

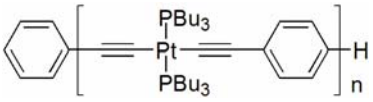

Figure 3-1. Structure of platinum acetylide oligomers Ptn (n = 1-5).

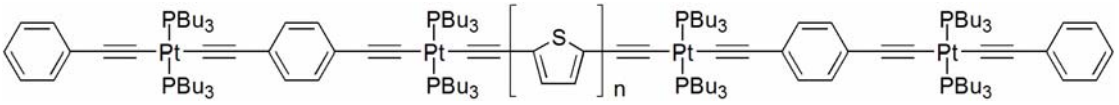

Figure 3-2. Structure of platinum acetylide oligomers Pt4Tn (n = 1-3).

Results

Electrochemistry

The oxidation and reduction of the platinum acetylide oligomers were explored using cyclic voltammetry (CV) and differential pulse voltammetry (DPV). Measurements

were carried out in nitrogen-degassed methylene chloride solutions with TBAH (0.1 M) as the supporting electrolyte. The reduction of all oligomers gave only irreversible waves around -1.0 and -1.3 V and this data will not be discussed. However, reversible (or quasi-reversible) waves were observed between +0.6 and +1.1 V for all oligomers and all the electrochemical data is summarized in Table 3-1.

Table 3-1. Redox potentials (V vs SCE) for Ptn and Pt4Tn oligomers series in CH_2Cl_2 containing 0.1 M TBAH.[a]

Oligomer	$E_{1,\,red}$	$E_{1,\,ox}$	$E_{2,\,ox}$	$E_{3,\,ox}$
Pt1	-1.29[(b)]	1.11[(b)]		
Pt2	-1.27[(b)]	0.89[(b)]		
Pt3	-1.19[(b)]	0.85 (1 e^-)	1.06 (1 e^-)	
Pt4	-1.30[(b)]	0.81 (1 e^-)	0.88 (1 e^-)	
Pt5	-1.29[(b)]	0.98 (1 e^-)	1.16 (1 e^-)	
Pt4T1	-1.08[(b)]	0.71 (1 e^-)	1.09 (2 e^-)	
Pt4T2	-1.02[(b)]	0.63 (1 e^-)	1.01 (2 e^-)	
Pt4T3	-1.01[(b)]	0.64 (1 e^-)	0.88 (1 e^-)	1.08 (2 e-)

[a] Number of electrons shown between parenthesis are only estimates from the current passed for each wave; [b] Irreversible wave.

The results of the CV and DPV measurements are complimentary and both instructive in the Pt oligomer series therefore all electrochemistry spectra are presented fro the Ptn oligomers series (Figure 3-3) but only CV voltammograms for the Pt4Tn oligomers series (Figure 3-4).

Starting with the Ptn oligomers series, it can be seen that **Pt1** and **Pt2** show only one irreversible wave at +1.11 V and +0.89 V, respectively. This implies that the radical

cation formed from **Pt1** and **Pt2** is not stable on the electrochemical timescale. In **Pt3**, two reversible waves are observed at +0.85 and +1.06 V. This is evidenced in the CV spectrum where the typical half-wave shape of a reversible electron process is present. In **Pt4**, it appears that the two waves observed in **Pt3** are "merged" into a single reversible wave centered at +0.85 V, while a new quasi-reversible wave appears at higher potentials. This merging of the two waves is clearly observed in the DPV spectrum of **Pt4** where the broad peak shows a shoulder due to the second oxidation process next to the maximum peak. The merging of these waves suggests charge localization on an electrophore. In **Pt3**, each reversible wave is attributed to the formation of radical cation centers on two sites in close proximity of each other on the oligomer. Due to this proximity, the second radical cation formed is affected by the presence of the first center already present. When the oligomer becomes longer, two radical cation centers can be formed without interacting with each other. This is almost entirely possible in **Pt4** where the waves have merged because the presence of a radical cation center does not influence the formation of a second center. In **Pt5**, the merging is complete and essentially one broad band is observed in the DPV spectrum. However, close inspection of the CV spectrum shows that the radical cation formed is not stable here again, as evidenced by the mostly irreversible wave observed. Several cycles revealed a loss of current after each cycle indicating that the oligomer was probably being deposited on the electrode during the oxidation.

All in all, the electrochemistry data on the Ptn oligomer series suggests that the radical cation electrophore is rather localized since two such sites can be created on **Pt4** with almost no electronic coupling or interaction between them.

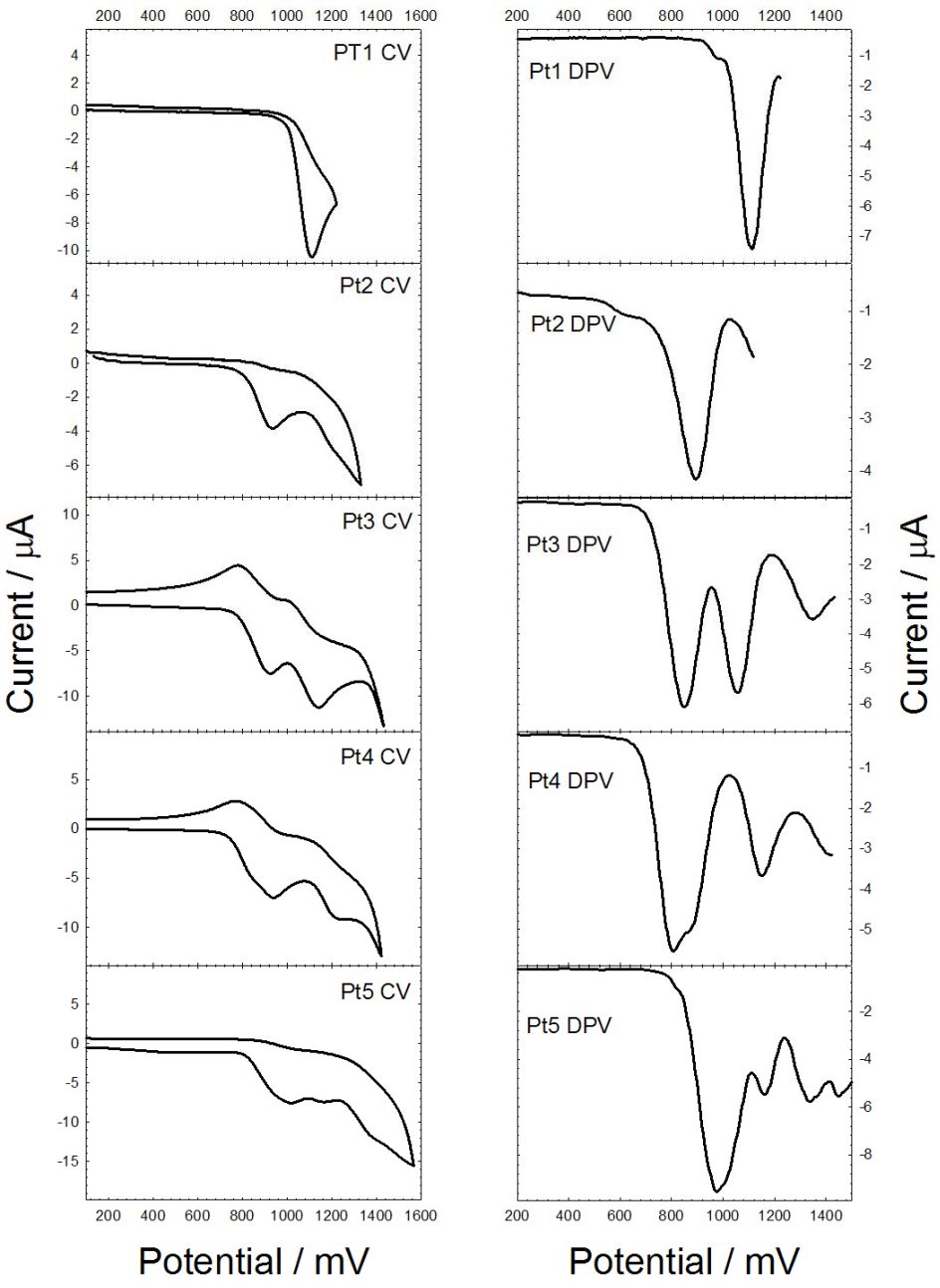

Figure 3-3. Cyclic voltammetry (CV, left) and differential pulse voltammetry (DPV, right) of oligomers Ptn.

In the Pt4Tn voltammograms, it can be seen that all Pt4Tn oligomers show two reversible bands around +1.0 V and +0.65 V. Based on the previous Ptn electrochemistry study and the lower oxidation potential of thiophene compared to benzene,[140] the high potential at +1.0 V is attributed to an oxidation of a phenyl-based electrophore and the

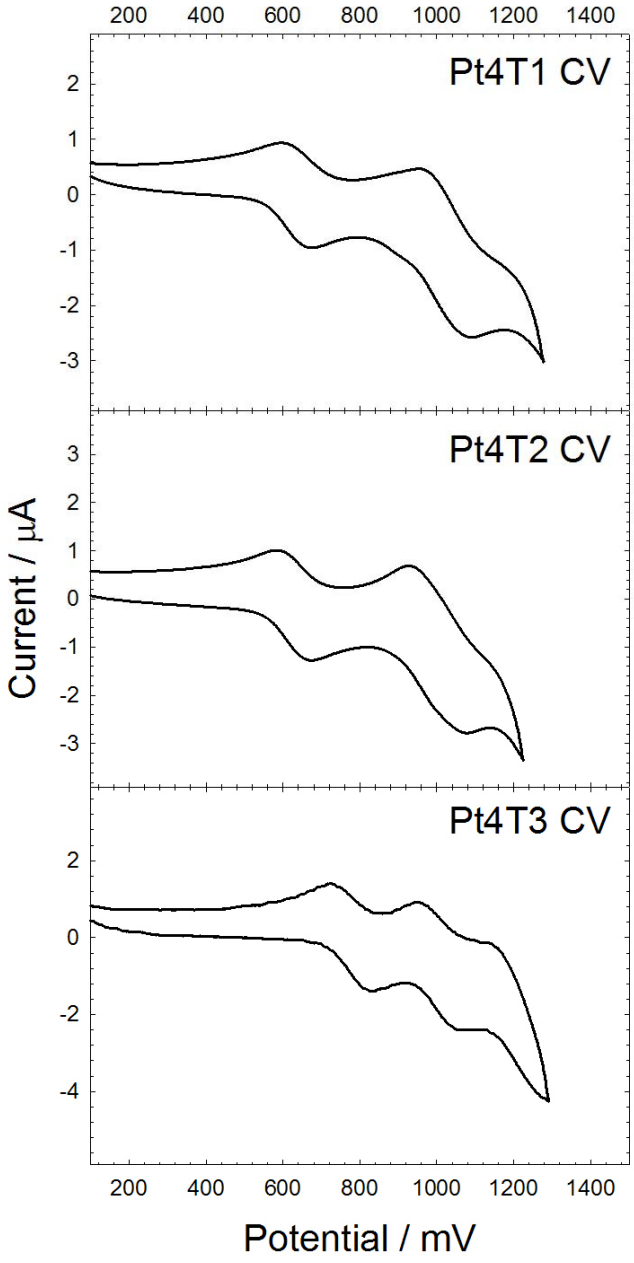

Figure 3-4. Cyclic voltammetry (CV) of oligomers Pt4Tn.

wave at +0.65 V to an oxidation of a thienyl-based electrophore. But while the first thienyl-based oxidation is attributed to a one-electron process, it appears that twice the current is passed in the phenyl-based oxidation in **Pt4T1** and **Pt4T2**. It is therefore believed that the phenyl-based wave is due to an oxidation on both end-phenylene electrophores. In addition, the DPV spectrum of **Pt4T3** (not shown) revealed a third band

at +0.88 V. This oxidation probably arises from the formation of a second oxidation on the terthiophene and formation of a dicationic terthienyl species, as observed in other oligothiophenes studies.[141]

Pulse Radiolysis – Ion Radical Spectra

Ion radicals were generated by pulse radiolysis at Brookhaven National Laboratory. The spectra were measured at 0.1-1.0 μs delay time following the growth of the radical ion species. Radical ions were produced from transfer of electron or hole from the solvated electrons and solvent-based holes created by the electron pulse.

Radical cations

The spectra of the radical cation obtained for both oligomers series are presented in Figure 3-5. All radical cation oligomers feature a strong band in the visible spectrum (400-800 nm) and a weaker and broader band in the near-IR (800-1600 nm). Looking at the Ptn oligomers first, it appears that the visible band around between $\lambda = 360$ and $\lambda = 520$ nm red-shifts strongly from **Pt1** to **Pt2**, but does not move after that. This is clearly evidenced in the inset of the visible region shown in Figure 3-5. In fact, the change levels off at **Pt3**, which has the same absorption band as **Pt4** and **Pt5**. The same trend is observed for the band in the near-IR, where the change levels off at **Pt2** in this case. Consistent with the electrochemistry data, this suggests a relatively localized radical cation species in these oligomers. Since no apparent stabilization energy is gained for oligomers longer than **Pt3**, it appears that the radical cation is delocalized over ca. three repeat units.

Turning to the Pt4Tn oligomers series, similar spectra consisting of two absorption bands in the visible and near-IR are observed. The spectra suggest that the radical cations

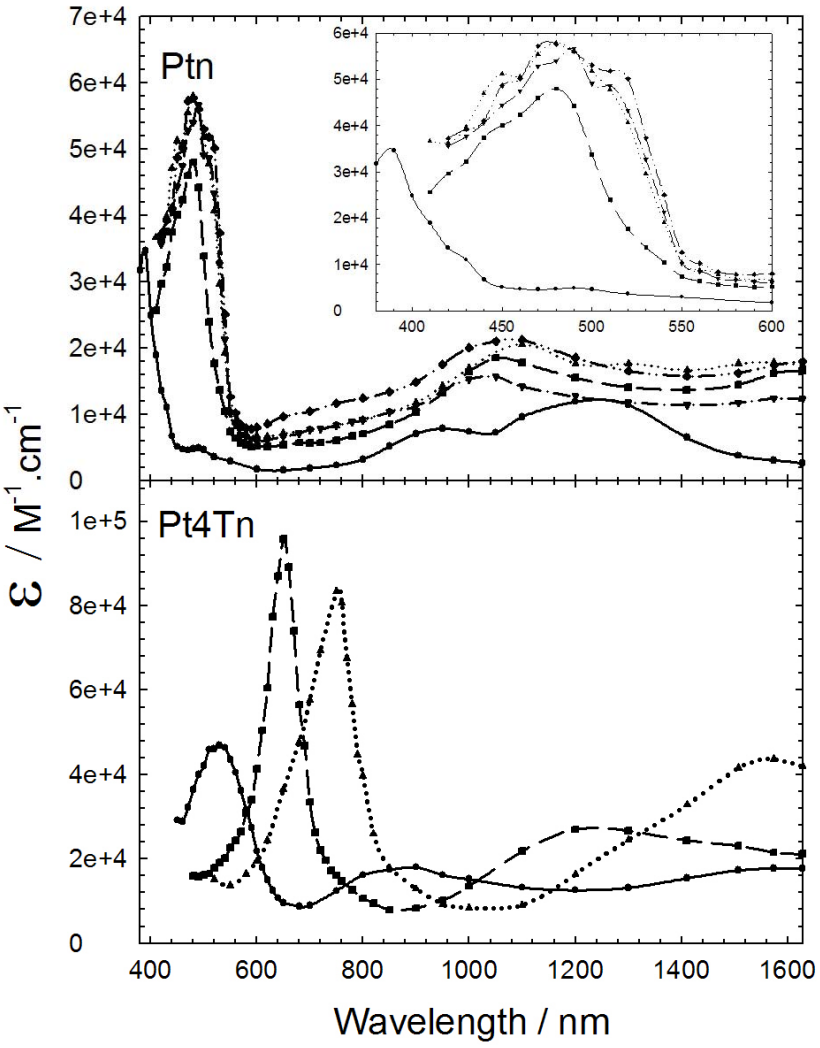

Figure 3-5. Radical cation spectra for Ptn (top) and Pt4Tn (bottom) oligomers series. In Ptn: Pt1 (●), Pt2 (■), Pt3 (▲), Pt4 (▼) and Pt5 (♦). In Pt4Tn: Pt4T1 (●), Pt4T2 (■), Pt4T3 (▲).

formed are essentially localized on the oligothienyl electrophore, as the visible bands are at much lower energies than the absorption bands in the Ptn oligomers series. Both of the bands undergo a significant bathochromic shift from **Pt4T1** to **Pt4T3**. This is attributed to the increasing stability of radical cation centers on the oligothienyl units of increasing length present in the oligomer.

Radical anions

The absorption spectra of the radical anions are presented in Figure 3-6 and all oligomers display two bands, one in the visible between λ = 380 and λ = 580 nm and one extending far in the IR (except for **Pt1**). Apart from **Pt1** which is blue-shifted from the rest of the series, the visible absorption band of all Ptn oligomers radical anions are almost superimposable. This suggests the presence of a very localized radical anion, which is not sensitive to an increase in chain length after **Pt2**.

The anion radicals of the Pt4Tn again display two bands as well, again in the visible between λ = 520 and λ = 800 nm and one extending in the IR. The visible band shows the same trend observed in the radical cation spectra, that is a bathochromic shift with increasing oligothiophene size. The second IR band however does not seem to follow any particular trend, although it is difficult to interpret as the bands are beyond the range of the instrument.

Discussion

Except from bulk conductivity of oligoPPE-based self-assembled films studied by Tour and co-workers,[142] there is no literature on the electrochemistry of phenyleneethynylene-based conjugated systems. However, platinum acetylide complexes, oligo(phenylenevinylene)s and oligo(thiophene)s have been studied by several groups and this provide a basis for the discussion.

Delocalization of Charge Carriers

The oxidation waves observed in the CV and DPV spectra of the Ptn and Pt4Tn oligomers are assigned to oxidation occurring on the phenyl or thienyl ligand rather than oxidation of the metal because of the oxidation potential and their reversibility. It is known that the one-electron oxidation of Pt(II) to Pt(III) is usually irreversible as the

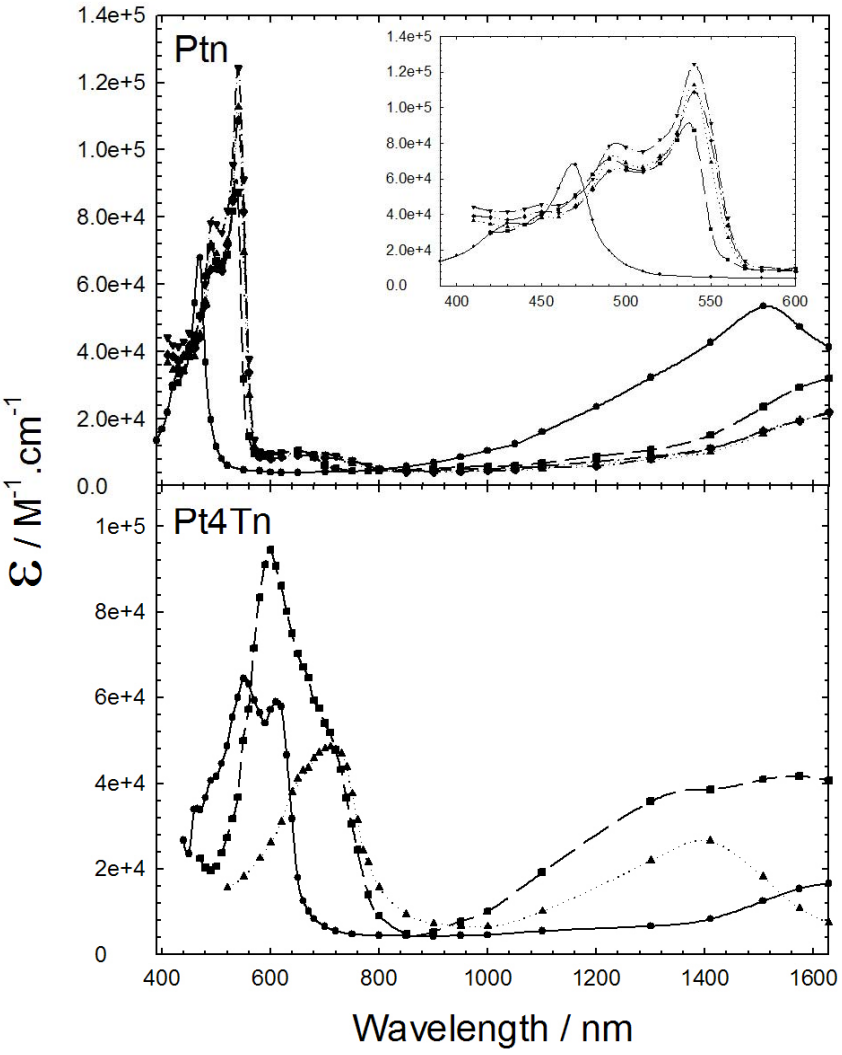

Figure 3-6. Radical anion spectra for Ptn (top) and Pt4Tn (bottom) oligomers series. In Ptn: Pt1 (●), Pt2 (■), Pt3 (▲), Pt4 (▼) and Pt5 (♦). In Pt4Tn: Pt4T1 (●), Pt4T2 (■), Pt4T3 (▲).

radical cation formed readily undergoes rapid interaction with the solvent, leading to decomposition products.[143] When observed,[144] the platinum oxidation has been reported at higher potential (~1.2 V) than all oxidation potential observed here. Moreover, the HOMO of platinum acetylide oligomers is believed to be located mostly on the aryl ligands with little metal character while the LUMO is located essentially on the aryl

ligands. It is therefore safe to rule out a metal oxidation for the reversible waves. The oxidations are thus referred to as ligand-based but bearing in mind that some metal character is probably mixed in as well. However, a Pt(II) to Pt(III) oxidation with decomposition could be responsible for the irreversible waves observed in **Pt1** and **Pt2**.

The merging of the two oxidation waves in **Pt3** into one wave in **Pt4** and the red-shift of the radical cation absorption bands leveling off for **Pt3** give an indication on the delocalization of the radical cation of platinum acetylide oligomers. The data suggest a fairly localized radical cation species, one that is probably localized over 2 to 3 repeat units. With 4 repeat units, two radical cation centers can form with little interaction or electronic coupling between them. The radical anions are more localized than the radical cations. The absorption spectra of radical anions of the Ptn series show no red-shift after **Pt2** for the visible band. Moreover, the electrochemistry of these platinum acetylide oligomers displayed only irreversible waves, implying that the radical anions are not stable. This means that these materials would probably perform better when p-doped rather than n-doped. The extent of delocalization of the radical ions observed in the Ptn series is somewhat smaller but comparable to the extent of delocalization of charge carriers in related all-organic conjugated oligomers studied recently.[72,145]

The merging of the oxidation waves in **Pt4** is reminiscent of mixed-valence systems which have been known for a long time.[146] And while it was first established for polymetallic complexes, the concept of mixed valence is also valid for organic molecules, as shown in several recent examples.[147-151] If two M^{II} metal centers are coupled by a strong electronic coupling, removal of one electron on one of the metal may lead to a delocalized cation with two equivalents metal each in a +2.5 oxidation state. If there is no

electronic coupling, the one-electron oxidation will lead to a mixed valence cation species with M^{II} and M^{III} metal centers. These two extreme cases represent the class III and I of the Robin and Day's classification of mixed-valence species.[152] In between those two cases lies a wide range of intermediate species with different degree of electronic coupling. Electronic coupling can be significantly improved by conjugation but it is also distance-dependent. Therefore it is probably favored and effective in the shorter oligomers of the Ptn series. For oligomers longer than **Pt3**, the distance between two radical cation centers becomes too great and the electronic coupling is greatly reduced.

The electrochemistry of thiophene-based conjugated materials is well documented in the literature. The oxidation potentials of unsubstituted oligothiophenes reported by Meerholz and Heinze[140] in methylene chloride are higher than the potential observed in the Pt4Tn oligomers series studied here. Values reported for the first oxidation are +1.7, +1.25 and +0.87 V for thiophene, bithiophenen and terthiophene, respectively, whereas they are +0.71, +0.63 and +0.64 V across the Pt4Tn oligomers series. Oxidation potentials for bis-(thiomethyl)bithiophene and bis-(thiomethyl)terthiophene as reported by Hill *et al.*[153] in acetonitrile are +0.93 and +0.89 V. Even with a good electron-donating substituent such as thiomethyl group, it appears the oligothiophenes located on the oligothiophenes of the Pt4Tn oligomers are easier to oxidize and their radical cations more stable. This is an indication that the platinum center is an excellent electron donor, that can bring a large stabilization energy to the radical cation.[141]

Electronic Transitions of the Radical Ions

Charge carriers are a key to opto-electrical processes in conjugated materials. The most promising polymers for these applications, poly(thiophene),[154] poly(*p*-phenylenevinylene)[130] and poly(*p*-phenylene)[155] have been studied extensively to

understand the nature and the dynamics of the charge carriers present. The absorption spectra of these extentded π-conjugated systems have been interpreted in terms of the polaron-bipolaron model, based on band theory. However, the oligomers such as the one studied here do not form real electronic band structures and it has been suggested that their spectra are better interpreted within the MO theory.[156,157] Since the electrochemistry study showed irreversible processes for the reduction of the platinum acetylide oligomers, the discussion will be focused on the radical cations.

Although the absorption spectra of the radical cations of oligo(phenyleneethynylene)s have not been reported, the related oligo(phenylenevinylene) has been investigated. Two bands are observed for oligomers up to the tetramer, one in the visible (λ = 500-700 nm) and one in the near-IR (λ = 800-1500 nm).[158] Both of these bands were shown to shift systematically to lower energy with increasing conjugation length. This implies an increasing delocalization of the radical cation in these all-organic oligomers and this is opposite to our Ptn oligomers series, where measurements have shown no shift of the absorption bands to lower energies after the dimer or the trimer. While the platinum center preserves conjugation in the neutral state, it is possible that conjugation becomes much more limited in the radical cation of these metal-organic oligomers. It is however interesting that the all-organic oligomers also exhibited two absorption bands, in the visible and in the near-IR. This is an indication that the metal centers do not drastically change the nature of the optical transitions of radical cations in metal-organic conjugated oligomers.

Different unsubstituted and substituted oligothiophene radical cations have been prepared and their absorption spectra recorded by several groups.[153,156,159,160] It is now

generally accepted that oxidized oligothiophenes can form intermolecular π-dimers and their spectra have been identified from the monomeric, non-aggregated oxidized species. Typically, the monomer radical cation shows two π,π* absorption bands (due to excitation from HOMO to SOMO and from SOMO to LUMO) at lower energy than the neutral oligomers, whereas the radical cation of the π-dimer displays two π,π* bands broader and blue-shifted compared to the "monomeric radical cation", as well as a third charge transfer band. Experimental conditions and factors such as a high concentration or a low temperature,[160] use of a polar solvent and the oligomer length[159] have been shown to favor the formation of π-dimers. Although one author has claimed that steric hindrance may prevent the formation of π-dimers,[161,162] these have been unambiguously identified in many examples of sterically hindered oligothiophenes. Therefore it is not clear whether steric hindrance has an effect on the monomer-dimer equilibrium constant.

The high energy transition observed in the visible for the radical cation of the Pt4Tn oligomers series is red-shifted compared to the visible absorption band observed for unsubstituted thiophene to terthiophene oligomers. The UV-vis band reported for this series is found between λ = 250 and λ = 545 nm,[156] whereas it is observed between λ = 530 and λ = 750 in the present Pt4Tn oligomers series. The visible absorption band also occurs at lower energy than various substituted oligothiophenes.[153,159,160] As mentioned earlier, this is consistent with the electrochemistry data and further supports the idea of a relatively stable radical cation in the platinum acetylide oligomers. The nature of the radical cation formed upon oxidation of the oligothienyl electrophore is confidently assigned to a monomeric, non-aggregated species, rather than a π-dimer for several reasons: 1) Measurements were carried out in 1,2-dichloroethane (not as polar as

acetonitrile); 2) The radical ion spectra were acquired on a short timescale (few μs) after the laser pulse, leaving little time for π-dimers to form; 3) The bis-(tri-*n*-butylphosphine) ligands may prevent π-dimer formation; 4) The equilibrium constant for the formation of π-dimers is probably too low for the short oligothiophenes investigated here.

It is difficult to unambiguously assign the absorption bands displayed by the platinum acetylide oligomers. The high energy band in the visible region probably is a ligand-localized π,π* transition. The nature of the broad band observed in the near-IR could be due to several possible transitions: 1) A second π,π* transition as in all-organic oligo(phenylene vinylene)s; 2) A Pt → (acetylide)$^+$ charge transfer transition (CT); 3) An intervalence charge transfer transition (IVCT). These last two transitions were observed in a platinum acetylide-bridged organic mixed valence compound recently studied by Jones *et al.*[163] at λ = 1000 nm (CT) and λ = 1530 nm. A triarylaminium ligand-based transition was also observed at λ = 670 nm in this study. Close inspection of the radical cation spectra of Ptn and Pt4Tn oligomers actually reveals the presence of two bands in the near-IR, in addition to the visible band for **Pt1** and **Pt4T1** only. Longer members of the Ptn and Pt4Tn series only display one broad near-IR band which extends beyond 1600 nm. Therefore it is not possible to tell whether a third transition occurs after 1600 nm or whether it is just the extension of the second band. A theoretical treatment of the radical cations would be needed to identify the exact orbitals involved in the electronic absorption of these species. Intervalence charge transfer transitions were first observed in mixed-valence inorganic systems and a theoretical model was developed by Hush in 1967.[164] More recently, intervalence charge transfer transitions have also been observed

in organic systems[147-149,165] and their presence can not be ruled out in platinum acetylide oligomers.

Conclusion

Two series of platinum acetylide oligomers have been studied by electrochemistry and pulse radiolysis. The first series of oligomers (Ptn) probed the effect of increasing chain length on the charge carriers while the effect of low-energy sites on these charge carriers was studied on the second series of oligomers (Pt4Tn).

The reduction of all oligomers gave irreversible waves between -1.0 and -1.3 V, indicating that the radical anions of these oligomers are not stable and probably fairly reactive. The oxidation however displayed a rich electrochemistry with reversible or quasi-reversible oxidations between +0.6 and +1.1 V. The electrochemical and pulse radiolysis data suggests the existence of a fairly localized radical ion in these oligomers, more so for the radical anions than for the radical cations. The extent of delocalization of the radical cation is estimated to be no more than three repeat units. This is comparable to the delocalization in all-organic conjugated oligomers and seems to indicate that the presence of platinum does not confine the charge carriers.

By comparison with the electronic absorption data available for related compound, the transitions observed by pulse radiolysis have been discussed. While the visible transition is almost certainly ligand-based, the origin of the near-IR transition is not clear and can not be assigned unambiguously. Several possibilities are envisaged such as charge transfer or intervalence charge transfer.

Experimental

Electrochemistry

Electrochemical measurements were performed in dry methylene chloride solutions containing 0.1 M tetra-n-butylammonimum hexafluorophosphate (TBAH, Aldrich) as the supporting electrolyte. The three-electrode setup consisted of a platinum microdisk (2 mm^2) working electrode, a platinum wire auxiliary electrode and a silver wire quasi-reference electrode. Solutions were bubble-degassed with nitrogen prior to measurements and a positive pressure of nitrogen was maintained during the measurements. The concentrations of oligomers in the solutions were all around 10 μM. Cyclic voltammetry (CV) was performed with a scan rate of 100 mV/s. Differential pulse voltammetry (DPV) was performed with a scan rate of 4 mV/s, a pulse amplitude of 50 mV and a pulse width of 50 ms. All potentials were internally calibrated against the ferrocene/ferricinium couple (E = 0.43 V vs SCE in methylene chloride[137]).

Pulse Radiolysis

This work was carried out at the Brookhaven National Laboratory Laser-Electron Accelerator Facility (LEAF). The facility has been described elsewhere.[93,166,167] The electron pulse (≤ 120 ps duration) was focused into a quartz cell with an optical path length of 20 mm containing the solution of interest. The concentration of oligomers was typically 0.2-2 mM. The monitoring light source was a 75 W Osram xenon arc lamp pulsed to a few hundred times its normal intensity. Wavelengths were selected using either 40 or 10 mm band-pass interference filters. Transient absorption signals were detected with either FND-100G silicon (≤ 1000 nm) or GAP-500L InGas (≥ 1100 nm) diodes and digitized with a Tektronix TDS-680B oscilloscope.

Synthesis

The synthesis of the Pt4Tn oligomers series was described in Chapter 2. The synthesis of the Ptn oligomers series was described elsewhere and all NMR data was identical to the data published previously.[67]

CHAPTER 4
CONSEQUENCES OF AGGREGATION ON THE TRIPLET EXCITED STATE IN PLATINUM ACETYLIDE OLIGOMERS

Introduction

The performance of electronic devices (LEDs, photovoltaic cells, field-effect transistors) made out of conjugated polymers depends on two main factors: the intrinsic photophysical properties of molecules, and the morphology of the molecules in the solid-state device. While the former has received the most attention in this field, the latter is generally accepted as being the most critical issue for device performance. For conjugated systems-based devices, the interchain electronic coupling determines the performance and is difficult to tune. Some studies have provided insights into the relationship between microstructure and device performance[115,168-170] but much work remains to be done in this particular area.

Conjugated oligomers have an important role to play in the fabrication of efficient devices because their precise chemical structure and conjugation length gives rise to well-defined functional properties and facilitates control over their supramolecular organization.[86,171] Controlled mesoscopic order can be created using supramolecular chemistry, the chemistry of molecular assemblies using noncovalent bonds.[172] Two important secondary interactions available for the supramolecular assembly of conjugated systems are π-π and hydrogen-bond interactions.[75] These interactions, individually or combined,[173] can provide a strong driving force for solution self-assembly, which contributes greatly to long-range macroscopic order in the final solid form.

The self-assembly process can take place in solution or in a liquid-crystalline phase. Conjugated oligomers such as derivatives of oligo(*m*-phenyleneethynylene)[174-176] and oligo(*p*-phenylenevinylene)[177-179] have shown very interesting self-assembling properties in solution, forming supramolecular helical or lamellar structures. In both systems, the expression of chirality was achieved over large supramolecular structures, as evidenced by circular dichroism experiments. Meijer and co-workers[177] use the "sergeants-and-soldiers" principle to convey the idea that chirality is achieved through a large number of achiral units (the soldiers) cooperating with a few chiral units (the sergeants). The supramolecular aggregates of phenylene vinylene oligomers have provided a system to study in moderately concentrated solutions phenomena usually encountered in the solid-state. Energy transfer,[180,181] exciton diffusion[182,183] and exciton annihilation[184] were hence studied with standard solution techniques.

More recently, Stupp and co-workers have prepared oligo(p-phenylene vinylene) amphiphiles and studied their luminescence properties.[179] These oligomers exhibited a liquid-crystalline mesophase and formed gels in water and DMSO (~30 wt%). The absorption spectrum of films displayed a blue-shifted absorption compared to solution, which was attributed to the presence of H-aggregates. A bilayer lamellar structure in films was proposed as a supramolecular architecture, brought upon by the amphiphilic character of the molecules.

Being purely organic systems, however only the singlet exciton was explored in these studies and no information regarding the triplet exciton was gained.

Recently, Cooper *et al.*[58] described a platinum acetylide oligomer exhibiting a glass phase at low temperature and a liquid state under ambient conditions. This was achieved

by using tri-*n*-octylphosphine ligands on the platinum complex instead of the more commonly used tri-*n*-butylphosphine ligand. In the liquid state, the chromophore density is increased 10 times compared to the chromophore density of a similar platinum acetylide oligomer (with tri-*n*-butylphosphine ligands) at the maximum concentration in solution. This is an interesting approach that should allow the study of triplet-triplet annihilation and triplet exciton dynamics in aggregated platinum acetylide oligomers. However to this date, no data on the triplet exciton dynamics in aggregated platinum oligomers is available on this system. This knowledge is nonetheless crucial for the design of efficient devices based on platinum acetylide oligomers, particularly in nonlinear optics and optical limiting.[69] While the properties of triplet excitons in platinum acetylide oligomers have been studied mostly in dilute solutions, questions remain on its fate in solid-state devices. There is a strong concern about this, as it is well-known that large and detrimental differences (red-shifted excimer emission, with lower quantum yield of emission) are observed between the solution and the solid-state properties of singlet excitons in organic conjugated polymers and oligomers.[74,185-187]

Inspired by the solution self-aggregating properties of the oligo(p-phenylenevinylene) derivatives designed by Meijer and co-workers, similar platinum acetylide oligomers have been prepared in hope of gaining some insight into the triplet exciton dynamics in aggregated states using standard photophysical solution techniques. Before plunging into the synthesis of relatively expensive platinum-containing oligomers, organic oligo(phenyleneethynylene) oligomers were prepared to assess the potential for self-assembling (Figure 4-1) in a preliminary study.

The first oligomer prepared, **PE1**, contained three phenyleneethynylene repeat units with both end-phenyl groups tri-substituted with *n*-dodecyloxy hydrocarbon chains, similar to the oligomers studied by Meijer and co-workers[177] as well as other aggregating systems studied in other groups.[188-190] However, no aggregates were clearly detected, either in concentrated solutions (up to 1 mM) or in the solid-state (drop-cast films). Since π-stacking is recognized to be an important driving force for the aggregation, a longer organic oligomer **PE3** was prepared, containing five phenyleneethynylene repeat units end-capped by the same 1,2,3-tri-dodecyloxyphenyl motif. In this case, clear evidence of aggregation was obtained from photoluminescence studies, both on thin films and in concentrated solutions (although only between 1 and 10

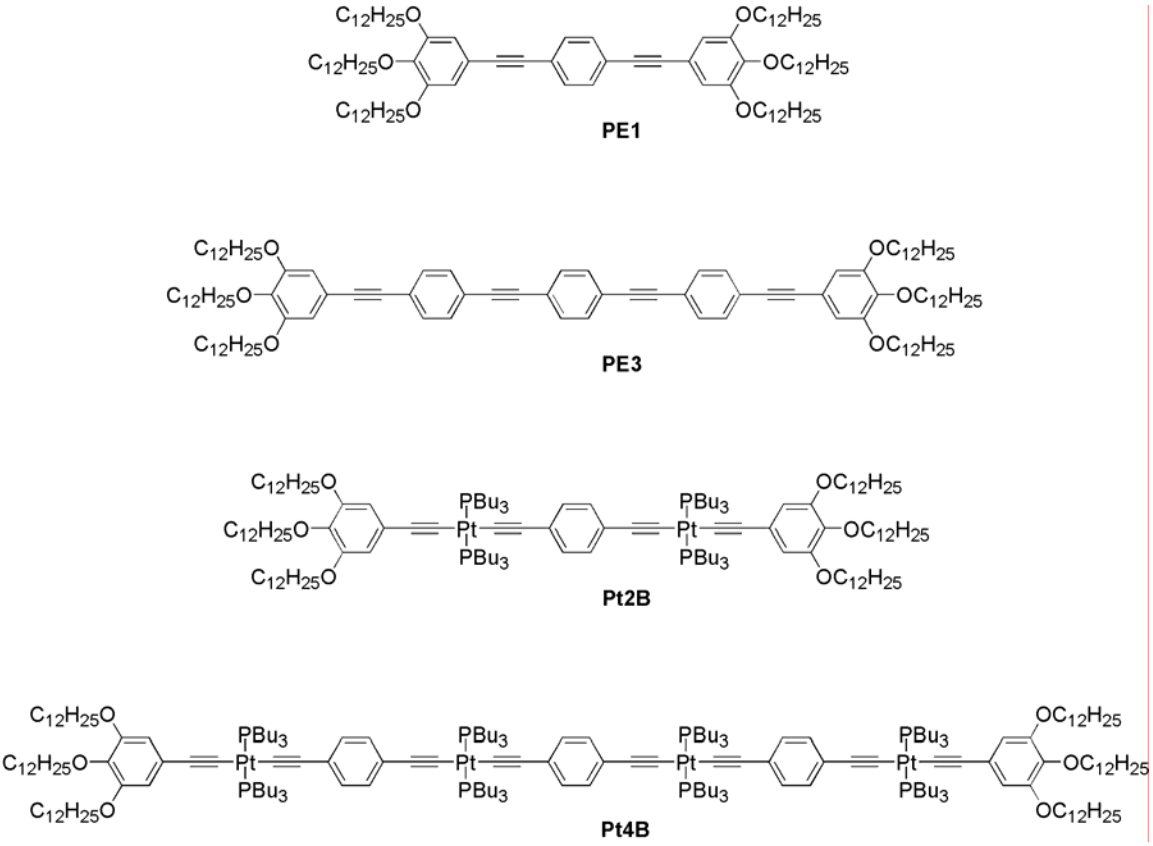

Figure 4-1. Structures of phenyleneethynylene and platinum acetylide oligomers synthesized for the preliminary study.

mM). Encouraged by this result, the synthesis of similarly end-capped platinum acetylide oligomers **Pt2B** and **Pt4B** was carried out. However, no sign of aggregation was observed from the photoluminescence of both oligomers. Recognizing that the bulky tri-*n*-butylphosphine ligands of the platinum complex may be sterically hindering the aggregation, a platinum acetylide oligomer with trimethylphosphine ligands on the platinum complex **Pt2M** (Figure 4-2) was prepared and this time, evidence for aggregation was obtained from photoluminescence and the immediate observation that this oligomer could form a gel in a dodecane solution (at 1 mM). With a desire to probe some structure-property relationships in the photophysics of aggregates of platinum acetylide oligomers, several variations of **Pt2M** were also prepared. As the photophysical evidence of aggregation was not entirely clear at first and not as dramatic as the eximer emission seen in **PE3**, an oligomer with a longer π-system **Pt2MP3** was prepared, the idea being that the longer π-conjugated segment would provide a strong driving force towards solution aggregation. A thiophene-containing oligomer **Pt2MT** was prepared to allow the study of the effect of a low-energy site and to probe energy transfer processes in aggregates. Finally, an oligomer with chiral side chains extending from the idle phenyl ring **Pt2MC** was also prepared to study the presence of chiral aggregates. These three oligomers are presented in Figure 4-2 along with **Pt2M**.

In the following, the synthesis of the oligomers presented in Figure 4-2 will be discussed. A brief look at some of the physical properties of these oligomers will be taken before presenting the photophysical properties of the aggregates of the oligomers. Finally, a discussion will propose a rationale for the photophysical observations made during the study.

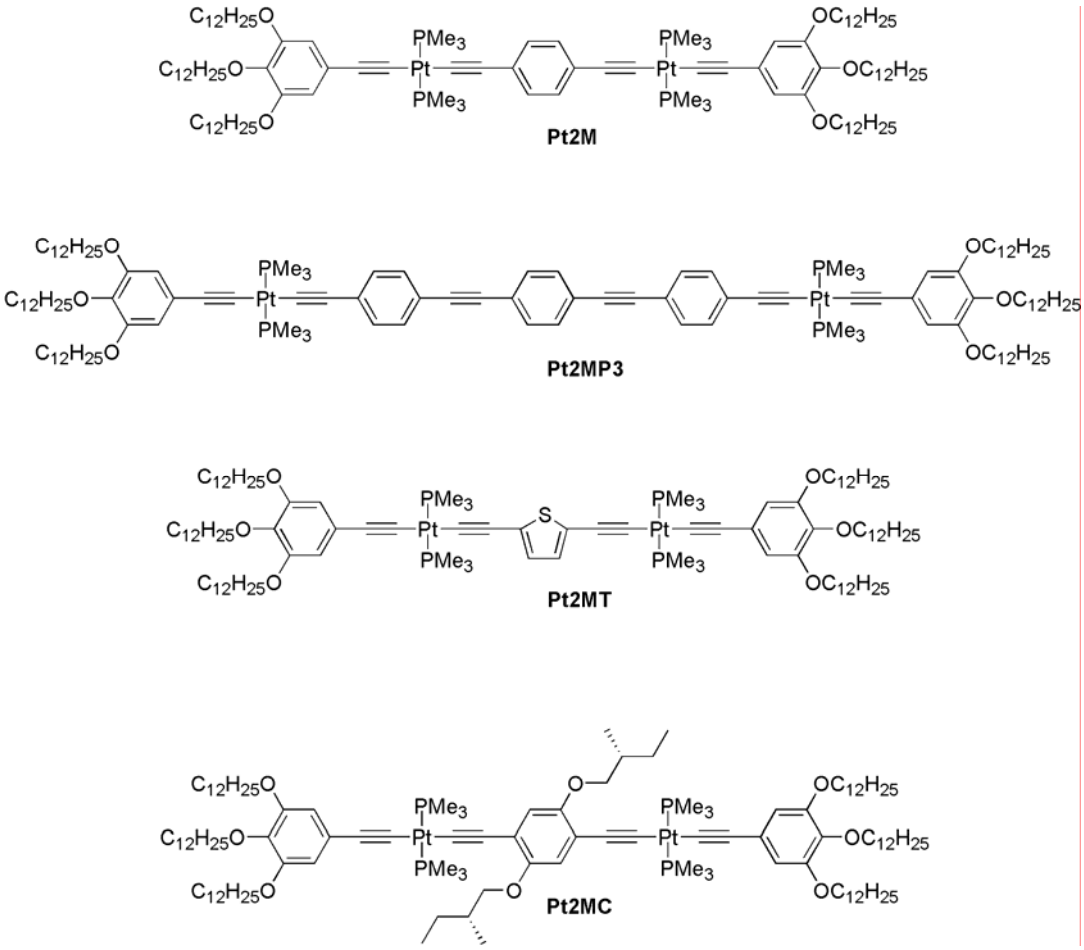

Figure 4-2. Structures of self-assembling platinum acetylide oligomers.

Synthesis

The synthesis of the platinum acetylide oligomers described above relies on a convergent strategy, as all oligomers share a common intermediate in *trans*-(tri-[3,4,5-dodecyloxy]phenylethynyl)-chloride-bis-(trimethylphosphine)-platinum(II) complex (Figure 4-3). This synthesis started with commercially available 3,4,5-trimethoxyaniline **12** which was converted to 1-iodo-3,4,5-trimethoxybenzene **13** in 83% yield through the in-situ formation of the diazonium salt and subsequent reaction with KI. The latter was treated with 4 eq. of boron tribromide[191] in CH_2Cl_2 to give 1-iodo-3,4,5-trihydroxybenzene **14** in a moderate 53% yield. Dodecyl chains were introduced by the

reaction of **14** with 4.5 eq. of 1-bromododecane in the presence of K_2CO_3 in DMF[188] to give **15** in 90% yield. Sonogashira coupling[90] of **15** and trimethylsilylacetylene (TMSA) gave the protected acetylene derivative **16** in good yield which was then treated with K_2CO_3 to afford the free acetylene derivative intermediate **17** in 91% yield.. Finally, the reaction of the latter with *cis*-dichloro-bis-(trimethylphosphine)platinum(II) gave the desired platinum complex **18** in excellent yield. The presence of a trans geometry around the platinum complex was assessed by ^{31}P NMR, which showed a single peak for the phosphorus resonance at δ = -13.6 ppm and the satellites arising from the coupling with ^{195}Pt with $^{1}J_{Pt\text{-}P}$ = 2332 Hz typical of trans platinum complexes.

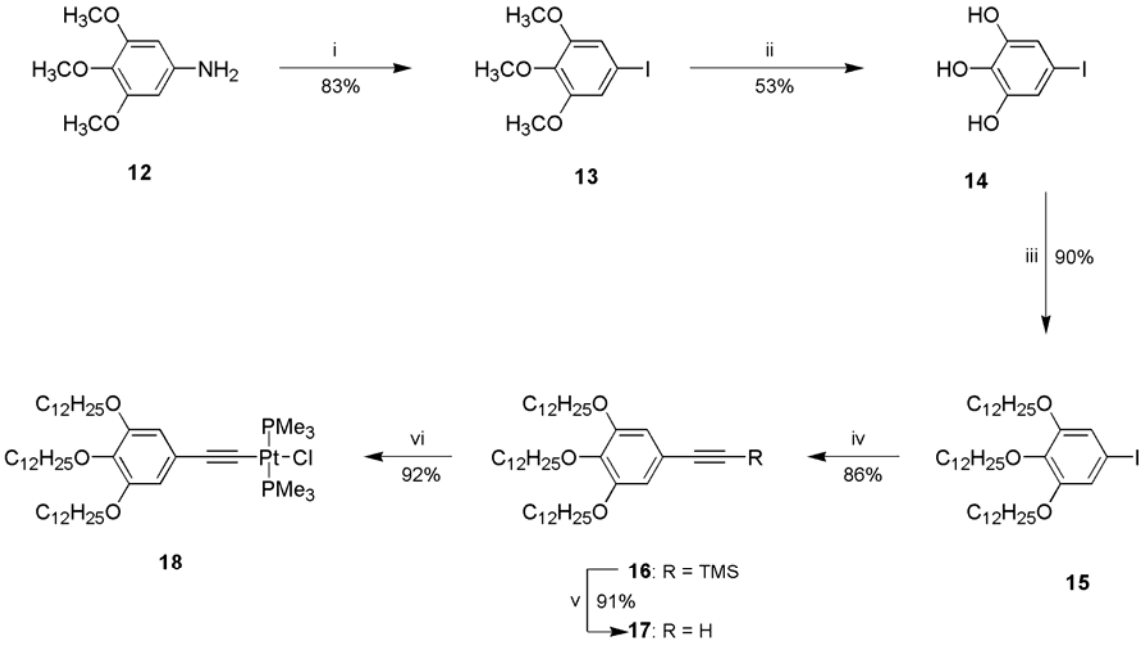

i. 1) $NaNO_2$, H_2SO_4; 2) KI, H_2O; ii. BBr_3, CH_2Cl_2, RT; iii. $C_{12}H_{25}Br$, K_2CO_3, DMF, heat; iv. TMSA, Pd/CuI (cat.), THF/*i*-Pr_2NH, heat; v. K_2CO_3, CH_2Cl_2/MeOH, RT; vi. *cis*-$Pt(PMe_3)_2Cl_2$, THF/Et_2NH, RT.

Figure 4-3. Synthesis of platinum complex intermediate **18**.

The synthesis of **Pt2MP3** required the preparation of a phenyleneethynylene trimer intermediate **20**. The latter was prepared from the Sonogashira coupling of 1,4-diiodobenzene and 1-ethynyl-4-(tri-*iso*-propylsilylethynyl)benzene **8** to give the protected

intermediate **19** in 69% yield. After desilylation with TBAF in THF, the desired free acetylene trimer **20** was obtained in 66% yield. These last two reactions were complicated by the limited solubility of compounds **19** and **20** but enough materials were obtained for the synthesis of **Pt2MP3**.

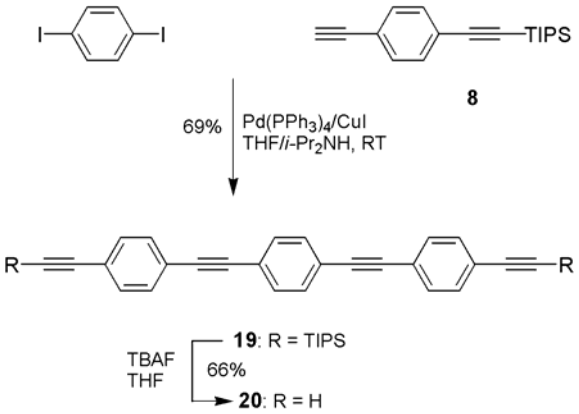

Figure 4-4. Synthesis of phenyleneethynylene derivative **20**.

The synthesis of **Pt2MC** necessitated the synthesis of a central benzene ring with chiral side chains. This began with commercially available 2,5-diiodohydroquinone which was reacted with (S)-(+)-1-bromo-2-methylbutane in the presence of K_2CO_3 to give 1,4-diiodo-2,5-bis-[(S)-(+)-2-methylbutanoxy]benzene **21**. The latter was then subjected to Sonogashira coupling with trimethylacetylene, which after deprotection with TBAF in THF, afforded the desired 1,4-bis-[(S)-(+)-2-methylbutanoxy]-2,5-bis-trimethylsilylethynylbenzene **22** in good yield. No loss of chirality was observed from ^{1}H NMR, as evidenced by the absence of diastereomers in the NMR spectrum of **23**.

Finally, the synthesis of the platinum acetylide oligomers was achieved by reacting 2 eq. of platinum complex **18** with the required bis-acetylene-aryl unit (1,4-diacetylenebenzene, 2,5-diacetylenethiophene, compound **20** and compound **23** for

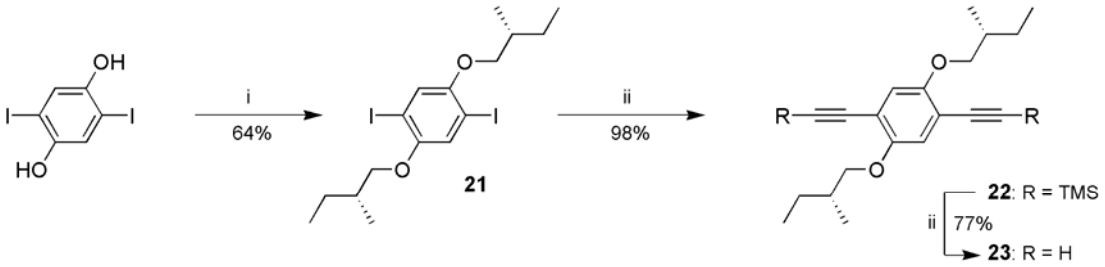

i. (S)-(+)-1-Bromo-2-methylbutane, K_2CO_3, DMF, RT; ii. TMSA, Pd/CuI (cat.), THF/*i*-Pr_2NH, heat; iii. TBAF, THF, RT.

Figure 4-5. Synthesis of chiral intermediate **23**.

Pt2M, **Pt2MT**, **Pt2MP3** and **Pt2MC**, respectively) under Hagihara conditions.[49] The synthesis of **Pt2M** only is shown in Figure 4-6 as a representative reaction of the series.

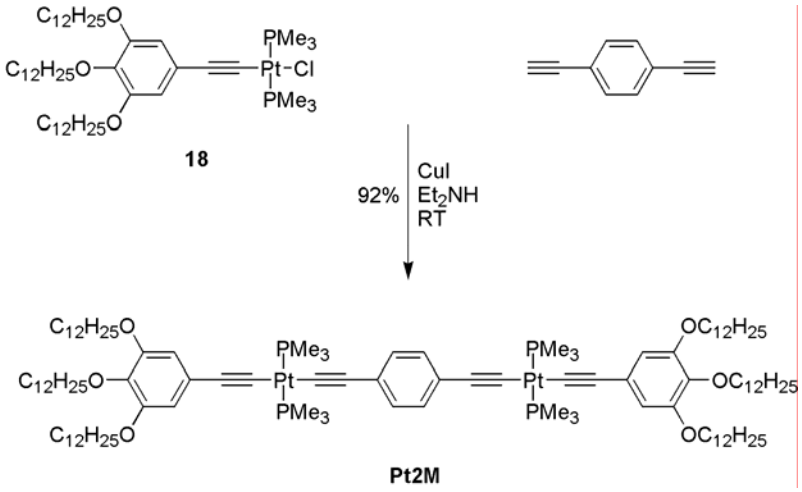

Figure 4-6. Synthesis of **Pt2M** as a representative reaction of the oligomer series.

Reactions were completed at room temperature within a few hours and the materials were obtained after column chromatography and recrystallization in moderate to excellent yields. All NMR spectra (^1H, ^{13}C and ^{31}P) were consistent with the assumed structures. In particular, ^{31}P NMR showed one peak only around δ = - 19.2 ppm along with the platinum satellites exhibiting a $^1J_{Pt\text{-}P}$ value between 2290 and 2310 Hz typical of trans geometry of such complexes.

Since the all-organic oligomer **PE3** will be mentioned in the following study, the synthesis is described here as well (Figure 4-7). The synthesis started with 1,4-diiodobenzene which was reacted with 0.67 eq. of propargyl alcohol under Sonogashira conditions[90] to afford the iodophenylpropynol intermediate **24** in 61% yield. The latter was then reacted with the previously prepared 3,4,5-tris-(dodecyloxy)ethynylbenzene **17** in a Sonogashira coupling reaction giving 25 in 87%, which after deprotection with MnO_2 and KOH gave the intermediate **26** in 50%. This deprotection step which usually proceeds in good yield was hampered here by the poor solubility of the starting material. Finally, the oligomer **PE3** was obtained by reacting 1,4-diiodobenzene with 2 eq. of intermediate **26** under Sonogashira coupling conditions giving oligomer **PE3** in 86% yield.

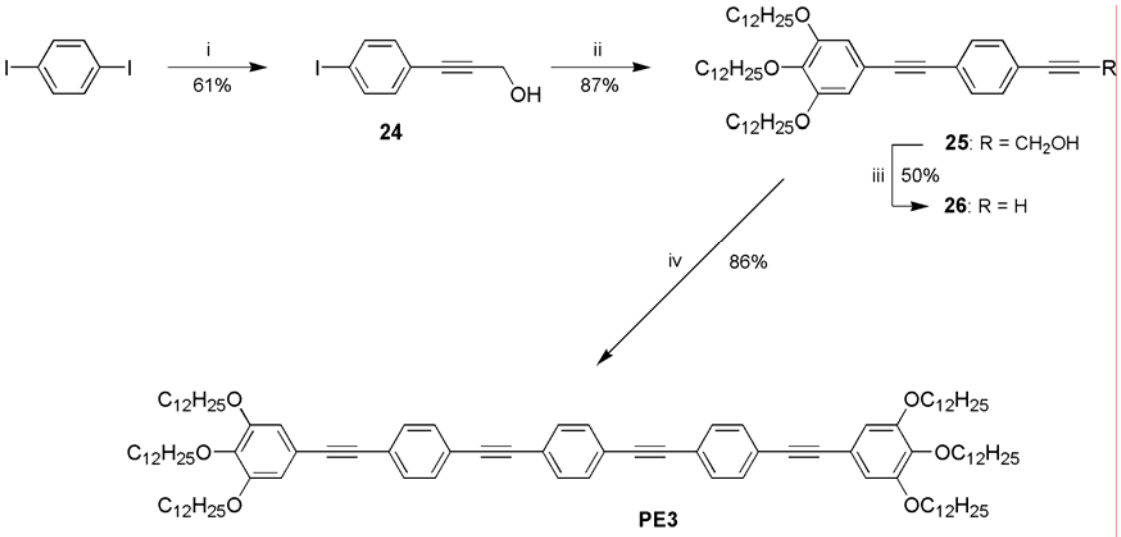

i. Propargyl alcohol, Pd/CuI (cat.), THF/*i*-Pr_2NH, RT; ii. **17**, Pd/CuI (cat.), THF/*i*-Pr_2NH, heat; iii.MnO_2, KOH, Et_2O, RT; iv. 1,4-Diiodobenzene, Pd/CuI (cat.), THF/*i*-Pr_2NH, heat.

Figure 4-7. Synthesis of oligomer **PE3**.

Results

Gel Formation

All of the oligomers presented in Figure 4-2 except **Pt2MP3** are able to gel hydrocarbon solvents such as *n*-dodecane, hexane and cyclohexane. The critical gel concentration was determined to be around 1 mM in dodecane and hexane for **Pt2M** and **Pt2MT** (~2 wt %), while it is 4 mM for **Pt2MC**. Moreover, while the gels are formed upon cooling of a hot concentrated solution within a few minutes for **Pt2M** and **Pt2MT**, the gel takes about 3 days to form for **Pt2MC**. This prevented advanced photophysical characterization of **Pt2MC** gels since solutions need to be oxygen-free for triplet excited state studies. Upon heating to ~50^{o}C, the gels melted to an isotropic liquid that could be reversibly brought back to the gel upon cooling. The gels are stiff enough that the flow of entrapped solvent molecules is frozen when a vial containing the gel is tilted or turned upside-down (Figure 4-8).

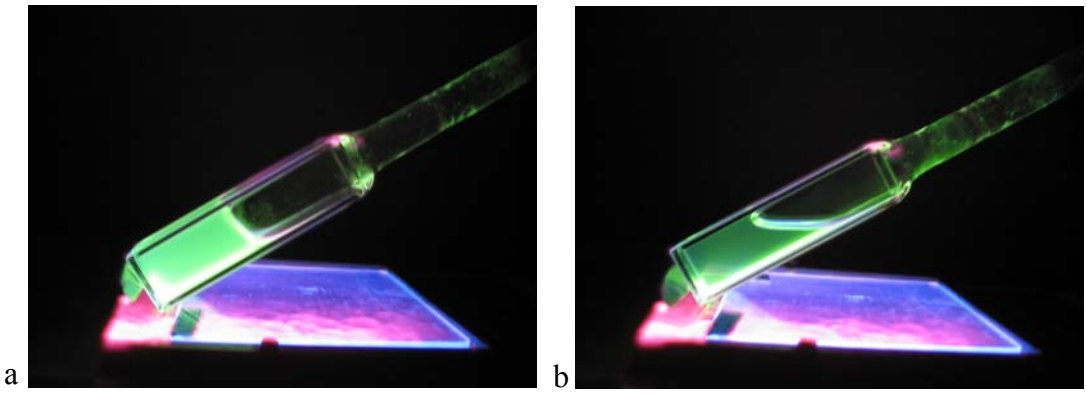

Figure 4-8. Picture of deoxygenated dodecane gel of **Pt2M** (10^{-3} M) under illumination with a UV light. (a) At room temperature. (b) At 50 ^{o}C. Notice the non-horizontal level of the solution in (a) due to the presence of the gel.

It is important to realize that the gel formation of these platinum acetylide oligomers is rather unique. While examples of luminescent organogels and

organometallic gels are numerous,[192,193] examples of low molecular weight luminescent gel-forming systems with extended conjugation are rare. In fact, there are only three examples found in the literature of fluorescent organogels based on a conjugated oligomer.[173,194,195] The platinum acetylide oligomer series studied here truly makes a remarkable system, which could contribute to make platinum acetylide oligomers into more attractive materials for technological applications.

Thermal Properties

The thermal properties of the oligomers were investigated by differential scanning calorimetry between -50 ^{o}C and 150 ^{o}C and the plot obtained for the second heating and second cooling are presented in Figure 4-9. The oligomers were also studied under polarized optical microscopy, both as neat samples and in their dodecane gels.

The thermogram of oligomer **Pt2M** shows one endotherm at 58 ^{o}C (19 J.g^{-1}) upon heating and a corresponding exotherm at 37 ^{o}C (20 J.g^{-1}) upon cooling. However, no transition was observed under polarized microscopy upon heating up to 190 ^{o}C. Upon cooling to room temperature, a glass phase was observed. Some fibers were seen in the dodecane gel sample, indicating the presence of a network structure.

For oligomer **Pt2MT**, two small endotherms are found at 54 ^{o}C and 79 ^{o}C (2.7 and 1.0 J.g^{-1}, respectively) and a larger one at 115 ^{o}C (11 J.g^{-1}). Upon cooling, three corresponding exotherms are observed. In this case, a liquid-crystalline phase was observed under polarized microscopy between 124 ^{o}C and 144 ^{o}C (Figure 4-10a), at which temperature the liquid-crystal melted into the isotropic liquid. Some fibers were also observed in the dodecane gel sample. Upon cooling to room temperature, no obvious change in appearance was observed, indicating a possible decomposition of the sample during the first heating.

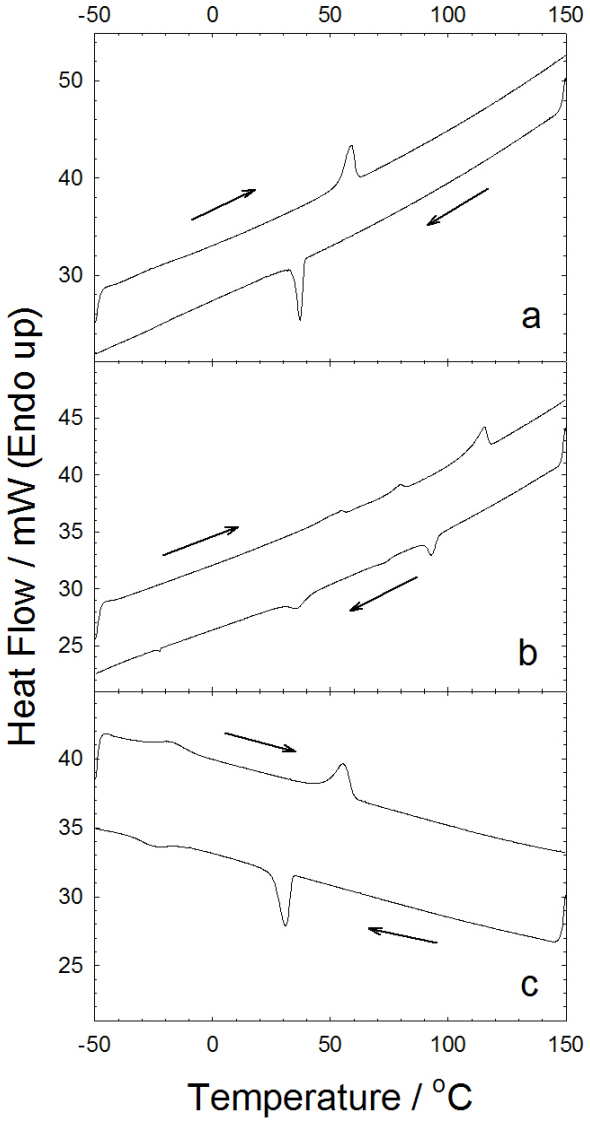

Figure 4-9. Differential scanning calorimetry thermograms for second heating and cooling cycle at a10 ^{o}C/min scan rate. (a) **Pt2M**. (b) **Pt2MT**. (c) **Pt2MC**.

In **Pt2MC**, the thermogram displays two endotherms, at -19 ^{o}C (7.1 J.g^{-1}) and 55 ^{o}C (17.1 J.g^{-1}), with corresponding exotherms upon cooling. Under polarized microscopy, the oligomer started melting at 84 ^{o}C and a liquid-crystal phase was observed between 114 ^{o}C and 181 ^{o}C (Figure 4-10b). No change was observed upon cooling to room temperature, again indicating a possible decomposition during the first heating. Some fibers were also observed in the dodecane gel sample.

Finally, **Pt2MP3** was only investigated with polarized microscopy where the oligomer started melting at 102 ^{o}C. A liquid-crystal phase was observed between 154 ^{o}C and 181 ^{o}C (Figure 4-10c), but no clearing point was detected at this temperature where the liquid-crystal phase remains. Upon cooling, the liquid-crystal phase disappeared at 143 ^{o}C and no further change was observed. On second heating, the mesoscopic phase was again observed at 143 ^{o}C but some crystals remained even up to 180 ^{o}C, indicating a possible decomposition during the first heating.

The mesoscopic properties of the platinum acetylide oligomers is not the main concern of this study, hence observations with polarized microscopy were not carried out extensively. Therefore, it is not possible to identify the type of mesophase (nematic, smectic) displayed by these materials. However, they are included to illustrate the potential of these oligomers as active elements in opto-electronic devices.

UV-Vis Absorption

The absorption spectra of the oligomers were recorded in dodecane solutions, where a concentration and a temperature-dependence were observed for all oligomers. The absorbance was kept below a value of one by using short path length (1 cm, 1 mm, or 0.1 mm) cells when necessary.

The absorption spectrum of **Pt2M** in dilute dodecane solutions (C = 10^{-4} M and below) is dominated by a strong band centered around λ = 358 nm, with some weaker transitions at higher energy (Figure 4-11a). This is similar to the absorption spectrum of **Pt4** from Chapter 2 and to Ptn oligomers from a previous study,[67] and this is confidently assigned to a "monomeric" chromophore absorption since the spectrum does not undergo any further change at lower concentrations. When the concentration is increased from 10^{-4} M, the spectrum broadens due to the decrease of the main absorption band to be finally

(a)

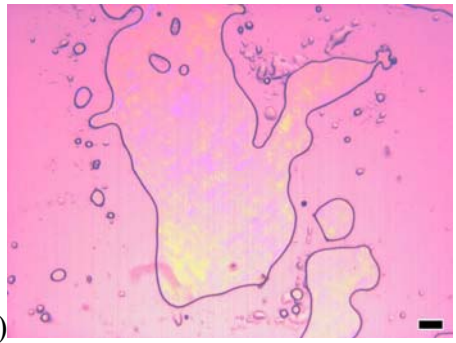

(b)

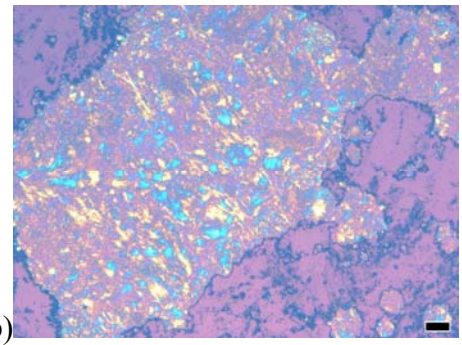

(c)

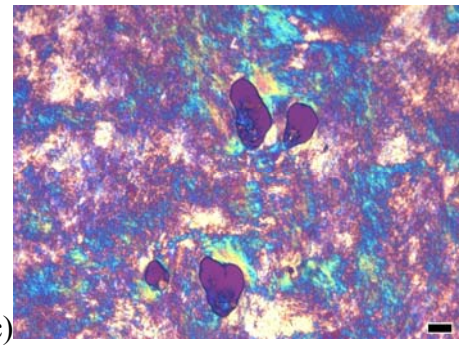

Figure 4-10. Pictures of liquid-crystal phases under a polarized optical microscope. (a) **Pt2MT** at 124 ^{o}C. (b) **Pt2MC** at 84 ^{o}C. (c) **Pt2MP3** at 144 ^{o}C. The black space bar indicates 100 μm. The presence of liquid-crystal phases was confirmed by lateral displacement of one cover slip with respect to the other.

dominated by a blue-shifted band at λ = 300 nm in the gel phase (C = 10^{-3} M). A similar trend is observed in the temperature-dependent absorption spectrum of **Pt2M** (Figure 4-11b). Starting in the gel phase at room temperature and increasing the temperature up to ~60^{o}C results in the melting of the gel into the isotropic solution and the recovery of the "monomeric" absorption at λ = 358 nm.

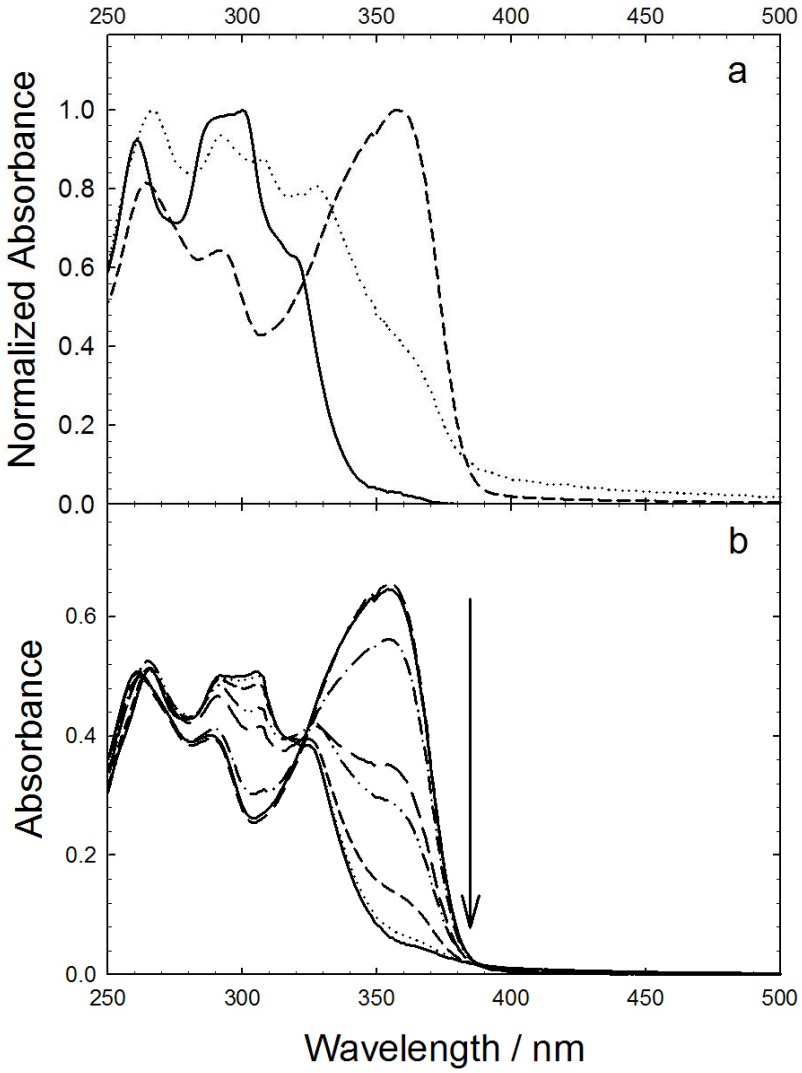

Figure 4-11. Absorption spectrum of **Pt2M** in dodecane. (a) Room temperature, C = 10^{-3} M and 0.1 mm pathlength (—), C = $5x10^{-4}$ M and 1 mm pathlength (• • •), C = 10^{-4} M and 1 mm pathlength (– – –). (b) C = 10^{-3} M and 0.1 mm pathlength, arrow indicates effect of increasing temperature from 21 ^{o}C to 66 ^{o}C.

A very similar behavior was observed for **Pt2MT**, for which only the temperature-dependent absorption is shown here (Figure 4-12). As can be seen, the main absorption band of the hot isotropic solution at λ = 378 nm decreases with decreasing temperature and at room temperature the spectrum is dominated by a higher energy transition at λ = 338 nm. Again, the "monomeric" absorption of **Pt2MT** disappears when the gel is formed, to be replaced by higher energy transitions in the gel phase, as in **Pt2M**. This

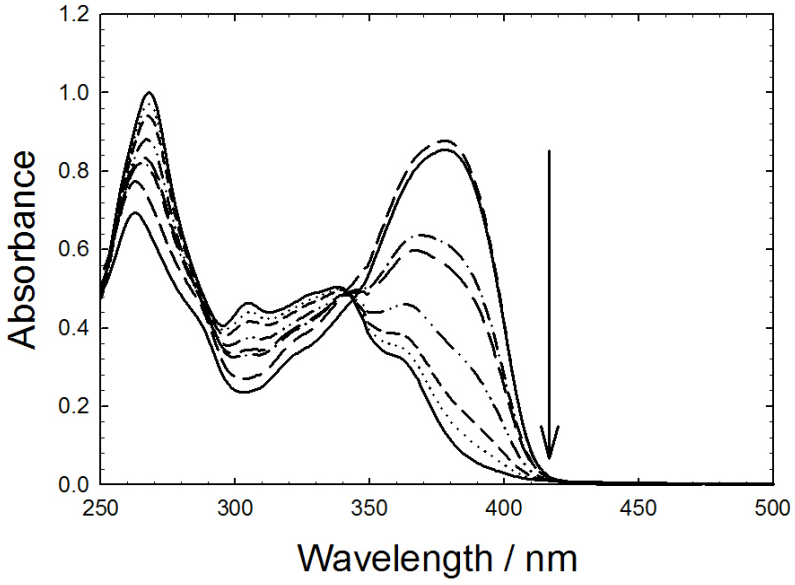

Figure 4-12. Absorption spectrum of **Pt2MT** in dodecane. C = 10^{-3} M and 0.1 mm pathlength. Arrow indicates effect of increasing temperature from 23 ^{o}C to 63 ^{o}C.

blue-shifting of the absorption in aggregated states is an indication of the presence of H-aggregates and this will be examined more closely in the discussion.

The absorption of **Pt2MP3** (Figure 4-13) showed a very different trend than the two previous oligomers. Note that in this case, no gel is formed in concentrated solutions but turbidity appears instead at a concentration of ~10^{-3} M. In the concentration-dependent absorption spectrum (Figure 4-13a), it can be seen that in the dilute solutions (10^{-5} - 10^{-4} M), the spectrum is dominated by a band at λ = 368 nm. This is again similar to what has been seen so far on the platinum acetylide absorption data and this is attributed to the absorption of a "monomeric" chromophore. However in concentrated solutions (10^{-3} M), this band becomes narrower, with a maximum at λ = 373 nm, and a new sharp band appears at λ = 405 nm. The "monomeric" absorption in concentrated solution can be restored by heating the solution to ~ 60 ^{o}C, where aggregates are broken

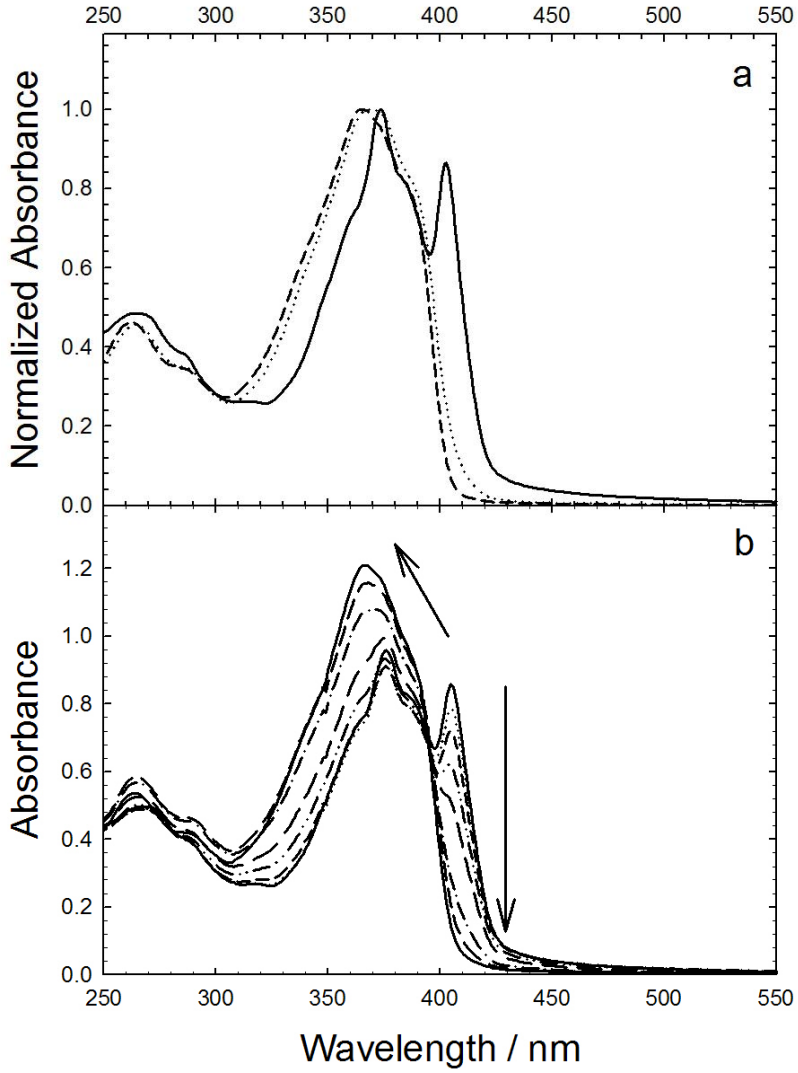

Figure 4-13. Absorption spectrum of **Pt2MP3** in dodecane. (a) Room temperature, C = 10^{-3} M and 0.1 mm pathlength (—), 10^{-4} M and 1 mm pathlength (• • •), 10^{-5} M and 1 cm pathlength (– – –). (b) C = 10^{-3} M and 0.1 mm pathlength, arrow indicates the effect of increasing temperature from 23 ^{o}C to 58 ^{o}C.

down and the same absorption spectrum as observed in dilute solutions is observed (Figure 4-13b).

In **Pt2MP3**, the effect of aggregation on the absorption of the oligomers is therefore opposed to what they are in **Pt2M** and **Pt2MT**. While the latter both show a broadening and a large blue shift of the absorption maximum, **Pt2MP3** show a small red-shift and a new sharp red-shifted peak. And while the change in absorption observed for

Pt2M and **Pt2MT** is often attributed to H-aggregates, the trend observed in **Pt2MP3** is usually assigned to J-aggregates.

As mentioned earlier, while **Pt2MC** also has the ability to gel dodecane, this process takes more time than **Pt2M** and **Pt2MT** oligomers. This is apparent in the absorption spectrum of **Pt2MC** (Figure 4-14), which is typical of platinum acetylide oligomers with a maximum at λ = 368 nm and two higher energy transitions. The spectrum is almost unchanged under dilute and concentrated conditions, except for a small increase in the higher energy bands absorption. However, if the solution is left sitting for several days and a gel has had time to settle, a large hypsochromic shift of the maximum of absorption to λ = 345 nm occurs. The higher energy bands are now stronger than the main absorption band and the reason for this is not clear.

Circular Dichroism

While the UV-vis absorption spectrum of **Pt2MC** offers some proof of aggregation, more evidence for the presence of aggregates in dodecane gels of **Pt2MC** is found in circular dichroism (CD) experiments (Figure 4-15). The CD spectrum of **Pt2MC** only shows a very weak negative signal in freshly prepared dodecane solutions at 4×10^{-3} M. However, after this solution is allowed to gel (over a period of a few days), a strong negative signal is observed in the CD spectrum in the region where **Pt2MC** absorbs. Since Meijer and co-workers[177] observed bisignate signals in their H-bonded helical self-assembled oligo(p-phenylenevinylene)s, this indicates that the chiral assemblies formed in this gel are not supramolecular helices. The possibility of a supramolecular lamellar structure is more likely in view of this result.

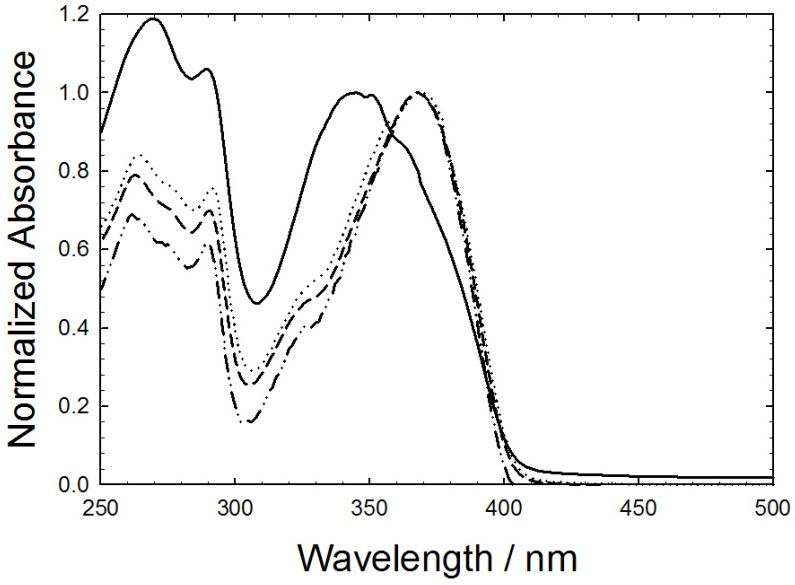

Figure 4-14. Absorption spectrum of **Pt2MC** at room temperature in dodecane. C = 4 x 10^{-3} M and 0.1 mm pathlength gelled for 40 days (—), C = 4 x 10^{-3} M and 0.1 mm pathlength freshly prepared (• • •), C = 10^{-3} M and 0.1 mm pathlength (– – –), C = 10^{-4} M and 1 mm pathlength (– • • –).

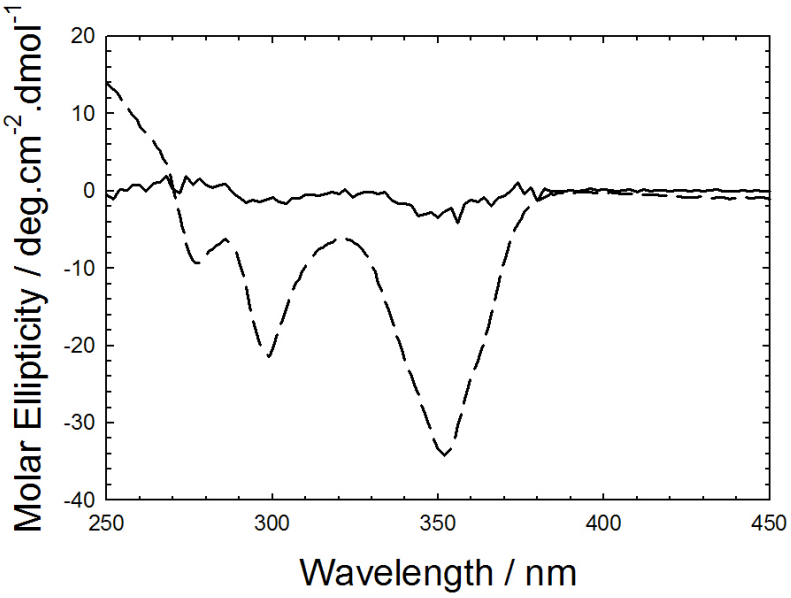

Figure 4-15. Circular dichroism (CD) absorption spectrum of **Pt2MC** in dodecane. C = 4 x 10^{-3} M and 0.3 mm pathlength freshly prepared (—), C = 4 x 10^{-3} M and 0.3 mm pathlength gelled after 4 days (– – –).

Steady-State Photoluminescence

The photoluminescence of the platinum acetylide oligomers were studied in dodecane. For gels, the solutions were bubble-degassed with argon from a hot isotropic state and heated regularly to prevent gel formation and ensure adequate degassing.

In order to determine what emission band may appear in the photoluminescence of self-assembled oligomers in the solution, the photoluminescence of drop-cast films of the oligomers were measured as well. Moreover, in order to stress the difference between the aggregate emission of an organic system and the aggregate emission of the metal-organic systems, the emission spectrum of **PE3** is presented in Figure 4-16. The effect of aggregation on the emission of **PE3** is typical of many organic conjugated systems. Whereas the emission in dilute solutions is dominated by sharp fluorescence emission, the emission in thin films often exhibits a red-shifted band due to excimer formation. In fact, the excimer emission entirely dominates the spectrum in thin film of **PE3** and no "monomeric" fluorescence is observed. A concentration study supports the excimer origin of the broad red-shifted emission band, which decreases as concentration decreases and is no longer observed for concentrations lower than 10^{-3} M.

The photoluminescence spectrum of **Pt2M** in gel (10^{-3} M) is excitation wavelength-dependent and is dominated by phosphorescence emission (Figure 4-17a). When exciting at λ = 326 nm, close to the maximum of absorption found in the gel, the emission spectrum displays a phosphorescence peak at λ = 495 nm. When exciting at λ = 366 nm, where the maximum of absorption is found in the dilute solution, the peak of maximum intensity is λ = 516 nm. With an intermediate excitation wavelength λ = 346 nm, a phosphorescence band exhibiting both peaks at λ = 495 and 516 nm is observed. Both bands are assigned to emission from a triplet excited state due to their similarity to the

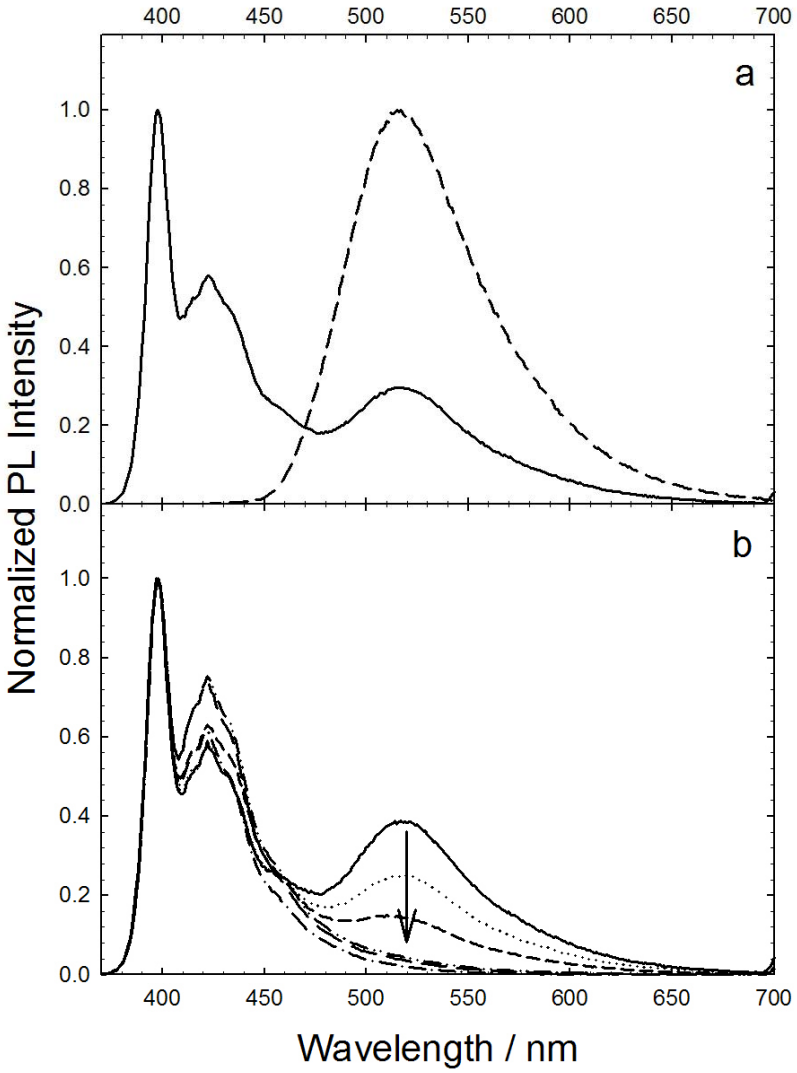

Figure 4-16. Photoluminescence spectrum of **PE3** with λ_{ex} = 354 nm. (a) C = 10^{-2} M deoxygenated dodecane (—), drop-cast film (– – –). (b) From 10^{-2} M to 10^{-3} M in deoxygenated dodecane. Arrow indicates effect of decreasing concentration.

Pt4 oligomer emission spectrum (see Chapter 2). Moreover, the "blue" emission band at λ = 495 nm is attributed to an aggregated state, while the "normal" emission band at λ = 516 nm is assigned to a monomeric state. Several experiments support these assignments:

1) The "blue" band is also present in the emission spectrum of thin films (Figure 4-17b);

2) The "blue" band is absent from the dilute solution emission spectrum (Figure 4-17c);

3) The "blue" band intensity decreases relative to the "normal" emission band as

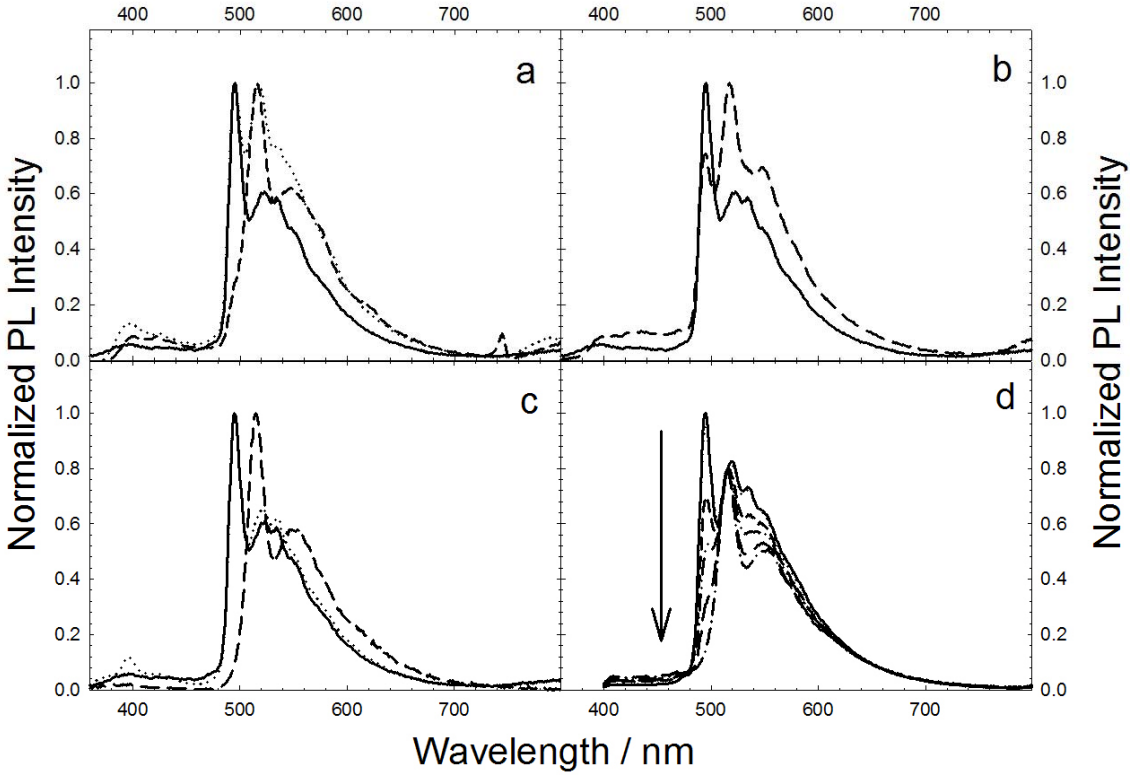

Figure 4-17. Photoluminescence spectrum of **Pt2M**. (a) C = 10^{-3} M with λ_{ex} = 326 nm (—), λ_{ex} = 346 nm (• • •) and λ_{ex} = 366 nm (– – –) in deoxygenated dodecane. (b) With λ_{ex} = 326 nm in deoxygenated dodecane at C = 10^{-3} M (—) and in drop-cast film (– – –). (c) With λ_{ex} = 326 nm in deoxygenated dodecane at C = 10^{-3} M (—), C = 10^{-4} M (• • •), C = 10^{-6} M (– – –). (d) In deoxygenated dodecane at C = 10^{-3} M, from 23 ^{o}C to 61 ^{o}C. The arrow indicates the effect of increasing temperature.

temperature increases (Figure 4-17d). All of these observations support the idea that the emission band observed at λ = 495 nm arises from a triplet excited state in an aggregated environment. Note that this is very different from organic systems, as illustrated with **PE3** in Figure 4-16, where aggregation is often accompanied by the appearance of red-shifted excimer emission.

Low-temperature photoluminescence in dilute MeTHF solutions (Figure 4-18) are also revealing as the "blue" emission band also appears at -53 ^{o}C, increases relatively to the "normal" emission until -33 ^{o}C, and then decreases to finally disappear at higher

temperatures. While the presence of the "blue" band only in this narrow temperature range is not entirely clear, it is interesting that it is present at all since the concentration is only ~7 μM. Aggregation of similar oligomers in dilute solutions at low temperature have been observed in our group before[196] and there is little doubt that the appearance of a blue-shifted emission band in this experiment has the same origin as the one observed in concentrated solutions.

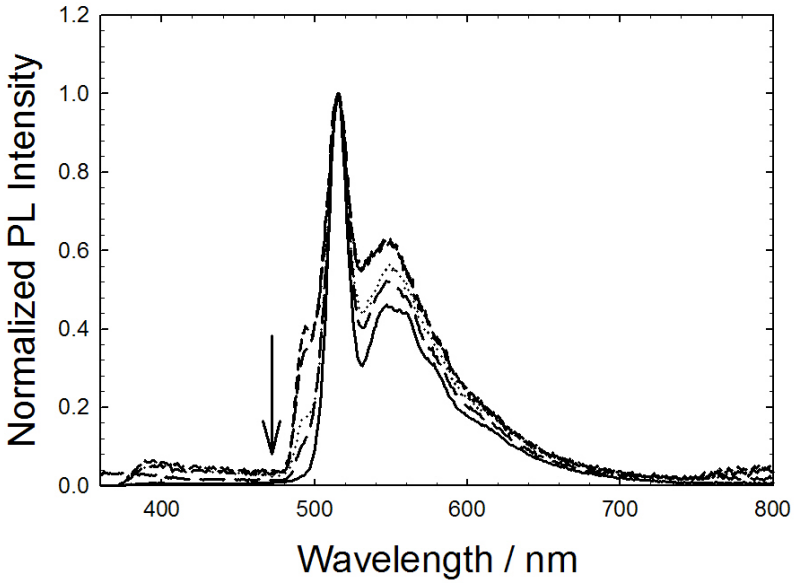

Figure 4-18. Photoluminescence spectrum of **Pt2M** in MeTHF at C = 7 x 10^{-6} M with λ_{ex} = 326 nm from -63 ^{o}C to -23 ^{o}C. The arrow indicates the effect of increasing temperature.

While the photoexcitation spectra obtained in concentrated solutions should be viewed with caution and therefore are not discussed here, the photoexcitation spectra obtained in dilute solutions (Figure 4-19) are not be plagued by high concentration effects and are hence useful in assessing the origin of the emission bands observed. At -63 ^{o}C, there is no emission at λ = 494 nm and no photoexcitation signal when this emission wavelength is monitored. The emission spectrum displays the "normal" emission at λ =

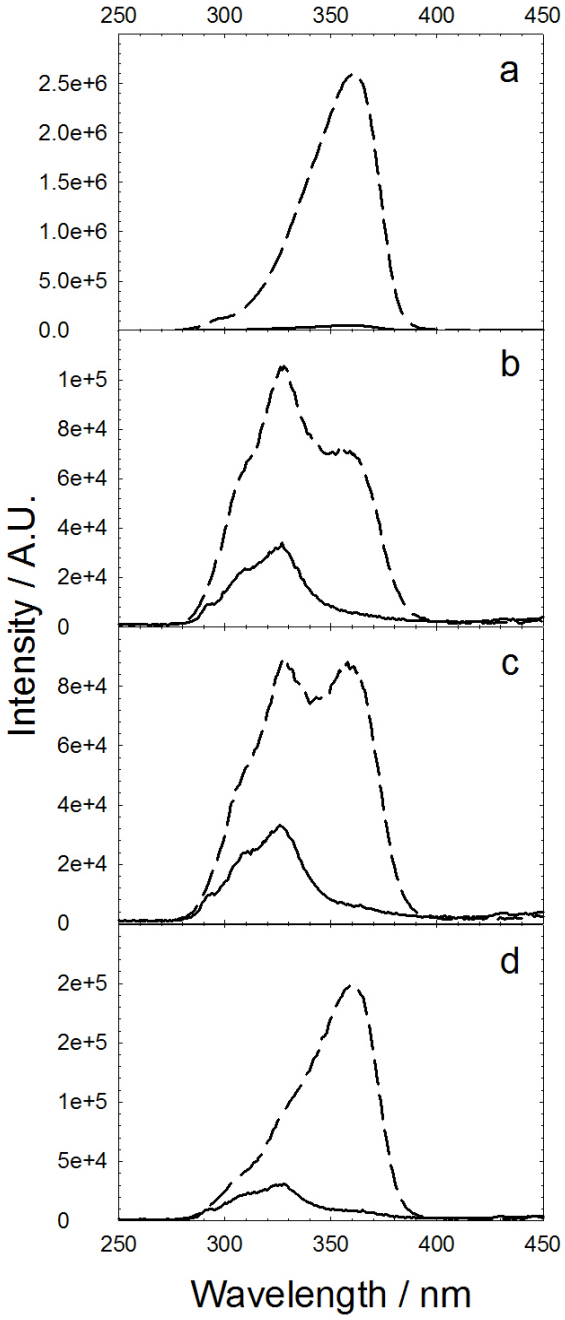

Figure 4-19. Low-temperature photoexcitation spectra of **Pt2M** in deoxygenated MeTHF monitoring λ_{em} = 494 nm (—) and λ_{em} = 516 nm (– – –). (a) -63 ^{o}C; (b) -53 ^{o}C; (c) -43 ^{o}C; (d) -33 ^{o}C.

516 nm and the photoexcitation spectrum shows the same band as the one observed in the dilute absorption spectrum of **Pt2M**. At temperatures of -53^{o}C and -43 ^{o}C, where the emission spectrum shows the "blue" emission band, the photoexcitation spectrum is

indeed revealing. While the "blue" emission band at $\lambda = 494$ nm seems to be coming from a state absorbing at $\lambda = 340$ nm, the "normal" emission now has contributions from both excited states. This implies that in the presence of aggregates, the higher-energy excited state can transfer the excitation to the lower "normal" excited state from which emission is then observed. At -43 ^{o}C, there is probably too much thermal energy for aggregates to form, the "blue" emission is almost entirely absent from the emission spectrum and the photoexcitation of the "normal" emission at $\lambda = 516$ nm originates now almost entirely from the "normal" non-aggregated excited state.

Although **Pt2MT** was not studied as extensively as **Pt2M**, there are indications that much of the same photophysics are found in this compound. For instance, the photoluminescence shows a blue shift of the emission band in dodecane gel (Figure 4-20) as well, although not as strong as in **Pt2M**.

For **PtMP3**, while the absorption spectrum displayed signs of possible aggregates absorption (see Figure 4-13), the photoluminescence spectrum does not show direct evidence of aggregates (Figure 4-21). The spectra of concentrated solutions and drop-cast films are very similar (Figure 4-21a), showing a strong fluorescence band at $\lambda = 440$ nm and a comparatively weak phosphorescence at $\lambda = 573$ nm. The emission band appearing at lower energy ($\lambda = 622$ nm) is a scattering peak, as evidenced by its strong dependence on the excitation wavelength (not shown here). The photoluminescence spectrum of **Pt2MP3** at different concentrations (Figure 4-21b) shows that under dilute conditions, the phosphorescence dominates the spectrum, as in all platinum acetylide oligomers studied here. Note the presence of the scattering peak at $\lambda \approx 670$ nm, clearly dependent on the excitation wavelength used ($\lambda_{ex} = 366$ nm in Figure 4-21a, $\lambda_{ex} = 393$ nm in Figure 4-

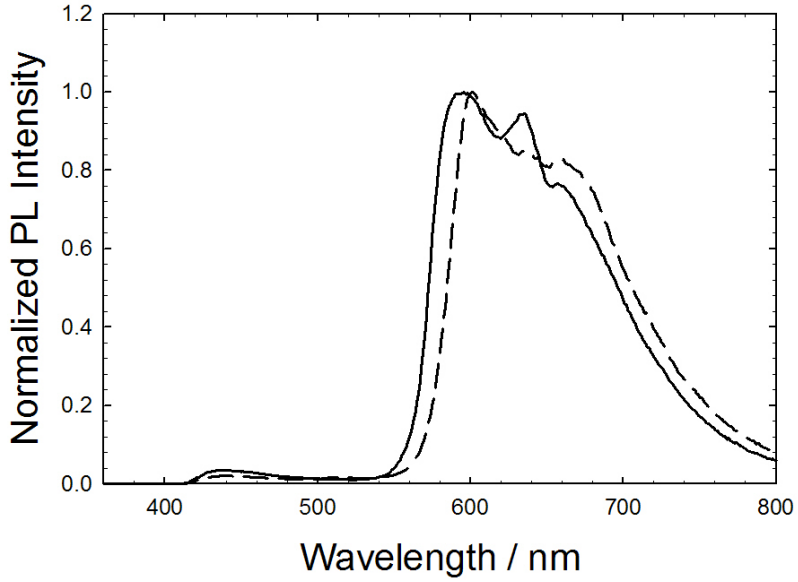

Figure 4-20. Photoluminescence spectrum of **Pt2MT** in deoxygenated dodecane with λ_{ex} = 340 nm at C = 10^{-3} M (—) and 10^{-4} M (– – –).

21b). While the relative increase in fluorescence at high concentrations can certainly be interpreted as originating from increased triplet-triplet annihilation, this has not been shown to be particularly more efficient in the high concentration photoluminescence spectra of **Pt2M** and **Pt2MT** where phosphorescence always dominates the emission spectra. However, this is consistent with the presence of J-aggregates, where increased fluorescence compared to monomer emission is usually observed. Further support for the presence of aggregates in concentrated dodecane solutions of **Pt2MP3** comes from the temperature dependent photoluminescence spectrum (Figure 4-21c), where it can be seen that the phosphorescence band increases as temperature increases. This is at first counter-intuitive, as nonradiative decay channels are typically activated at high temperature but it is in fact consistent with a breakdown of the aggregates at elevated temperatures and a return to a “monomeric” photoluminescence dominated by the phosphorescence.

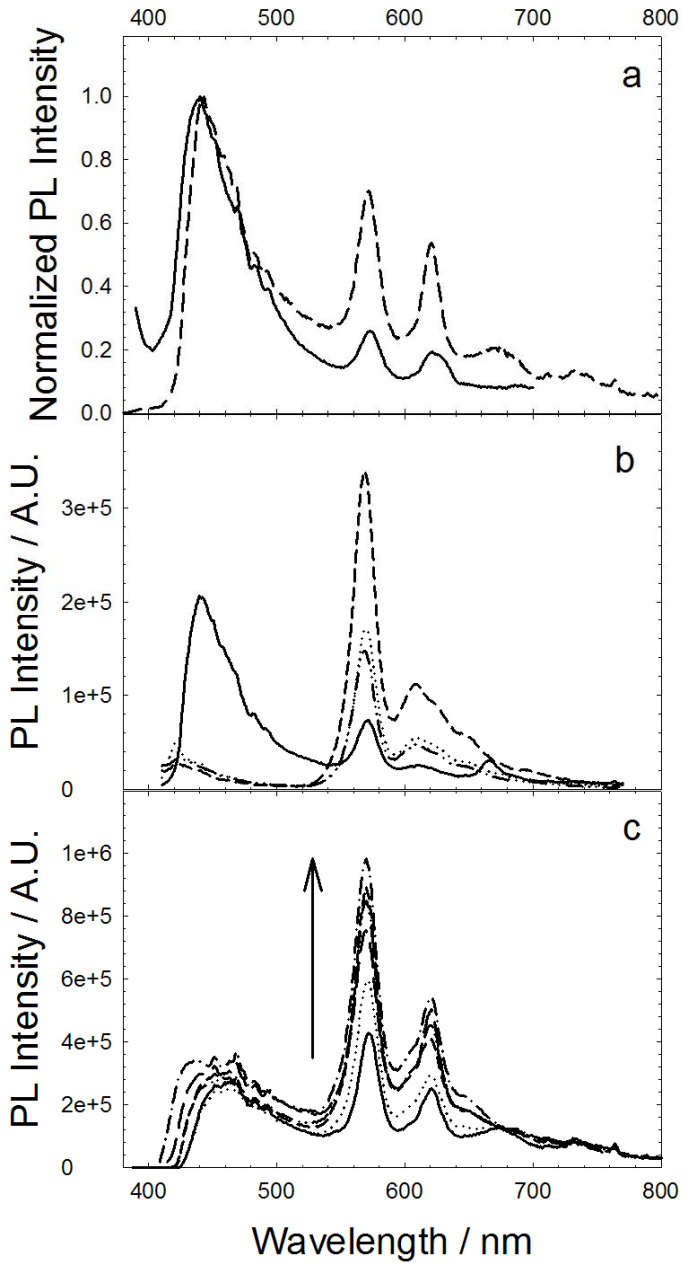

Figure 4-21. Photoluminescence spectrum of **Pt2MP3**. (a) With λ_{ex} = 366 nm from drop-cast film (—) and from deoxygenated dodecane at 10^{-3} M (– – –). (b) With λ_{ex} = 393 nm in deoxygenated solution at C = 10^{-3} M (—), 10^{-4} M (• • •), 10^{-5} M (– – –), 10^{-6} M (– •• –). (c) With λ_{ex} = 366 nm from deoxygenated dodecane at 10^{-3} M. Arrow indicates the effect of increasing temperature from 23 ^{o}C to 48 ^{o}C.

As the photophysical data obtained so far for **Pt2M** indicated that emission from aggregates could be detected and identified, the possibility of observing energy transfer within those aggregates was envisaged. For this, doping levels of **Pt2MT** were mixed in a gel of **Pt2M** and the photoluminescence was measured. In order to minimize direct excitation of **Pt2MT**, the excitation wavelength used for photoluminescence was λ_{ex} = 300 nm. This is where the least direct absorption of **Pt2MT** will occur while still allowing the observation of the "blue" emission band of **Pt2M** (Figure 4-22). Note that in the following photoluminescence energy transfer experiments, the concentration of **Pt2MT** is at doping levels, so its effective absorption is of a few percent to what is apparent in Figure 4-22.

Energy transfer from **Pt2M** to **Pt2MT** at doping levels was indeed observed in dodecane gels (Figure 4-23a). At only 3 mol% doping of **Pt2MT** in **Pt2M** at 10^{-3} M, the photoluminescence displays equally intense phosphorescence from both oligomers. At 5 mol% doping level, the phosphorescence of **Pt2MT** dominates the emission spectrum. Note that the photoluminescence spectrum in Figure 4-23a is normalized to the PL intensity at λ = 494 nm. The slight increase in the phosphorescence at λ = 526 nm as the **Pt2MT** doping level increases suggests a stronger quenching of the "blue" emission band than of the "normal" emission. This is consistent with the idea that energy transfer will occur more efficiently in aggregates than in non-aggregated domains. In order to provide evidence that the emission from **Pt2MT** is not due to its direct excitation and that energy transfer occurs preferentially in aggregates, the photoluminescence of **Pt2M** at different concentrations with a constant 5% doping level of **Pt2MT** was measured (Figure 4-23b). As expected, the phosphorescence emission from **Pt2MT** decreases with concentration.

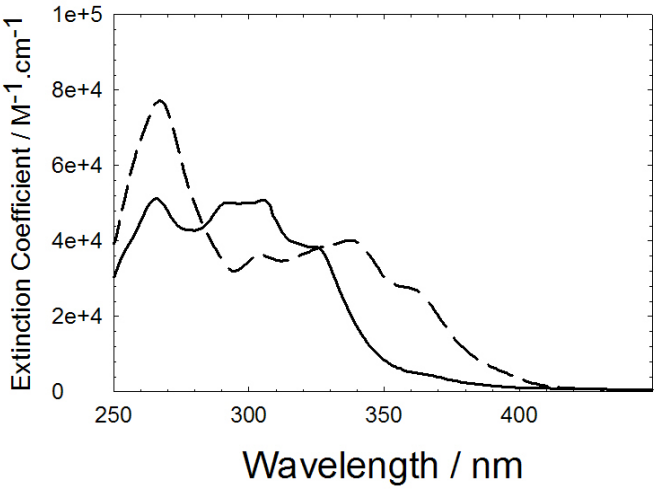

Figure 4-22. Absorption spectrum of **Pt2M** (—) and **Pt2MT** (– – –) in dodecane at C = 10^{-3} M.

At a **Pt2M** concentration of 10^{-4} M, where the solution is in a liquid state and aggregates formation is limited, almost no phosphorescence from **Pt2MT** is detected and the emission is essentially that of **Pt2M**.

These experiments point to a very efficient energy transfer when aggregates are present, especially considering that the quantum yield of phosphorescence of **Pt2MT** is much less than that of **Pt2M**. Indeed, while Φ_p = 9.1% for **Pt2M**, Φ_p = 0.7% for **Pt2MT** in dilute dodecane solutions. This is consistent with what has been observed in Chapter 2, where lower phosphorescence quantum yields were obtained in the thiophene-containing oligomers due in part to their lower triplet excited state energy. Therefore, from the ratio of the phosphorescence quantum yields of **Pt2M** and **Pt2MT**, approximately one in ten excitons transferred results in detectable phosphorescence from **Pt2MT**.

Time-Resolved Photoluminescence

The time-resolved photoluminescence of the platinum acetylide oligomers were investigated in order to extract some information regarding the dynamics of their excited state in aggregates. All lifetimes obtained from the decay of the emission bands are

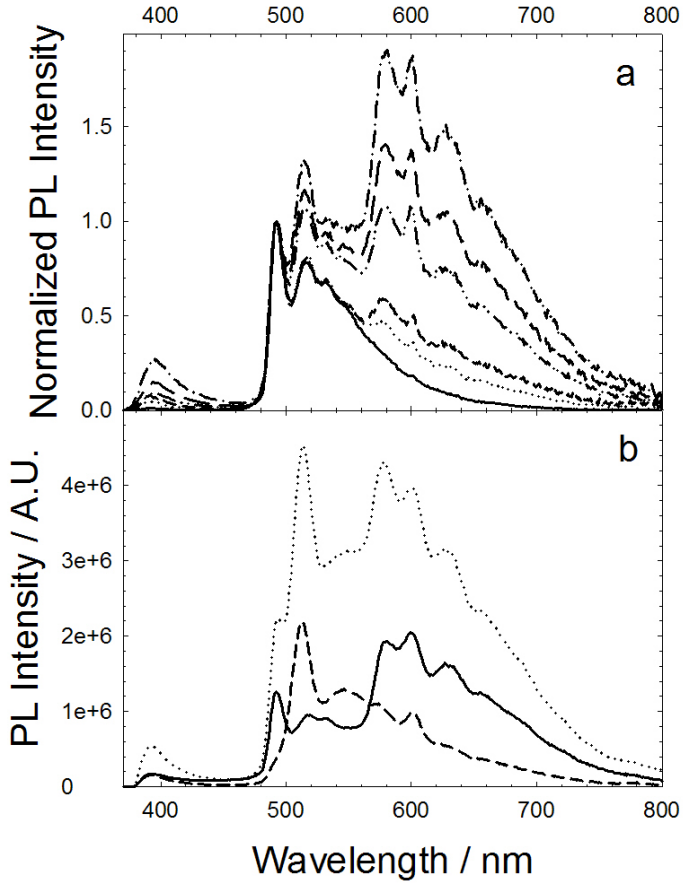

Figure 4-23. Photoluminescence spectrum of **Pt2M**-**Pt2MT** mixed-oligomer system. (a) With [**Pt2M**] = 10^{-3} M and [**Pt2MT**] = 0 mol% (—), 1 mol% (• • •), 2 mol% (– – –), 3 mol% (– • • –), 4 mol% (— —) and 5 mol% (– • –) in deoxygenated dodecane, with λ_{ex} = 300 nm. (b) **Pt2M** with 5 mol% **Pt2MT** mixed-oligomer system in deoxygenated dodecane with [**Pt2M**] = 10^{-3} M (—), 5x10^{-4} M (• • •), 10^{-4} M (– – –), with λ_{ex} = 300 nm.

summarized in Table 4-1. When the decay was better fitted with a bi-exponential, the lifetime and the relative contribution of each component are shown.

The time-resolved photoluminescence of **Pt2M** (Figure 4-24) shows a much slower decay for the "blue" emission (λ = 494 nm) than for "normal" emission (λ = 516 nm) in aggregates. While the lifetime of the emission at λ = 516 m is about 10 μs at all concentrations studied, the lifetime of the emission at λ = 494 nm is about 59 μs. The lifetime of the "normal" emission band is somewhat smaller but comparable to the

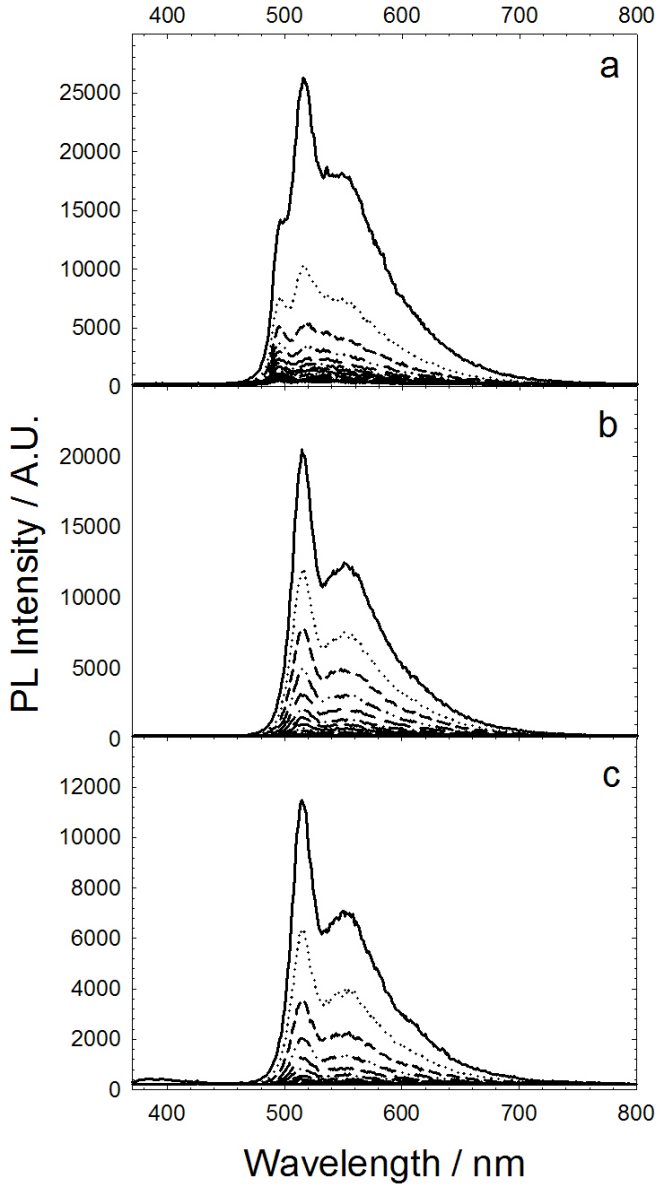

Figure 4-24. Time-resolved photoluminescence spectrum of **Pt2M** in deoxygenated dodecane following λ_{ex} = 337 nm. (a) C = 10^{-3} M, 100 ns camera delay, 10.5 µs delay increment; (b) C = 10^{-4} M, 100 ns camera delay, 5.2 µs delay increment; (c) C = 10^{-5} M, 100 ns camera delay, 5.2 µs delay increment.

emission lifetime of **Pt4** (see Chapter 2). However, the lifetime of the "blue" emission is surprisingly longer. This is at first unexpected because triplet-triplet annihilation could have been thought to be efficient in aggregates and therefore shorter lifetimes could have been expected in aggregates. This is clearly not the case for **Pt2M** and possible

explanations for this will be provided in the discussion. The photoluminescence decay of **Pt2M** was deconvoluted into two components (Figure 4-25). The decay of the blue emission band, while longer, contributes only 22% of the emission decay observed. The decay of the normal emission band contributes 78% of the emission decay observed. This seems to imply that a significant proportion of photoluminescence is arising from non-aggregated domains of the gel.

While the time-resolved photoluminescence spectrum of **Pt2MT** (not shown here) does not display two emission bands as **Pt2M**, the lifetime obtained in concentrated solution is also much longer than what could have expected (τ = 23 μs). As a comparison, the lifetime of the thiophene-based excited state in **Pt4T1** in dilute solutions was much shorter (τ = 7 μs, see Chapter 2) than the lifetime of emission of **Pt2MT** in concentrated solutions, which may appear counter-intuitive but is consistent with the trend observed in the lifetimes of **Pt2M**.

The time-resolved photoluminescence of **Pt2MP3** (Figure 4-26) shows trends different than those observed in **Pt2M**, further supporting the different structure of the aggregates formed in **Pt2MP3**. The first noticeable feature is the presence of some delayed fluorescence in the photoluminescence at high concentration solution (10^{-3} and 10^{-4} M) acquired 1 μs after laser pulse, indicating that triplet-triplet annihilation is taking place in aggregates of **Pt2MP3**. However, it does not appear as though the delayed fluorescence observed here can account for the strong fluorescence observed in the steady-state spectrum (Figure 4-21). This implies that the strong fluorescence in the steady-state emission is prompt-type fluorescence, rather than a delayed fluorescence originating from triplet-triplet annihilation.

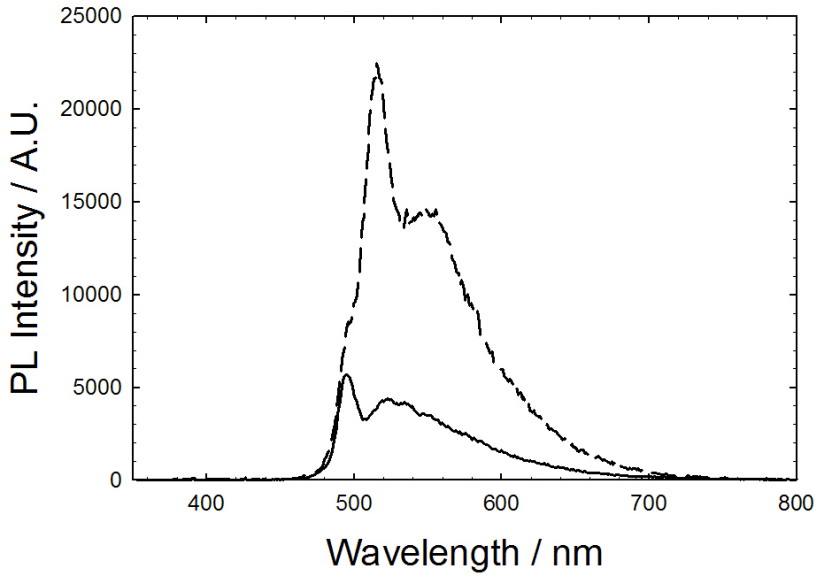

Figure 4-25. Principal components of emission decay of **Pt2M** at 10^{-3} M in dodecane for slow component τ = 59 μs (—) and fast component τ = 9 μs (– –).

Another noteworthy feature extracted from the time-resolved emission is the lifetime of the emission band. As can be seen from Table 4-1, the lifetime of the phosphorescence band was fitted well with a mono-exponential decay function. Looking at the overall evolution of these lifetimes as concentration increases, it appears that in this case, the trend follows the expected lifetime increase as concentration decreases and excited states quenching becomes less prone to occur. Hence, the lifetimes vary from 37 μs at 10^{-3} M to 148 μs at 10^{-6} M. However, experiments carried out with increasing laser intensity (not shown here) did not show a decrease in lifetime, as expected if quenching is due to triplet-triplet annihilation at higher laser energies. This again supports the idea that delayed fluorescence is not the main origin for the strong fluorescence observed in the steady-state experiment. The decay of the phosphorescence band in **Pt2MP3** was also fitted well with a bi-exponential function (not shown here) for all concentrations, consisting of a short (9-25 μs) and a long (52-160 μs) component. The relative

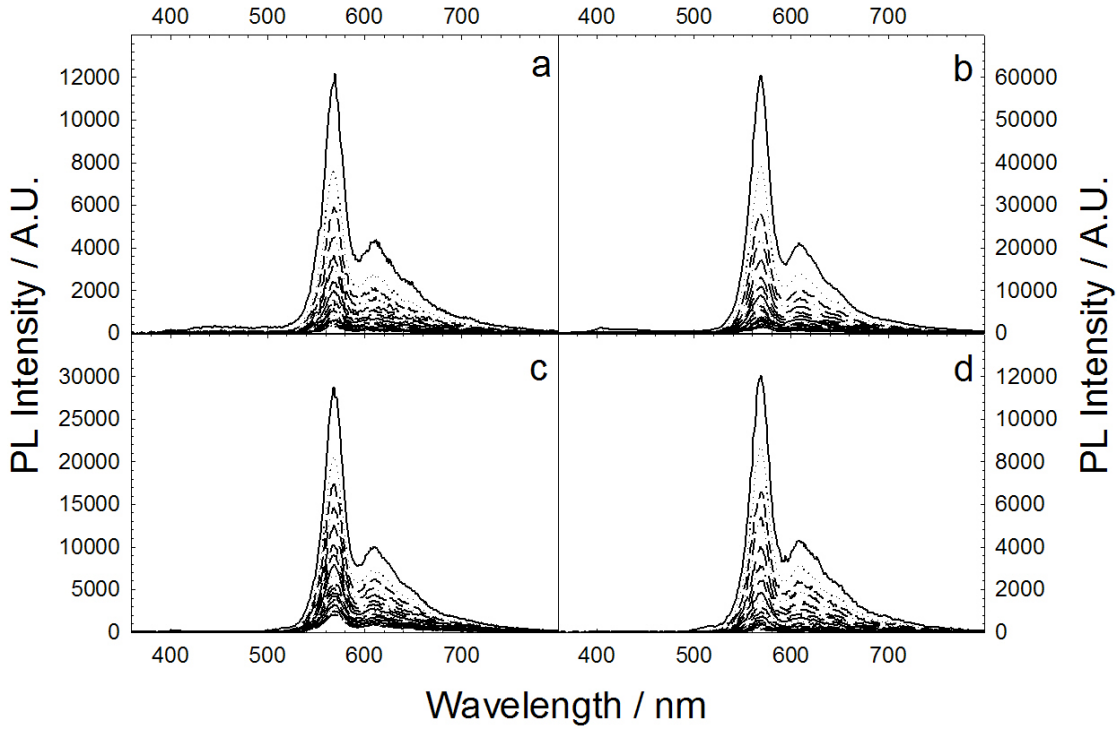

Figure 4-26. Time-resolved photoluminescence spectrum of **Pt2MP3** in deoxygenated dodecane following λ_{ex} = 355 nm. (a) C = 10^{-3} M, 1 μs camera delay, 10 μs delay increment. (b) C = 10^{-4} M, 1 μs camera delay, 20 μs delay increment. (c) C = 10^{-5} M, 1 μs camera delay, 20 μs delay increment. (d) C = 10^{-6} M, 1 μs camera delay, 40 μs delay increment.

contribution of the short component decreased from 42% at 10^{-3} M to 13% at 10^{-6} M, at the expense of the longer component. The trend displayed by these two components would be consistent with triplet-triplet annihilation responsible for the short component, however again power-dependent lifetime measurements did not reveal any effect on the lifetime. The reason for this is not clear at this time.

The **Pt2M-Pt2MT** mixed oligomer system was also examined with time-resolved photoluminescence in order to gain some understanding on the dynamics of energy transfer. The time-resolved photoluminescence was measured in a dodecane gel of **Pt2M** containing 5 mol% **Pt2MT** (Figure 4-27) 1 μs after laser excitation (λ_{ex} = 337 nm). The spectrum clearly shows a much shorter decay for the phosphorescence bands of **Pt2M**,

resulting from the energy transfer to **Pt2MT**. The fitting of the decay curves did not deconvolute both bands from **Pt2M**, but gives an overall lifetime of 5 μs, much shorter than the lifetimes of pure **Pt2M** in dodecane (τ_1 = 9 μs, τ_2 = 59 μs). The energy transfer is also reflected in the lifetime of **Pt2MT** in the mixed-oligomers system (τ = 62 μs, with some contribution from the "blue" band of **Pt2M**), which is considerably longer than the lifetime of pure **Pt2MT** (τ = 23 μs). The photoluminescence decay was deconvoluted into phosphorescence components of **Pt2M** (71%) and **Pt2MT** (29%), although the component from **Pt2MT** has some contribution from the "blue" emission of **Pt2M** (Figure 4-28). A control experiment under dilute concentration (10^{-5} M) at with 1:1 **Pt2M**/**Pt2MT** (not shown here) shows no change on the lifetime of **Pt2M** emission. This supports the idea that the presence of aggregates is necessary for efficient energy transfer and that quenching does not occur by a diffusional process.

In an effort to determine whether both emission bands of **Pt2M** are quenched to the same extent by **Pt2MT**, measurements were carried out in dodecane gel of **Pt2M** with different doping levels of **Pt2MT** ranging from 0.25 to 4 mol%. The decay of the each emission band is plotted as a function time and can be at least qualitatively commented (Figure 4-29).

First, it is clear that **Pt2MT** has an effect on both emission bands, as the lifetime of both bands gets shorter with increasing content of **Pt2MT**. However, it appears that the effect is somewhat more pronounced for the "blue" emission band at λ = 494 nm (Figure 4-29a) than for the "normal" emission at λ = 516 nm (Figure 4-29b). Since several pieces of evidence point out to efficient energy transfer only in the aggregates. This is evidenced by the apparent faster decays at λ = 494 nm than at λ = 516 nm as well as by the relative

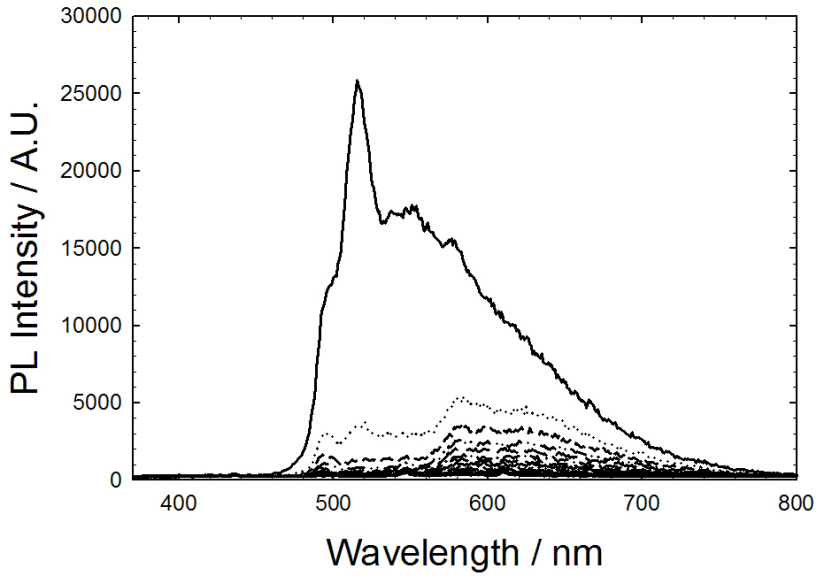

Figure 4-27. Time-resolved photoluminescence spectrum of **Pt2M** with 5 mol% **Pt2MT** in deoxygenated dodecane following λ_{ex} = 337 nm. [**Pt2M**] = 10^{-3} M, 1 μs camera delay, 10.5 μs delay increment.

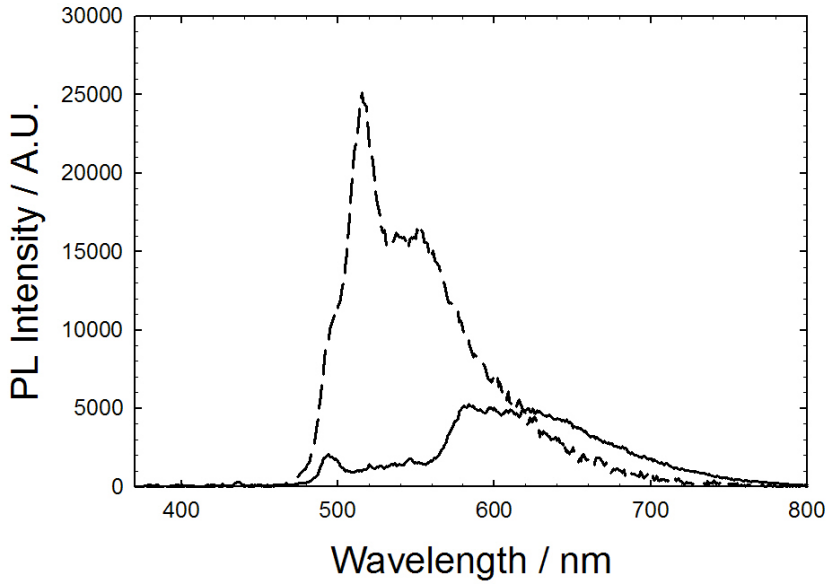

Figure 4-28. Principal components of emission decay of **Pt2M** at 10^{-3} M with 5 mol% **Pt2MT** in dodecane for slow component τ = 41 μs (—), fast component τ = 5 μs (– –).

quenching of instantaneous amplitude (t = 0). This further supports the idea that the "blue" emission band is the emission of **Pt2M** in aggregates. This is not contradictory with an energy transfer working also for the "normal" emission as there appears to be a significant proportion of oligomers in "liquid" non-aggregated domains in the gel.

Table 4-1. Lifetime[a] of photoluminescence of self-assembling platinum acetylide oligomers.[b]

Pt2M			**Pt2MT**	**Pt2MP3**				**Pt2M/Pt2MT**
10^{-3} M	10^{-4} M	10^{-5} M	10^{-3} M	10^{-3} M	10^{-4} M	10^{-5} M	10^{-6} M	10^{-3} M Pt2M + 5% Pt2MT
59 (22%)[c] 9 (78%)[d]	11	10	23	37	70	119	148	5 (71%)[e] 41 (29%)[f]

[a]: all lifetimes are in μs. [b]: number in parenthesis is the relative contribution of the individual decay component; [c]: decay of "blue" band; [d]: decay of "normal" band"; [e]: decay of **Pt2M** only; [f]: decay of **Pt2MT** and "blue" band of **Pt2M**.

Discussion

Nature of Aggregates

The photophysical properties of platinum acetylide oligomers studied here have clearly shown signs of aggregation in dodecane solution. For all oligomers except **Pt2MP3**, the solutions of oligomers at concentrations of ~1 mM were found to form a gel in saturated hydrocarbon solvents. The observation of the gelation effect is a clear indication that some network structures are present, such that the flow of the solvent is frozen. While the concentration necessary to reach gelation may appear high when compared to concentrations typically used in photophysical studies in solution, they are not. A concentration of 1 mM of **Pt2M** in dodecane corresponds to about 2 wt%, which is in fact on the low end of concentration range of efficient low molecular mass organogelators.[192] This is an important finding that would allow these materials to be

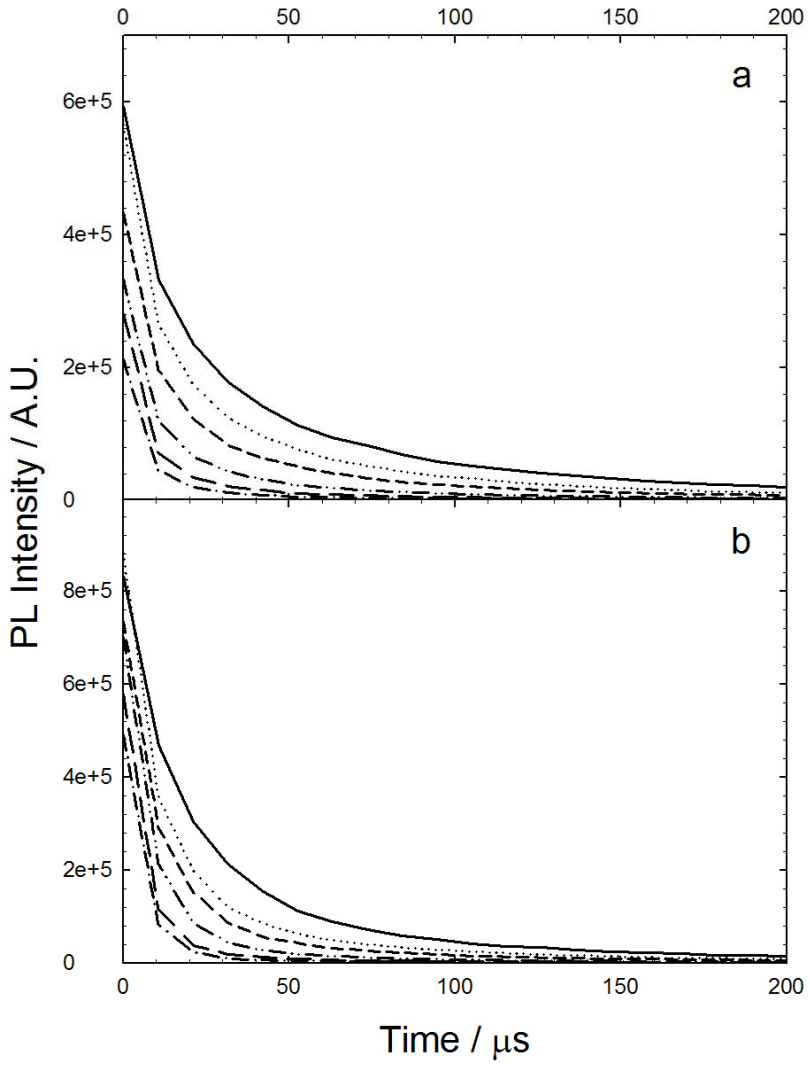

Figure 4-29. Plot of emission decay of **Pt2M** at 494 nm (a) and 516 nm (b) with x mol% doping levels of **Pt2MT**. Doping x = 0% (—), 0.25% (• • •), 0.50% (– – –), 1% (– • • –), 2% (— —) and 3% (— • —). Lines are only an indication of the decays and do not represent an actual fit of the data points.

easily processed, when most short oligomers do not usually have the advantageous processable properties of long chain polymers. Their apparent liquid-crystalline behavior is also a clear advantage in terms of processability and technological application. Moreover, organogels based on π-conjugated systems are relatively very few and therefore makes these platinum acetylide oligomers an elegant and original system.

While a direct characterization of the gels and the solution aggregates could be desirable, the photophysical study conducted here can give a wealth of information regarding the structure of aggregates. As briefly introduced in Chapter 1, the interaction of aggregated chromophores has been fairly accurately described by McRae and Kasha in terms of the molecular exciton model.[27] The model predicts a splitting of the excited state in the aggregate due to the interaction between neighboring transition dipole moments. The exciton interaction energy (ΔE) depends on the transition dipole moment of the molecule ($\Delta E \propto M^2$), the distance between them ($\Delta E \propto R^{-3}$) and their relative orientation. Depending on the position of the absorption band of the aggregate relative to the monomer, the aggregates are called J-aggregates (for an observed bathochromic shift) or H-aggregates (for an observed hypsochromic shift).

From the absorption spectra of the oligomers, it appears that **Pt2M** and **Pt2MT** form H-aggregates in concentrated dodecane solutions. The hypsochromic shift of the absorption band compared to the one observed in dilute solutions is a typical signature of H-aggregates, as observed in various systems such as trans-stilbene,[38] squaraine dye[197], perylene bisimide polymers,[198] terthiophene[199] and different dyes.[31,200,201] In this case, the interaction of the transition dipoles splits the excited state into two excitonic levels E' and E'' (see Chapter 1). Transition between ground state and E' are forbidden, so excitation occurs to the higher excitonic level E'', resulting in absorption at higher energy and shorter wavelength. The spectral shift of the absorption bands observed here ($\Delta\lambda$ = - 58 nm for **Pt2M**, $\Delta\lambda$ = - 40 nm for **Pt2MT** with $\Delta\lambda = \lambda_{agg} - \lambda_m$) are comparable though somewhat smaller than those observed in the examples cites above. For instance in the *trans*-stilbene system,[38] a spectral blue shift of 70 nm was observed upon aggregation,

while the squaraine system[197] exhibited a strong blue shift of 130 nm in aggregates. This indicates that the exciton coupling in the aggregates of platinum acetylide oligomers may not be as strong as in these other systems.

The absorption spectrum of **Pt2MP3** displays a red-shift that could be attributed to J-aggregates. In this case, absorption is only allowed from the ground state to the lower excitonic level E'. This results in absorption at lower energy and longer wavelength for the aggregate. J-aggregates have also been observed in many different systems such as bis-(biphenyl)-ethylene[37] and diphenylbutadiene[202] derivatives, carbocyanine dyes[40,203], as well as H-bonded oligo(*p*-phenylenevinylene)s.[177] The spectral shift of the absorption band in **Pt2MP3** ($\Delta\lambda$ = 40 nm, with $\Delta\lambda = \lambda_{agg} - \lambda_{m}$) is also smaller than those observed in the examples cited above, again indicating that exciton coupling in aggregates of **Pt2MP3** may relatively weak.

The bathochromic shift of the absorption band in the aggregate of **Pt2MP3** can also be explained by an intramolecular phenomenon, rather than an intermolecular one in the form of J-aggregates. Indeed, Bunz and co-workers[204] have studied the aggregation behavior of poly(*p*-phenenyleneethynylene)s (PPEs) and observed a sharp red-shifted absorption in films, very similar to the one observed in **Pt2MP3**. The red-shifted band disappeared once the polymer reached an isotropic state. The same behavior was observed more recently by Li and Wang[205] in a polystyrene-oligo(*p*-phenyleneethynylene)-polystyrene triblock copolymer. Upon addition of a poor solvent to the dissolved polymer, a red-shifted shoulder appeared in the absorption spectrum, almost superimposable to the absorption spectrum in thin films. The general consensus about the bathochromic shift in these aggregates is that it is due to a planarization of the conjugated

backbone induced by aggregation.[206] Therefore, it is not excluded that the red-shifted absorption in aggregates of **Pt2MP3** could also be simply due to a planarization of the phenyleneethynylene segment of the oligomer. However, there are some indications that J-aggregates are indeed formed in **Pt2MP3**. Firstly, H-aggregates are clearly formed in **Pt2M** and **Pt2MT** so it appears likely that similar aggregates should form in **Pt2MP3**. More importantly, when aggregate formation was observed in thin films of PPEs, the photoluminescence spectrum was entirely dominated by a broad strongly red-shifted band attributed to excimer emission. The intensity of the excimer band was also weaker than the emission of non-aggregated PPEs. From the photoluminescence experiments of **Pt2MP3** (Figure 4-21), it does not appear as though emission from excimers is observed. While the fluorescence of **Pt2MP3** in aggregates does seem broader and red-shifted compared to the photoluminescence in dilute solutions, it is clearly not similar to the excimer emission at $\lambda = 516$ nm observed in **PE3** (Figure 4-16). Moreover, thin films of **PE3** exhibiting excimer emission did not display the sharp red-shifted absorption band observed in **Pt2MP3** but only a slight broadening of the "monomeric" absorption band (not shown here). Time-resolved photoluminescence measurements of **Pt2MP3** at early times after laser excitation (not shown) did not reveal excimer emission either. Moreover, the fluorescence of **Pt2MP3** seems stronger in aggregates than it is in dilute solutions, further supporting the idea that J-aggregates are indeed formed for **Pt2MP3**. Increased red-shifted fluorescence in J-aggregates has been observed before in similar systems,[37,194] and is attributed to the synergic effects of intramolecular planarization (which leads to a slight increase in oscillator strength), restricted excimer formation and increased transition dipole moment of the $E' \rightarrow S_0$ transition.[27,207]

Although it appears that the absorption properties of the oligomers studied here can be rationalized in terms of face-to-face H- and J-aggregates, other structures have been proposed for aggregates consisting of small aromatic systems. Whitten and co-workers[208] have studied a wide variety of aromatic-functionalized amphiphiles-fatty acid and phospholipids derivatives and the results of their experimental and simulation studies indicate that in many cases, aggregates are characterized by strong noncovalent edge-to-face interactions. Pinwheel and herringbone structures based on a chiral tetramer unit[209] were proposed for the aggregates which exhibited blue-shifted absorption and red-shifted fluorescence compared to the monomer. Close energetic balance and competing factors such as topology and steric constraints do not allow an easy identification between edge-to-face and face-to-face. The remaining of the discussion will therefore assume a face-to-face arrangement for the aggregates of platinum acetylide oligomers studied here, bearing in mind that other supramolecular arrangement are also possible.

Photoluminescence of Aggregates

The photoluminescence of H- and J-aggregates is rationalized with the molecular exciton model introduced in Chapter 1. For organic H-aggregates, quenching of fluorescence and long lifetimes are usually observed. After excitation to the upper excitonic level E'' (excitation to lower excitonic level E' is forbidden), rapid internal conversion occurs to the E' level. The radiative relaxation from E' to the ground state being forbidden, radiationless transitions are necessary to return to ground state. Two possibilities are nonradiative decay from E' to S_0 and intersystem crossing to triplet excited state. The latter is considered to be nondegenerate in the molecular exciton model, since the oscillator strength of the S_0-T_1 is zero. The consequence on photoluminescence are therefore quenching of fluorescence with long lifetime and

phosphorescence enhancement in some cases. This effect was observed by Kasha and co-workers[28,36] as early as 1958. For J-aggregates, absorption from ground state to the lower excitonic level E' is allowed, therefore red-shifted fluorescence is observed.

Platinum acetylide oligomers aggregates fit into the molecular exciton model, the only difference being that phosphorescence is intrinsically favored due to the presence of strong spin-orbit coupling induced by platinum. A simplified energy diagram for monomers and aggregates is shown in Figure 4-30.

The diagram shows the different photophysical processes involved in monomers and aggregates. For monomers, excitation of the oligomer to S_1 results in radiative decay from S_1 and T_{1A}, via ISC. From the photoluminescence in dilute solutions, for which almost no fluorescence is observed, ISC is fast and relaxation occurs by phosphorescence from T_{1A}. For **Pt2M** and **Pt2MT**, which are believed to form H-aggregates, excitation of the oligomers occurs to the upper excitonic level E'', as evidenced by the blue-shifted absorption in gels. Rapid internal conversion relaxes the molecule to the lower excitonic level E', from which the radiative decay is forbidden. Nonradiative decays can provide a channel for relaxation to ground state but fast intersystem crossing provide an alternate pathway to the triplet excited state T_{1B}. The triplet excited state in H-aggregate is denoted T_{1B} and shown slightly higher in energy than T_{1A} (triplet excited state for monomer). As photoluminescence experiments have shown, phosphorescence from the aggregates displays two bands. The "normal" phosphorescence band at $\lambda = 516$ nm (similar to the one observed for the monomer), as well as a higher-energy, "blue" phosphorescence band at $\lambda = 494$ nm, only observed when aggregates are present. Preliminary theoretical calculations carried out in our group indicate that the preferred conformation of the triplet

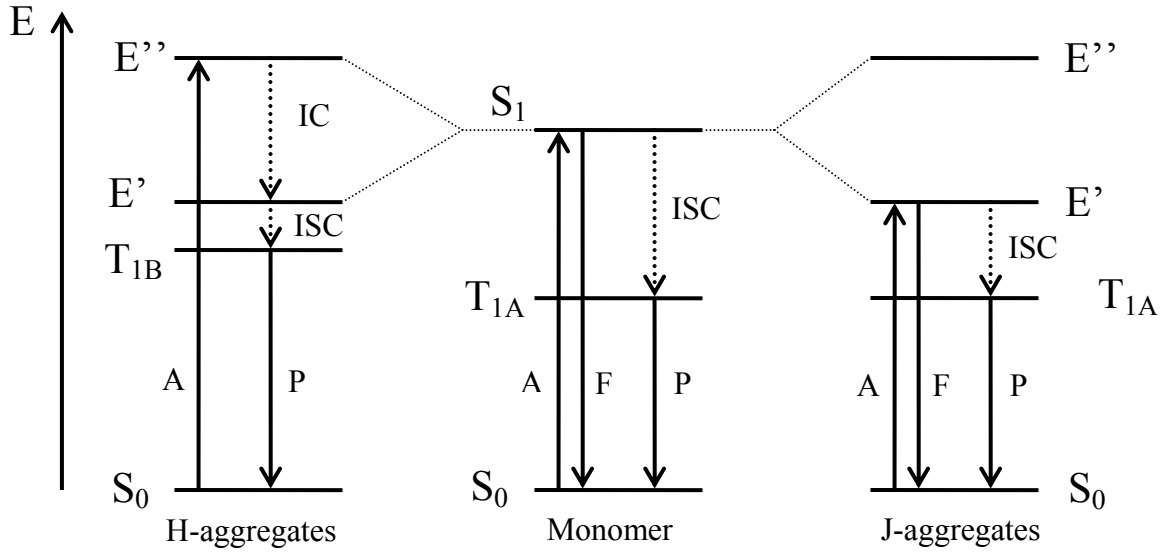

Figure 4-30. Energy diagram for monomer and aggregates in self-assembling platinum acetylide oligomers. Energy levels are only relative. A: absorption; F: fluorescence; P: phosphorescence; IC: internal conversion; ISC: intersystem crossing; S_0: singlet ground state; S_1: singlet excited state; $T_{1A,B}$: triplet excited state; E',E'': excitonic levels.

excited state in a **Pt2** oligomer has the central phenyl ring co-planar to the planes of the platinum square complex, while the two outer phenyl rings are perpendicular to the plane of the platinum complex. Other conformations (obtained by a rotation of 90^o of one or several of the phenyl rings) were found to have energies higher

by as much as 3 kcal/mol. It is proposed that the triplet excited in H-aggregates is a conformer higher in energy than the conformation of the triplet excited state in dilute solution. Indeed, for H-aggregates and even if the slippage angle θ is significant, there must be some planarization to allow the oligomers to come close to each other. A proposed conformation for the triplet excited state in H-aggregates of **Pt2M** is depicted in Figure 4-31, along with the ideal triplet excited state conformation found in solution. The difference in energy between the "blue" and the "normal" emission band is ~2.5

kcal/mol, therefore it is within the limit of the conformer of highest energy calculated (with all phenyl rings co-planar and perpendicular to the planes of the square platinum complex). Note that the photoluminescence of dodecane gel of **Pt2M** also shows "normal" phosphorescence. This implies that even in the gel, there must be domains where the oligomer is in a dodecane solvent cage and retains some configurational freedom.

(a)

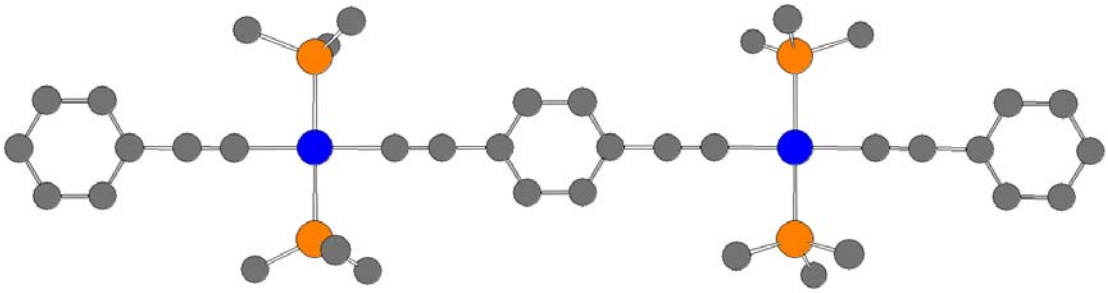

(b)

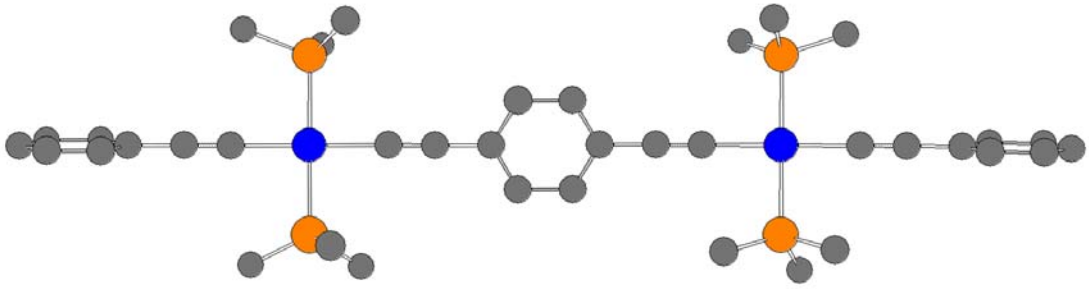

Figure 4-31. Proposed conformation of the triplet excited state of **Pt2M**. (a) All-planar high energy conformation in H-aggregates. (b) Ideal conformation in dilute solution. Hydrogen atoms and dodecanoxy end-chains have been omitted for clarity.

For **Pt2MP3**, the photoluminescence spectrum can also be explained using the energy diagram in Figure 4-30. In this case, the oligomer is excited to the lower excitonic

level E'. The radiative decay from E' to S_0 is allowed so the oligomer can relax to ground state by emission of fluorescence. Efficient intersystem crossing due to the presence of platinum may also provide access to the triplet excited T_{1A}, from which relaxation occurs by emission of phosphorescence. Time-resolved photoluminescence experiments have shown that strong fluorescence observed in concentrated dodecane solution is prompt fluorescence (fluorescence lifetime on the order of the ns) and that triplet-triplet annihilation does not play a significant part (no excitation power dependence). This reinforces the proposed J-aggregation of **Pt2MP3** (as opposed to a simple planarization induced by aggregation) because increased fluorescence is expected from J-aggregates (intensity scales as $N^{1/2}$ for aggregates smaller than the emission wavelength, with N the number of monomers in the aggregate).[33] Fluorescence enhancement in aggregates has been observed previously in related systems and is usually attributed to a combination of inter- and intramolecular effects.[210-212]

A brief mention of the phosphorescence lifetimes measured by time-resolved photoluminescence experiments should be made at this point. The interpretation of the lifetimes is speculative as no example of phosphorescence lifetime from aggregates in similar systems is found in the literature. As mentioned earlier, phosphorescence enhancement may observed in an H-aggregate, because fluorescence from the lower excitonic level E' is forbidden. However in H-aggregates of platinum acetylide oligomers, phosphorescence is always the dominant radiative process, regardless of concentration. The longer lifetime of the "blue" band (τ = 59 μs) of **Pt2M** (attributed to triplet excited states in aggregates) compared to the "normal" band (τ = 9 μs) is hypothetically attributed to two factors: 1) Constrained environment in aggregate may

limit vibrational coupling through which nonradiative decays occur.[7,64] This situation is similar to phosphorescence measurements made in frozen solvent matrix, where increased phosphorescence is usually observed due to decreased nonradiative decay rates; 2) Phosphorescence from the aggregated triplet excited state appears to arise from a high-energy conformer, which may slow down the rate of radiative decay.

The case of **Pt2MP3**, where lifetimes decreases with concentration, is not clear at this time. While it may appear as though increasing concentration should increase triplet-triplet annihilation and therefore reduce the lifetime, no evidence for this process which should result in delayed fluorescence was observed. The observed trend can be explained by assuming the presence of J-aggregates. As concentration decreases, less aggregates are present in solution, which limits highly efficient fluorescence from lower excitonic level to ground state. This would imply that aggregates are present even in relatively dilute solution as the lifetime increases regularly from 10^{-3} M (τ = 37 μs) to 10^{-6} M (148 μs). While the aggregate band disappears from the absorption spectrum below 10^{-4} M, it is not impossible that aggregates are still present below 10^{-4} M.

Molecular Exciton Modeling

In an effort to further characterize the supramolecular arrangement of the aggregates, the molecular exciton model is used to predict the geometry of aggregates of platinum acetylide oligomers. For the sake of simplicity, it is assumed that spectral changes in the absorption spectra of the oligomers are due to dimers of J- or H-aggregates and the point-dipole approximation introduced in Chapter 1 is used. This model has been used recently on studies concerned with aggregates of porphyrins,[213] sapphyrins[214] and lutein,[32] and provides a simple, semi-quantitative analysis of aggregate effects. Parameters needed are the interaction energy ΔE (obtained from the energy difference

between monomer absorption and aggregate absorption maxima), the transition moment of the monomer absorption μ (obtained through the calculation of the oscillator strength of monomer absorption), and the distance R between point-dipoles of oligomers in aggregates. The latter is critical and will have a large influence on the result of the calculation since the exciton interaction energy is proportional to the inverse cube of R. Since no crystallographic data on the oligomers was obtained in this study, the distance R has to be estimated. A maximum limit on R can be obtained by taking the intermolecular distance obtained from a non-aggregating platinum acetylide complex bearing bulky iptycene unit studied recently in our group,[215] which was found to have R = 11.782 Å. Other crystallographic data available for a stilbene platinum acetylide complex[216] and a simple platinum acetylide complex[217] are R = 12.812 Å and 10.032 Å, respectively. Note that in both cases, tri-*n*-butylphosphine ligands are used, which most likely creates significant steric hindrance compared to the trimethylphosphine ligand used in the present study. Relevant parameters for the calculation are presented in Table 4-2 below. The evolution of the spectral shift Δλ is plotted as a function of the angle θ in Figure 4-28. Several possible distances are examined and calculated angles θ for the experimental spectral shifts are presented in Table 4-3 (see Experimental section for detail).

From the plots of the angle θ versus Δλ (Figure 4-32), some limits can be assigned on the dipole-dipole distance in the aggregates. For **Pt2M** and **Pt2MT**, it can be seen that only distances shorter than 8 Å can account for the exciton splitting observed. Above 8 Å, exciton splitting is too small to induce spectral shifts of 58 and 40 nm found in the absorption study of **Pt2M** and **Pt2MT**, respectively. Since the model assumes no ground

Table 4-2. Absorption data of self-assembling platinum acetylide oligomers.

	Pt2M	**Pt2MT**	**Pt2MP3**
λ_m (nm)[a]	358	378	365
ε_{max} ($M^{-1}.cm^{-1}$)[b]	100,520	52,500	123,000
λ_{agg} (nm)[c]	300	338	405
$\Delta\lambda$ (nm)[d]	- 58	- 40	40
FWHM (cm^{-1})[e]	4709	4673	4895
f[f]	3.21	1.66	4.08
μ (D)[g]	15.6	11.5	17.8

[a]: absorption maximum of monomer; [b]: molar extinction coefficient of monomer at absorption maximum; [c]: absorption maximum of aggregate; [d]: absorption spectral shift ($\lambda_{agg} - \lambda_m$); [e]: full width at half maximum for monomer; [f]: oscillator strength; [g]: transition dipole moment for absorption of monomer.

state interaction, R must be larger than van der Waalls distances, which are about 3-4 Å in the π-stacking of neutral aromatic compounds.[214] Therefore the dipole-dipole distance in the aggregates of **Pt2M** can be estimated to be between 8 and 4 Å. The angle θ calculated for some possible distances R are presented in Table 4-3. For a perfect face-to-face arrangement with $\theta = 90^o$, the calculated distance R is 7.7 Å for **Pt2M**, while it is 7.5 Å for **Pt2MT**.

For **Pt2MP3**, a large exciton splitting is obtained for a dipole-dipole distance R = 12 Å that can account for the absorption spectral shift observed in the aggregate. For a perfectly arranged head-to-tail geometry with $\theta = 0^o$, the calculated dipole-dipole distance is 13.3 Å (Table 4-3).

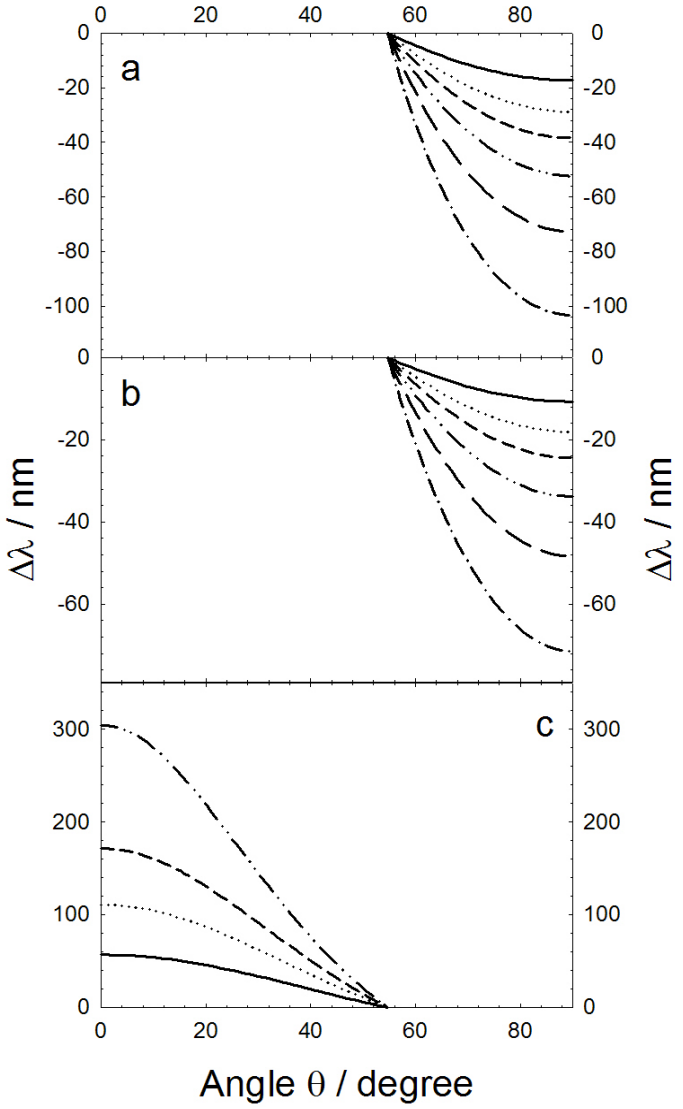

Figure 4-32. Plot of angle θ versus $\Delta\lambda = \lambda_{agg} - \lambda_m$ for different dipole-dipole distance R. (a) **Pt2M**. (b) **Pt2MT**. (c) **Pt2MP3**; (—) R = 12 Å; (•••) R = 10 Å; (– – –) R = 9 Å; (– • • –) R = 8 Å; (— —) R = 7 Å; (– • –) R = 6 Å.

Conclusion

A series of platinum acetylide oligomers designed to self-assemble in solution have been synthesized in order to study the consequences of aggregation on the triplet excited state. The oligomers were indeed found to form aggregates in dodecane solution, as evidenced physically by the formation of gels at relatively low concentrations (~2 wt%).

Table 4-3. Some angles and dipole-dipole distances calculated with the molecular exciton model.

	Pt2M			Pt2MT			Pt2MP3		
R (Å)	7.7	7	6	7.5	7	6	13.3	10	8
α (degree)	90	73	65	90	75	66	0	38	46

A preliminary study of the mesoscopic properties of the oligomers revealed liquid-crystalline phases between 120 ^{o}C and 180 ^{o}C. This is important for opto-electronic applications because it may improve the processability of these oligomers, which are often not as processable as polymers.

The photophysical study carried out on these oligomers revealed very different behavior among the oligomer series. The presence of aggregates has been identified spectroscopically, and the formation of H- and J-aggregates has been proposed from the direction of spectral shifts observed in absorption spectrometry of the aggregates. The mode of aggregation was found to have very different consequences on the photoluminescence. Oligomers that formed H-aggregates showed intact phosphorescence upon aggregation. The emission spectrum of H-aggregates was dependent on the excitation wavelength, and exciting on the J-aggregate absorption band showed a blue-shifted phosphorescence band in addition to the phosphorescence usually observed. The "blue" phosphorescence band is assumed to arise from a high energy conformer present in aggregate, where the restrained environment forces the molecule to adopt an unfavorable conformation. Overall, the photophysical properties of the oligomer are preserved in H-aggregates, which is particularly important for technological applications relying on the triplet excited state. On the other hand, the photoluminescence spectrum of

an oligomer believed to form J-aggregate showed a drastic change upon aggregation, where strong fluorescence was observed instead of phosphorescence, as in dilute solutions. Although shorter lifetime of phosphorescence are observed in aggregates compared to those in dilute solution, triplet-triplet annihilation is not believed to be significatly responsible for the relative increase of fluorescence in aggregates.

Efficient energy transfer has been observed in mixed-oligomer systems, where one oligomer was used a dopant. Donor emission was significantly quenched with only 5% of dopant in gel. Both "blue" and "normal" emission bands were found to be affected by the presence of the dopant, although to a lesser extent for the latter. This implies that the gel contains domains where oligomer are not aggregated but rather trapped in a solvent cage with some conformational freedom.

Finally, the molecular exciton model has been used under the dipole-dipole approximation on the absorption data collected. For H-aggregates, the maximum dipole-dipole distance was found to be ~7.5 Å, while it was found to be 13.3 Å for a J-aggegate.

Experimental

Thermal Properties

Differential scanning calorimetry (DSC) analysis was performed using a Perkin-Elmer DSC 7 equipped with a controlled cooling accessory (CCA-7) at a heating and cooling rate of 10 ^{o}C/min. Calibrations were made using indium and freshly distilled n-octane as the standards for peak temperature transitions and indium for the enthalpy standard. All samples were prepared in hermetically sealed pans (5-10 mg/sample) and were run using an empty pan as a reference and an empty cells as a subtracted baseline.

Optical microscopic images of organogelators and organogels were observed on a Leitz 585 SM-LUX-POL microscope equipped with crossed polars, a Leitz 350 heating

stage, a Photometrics CCD camera interfaced to a computer, and an Omega HH503 microprocessor thermometer connected to a J-K-T thermocouple. All solids were sandwiched between thin cover slides. Organogel samples were smeared between two glass slides. Temperature was increased approximately 3 - 4 ºC/min from room temperature. All micrograph images were taken with a full-wave plate.

Photophysical Measurements

Steady-state absorption spectra were recorded on a Varian Cary 100 dual-beam spectrophotometer. Samples were placed in adequate short path length cell (1 or 0.1 mm) and absorbance was kept below 1. Corrected steady-state photoluminescence measurements were conducted on a SPEX F-112 fluorescence spectrometer. Samples were degassed by argon purging for 30 min and heated to an isotropic state regularly during this time for adequate degassing of gel-forming solutions. Samples were placed in a triangular-shaped cell and spectra recorded under pseudo front-face geometry to limit self-absorption. The sample cell was positioned so that the incident beam was at 45^{o} from the face of the cell and emission detected at 45^{o}. Low-temperature fluorescence measurements were carried out similarly to the procedure described in Chapter 2.

Time-resolved photoluminescence measurements were carried out on the same apparatus described in Chapter 2, except a N_2 laser (λ = 337 nm, 10 ns fwhm) was used as well for some oligomers. Photoluminescence was measured by front-face detection to limit self-absorption.

Circular dichroism (CD) measurements were carried out on an Aviv-202 circular dichroism spectrometer with a cell path length of 0.3 mm.

Calculation of Exciton Interaction Energy

The oscillator strength *f* of the monomer absorption was calculated using the following equation:[2]

$$f_{nm} = 4.319 \times 10^{-9} \frac{\pi \varepsilon_{\max} \Gamma}{2} = 6.784 \times 10^{-9} \varepsilon_{\max} \Gamma \quad (19)$$

where the constant is in $cm^2.mol.L^{-1}$, ε is the molar extinction coefficient in $L.mol^{-1}.cm^{-1}$ and Γ is the full width at half maximum in cm^{-1}.

The transition dipole moment μ of the monomer absorption band was calculated by

$$\mu = \sqrt{\frac{f}{4.702 \times 10^{-7} \tilde{\nu}}} \quad (20)$$

where *f* has no dimension, the constant is in $D^{-2}.cm$ and the absorption maximum $\tilde{\nu}$ is in cm^{-1}. The dipole moment was converted to C.m using:

1 D = 3.33564 x 10^{-30} C.m

The angle θ between the dipole moment of the monomers and the line of molecular centers was calculated according to Kasha's model[27,28] of the molecular exciton in the point-dipole approximation, assuming co-planar monomers in the aggregates and using the following equation:

$$\Delta E = 4\left(\frac{N-1}{N}\right)\frac{1}{4\pi\varepsilon_0}\left(\frac{\mu^2}{R^3}\right)\left(1-3\cos^2\theta\right) \quad (21)$$

For dimers (N = 2), this equation becomes:

$$\Delta E = \frac{1}{2\pi\varepsilon_0}\left(\frac{\mu^2}{R^3}\right)\left(1-3\cos^2\theta\right) \quad (22)$$

where ΔE is in Joules, ε_0 is the permittivity of free space (ε_0 = 8.8542 x 10^{-12} $C^2.N^{-1}.m^{-2}$), μ is the transition dipole moment in C.m, R is the point-dipole—point-dipole distance in

m and θ is the angle between the dipole moment of the monomer and the line of molecular centers in degree.

The interaction energy was obtained from the energy difference of the monomer and aggregate maximum of absorption using

$$\Delta E = \frac{hc}{\lambda_{agg}} - \frac{hc}{\lambda_m} \quad (23)$$

where h is Plank's constant (h = 6.626 x 10^{-34} J.s), c is the speed of light (c = 2.998 x10^8 m.s^{-1}, λ_{agg} and λ_m are the wavelengths in nm of absorption maximum of the aggregate and of the monomer, respectively.

Synthesis

General. The same procedures as described in Chapter 2 were used. Compounds were loaded on column for flash chromatography by dry-loading. For this, the crude product was first dissolved in a few mL of CH_2Cl_2, silica (1:1 crude/silica by weight) was added and the solvent removed. Crude adsorbed on silica was then loaded on column. *cis*-Dichloro-bis-(trimethylphosphine)-platinum(II) was prepared in two steps by an adapted literature method.[218,219]

***cis*-Bis(trimethylphosphine)dichloroplatinum(II)**. Potassium tetrachloroplatinate (3.0 g, 7.27 mmol) was placed in water (60 mL) and the suspension degassed with nitrogen. Then, diethyl sulfide (1.97 g, 21.8 mmol) was added via syringe and the mixture stirred for 2 hours under reflux, during which time the mixture turned clear and yellow. After cooling down, the solution was extracted with CH_2Cl_2 (3 x 60 mL), the organic phase dried on $MgSO_4$, and the solvent was removed to give the desired product as a bright yellow solid. Yield = 2.815 g (87%). The next step was carried out without characterization and *cis*-bis(diethylsulfide)dichloroplatinum(II) (2.815 g, 6.3 mmol) was

dissolved in CH_2Cl_2 and the solution degassed with nitrogen. Then trimethylphosphine (13.9 mL of 1 M THF sol., 13.9 mmol) was added via syringe. A fine white solid precipitated immediately and the mixture was further stirred for 30 min at room temperature. After this time, the white solid was collected by filtration, washed with cold Et_2O, recrystallized from Et_2O and dried under vacuum for 2 days. After this time, a faint smell of diethyl sulfide could still be detected, although NMR does not reveal the presence of diethyl sulfide. Yield = 2.483 g (94%). ^{1}H NMR (300 MHz, $CDCl_3$) δ 1.80 (m, 18H); ^{31}P NMR (75 MHz, $CDCl_3$) δ -23.53 (J_{Pt-P} = 3474.6 Hz).

5-Iodo-1,2,3-trimethoxybenzene (13). 3,4,5-Trimethoxyaniline (10.0 g, 54.6 mmol) was placed in a 500 mL beaker and water (120 mL) and sulfuric acid (8 mL) were added. The beaker was placed in an ice-bath and stirred with a mechanical stirrer. Then sodium nitrite (37.7 g, 564.6 mmol) in 60 mL of water was added dropwise and the temperature was maintained between -5 ^{o}C and 0 ^{o}C. After addition of sodium nitrite was complete, the reaction mixture was poured onto a 30 mL aqueous solution of potassium iodide (14.0 g, 84.3 mmol) at 50 ^{o}C under strong magnetic stirring. After the addition of the diazonium salt solution was complete, the mixture was stirred for 30 min. After cooling down, an aqueous solution of sodium sulfite was added to neutralize excess iodine until no further change in color was observed. The resulting aqueous solution was extracted with Et_2O (3 x 100 mL), the organic phase dried on $MgSO_4$ and the solvent removed to give the desired product as a yellow-orange solid. Yield = 13.3 g (83%). ^{1}H NMR (300 MHz, $CDCl_3$) δ 3.82 (s, 3H), 3.84 (s, 6H), 6.89 (s, 2H); ^{13}C NMR (75 MHz, $CDCl_3$) δ 56.5, 56.6, 86.4, 115.1, 147.4, 154.2.

5-Iodo-1,2,3-trihydroxybenzene (14). 5-Iodo-1,2,3-trimethoxybenzene (9 g, 30.6 mmol) was placed in a 250 mL three-neck round-bottom flask fitted with a condenser and CaCl2 drying tube, dissolved in 60 mL of freshly distilled methylene chloride, degassed with nitrogen and the solution cooled to -78 ^{o}C. Then boron tribromide (91.8 mL of 1M CH_2Cl_2 solution, 91.8 mmol) was added slowly via syringe. After the addition was complete, the mixture was allowed to warm to room temperature and further stirred for 24 h. The reaction was then carefully quenched with ice-water (40 mL) and stirred for 30 min. The mixture was then extracted with ethyl acetate (3 x 100 mL), the organic phase washed with aqueous Na_2SO_3, dried on $MgSO_4$ and solvent removed to give a brown oil. Finally, the product was precipitated from the crude oil by addition of $CHCl_3$, collected by filtration, washed with cold $CHCl_3$ and dried overnight to give the desired product as a white solid. Yield = 4.06 g (53%). ^{1}H NMR (300 MHz, acetone-d_6) δ 6.78 (s, 2H), 7.56 (s, 1H), 8.22 (s, 2H); ^{13}C NMR (75 MHz, acetone-d_6) δ 60.7, 80.5, 117.2, 147.6.

1,2,3-Tris(dodecyloxy)-5-iodo-benzene (15). 5-Iodo-1,2,3-trihydroxybenzene (4.0 g, 15.9 mmol) was dissolved in DMF (80 mL) and the solution was degassed with nitrogen for 15 min. Then K_2CO_3 (17.5 g, 127 mmol) was added and the mixture stirred at room temperature for 30 min. Then bromododecane (17.1 mL, 17.8 g, 71.4 mmol) was added and the mixture stirred at 60 ^{o}C for 7 h. After cooling down, the brown crude solid was filtered and washed with ice-cold water. Chromatography (silica gel, hexane then 4:1 hexane/CH_2Cl_2) gave the desired product as a white solid. Yield = 10.79 g (90%). ^{1}H NMR (300 MHz, $CDCl_3$) δ 0.88 (t, 9H), 1.26 (s, 48H), 1.45 (m, 6H), 1.78 (m, 6H), 3.92 (m, 6H), 6.84 (s, 2H); ^{13}C NMR (75 MHz, $CDCl_3$) δ 14.34, 22.92, 26.24, 26.31, 29.49,

29.58, 29.61, 29.80, 29.84, 29.88, 29.91, 29.95, 30.48, 32.15, 69.50, 73.64, 85.86, 116.39, 138.56, 154.15.

3,4,5-Tris(dodecyloxy)trimethylsilylethynylbenzene (16). 1,2,3-Tris(dodecyloxy)-5-iodo-benzene (10.70 g, 14.14 mmol) was dissolved in THF (60 mL) and *i*-Pr_2NH (40 mL) and the solution was degassed with argon. Then trimethylsilylacetylene (3.0 mL, 2.08 g, 21.2 mmol), $Pd(PPh_3)_4$ (489.6 mg, 0.42 mmol) and CuI (80.7 mg, 0.42 mmol) were added. The mixture turned dark right away and was stirred at 60 ^oC overnight. After cooling down, the mixture was passed through a bed of Celite and the solvents were removed. The crude mixture was dissolved in CH_2Cl_2 (100 mL), washed with 10% aqueous NH_4OH (2 x 100 mL), water (2 x 200 mL), dried on $MgSO_4$, and the solvent removed. The crude product was purified by flash chromatography (silica gel, hexane then 4:1 hexane/CH_2Cl_2) to give the desired product as a yellow solid. Yield = 6.0 g (58%). ^1H NMR (300 MHz, $CDCl_3$) δ 0.24 (s, 9H), 0.88 (t, 9H), 1.28 (s, 48H), 1.46 (m, 6H), 1.78 (m, 6H), 3.94 (m, 6H), 6.66 (s, 2H); ^{13}C NMR (75 MHz, $CDCl_3$) δ 0.19, 14.27, 22.90, 26.28, 26.32, 29.55, 29.58, 29.61, 29.79, 29.85, 29.88, 29.91, 29.94, 29.97, 30.52, 32.14, 32.16, 53.50, 69.23, 73.32, 73.57, 92.55, 105.71, 110.68, 117.06, 117.69, 139.53, 153.01.

3,4,5-Tris(dodecyloxy)ethynylbenzene (17). 3,4,5-Tris(dodecyloxy)trimethylsilyl-ethynylbenzene (5.58 g, 7.68 mmol) was dissolved in CH_2Cl_2 (40 mL) and MeOH (40 mL). Then K_2CO_3 (3.18 g, 23 mmol) was added and the mixture stirred at room temperature for 4 h. Then, the mixture was transferred to a separatory funnel and water (100 mL) was added. The aqueous phase was extracted with CH_2Cl_2 (2 x 50 mL), the organic phase washed with water (3 x 50 mL), dried on $MgSO_4$ and the solvent removed

to give the desired product as an off-white solid. Yield = 4.57 g (91%). ^{1}H NMR (300 MHz, $CDCl_3$) δ 0.88 (t, 9H), 1.28 (s, 48H), 1.46 (m, 6H), 1.78 (m, 6H), 2.98 (s, 1H), 3.94 (m, 6H), 6.68 (s, 2H); ^{13}C NMR (75 MHz, $CDCl_3$) δ 14.29, 22.90, 22.26, 26.26, 29.49, 29.59, 29.84, 29.91, 30.50, 32.13, 69.19, 73.62, 75.91, 75.98, 76.81, 84.16, 110.70, 116.64, 139.55, 153.08.

***trans*-[3,4,5-Tris(dodecyloxy)phenylethynyl]-chloro-bis(trimethylphosphine)-platinum(II) (18)**. *cis*-Dichloro-bis(trimethylphosphine)platinum(II) (382.2 mg, 0.91 mmol) was placed in THF (3 mL) and Et_2NH (3 mL) and the solution was degassed with nitrogen. Then **17** (500 mg, 0.76 mmol) was added and the reaction stirred at room temperature for 24 h after which time TLC showed no more organic **17** (R_F = 0.78, 1:1 hexane/CH_2Cl_2) and a new spot (R_F = 0.45, 1:2 hexane/CH_2Cl_2) was apparent. The solvents were removed and the crude product was purified by flash chromatography (silica gel, hexane then 7:3, 1:1, 3:7 hexane/CH_2Cl_2 and finally pure CH_2Cl_2) to give the desired product as a pale yellow solid. Yield = 724.1 mg (96%). ^{1}H NMR (300 MHz, $CDCl_3$) δ 0.85 (t, 9H), 1.28 (s, 48H), 1.48 (m, 6H), 1.63 (t, 18H), 1.76 (m, 6H), 3.93 (m, 6H), 6.51 (s, 2H); ^{13}C NMR (75 MHz, $CDCl_3$) δ 13.12, 13.37, 13.63, 13.99, 22.55, 25.98, 29.25, 29.27, 29.53, 29.57, 29.60, 29.62, 30.20, 31.80, 68.74, 73.13, 80.43, 101.75, 109.47, 122.65, 137.12, 152.45; ^{31}P NMR (121 MHz, $CDCl_3$) δ -13.66 ($J_{Pt\text{-}P}$ = 2332.2 Hz).

Compound (19). 1,4-Diiodobenzene (33.0 mg, 0.1 mmol) was dissolved in THF (6 mL) and *i*-Pr_2NH (4 mL) in a Schlenk flask and the solution degassed with argon. Then 1-ethynyl-4-(tri-*iso*-propylsilylethynyl)benzene (59.2 mg, 0.21 mmol), $Pd(PPh_3)_4$ (11.5 mg, 0.01 mmol) and CuI (1.9 mg, 0.01 mmol) were added and the mixture was stirred at

room temperature for 2 days. After the solvents were removed, the crude product was purified by flash chromatography (silica gel, hexane then 4:1 hexane/CH_2Cl_2) to give the desired product as a white solid. Yield = 43.9 mg (69%). ^{1}H NMR (300 MHz, $CDCl_3$) δ 1.15 (s, 42H), 7.45 (s, 8H), 7.50 (s, 4H); ^{13}C NMR (75 MHz, $CDCl_3$) δ 11.51, 18.88, 91.06, 91.31, 93.19, 106.79, 123.03, 123.23, 123.76, 131.57, 131.78, 132.22, 147.43.

Compound (20). Compound **19** (43.9 mg, 0.07 mmol) was dissolved in THF (3 mL) and the solution degassed with argon. Then TBAF (0.40 mL of 1 M THF solution, 0.40 mmol) was added via syringe. A white solid precipitated immediately and the mixture was left stirring at room temperature for 5 h. After this time, the solvent was removed and the crude redissolved in CH_2Cl_2 (50 mL), transferred to a separatory funnel, washed with brine (2 x 50 mL) and water (2 x 50 mL), dried on $MgSO_4$, and the solvent was removed. The crude product was further purified by flash chromatography (silica gel, hexane then 4:1, 7:3 hexane/CH_2Cl_2 to give the desired product (R_F = 0.34 in 4:1 hexane/CH_2Cl_2) as a white crystalline solid. Yield = 14.7 mg (66%). ^{1}H NMR (300 MHz, $CDCl_3$) δ 4.00 (s, 2H), 7.45 (s, 8H), 7.50 (s, 4H).

1,4-Diiodo-2,5-bis-[(S)-(+)-2-methylbutanoxy]benzene (21). 2,5-Diiodohydroquinone (200 mg, 0.55 mmol) was dissolved in DMF (3 mL) and the solution degassed with argon for 15 min. Then K_2CO_3 (455 mg, 3.3 mmol) was added and the mixture stirred at room temperature for 30 min. Then (S)-(+)-1-bromo-2-methylbutane (0.2 mL, 249.2 mL, 1.65 mmol) was added via syringe and the mixture was stirred at 60 ^{o}C for 3 h. After this time, TLC (1:1 hexane/CH_2Cl_2) showed no more starting material (R_F = 0.05) and a new spot (R_F = 0.25) was apparent. After cooling to room temperature, water (10 mL) was added and mixture transferred to a separatory

funnel. The aqueous phase was extracted with CH_2Cl_2 (3 x 20 mL), the organic phase dried on $MgSO_4$, and the solvent was removed. The crude red oil obtained was further purified by flash chromatography (silica gel, hexane then 4:1, 3:2 hexane/CH_2Cl_2) to give the desired product as white crystalline solid. Yield = 176 mg (64%). ^{1}H NMR (300 MHz, $CDCl_3$) δ 0.97 (t, 6H), 1.08 (d, 6H), 1.32 (m, 2H), 1.62 (m, 2H), 1.90 (m, 2H), 3.80 (m, 4H), 7.17 (s, 2H); ^{13}C NMR (75 MHz, $CDCl_3$) δ 11.61, 16.90, 26.26, 34.96, 74.96, 86.24, 122.48, 152.87.

1,4-Bis-[(S)-(+)-2-methylbutanoxy]-2,5-bis(trimethylsilylethynyl)benzene (22). 1,4-Diiodo-2,5-bis-[(S)-(+)-2-methylbutanoxy]benzene (175 mg, 0.35 mmol) was dissolved in THF (6 mL) and *i*-Pr_2NH (4 mL) in a Schlenk flask and the solution was degassed with argon for 15 min. Then trimethylsilylacetylene (75.2 mg, 0.11 mL, 0.76 mmol), $Pd(PPh_3)_4$ (40.1 mg, 0.035 mmol) and CuI (3.8 mg, 0.02 mmol) were added and the reaction mixture stirred at 50 ^{o}C for 4 h. After this time, TLC (2:1 CH_2Cl_2/hexane) showed no more starting material (R_F = 0.36) and a new blue fluorescent spot (R_F = 0.19) was apparent. After cooling down, the solvents were removed and the crude product was purified by flash chromatography (silica gel, hexane then 4:1, 3:2, 1:1, 1:2, 1:4 hexane/CH_2Cl_2 and finally pure CH_2Cl_2) to give the desired product as a white solid. Yield = 151.7 mg (98%). ^{1}H NMR (300 MHz, $CDCl_3$) δ 0.26 (s, 18H), 0.96 (t, 6H), 1.08 (d, 6H), 1.30 (m, 2H), 1.64 (m, 2H), 1.88 (m, 2H), 3.78 (m, 4H), 6.90 (s, 2H); ^{13}C NMR (75 MHz, $CDCl_3$) δ 0.15, 11.66, 16.71, 26.30, 35.16, 74.27, 100.15, 101.25, 114.01, 116.96, 154.29.

1,4-Bis-[(S)-(+)-2-methylbutanoxy]-2,5-bis-ethynylbenzene (23). 1,4-Bis-[(S)-(+)-2-methylbutanoxy]-2,5-bis-trimethylsilylethynylbenzene (151 mg, 0.34 mmol) was

dissolved in THF (8 mL) and the solution was degassed with argon. Then TBAF (2 mL of 1 M THF solution, 2.04 mmol) was added via syringe and the mixture stirred at room temperature protected from light for 2 h. After this time, TLC (CH_2Cl_2) showed no more starting material ($R_F = 0.5$) and a new spot below it ($R_F = 0.36$). The solvent was removed at room temperature and the crude product was purified by flash chromatography (silica gel, hexane then 1:1 and 2:3 hexane/CH_2Cl_2) to give the desired product as a brown crystalline solid. Yield = 78.0 mg (77%). ^{1}H NMR (300 MHz, $CDCl_3$) δ 0.95 (t, 6H), 1.03 (d, 6H), 1.28 (m, 2H), 1.58 (m, 2H), 1.88 (m, 2H), 3.33 (s, 2H), 3.78 (m, 4H), 6.95 (s, 2H); ^{13}C NMR (75 MHz, $CDCl_3$) δ 11.55, 16.71, 26.26, 34.88, 75.48, 79.92, 82.57, 113.32, 117.66, 154.24.

3-(4-iodophenyl)-prop-2-yn-1-ol (24). 1,4-Diiodobenzene (1.13 g, 3.44 mmol) was dissolved in THF (12 mL) and *i*-Pr_2NH (8 mL) in a Schlenk flask and the solution was degassed with argon. Then propargyl alcohol (128 mg, 2.29 mmol), $Pd(PPh_3)_4$ (198 mg, 0.17 mmol) and CuI (65 mg, 0.34 mmol) were added and the mixture stirred at room temperature for 20 h. Then, water (50 mL) and Et_2O (50 mL) were added and the mixture transferred to a separatory funnel. The aqueous phase was extracted with Et_2O (3 x 50 mL), the combined organic phase washed with brine (3 x 50 mL), dried on $MgSO_4$, and the solvent was removed. The crude product was purified by flash chromatography (silica gel, 4:1, 3:2, 2:3, 1:4 hexane/CH_2Cl_2 and finally pure CH_2Cl_2) to give the desired product as a light yellow solid. Yield = 360.7 mg (61%). ^{1}H NMR (300 MHz, $CDCl_3$) δ 2.30 (s, 1H), 4.48 (s, 2H), 7.40 (dd, 4H); ^{13}C NMR (75 MHz, $CDCl_3$) δ 51.69, 84.91, 88.79, 94.64, 122.15, 133.29, 137.62.

3-[4-(3,4,5-tris(dodecyloxy)ethynylbenzene)-phenyl]-prop-2-yn-1-ol (25). 3-(4-iodophenyl)-prop-2-yn-1-ol (360.7 mg, 1.4 mmol) was dissolved in THF (9 mL) and *i*-Pr_2NH (6 mL) in a Schlenk flask and the solution was degassed with argon for 30 min. Then, 3,4,5-tris-(dodecyloxy)ethynylbenzene (962.2 mg, 1.47 mmol), $Pd(PPh_3)_4$ (80.8 mg, 0.07 mmol) and CuI (26.6 mg, 0.14 mmol) were added and the mixture stirred at 70 ^oC for 2 hours. After this time, TLC (CH_2Cl_2) showed no more starting material and a new bright blue fluorescent spot (R_F = 0.52) was apparent. Therefore, Et_2O (20 mL) and water (20 mL) were added and the mixture transferred to a separatory funnel. The aqueous phase was extracted with Et_2O (3 x 20 mL), the combined organic phase was washed with 5% HCl (2 x 50 mL) and brine (2 x 50 mL), dried on $MgSO_4$, and the solvent was removed. The crude product was purified by flash chromatography (silica gel, 4:1, 3:2, 2:3, 1:4 hexane/CH_2Cl_2 and finally pure CH_2Cl_2) to give the desired product a sticky orange solid. Yield = 956.6 mg (87%). ^1H NMR (300 MHz, $CDCl_3$) δ 0.88 (t, 9H), 1.26 (s, 48H), 1.46 (m, 6H), 1.78 (m, 6H), 2.66 (s, 1H), 3.96 (m, 6H), 4.47 (s, 2H), 6.72 (s, 2H), 7.40 (dd, 4H); ^{13}C NMR (75 MHz, $CDCl_3$) δ 14.27, 22.87, 26.26, 29.50, 29.55, 29.58, 29.77, 29.83, 29.84, 29.88, 29.91, 29.93, 30.47, 32.10, 51.57, 69.26, 73.74, 85.18, 87.86, 89.39, 91.81, 110.26, 117.57, 122.42, 123.54, 131.46, 131.70, 153.09.

5-(4-ethynyl-phenylethynyl)-1,2,3-tris(dodecyloxy)benzene (26). 3-[4-(3,4,5-Tris(dodecyloxy)ethynylbenzene)-phenyl]-prop-2-yn-1-ol (956.6 mg, 1.22 mmol) was dissolved in dry Et_2O and the solution degassed with nitrogen. Then, activated MnO_2 (1.70 g, 19.52 mmol) and KOH (548 mg, 9.76 mmol) were added in four fractions every hour and mixture was stirred at room temperature for 22 hours protected from light. After this time, the mixture was passed through a bed of Celite and transferred to a separatory

funnel. The solution was washed with 5% HCl (2 x 100 mL) and water (2 x 50 mL), dried on $MgSO_4$, and the solvent was removed. The crude product was purified by flash chromatography (silica gel, hexane, then 7:3, 3:2 hexane/CH_2Cl_2) to give the desired product as an orange solid. Yield = 457.9 mg (50 %). ^{1}H NMR (300 MHz, $CDCl_3$) δ 0.88 (t, 9H), 1.26 (s, 48H), 1.46 (m, 6H), 1.78 (m, 6H), 3.14 (s, 1H), 3.96 (m, 6H), 6.72 (s, 2H), 7.44 (s, 4H); ^{13}C NMR (75 MHz, $CDCl_3$) δ 14.28, 22.89, 26.27, 26.30, 29.52, 29.59, 29.60, 29.80, 29.85, 29.87, 29.91, 19.94, 30.52, 32.13, 69.22, 73.64, 79.05, 83.39, 87.74, 92.05, 110.24, 117.48, 121.89, 124.05, 131.48, 132.16, 139.42, 153.17.

Pt2M. *trans*-[3,4,5-Tris(dodecyloxy)phenylethynyl]-chloro-bis(trimethylphosphine)platinum(II) **18** (297.2 mg, 0.287 mmol) was placed in THF (10 mL) and Et_2NH (10 mL) in a Schlenk flask and the solution was degassed with argon for 15 min. Then, 1,4-diethynylbenzene (18.0 mg, 0.14 mmol) and CuI (2.6 mg, 0.014 mmol) were added and the mixture stirred at room temperature for 3 h. After this time, TLC showed no more platinum complex starting material and a new yellow-green phosphorescent spot (R_F = 0.65, CH_2Cl_2) was apparent. Therefore the solvents were removed and the crude product purified by flash chromatography (silica gel, 2:3, 3:2, 4:1 $CHCl_3$/hexane, $CHCl_3$, and finally $CHCl_3$ + 3% MeOH) to give a yellow solid. The product was precipitated from 10:1 acetone/CH_2Cl_2 to give the desired product as an off-white solid. Yield = 275.5 mg (92%). ^{1}H NMR (300 MHz, $CDCl_3$) δ 0.90 (t, 18H), 1.35 (s, 96 H), 1.50 (m, 12H), 1.80 (m, 48H), 3.98 (m, 12H), 6.55 (s, 4H), 7.18 (s, 4H); ^{13}C NMR (75 MHz, $CDCl_3$) δ 14.24, 15.29, 15.55, 15.81, 22.81, 26.24, 29.49, 29.55, 29.78, 29.82, 29.86, 30.44, 32.05, 69.16, 73.54, 109.07, 109.19, 109.96, 123.02, 125.37, 130.78,

137.34, 152.76; ^{31}P NMR (121 MHz, $CDCl_3$) δ – 19.39 (J_{Pt-P} = 2293.0 Hz); Elemental anal. calc'd C 62.12, H 9.19, found C 62.37, H 9.48.

Pt2MT. *trans*-[3,4,5-Tris(dodecyloxy)phenylethynyl]-chloro-bis(trimethylphosphine)platinum(II) **18** (127.0 mg, 0.122 mmol) was placed in Et_2NH (5 mL) in a Schlenk flask and the solution was degassed with argon for 15 min. Then, 2,5-diethynylthiophene (7.9 mg, 0.06 mmol) and CuI (1.1 mg, 0.006 mmol) were added and the mixture stirred at room temperature for 4 h. After this time, TLC showed no more evolution, with some platinum complex starting material remaining, and a new red phosphorescent spot (R_F = 0.43, CH_2Cl_2) was apparent. Therefore the solvents were removed and the crude product purified by flash chromatography (silica gel, 1:1, 3:2, 7:3, 4:1 $CHCl_3$/hexane and finally pure $CHCl_3$) to give a yellow solid. The product was precipitated from 10:1:1 acetone/CH_2Cl_2/MeOH to give the desired product as an off-white solid. Yield = 69.3 mg (54%). ^{1}H NMR (300 MHz, $CDCl_3$) δ 0.88 (t, 18H), 1.26 (s, 96H), 1.46 (m, 12H), 1.74 (m, 48H), 3.92 (m, 12H), 6.53 (s, 4H), 6.68 (s, 2H); ^{13}C NMR (75 MHz, $CDCl_3$) δ 14.32, 15.36, 15.62, 15.89, 22.88, 26.29, 29.56, 29.58, 29.61, 29.85, 29.89, 29.93, 30.49, 32.11, 53.62, 69.18, 73.62, 109.85, 122.97, 127.86, 137.32, 152.80; ^{31}P NMR (75 MHz, $CDCl_3$) δ – 19.24 (J_{Pt-P} = 2296.3 Hz); Elemental anal. calc'd 60.82, H 9.07, found C 61.22, H 9.41.

Pt2MP3. Compound **20** (14.7 mg, 0.045 mmol) and *trans*-[3,4,5-tris(dodecyloxy)phenylethynyl]-chloro-bis(trimethylphosphine)platinum(II) **18** (95.7 mg, 0.092 mmol) were placed in THF (3 mL) and Et_2NH (3 mL) in a Schlenk flask and the solution was degassed with argon for 15 min. Then CuI (0.8 mg, 0.004 mmol) was added and the mixture stirred at room temperature for 6 h. After this time, TLC showed no more

starting material **20** and a new orange phosphorescent spot (R_F = 0.35, 2:1 CH_2Cl_2/hexane) was apparent. Therefore the solvents were removed and the crude product was purified by flash chromatography (silica gel, hexane then 4:1, 3:2, 2:3, 1:4 hexane/CH_2Cl_2, pure CH_2Cl_2 and finally CH_2Cl_2 + 3% MeOH) to give a yellow solid. The product was precipitated from 10:1:1 acetone/CH_2Cl_2/MeOH to give the desired product as a sticky orange solid. Yield = 64.0 mg (61%). ^{1}H NMR (300 MHz, $CDCl_3$) δ 0.90 (t, 18H), 1.25 (s, 96H), 1.45 (m, 12H), 1.75 (m, 48H), 3.90 (m, 12H), 6.55 (s, 4H), 7.30 (dd, 8H), 7.45 (s, 4H); ^{13}C NMR (75 MHz, $CDCl_3$) δ 14.34, 15.37, 15.64, 15.90, 22.90, 26.32, 29.58, 29.60, 29.63, 29.87, 29.91, 29.95, 30.52, 32.13, 69.22, 73.65, 109.94, 131.22, 131.48, 131.58, 152.84; ^{31}P NMR (121 MHz, $CDCl_3$) δ – 19.23 (J_{Pt-P} = 2294.1 Hz); Elemental anal. calc'd C 65.03, H 8.75, found C 65.24, H 9.07.

Pt2MC. *trans*-[3,4,5-Tris(dodecyloxy)phenylethynyl]-chloro-bis(trimethylphosphine)platinum(II) **18** (168.2 mg, 0.162 mmol) was placed in THF (5 mL) and Et_2NH (5 mL) in a Schlenk flask and the solution was degassed with argon for 15 min. Then 1,4-bis-[(S)-(+)-2-methylbutanoxy]-2,5-bis(ethynyl)benzene (23.6 mg, 0.08 mmol) and CuI (1.0 mg, 0.008 mmol) were added and the mixture stirred at room temperature for 3 h. After this time, TLC showed no more starting material and a new yellow phosphorescent spot (R_F = 0.47, CH_2Cl_2) was apparent. Therefore the solvents were removed and the crude product was purified by flash chromatography (silica gel, hexane then 3:2, 2:3, 1:4 hexane/$CHCl_3$ and finally pure $CHCl_3$) to give a red solid. The product was precipitated from 10:1:1 acetone/CH_2Cl_2/MeOH to give the desired product as yellow solid. Yield = 140.7 mg (78%). ^{1}H NMR (300 MHz, $CDCl_3$) δ 0.88 (m, 24H), 0.98 (d, 6H), 1.26 (s, 98H), 1.46 (m, 12H), 1.62 (m, 2H), 1.76 (m, 50H), 3.74 (dt, 4H),

3.92 (m, 12H), 6.50 (s, 4H), 6.76 (s, 2H); ^{13}C NMR (75 MHz, $CDCl_3$) δ 11.50, 14.28, 15.37, 15.63, 15.89, 16.81, 22.83, 26.24, 26.30, 29.51, 29.29.80, 29.84, 29.89, 30.44, 32.06, 34.62, 69.08, 73.54, 74.24, 109.42, 109.83, 117.25, 123.04, 136.38, 137.17, 147.35, 147.37, 152.72, 153.08; ^{31}P NMR (121 MHz, $CDCl_3$) δ – 19.10 (J_{Pt-P} = 2309.5 Hz); Elemental anal. calc'd C 62.69, H 9.38, found C 63.20, H 9.73.

PE3. 1,4-Diiodobenzene (97.6 mg, 0.3 mmol) was dissolved in THF (18 mL) and *i*-Pr_2NH (12 mL) in a Schlenk flask and the solution was degassed with argon. Then, 5-(4-ethynyl-phenylethynyl)-1,2,3-tris(dodecyloxy)benzene (457.9 mg, 0.61 mmol), $Pd(Ph_3)_4$ (17.1 mg, 0.015 mmol) and CuI (5.6 mg, 0.03 mmol) were added and the mixture stirred at 50 ^{o}C for 3 hours. After this time, TLC (2:1 hexane/CH_2Cl_2) showed no more 1,4-diiodobenzene (R_F = 0.87) and a new bright blue fluorescent spot (R_F = 0.44) was apparent. The mixture was diluted to 6 mL with CH_2Cl_2, transferred to a separatory funnel, washed with water (3 x 40 mL), dried on $MgSO_4$, and the solvents were removed. The crude product was purified by flash chromatography (silica gel, hexane then 4:1, 7:3 and 3:2 hexane/CH_2Cl_2) to give the desired product as a bright yellow solid. Yield = 405.1 mg (86%). ^{1}H NMR (300 MHz, $CDCl_3$) δ 0.88 (t, 18H), 1.26 (s, 96H), 1.46 (m, 12H), 1.78 (m, 12H), 3.96 (m, 12H), 6.73 (s, 4H), 7.48 (s, 12H); ^{13}C NMR (75 MHz, $CDCl_3$) δ 14.30, 22.89, 26.28, 29.52, 29.58, 29.60, 29.79, 29.85, 29.91, 29.95, 30.52, 32.13, 69.22, 73.65, 87.99, 91.05, 91.31, 92.13, 110.23, 117.53, 122.76, 123.20, 123.64, 131.70, 132.64, 139.39, 153.17; Elemental anal. calc'd C 83.38, H 10.56, found C 84.48, H 11.03.

CHAPTER 5
CONCLUSION

In previous chapters, different aspects of the photophysical properties of platinum acetylide oligomers have been presented. The oligomers were designed to gain some insight into the photophysical properties of these promising materials, but also on the triplet excited state in general as it has been studied less than the singlet excited state. The importance of the triplet excited state in all-organic systems where it is usually silent has only recently been recognized. The studies presented in previous chapters may therefore help understand the photophysical properties of triplet excited states in all-organic and metal-organic conjugated systems.

A series of platinum acetylide oligomers containing oligothiophene units incorporated in the main chain have been prepared in an effort to examine the effect of low-energy traps on the triplet excited state. Although more localized than the singlet exciton, the triplet exciton was found to be very sensitive to the presence of low-energy sites. Triplet excitons were efficiently trapped by the oligothienyl-based units, from which relaxation occurred. Depending on the energy level of the trap, two scenarios were observed. In one case where the trap is relatively close in energy to the normal energy level, relaxation occurred by radiative decay of the triplet excited state of the trap. Evidence for an equilibrium between two excited states was observed and phosphorescence remained the main channel of deactivation. In a second case, where the energy of the trap is much lower than the normal triplet excited, phosphorescence was almost entirely lost. Governed by the energy gap law, the triplet excited state of the

lowest energy traps relaxed through nonradiative channels and their emission spectra were dominated by short lived fluorescence. Moreover, experimental evidence suggests that the equilibrium is not operating when the energy gap between excited state is large. This study suggests that the triplet exciton can migrate as well as the singlet exciton and is therefore subject to being quenched by low energy sites.

In a second study, the same oligothiophene-containing platinum acetylide oligomer series, as well as a series of oligomers of increasing chain length were studied by electrochemistry and pulse radiolysis. The radical anions of the platinum acetylide oligomers were found to be relatively unstable and very localized. On the other hand, the radical cations displayed reversible oxidations and seemed more stable on the electrochemical timescale. The radical cations seemed relatively localized, although not as much as the radial anions. Evidence for possible multiple oxidations was found, suggesting a relatively weak electronic coupling. Electronic absorption of the radical ions displayed two transition bands, one in the visible attributed to a transition from ligand-localized HOMO to SUMO and a second transition in the near-IR which origin was not clearly determined.

Finally, a third study was devoted to self-assembling platinum acetylide oligomers in order to probe the consequences of aggregation on the triplet excited state. A series of different oligomers sharing long alkyl end-chains were synthesized toward this goal. The materials displayed rich physical properties with liquid-crystalline mesophases and the formation of gel in saturated hydrocarbon solvents. The consequences of aggregation were found to fall into one of two categories. In one group, absorption of aggregates was manifested by a blue-shifted absorption, attributed to H-aggregates. The photophysical

properties were almost intact and strong phosphorescence was observed even in aggregates. Phosphorescence from a high-energy triplet excited state conformer was observed but no dramatic change on the photoluminescence was otherwise observed. In a second group, aggregation resulted in the appearance of a sharp red-shifted peak in the absorption spectrum. The possibility that this could be due to a simple planarization induced by aggregation was considered but other signs point out to the presence of J-aggregates. In this case, the phosphorescence was seen to disappear almost completely from the photoluminescence of aggregates, at the expense of a strong fluorescence emission. The molecular exciton model was used assuming co-planar dimers and some geometrical parameters of the aggregates were calculated. This study highlights the fact that while aggregation may have practically no impact on the triplet excited state, in some cases, the consequences are dramatic and the photophysical properties of the material may be entirely compromised.

APPENDIX
NMR SPECTRA

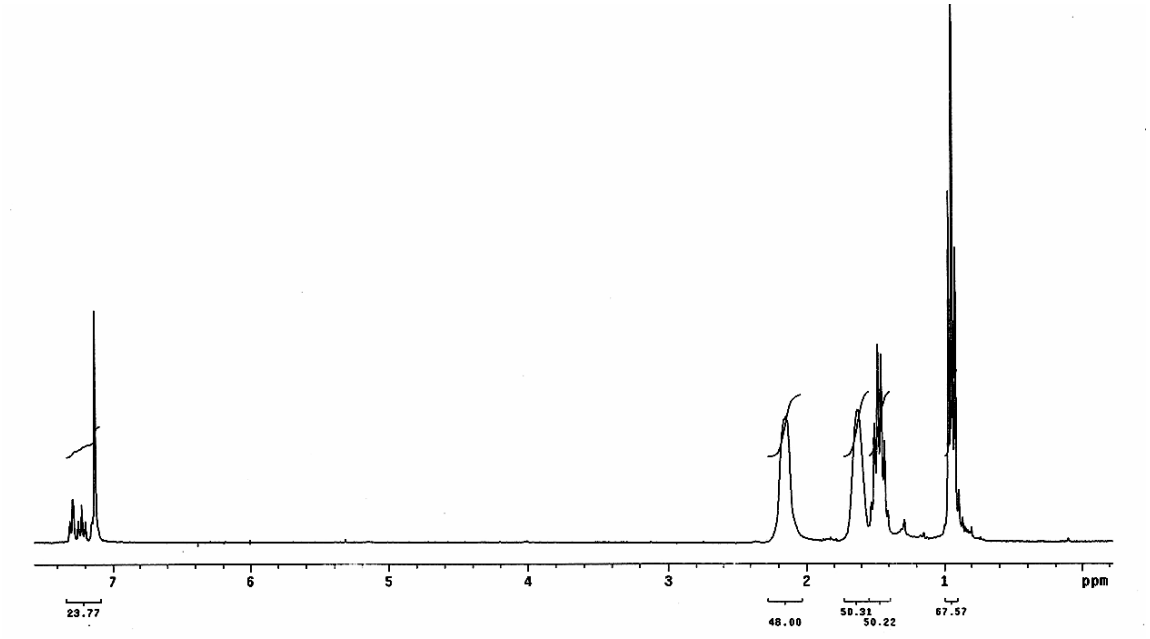

Figure A-1. ^{1}H NMR (300 MHz, $CDCl_3$) spectrum of **Pt4**.

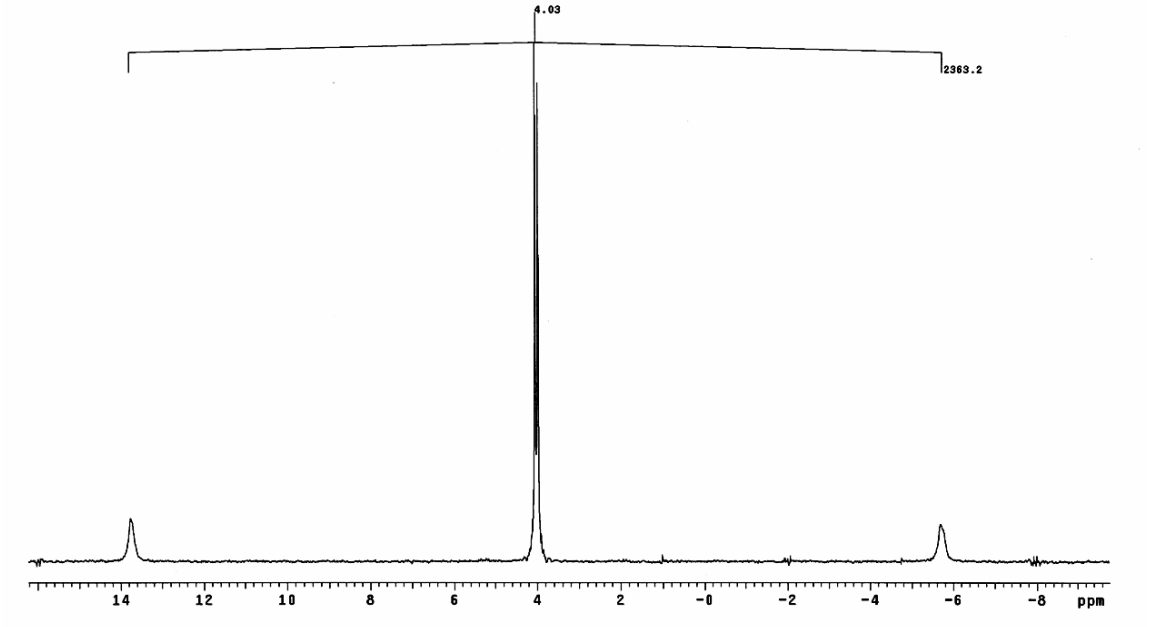

Figure A-2. ^{31}P NMR (121 MHz, $CDCl_3$) spectrum of **Pt4**.

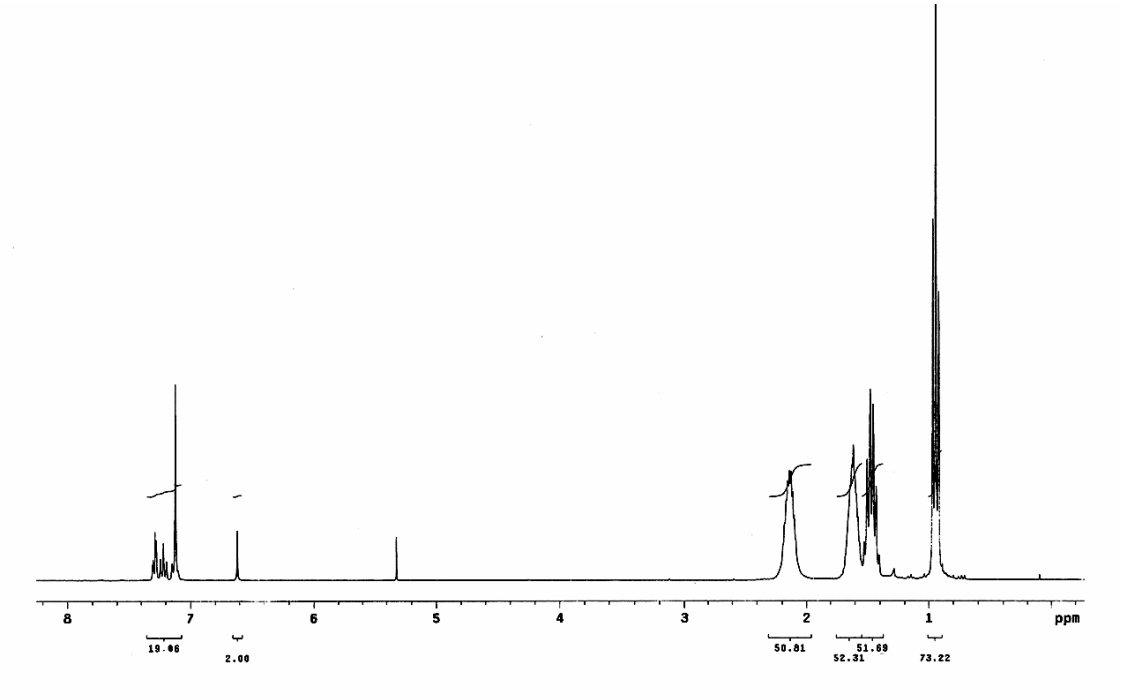

Figure A-3. ^{1}H NMR (300 MHz, $CDCl_3$) spectrum of **Pt4T1**.

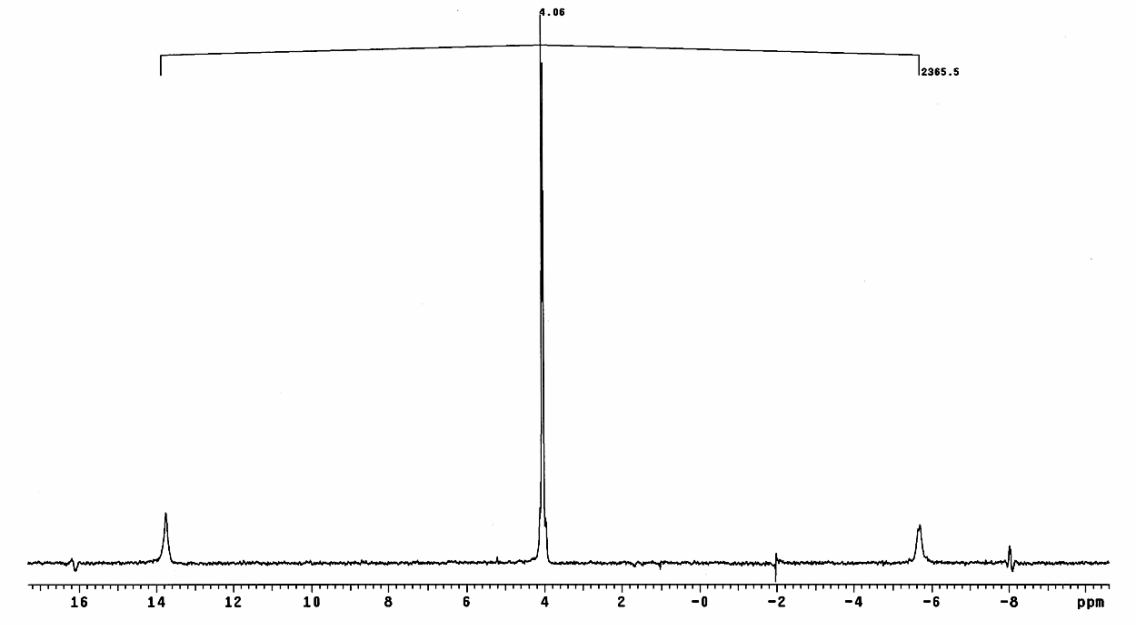

Figure A-4. ^{31}P NMR (121 MHz, $CDCl_3$) spectrum of **Pt4T1**.

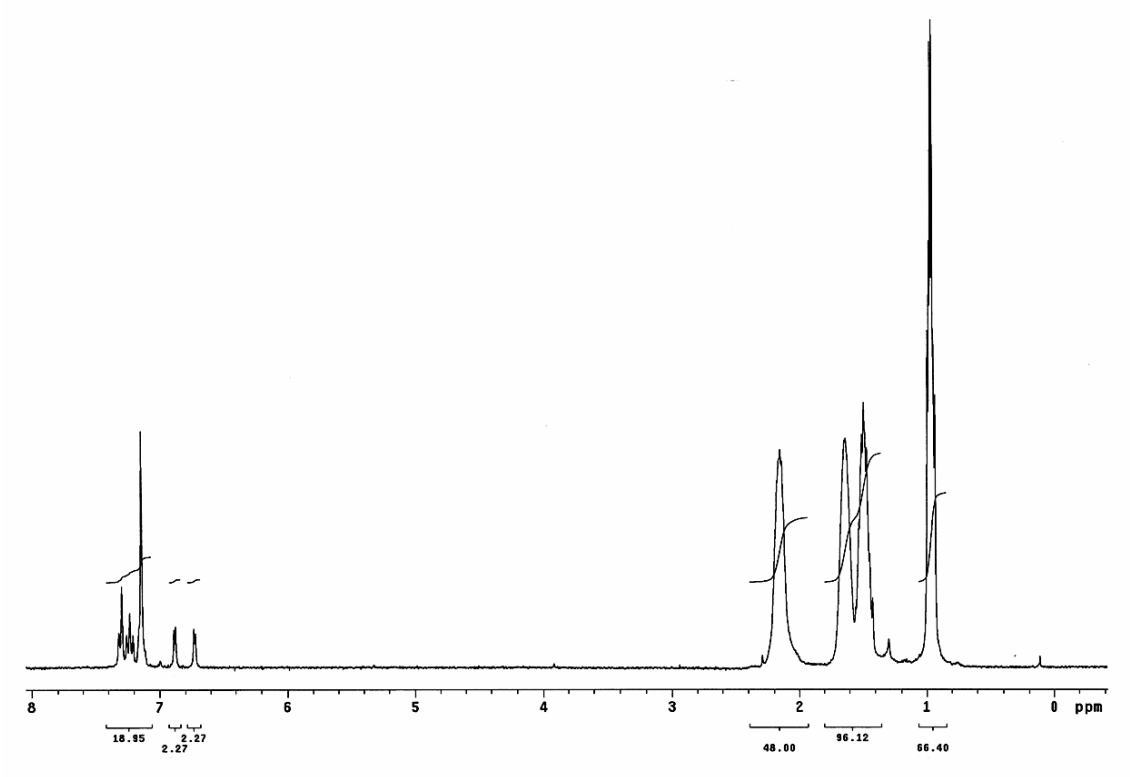

Figure A-5. ^{1}H NMR (300 MHz, $CDCl_3$) spectrum of **Pt4T2**.

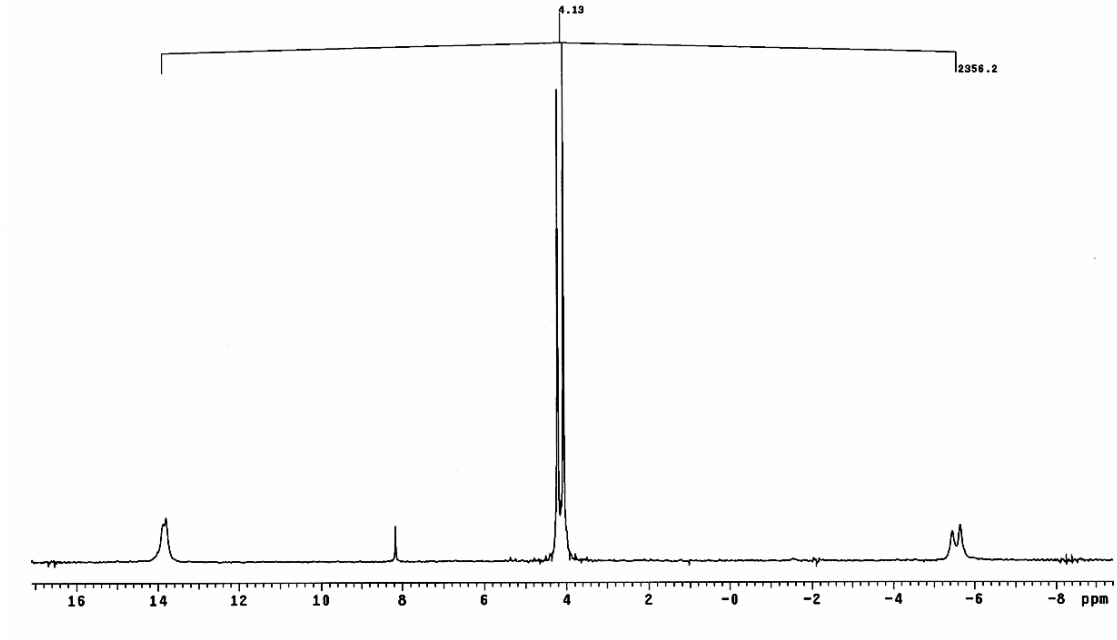

Figure A-6. ^{31}P NMR (121 MHz, $CDCl_3$) spectrum of **Pt4T2**.

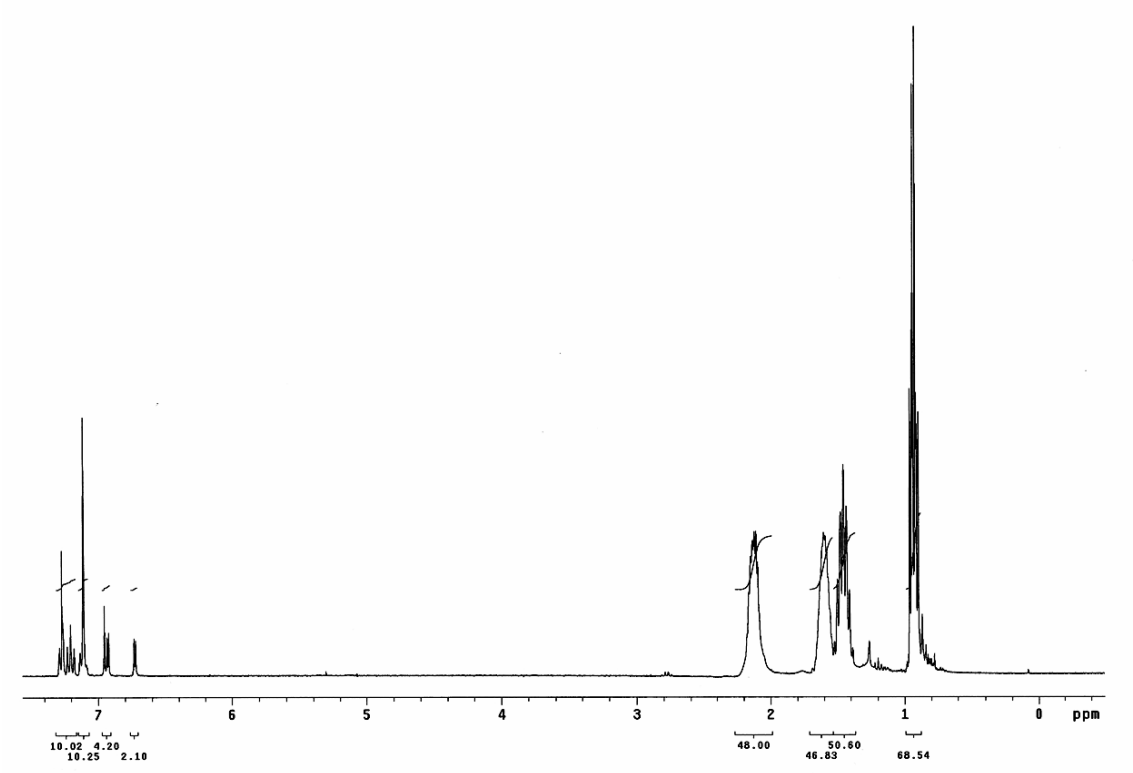

Figure A-7. ^{1}H NMR (300 MHz, $CDCl_3$) spectrum of **Pt4T3**.

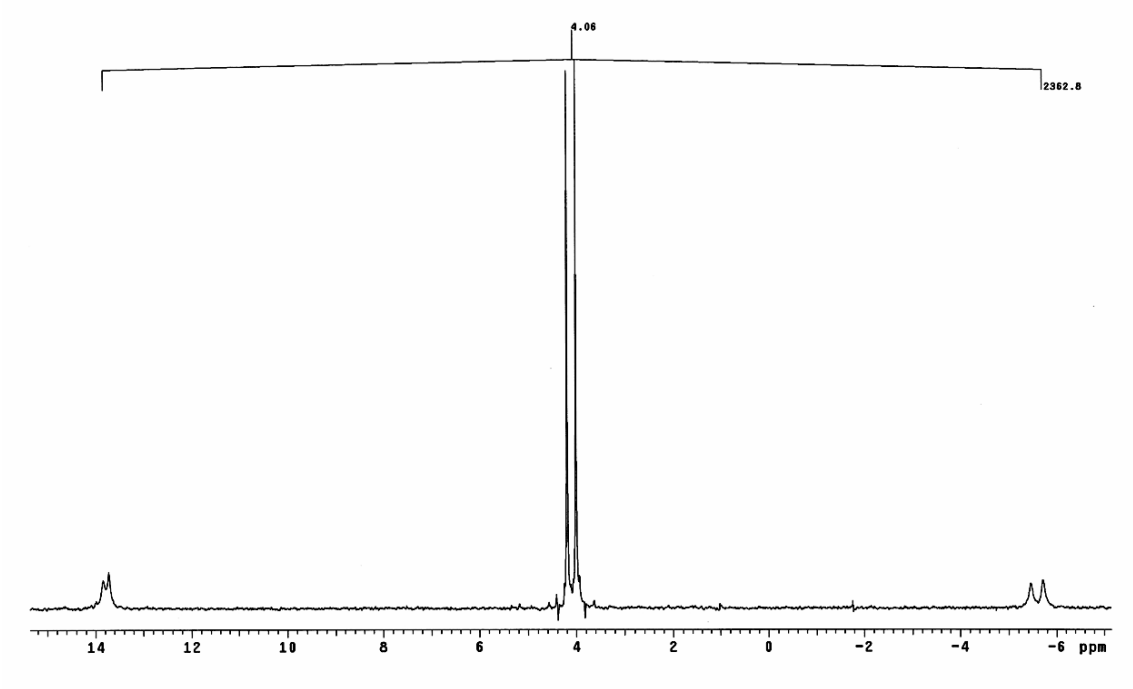

Figure A-8. ^{31}P NMR (121 MHz, $CDCl_3$) spectrum of **Pt4T3**.

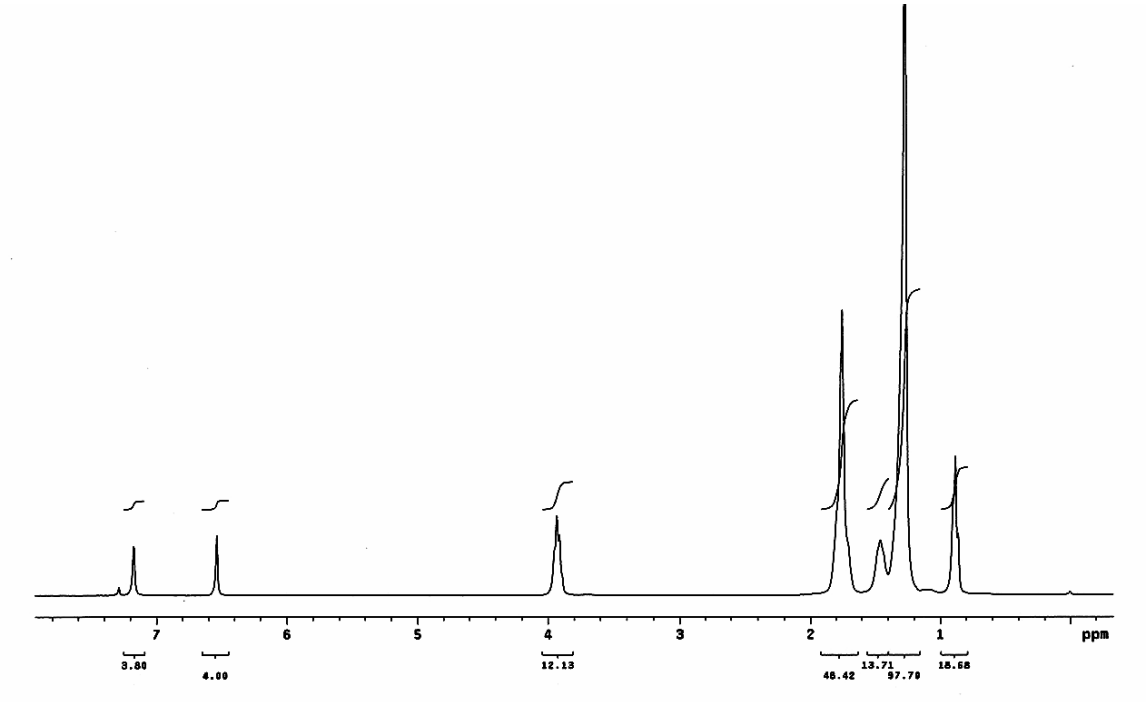

Figure A-9. ^{1}H NMR (300 MHz, $CDCl_3$) spectrum of **Pt2M**.

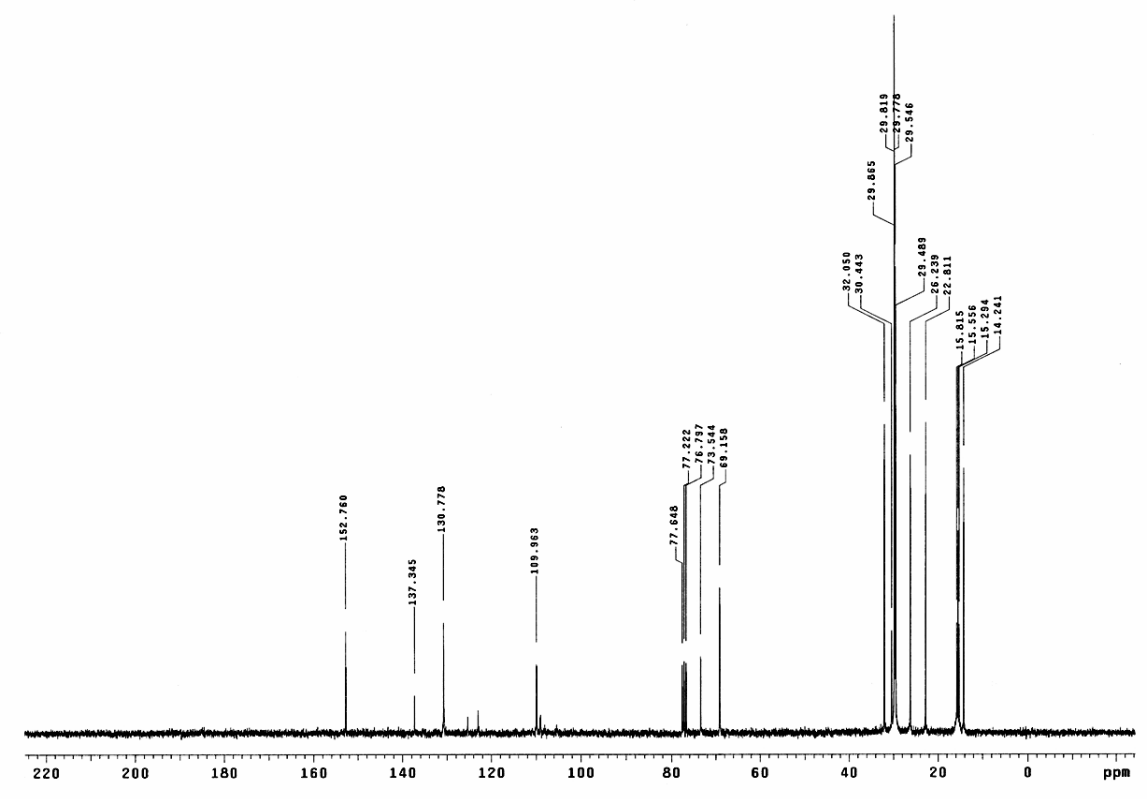

Figure A-10. ^{13}C NMR (75 MHz, $CDCl_3$) spectrum of **Pt2M**.

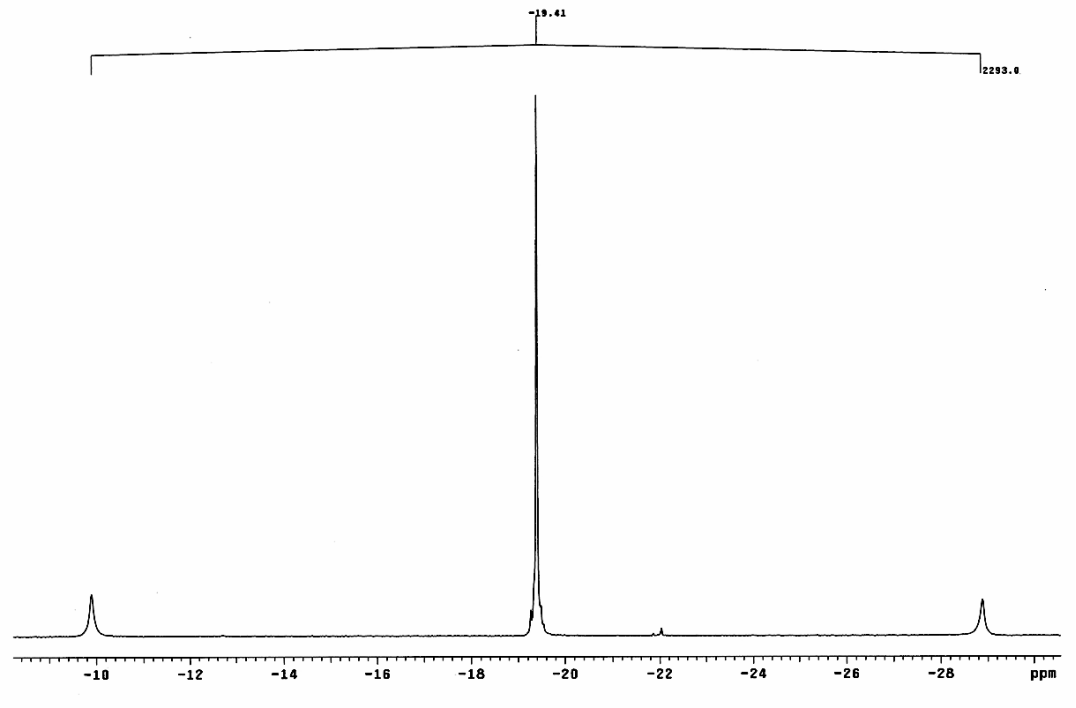

Figure A-11. ^{31}P NMR (121 MHz, $CDCl_3$) spectrum of **Pt2M**.

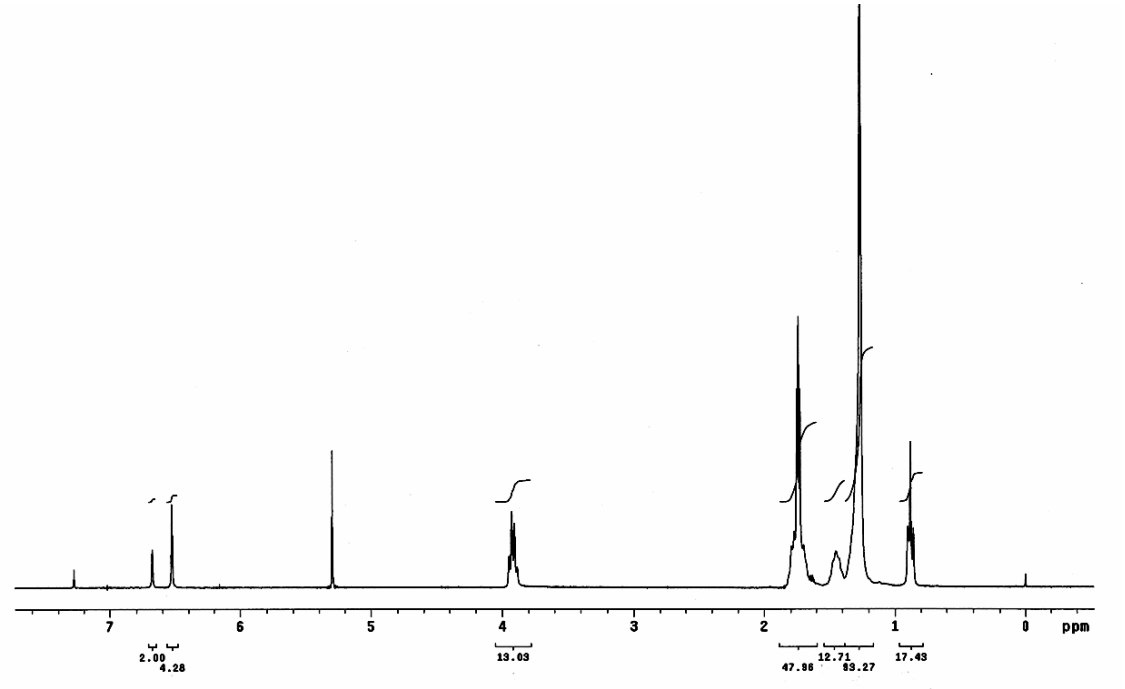

Figure A-12. ^{1}H NMR (300 MHz, $CDCl_3$) spectrum of **Pt2MT**.

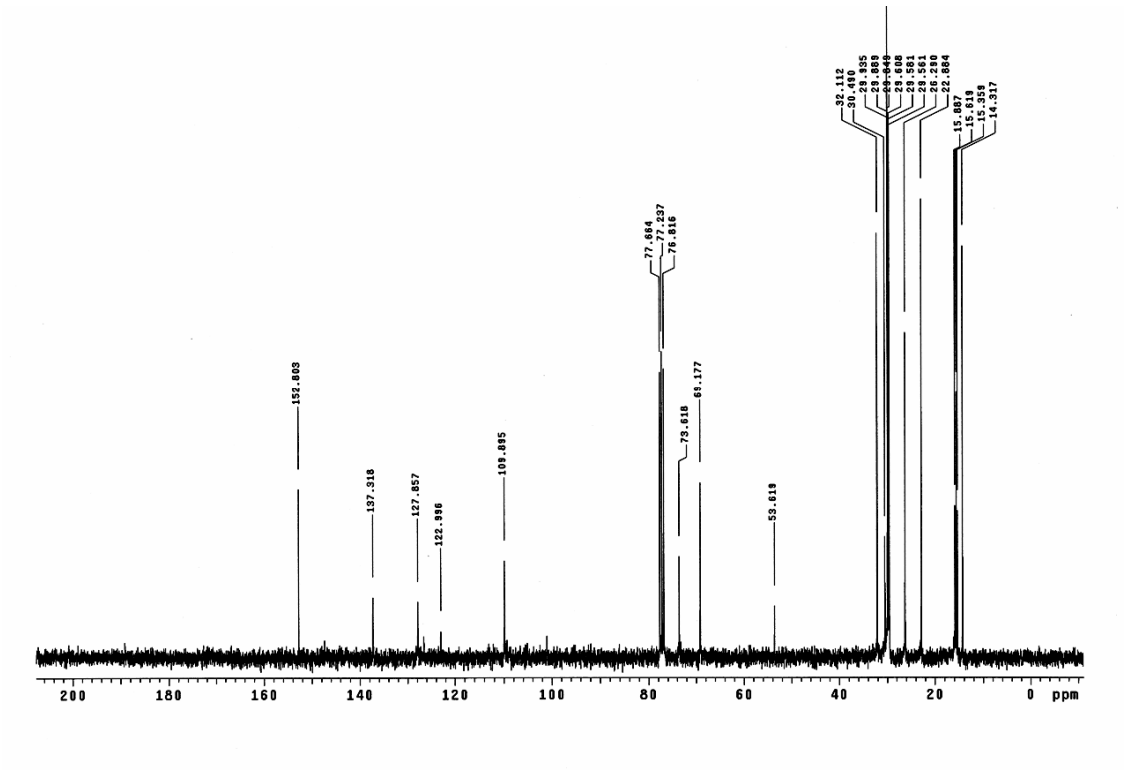

Figure A-13. ^{13}C NMR (75 MHz, $CDCl_3$) spectrum of **Pt2MT**.

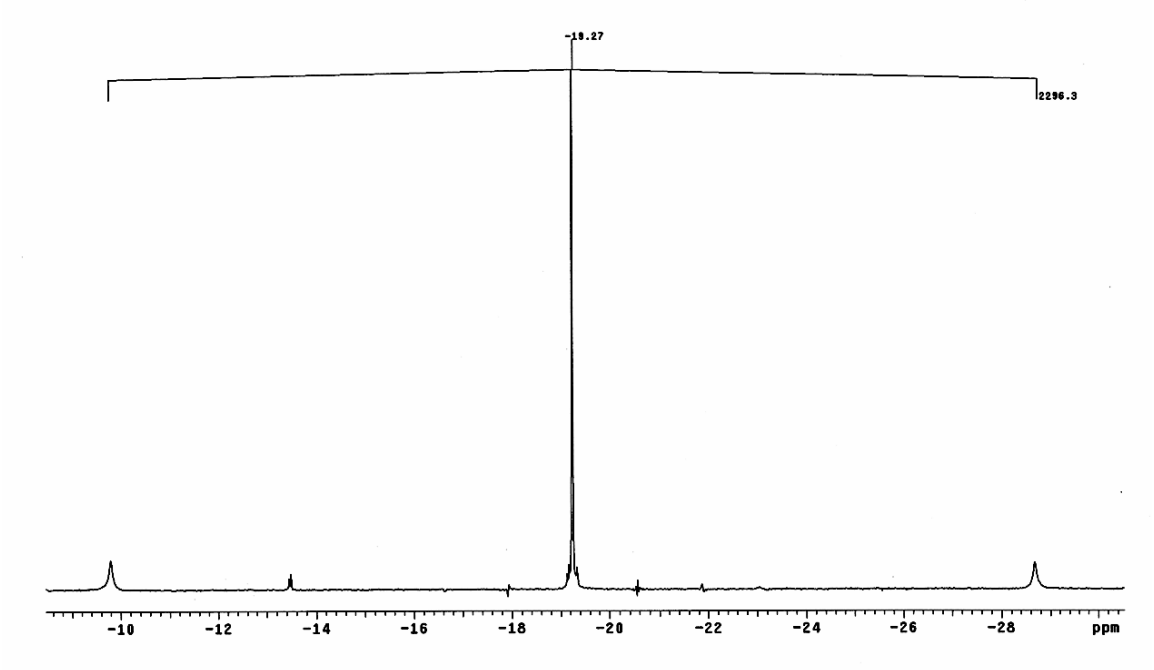

Figure A-14. ^{31}P NMR (121 MHz, $CDCl_3$) spectrum of **Pt2MT**.

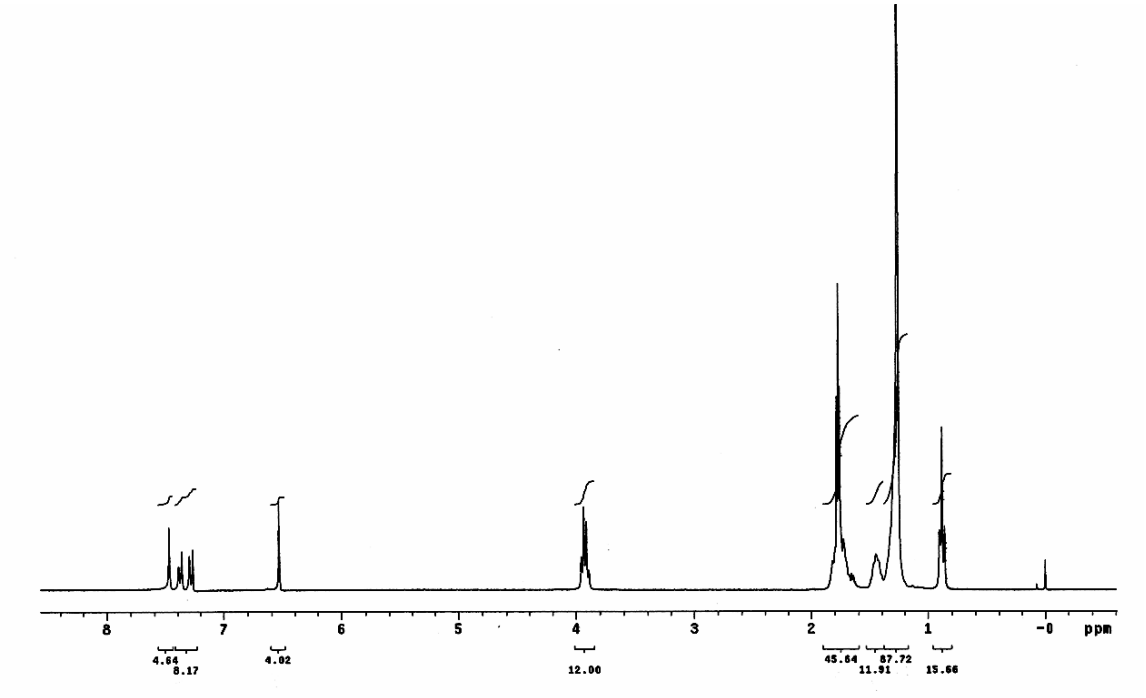

Figure A-15. ^{1}H NMR (300 MHz, $CDCl_3$) spectrum of **Pt2MP3**.

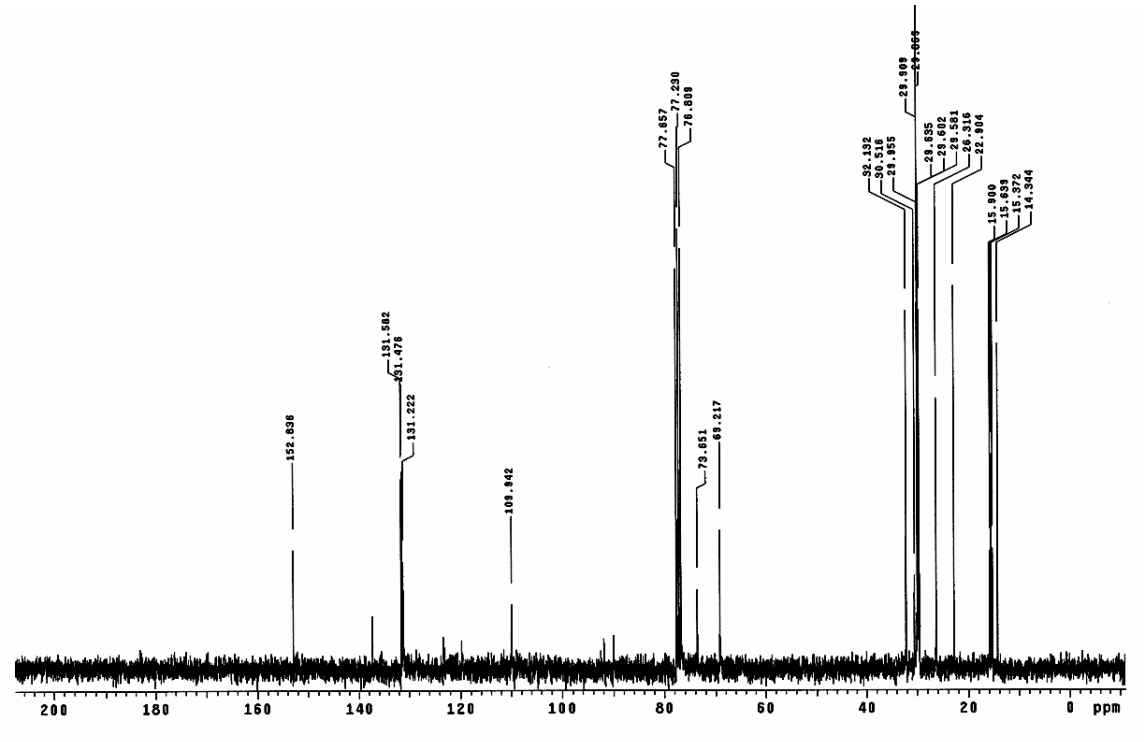

Figure A-16. ^{13}C NMR (75 MHz, $CDCl_3$) spectrum of **Pt2MP3**.

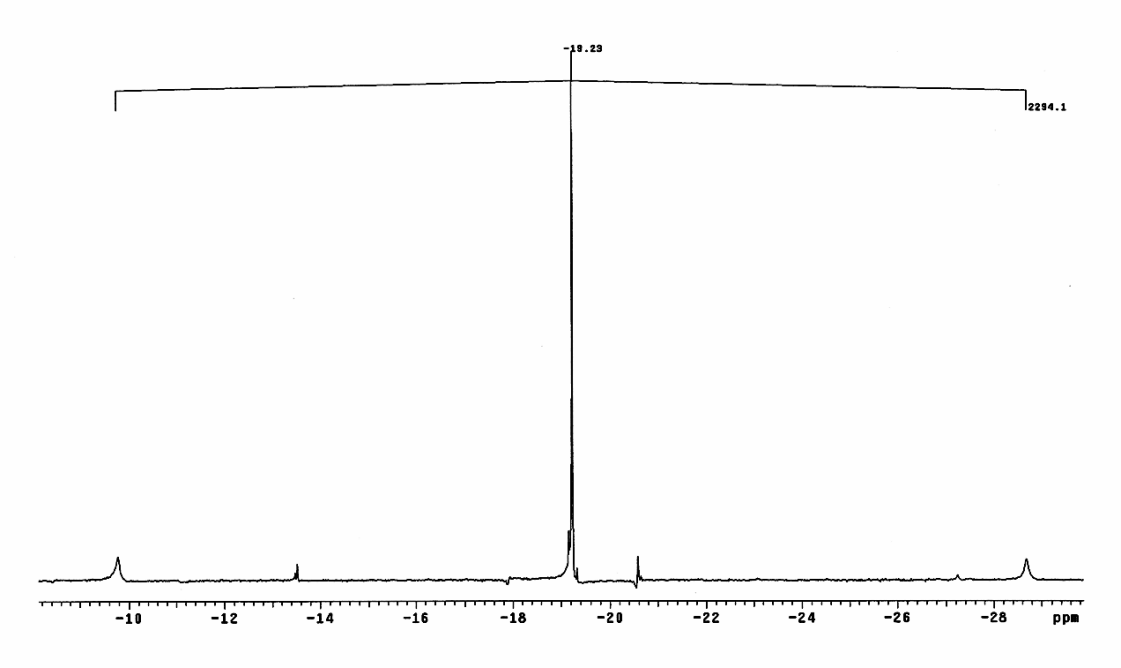

Figure A-17. ^{31}P NMR (121 MHz, $CDCl_3$) spectrum of **Pt2MP3**.

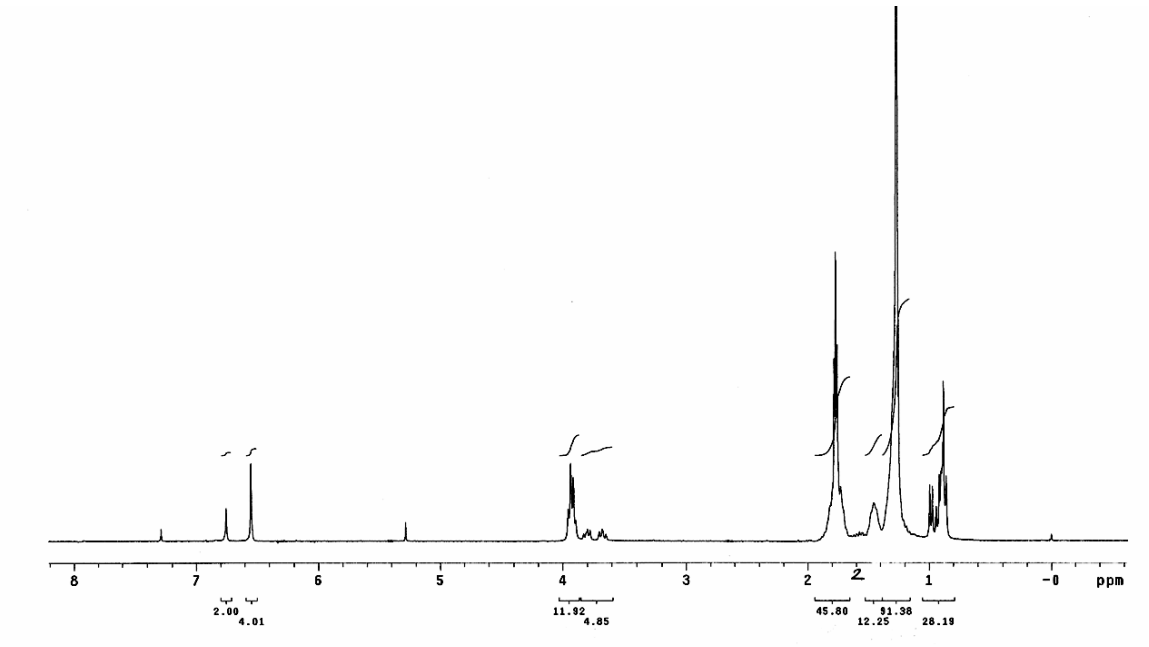

Figure A-18. ^{1}H NMR (300 MHz, $CDCl_3$) spectrum of **Pt2MC**.

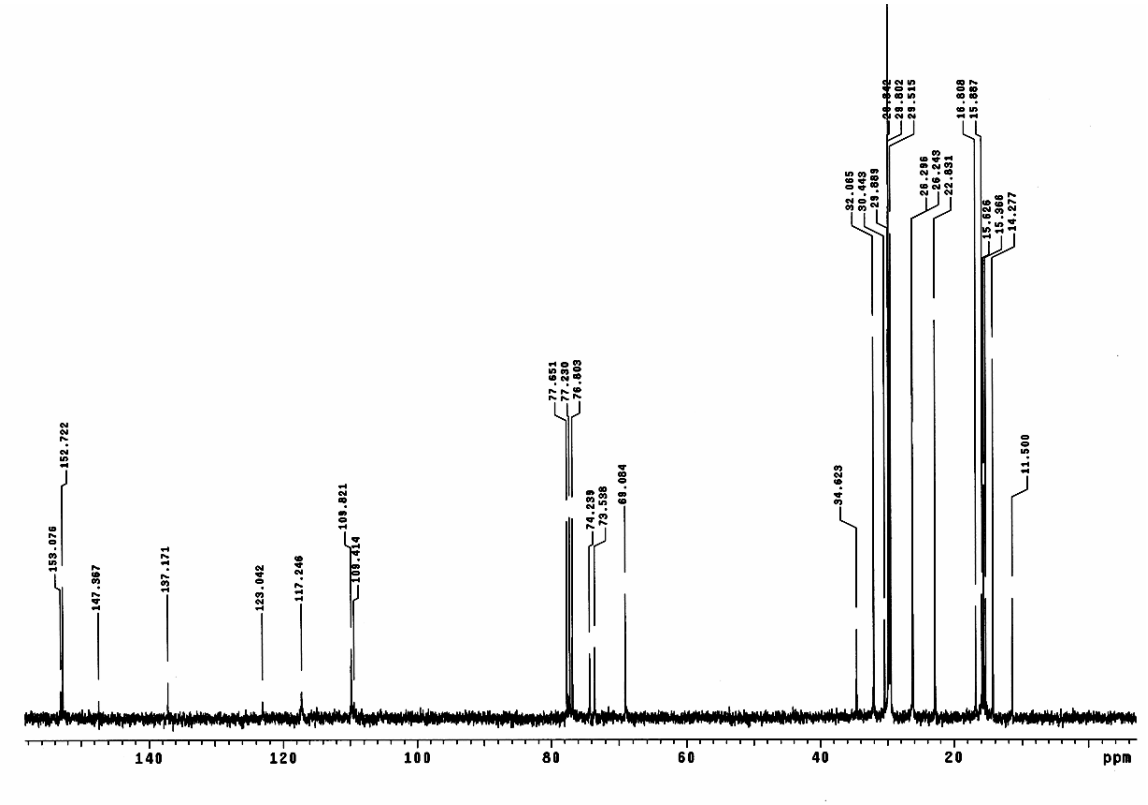

Figure A-19. ^{13}C NMR (75 MHz, $CDCl_3$) spectrum of **Pt2MC**.

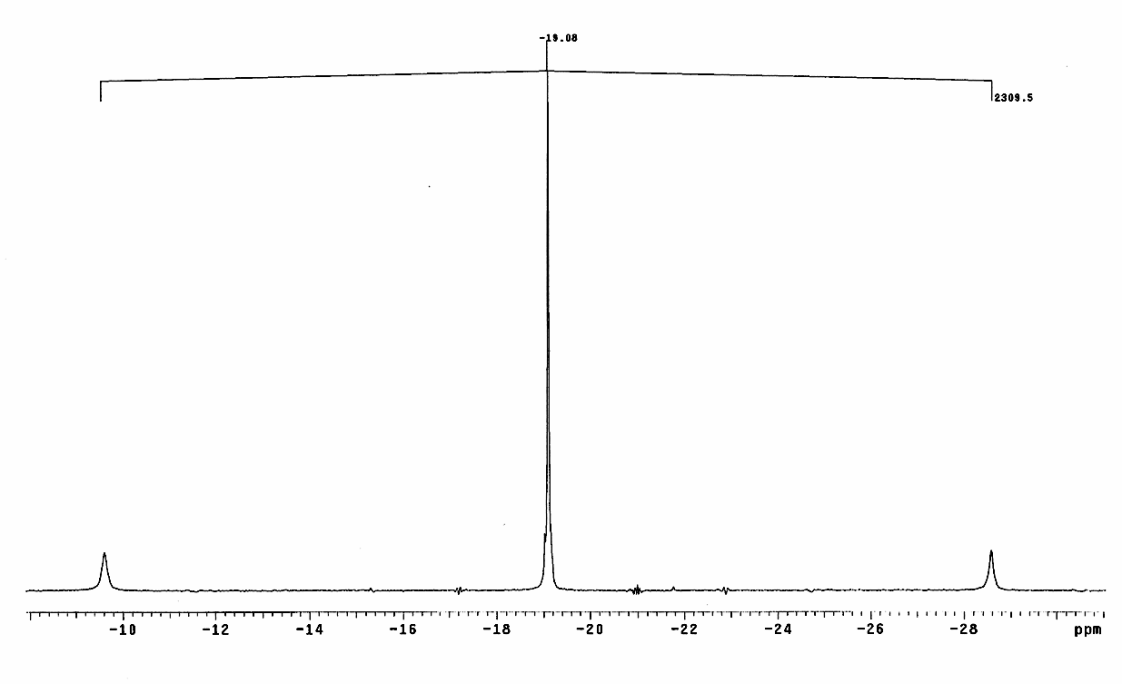

Figure A-20. ^{31}P NMR (121 MHz, $CDCl_3$) spectrum of **Pt2MC**.

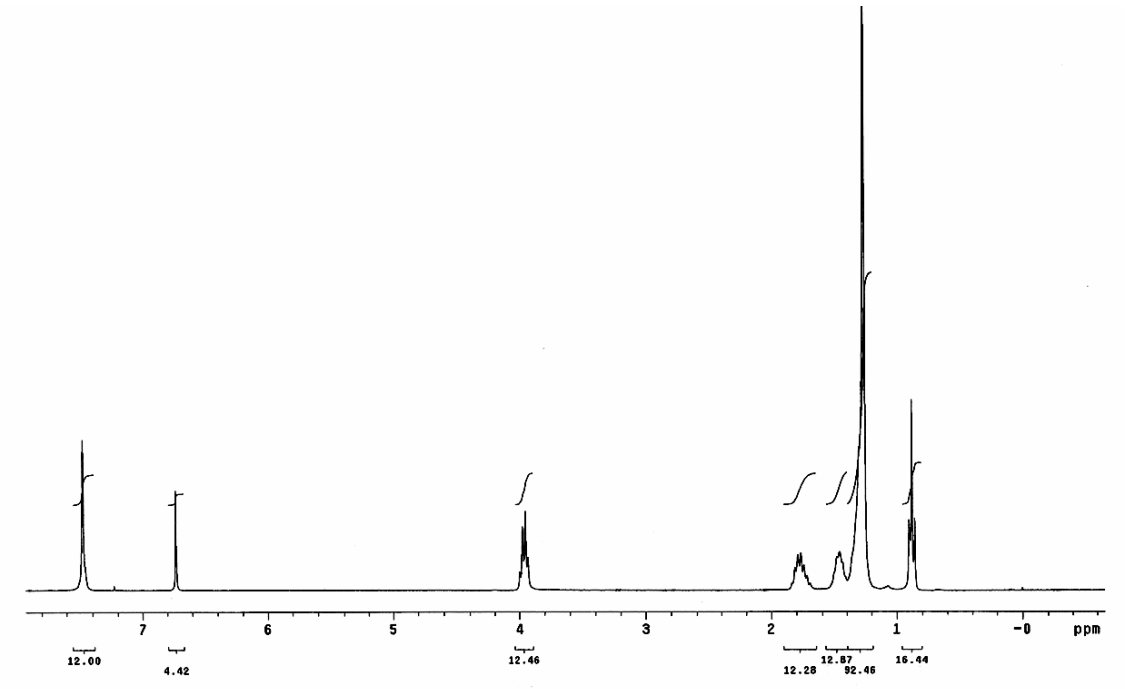

Figure A-21. ^{1}H NMR (300 MHz, $CDCl_3$) spectrum of **PE3**.

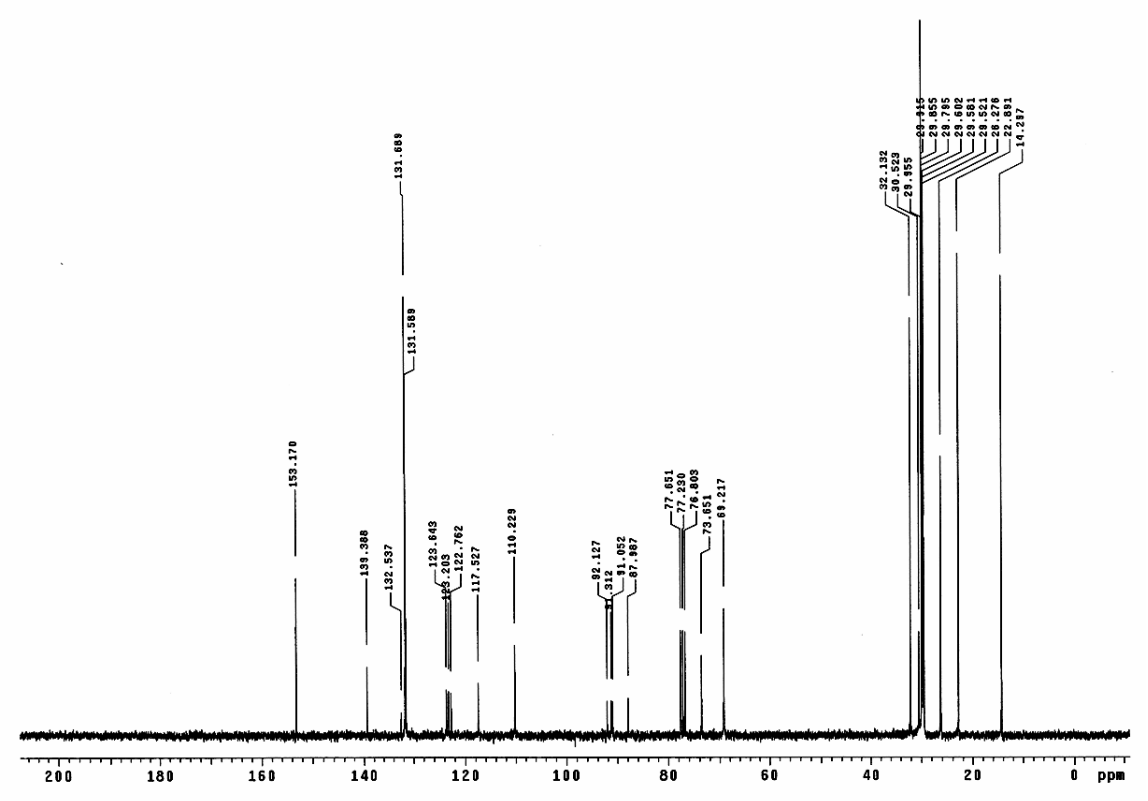

Figure A-22. ^{13}C NMR (75 MHz, $CDCl_3$) spectrum of **PE3.**

LIST OF REFERENCES

1. Atkins, P.; de Paula, J. In *Physical Chemistry*; W.H. Freeman and Company: New York, 2001, p 304.

2. Gilbert, A.; Baggot, J. *Essentials of Molecular Photochemistry*; CRC Press, Inc.: Boca Raton, 1991.

3. Turro, N. J. In *Modern Molecular Photochemistry*; The Benjamin/Cummings Publishing Co., Inc.: Menlo Park, 1978, p 185.

4. Ingle, J. D. J.; Crouch, S. R. In *Spectrochemical Analysis*; Prentice-Hall, Inc.: Upper Saddle River, 1988, p 342.

5. Englman, R.; Joshua, J. Energy Gap Law for Radiationless Transitions in Large Molecules. *Mol. Phys.* **1970**, *18*, 145.

6. Lin, S.-H. Energy Gap Law and Franck-Condon Factor in Radiationless Transitions. *J. Chem. Phys.* **1970**, *53*, 3766.

7. Caspar, J. V.; Meyer, T. J. Application of the Energy Gap Law to Nonradiative, Excited-State Decay. *J. Phys. Chem.* **1983**, *87*, 952.

8. Dexter, D. L. A Theory of Sensitized Luminescence in Solids. *J. Chem. Phys.* **1953**, *21*, 836.

9. Lakowicz, J. R. In *Principles of Fluorescence Spectroscopy*; Kluwer Academic/Plenum Publishers: New York, 1999, p 239.

10. Förster, T. 10th Spiers Memorial Lecture. Transfer Mechanism of Electronic Excitation. *Discuss. Faraday Soc.* **1959**, *27*, 7.

11. Lakowicz, J. R. In *Principles of Fluorescence Spectroscopy*; Kluwer Academic/Plenum Publishers: New York, 1999, p 367.

12. Elisha, H. The Study of Protein Folding and Dynamics by Determination of Intramolecular Distance Distributions and Their Fluctuations Using Ensemble and Single-Molecule FRET Measurements. *ChemPhysChem* **2005**, *6*, 858.

13. Heidecker, M.; Yan-Marriott, Y.; Marriott, G. Proximity Relationships and Structural Dynamics of the Phalloidin Binding Site of Actin Filaments in Solution and on Single Actin Filaments on Heavy Meromyosin. *Biochemistry* **1995**, *34*, 11017.

14. Qu, Q.; Sharon, F. J. Proximity of Bound Hoechst 33342 to the ATPase Catalytic Sites Places the Drug Binding Site of P-glycoprotein within the Cytoplasmic Membrane Leaflet. *Biochemistry* **2002**, *41*, 4744.

15. Birks, J. B. *Photophysics of Aromatic Molecules*; Wiley-Interscience: London, 1970.

16. Stevens, B. Some Effects of Molecular Orientation on Fluorescence Emission and Energy Transfer in Crystalline Aromatic Hydrocarbons. *Spectrochim. Acta* **1962**, *18*, 439.

17. Chandross, E. A.; Ferguson, J.; McRae, E. G. Absorption and Emission Spectra of Anthracene Dimers. *J. Chem. Phys.* **1966**, *45*, 3546.

18. Chandross, E. A.; Dempster, C. J. Intramolecular Excimer Formation and Fluorescence Quenching in Dinaphthylalkanes. *J. Am. Chem. Soc.* **1970**, *92*, 3586.

19. Bernhard, N.; Rodriguez Prieto, M. F. On the Alleged Triplet-Excimer Phosphorescence from Liquid Solutions of Naphtalene and Di-α-Naphtylalkanes in Isooctane. *Chem. Phys. Lett.* **1988**, *146*, 125.

20. Locke, R. J.; Lim, E. C. Comment. Triplet excimers: Further Verification by Emission Measurements. *Chem. Phys. Lett.* **1989**, *160*, 96.

21. Lim, E., C. Molecular Triplet Excimers. *Acc. Chem. Res.* **1987**, *20*, 8.

22. Subudhi, P. C.; Lim, E. C. Phosphorescence from Fluid Solutions of Dinaphthylpropane: Evidence for a Conformational Difference Between Singlet and Triplet Excimers. *J. Chem. Phys.* **1975**, *63*, 5491.

23. Haggquist, G. W.; Burkhart, R. D. Triplet Photophysics of Multichromophoric Molecules. A Study of Poly(N-ninylcarbazole) and *meso*-2,4-Dicarbazolylpentane in Fluid Solutions. *Macromolecules* **1995**, *28*, 2465.

24. Etheridge, H. T., III; Weisman, R. B. C70 Triplet Excimers: Evidence from Transient Absorption Kinetics. *J. Phys. Chem.* **1995**, *99*, 2782.

25. D'Andrade, B. W.; Brooks, J.; Adamovich, V.; Thompson, M. E.; Forrest, S. R. White Light Emission Using Triplet Excimers in Electrophosphorescent Organic Light-Emitting Devices. *Adv. Mater.* **2002**, *14*, 1032.

26. Davydov, A. S. *Theory of Molecular Excitons*; McGraw-Hill: New York, 1962.

27. McRae, E. G.; Kasha, M. In *Physical Processes in Radiation Biology*; Augenstein, L., Mason, R., Rosenberg, B., Eds.; Academic Press: New York, 1964, pp 23.

28. Kasha, M.; Rawls, H. R.; Ashraf El-Bayoumi, M. The Exciton Model in Molecular Spectroscopy. *Pure Appl. Chem.* **1965**, *11*, 371.

29. Doan, S. C.; Shanmugham, S.; Aston, D. E.; McHale, J. L. Counterion Dependent Dye Aggregates: Nanorods and Nanorings of Tetra(*p*-carboxyphenyl)porphyrin. *J. Am. Chem. Soc.* **2005**, *127*, 5885.

30. Kubát, P.; Lang, K.; Procházková, K.; Anzenbacher, P. J. Self-Aggregates of Cationic *meso*-Tetratolylporphyrins in Aqueous Solutions. *Langmuir* **2003**, *19*, 422.

31. Nasr, C.; Hotchandani, S. Excited-State Behavior of Nile Blue H-Aggregates Bound to SiO_2 and SnO_2 Colloids. *Chem. Mater.* **2000**, *12*, 1529.

32. Zsila, F.; Bikádi, Z.; Keresztes, Z.; Deli, J.; Simonyi, M. Investigation of the Self-Organization of Lutein and Lutein Diacetate by Electronic Absorption, Circular Dichroism Spectroscopy, and Atomic Force Microscopy. *J. Phys. Chem. B* **2001**, *105*, 9413.

33. Kasha, M. In *Spectroscopy of the Excited State.*; Di Bartolo, B., Ed.; Plenum Press: New York, 1975, p 340.

34. Bellin, J. S. Photoreduction of Eosin in the Bound State. *J. Am. Chem. Soc.* **1957**, *79*, 2461.

35. Levinson, G. S.; Simpson, W. T.; Curtis, W. Electronic Spectra of Pyridocyanine Dyes with Assignments of Transitions. *J. Am. Chem. Soc.* **1957**, *79*, 4314.

36. McRae, E. G.; Kasha, M. Enhancement of Phosphorescence Ability upon Aggregatation of Dye Molecules. *J. Chem. Phys.* **1958**, *28*, 721.

37. An, B.-K.; Kwon, S.-K.; Jung, S.-D.; Park, S. Y. Enhanced Emission and its Switching in Fluorescent Organic Nanoparticles. *J. Am. Chem. Soc.* **2002**, *124*, 14410.

38. Mooney, W. F.; Brown, P. E.; Russel, J. C.; Costa, S. B.; Pedersen, L. G.; Whitten, D. G. Photochemistry and Photophysics of Surfactant *trans*-Stilbenes in Supported Multilayers and Films at the Air-Water Interface. *J. Am. Chem. Soc.* **1984**, *106*, 5659.

39. Whitten, D. G. Photochemistry and Photophysics of *trans*-Stilbene and Related Alkenes in Surfactant Assemblies. *Acc. Chem. Res.* **1993**, *26*, 502.

40. Pawlik, A.; Ouart, A.; Kirstein, S.; Abraham, H.-W.; Daehne, S. Synthesis and UV/Vis Spectra of J-Aggregating 5,5',6,6'-Tetrachlorobenzimidacarbocyanine Dyes for Artificial Light-Harvesting Systems and for Asymmetrical Generation of Supramolecular Helices. *Eur. J. Org. Chem.* **2003**, 3065.

41. Wohlgenannt, M.; Jiang, X. M.; Vardeny, Z. V.; Janssen, R. A. J. Conjugation-Length Dependence of Spin-Dependent Exciton Formation Rates in π-Conjugated Oligomers and Polymers. *Phys. Rev. Lett.* **2002**, *88*, 197401.

42. Beljonne, D.; Ye, A.; Shuai, Z.; Brédas, J.-L. Chain-Length Dependence of Singlet and Triplet Exciton Formation Rates in Organic Light-Emitting Diodes. *Adv. Funct. Mater.* **2004**, *14*, 631.

43. Burrows, H. D.; Seixas de Melo, J.; Serpa, C.; Arnaut, L. G.; Miguel, M. d. G.; Monkman, A. P.; Hamblett, I.; Navaratnam, S. Triplet State Dynamics on Isolated Conjugated Polymer Chains. *Chem. Phys.* **2002**, *285*, 3.

44. Monkman, A. P.; Burrows, H. D. Backbone Planarity Effects on Triplet Energies and Electron-Electron Correlation in Luminescent Conjugated Polymers. *Synth. Met.* **2004**, *141*, 81.

45. Köhler, A.; Wilson, J. S.; Friend, R. H.; Al-Suti, M. K.; Khan, M. S.; Gerhard, A.; Bässler, H. The Singlet-Triplet Energy Gap in Organic and Pt-Containing Phenylene Ethynylene Polymers and Monomers. *J. Chem. Phys.* **2002**, *116*, 9457.

46. Hertel, D.; Setayesh, S.; Nothofer, H.-G.; Scherf, U.; Müllen, K.; Bässler, H. Phosphorescence in Conjugated Poly(*para*-phenylene)-Derivatives. *Adv. Mater.* **2001**, *13*, 65.

47. Laquai, F.; Im, C.; Kadashchuk, A.; Bässler, H. Sensitized Intrinsic Phosphorescence from a Poly(phenylene-vinylene) Derivative. *Chem. Phys. Lett.* **2003**, *375*, 286.

48. Köhler, A.; Beljonne, D. The Singlet-Triplet Energy Exchange Energy in Conjugated Polymers. *Adv. Funct. Mater.* **2004**, *14*, 11.

49. Sonogashira, K.; Fujikura, Y.; Yatake, T.; Toyoshima, N.; Takahashi, S.; Hagihara, N. Syntheses and Properties of *cis* and *trans*-Dialkynyl Complexes of Platinum(II). *J. Organomet. Chem.* **1978**, *145*, 101.

50. Mather, G. G.; Pidcock, A.; Rapsey, G. J. N. Correlation of NMR Coupling Constants with Transition Metal-Ligand Bond Lengths in Tertiary Phosphine Complexes. *J. Chem. Soc., Dalton Trans.* **1973**, 2095.

51. Sonogashira, K.; Kataoka, S.; Takahashi, S.; Hagihara, N. Studies of Poly-yne Polymers Containing Transition Metals in the Main Chain. *J. Organomet. Chem.* **1978**, *160*, 319.

52. Lewis, J.; Long, N. J.; Raithby, P. R.; Shields, G. P.; Wong, W.-Y.; Younus, M. Synthesis and Characterization of New Acetylide-Functionalised Oligothiophenes and Their Dinuclear Platinum Complexes. *J. Chem. Soc., Dalton Trans.* **1997**, 4283.

53. McKay, T. J.; Bolger, J. A.; Staromlynska, J.; Davy, J. R. Linear and Nonlinear Optical Properties of Platinum-Ethynyl. *J. Chem. Phys.* **1998**, *108*, 5537.

54. Staromlynska, J.; Chapple, P. B.; Davy, J. R.; McKay, T. J. A Platinum Ethynyl Compound for Optical Limiting. *Proceedings of SPIE-The International Society for Optical Engineering* **1994**, *2229*, 59.

55. Vestberg, R.; Westlund, R.; Carlsson, M.; Ellasson, B.; Glimsdal, E.; Oertengren, J.; Lindgren, M.; Malmstroem, E. Photophysical Properties of Dendronized Platinum(II) Acetylides for Optical Power Limiting. *Polym. Mater. Sci. Eng.* **2005**, *92*, 622.

56. Onitsuka, K.; Shimizu, A.; Takahashi, S. A Divergent Approach to the Precise Synthesis of Giant Organometallic Dendrimers using Platinum-Acetylides as Building Blocks. *Chem. Comm.* **2003**, 280.

57. Onitsuka, K.; Fujimoto, M.; Kitajima, H.; Ohshiro, N.; Takei, F.; Takahashi, S. Convergent Synthesis of Platinum-Acetylide Dendrimers. *Chem. Eur. J.* **2004**, *10*, 6433.

58. Cooper, T. M.; Hall, B. C.; Burke, A. R.; Rogers, J. E.; McLean, D. G.; Slagle, J. E.; Fleitz, P. A. Glass-Forming Liquid Platinum Acetylides. *Chem. Mater.* **2004**, *16*, 3215.

59. Campbell, K.; Johnson, C. A., III; McDonald, R.; Ferguson, M. J.; Haley, M. M.; Tykwinski, R. R. A Simple, One-Step Procedure for the Formation of Chiral Metallamacrocycles. *Angew. Chem., Int. Ed.* **2004**, *43*, 5967.

60. Beljonne, D.; Wittmann, H. F.; Köhler, A.; Graham, S.; Younus, M.; Lewis, J.; Raithby, P. R.; Khan, M. S.; Friend, R. H.; Brédas, J.-L. Spatial Extent of the Singlet and Triplet Excitons in Transition Metal-Containing Poly-ynes. *J. Chem. Phys.* **1996**, *105*, 3868.

61. Cooper, T. M.; Blaudeau, J.-P.; Hall, B. C.; Rogers, J. E.; McLean, D. G.; Liu, Y.; Toscano, J. P. The Triplet State of Platinum Acetylide Chromophore Examined by Time-Resolved Infrared Spectroscopy and Density Functional Theory. *Chem. Phys. Lett.* **2004**, *400*, 239.

62. Emmert, L. A.; Choi, W.; Marshall, J. A.; Yang, J.; Meyer, L. A.; Brozik, J. A. The Excited State Symmetry Characteristics of Platinum Phenylacetylene Compounds. *J. Phys. Chem. A* **2003**, *107*, 11340.

63. Chawdhury, N.; Köhler, A.; Friend, R. H.; Wong, W.-Y.; Lewis, J.; Younus, M.; Raithby, P.; Corcoran, T. C.; Al-Mandhary, M. R. A.; Khan, M. S. Evolution of Lowest Singlet and Triplet Excited States with Number of Thienyl Rings in Platinum Poly-ynes. *J. Chem. Phys.* **1999**, *110*, 4963.

64. Wilson, J. S.; Chawdhury, N.; Al-Mandhary, M. R. A.; Younus, M.; Khan, M. S.; Raithby, P.; Köhler, A.; Friend, R. H. The Energy Gap Law for Triplet States in Pt-Containing Conjugated Polymers and Monomers. *J. Am. Chem. Soc.* **2001**, *123*, 9412.

65. Penner, A. P.; Siebrand, W.; Zgierski, M. Z. Radiationless Decay of Vibronically Coupled Electronic States. *J. Chem. Phys.* **1978**, *69*, 5496.

66. Rogers, J. E.; Cooper, T. M.; Fleitz, P. A.; Glass, D. J.; McLean, D. G. Photophysical Characterization of a Series of Platinum(II)-Containing Phenyl-Ethynyl Oligomers. *J. Phys. Chem. A* **2002**, *106*, 10108.

67. Liu, Y.; Jiang, S.; Glusac, K.; Powell, D. H.; Anderson, D. F.; Schanze, K. S. Photophysics of Monodisperse Platinum-Acetylide Oligomers: Delocalization in the Singlet and Triplet Excited States. *J. Am. Chem. Soc.* **2002**, *124*, 12412.

68. Glusac, K. D.; Schanze, K. S. Photophysics and Photochemistry of Platinum-Acetylide Complexes: Models for Metal-Acetylide Polymers. *Polym. Prep.* **2002**, *43*, 87.

69. Staromlynska, J.; McKay, T. J.; Bolger, J. A.; Davy, J. R. Evidence for Broadband Optical Limiting in a Pt-Ethynyl Compound. *J. Opt. Soc. Am. B* **1998**, *15*, 1731.

70. Lammi, R. K.; Barbara, P. F. Influence of Chain Length on Exciton Migration to Low-Energy Sites in Single Fluorene Copolymers. *Photochem. Photobiol. Sci.* **2005**, *4*, 95.

71. Kraabel, B.; Klimov, I.; Kohlman, R.; Xu, S.; Wang, H.-L.; McBranch, D. W. Unified Picture of the Photoexcitations in Phenylene-Based Conjugated Polymers: Universal Spectral and Dynamical Features in Subpicosecond Transient Absorption. *Phys. Rev. B: Condens. Matter* **2000**, *61*, 8501.

72. Koizumi, Y.; Seki, S.; Acharya, A.; Saeki, A.; Tagawa, S. Delocalization of Positive and Negative Charge Carriers on Oligo- and Poly-Fluorenes Studied by Low-Temperature Matrix Isolation Technique. *Chem. Lett.* **2004**, *33*, 1290.

73. Peng, K.-Y.; Chen, S.-A.; Fann, W.-S.; Chen, S.-H.; Su, A. C. Well-Packed Chains and Aggregates in the Emission Mechanism of Conjugated Polymers. *J. Phys. Chem. B* **2005**, *109*, 9368.

74. Menon, A.; Galvin, M.; Walz, K. A.; Rothberg, L. Structural Basis for the Spectroscopy and Photophysics of Solution-Aggregated Conjugated Polymers. *Synth. Met.* **2004**, *141*, 197.

75. Hoeben, F. J. M.; Jonkheijm, P.; Meijer, E. W.; Schenning, A. P. H. J. About Supramolecular Assemblies of π-Conjugated Systems. *Chem. Rev.* **2005**, *105*, 1491.

76. Burroughes, J. H.; Bradley, D. D. C.; Brown, A. R.; Marks, R. N.; Mackay, K.; Friend, R. H.; Burns, P. L.; Holmes, A. B. Light-Emitting Diodes Based on Conjugated Polymers. *Nature* **1990**, *347*, 539.

77. Braun, D.; Heeger, A. J. Visible Light Emission from Semiconducting Polymer Diodes. *Appl. Phys. Lett.* **1991**, *58*, 1982.

78. Friend, R. H.; Gymer, R. W.; Holmes, A. B.; Burroughes, J. H.; Marks, R. N.; Taliani, C.; Bradley, D. D. C.; Dos Santos, D. A.; Brédas, J.-L.; Lögdlund, M.; Salaneck, W. R. Electroluminescence in Conjugated Polymers. *Nature* **1999**, *397*, 121.

79. List, E. J. W.; Kim, C. H.; Graupner, W.; Leising, G.; Shinar, J. Nonradiative Quenching of Singlet Excitons by Polarons in π-Conjugated Polymers. *Synth. Met.* **2001**, *119*, 511.

80. Campbell, A. J.; Bradley, D. D. C.; Lidzey, D. G. Charge Trapping in Polymer Diodes. *Opt. Mater.* **1998**, *9*, 114.

81. Zhao, W.; Cao, T.; White, J. M. On the Origin of Green Emission in Polyfluorene Polymers: The Roles of Thermal Oxidation Degradation and Crosslinking. *Adv. Funct. Mater.* **2004**, *14*, 783.

82. Romaner, L.; Pogantsch, A.; Scandiucci de Freitas, P.; Scherf, U.; Gaal, M.; Zojer, E.; List, E. J. W. The Origin of Green Emission in Polyfluorene-Based Conjugated Polymers: On-Chain Defect Fluorescence. *Adv. Funct. Mater.* **2003**, *13*, 597.

83. Yan, M.; Rothberg, L. J.; Papadimitrakopoulos, F.; Galvin, M. E.; Miller, T. M. Defect Quenching of Conjugated Polymer Luminescence. *Phys. Rev. Lett.* **1994**, *73*, 744.

84. Lupton, J. M.; Craig, M. R.; Meijer, E. W. On-Chain Defect Emission in Electroluminescent Polyfluorenes. *Appl. Phys. Lett.* **2002**, *80*, 4489.

85. Tretiak, S.; Igumenschchev, K.; Chernyak, V. Exciton Sizes of Conducting Polymers Predicted by Time-Dependent Density Functional Theory. *Phys. Rev. B: Condens. Matter* **2005**, *71*, 033201.

86. Martin, R. E.; Diederich, F. Linear Monodisperse π-Conjugated Oligomers: Model Compounds for Polymers and More. *Angew. Chem., Int. Ed.* **1999**, *38*, 1350.

87. Hennebicq, E.; Pourtois, G.; Scholes, G. D.; Herz, L. M.; Russel, D. M.; Silva, C.; Setayesh, S.; Grimsdale, A. C.; Müllen, K.; Brédas, J.-L.; Beljonne, D. Exciton Migration in Rigid-Rod Conjugated Polymers: an Improved Förster Model. *J. Am. Chem. Soc.* **2005**, *127*, 4744.

88. Wasserberg, D.; Marsal, P.; Meskers, S. C. J.; Janssen, R. A. J.; Beljonne, D. Phosphorescence and Triplet State Energies of Oligothiophenes. *J. Phys. Chem. B* **2005**, *109*, 4410.

89. Seixas de Melo, J.; Silva, L. M.; Arnaut, L. G.; Becker, R. S. Singlet and Triplet Energies of Oligothiophenes: A Spectroscopic, Theoritical, and Photoacoustic Study: Extrapolation to Polythiophene. *J. Chem. Phys.* **1999**, *111*, 5427.

90. Sonogashira, K.; Tohda, Y.; Hagihara, N. A Convenient Synthesis of Acetylenes: Catalytic Substitutions of Acetylenic Hydrogens with Bromoalkenes, Iodoarenes and Bromopyridine. *Tet. Lett.* **1975**, *16*.

91. Wilson, J. S.; Wilson, R. J.; Friend, R. H.; Köhler, A.; Al-Suti, M. K.; Al-Mandhary, M. R. A.; Khan, M. S. Polarization of Singlet and Triplet Excited States in a Platinum-Containing Conjugated Polymer. *Phys. Rev. B: Condens. Matter* **2003**, *67*, 125206.

92. Cummings, S. D.; Eisenberg, R. Tuning the Excited-State Properties of Platinum(II) Diimine Dithiolate Complexes. *J. Am. Chem. Soc.* **1996**, *118*, 1949.

93. Funston, A. M.; Silverman, E. E.; Miller, J. R.; Schanze, K. S. Charge Transfer Through Terthiophene End-Capped Poly(arylene ethynylene)s. *J. Phys. Chem. B* **2004**, *108*, 1544.

94. List, E. J. W.; Leising, G. Excitation Energy Migration Assisted Processes in Conjugated Polymers. *Synth. Met.* **2004**, *141*, 211.

95. Liu, S.; Schanze, K. S. Solvent Tuned Excited State Configuration Mixing in a π-Conjugated Metal-Organic Oligomer. *Chem. Comm.* **2004**, 1510.

96. Hissler, M.; Harriman, A.; Khatyr, A.; Ziessel, R. Intramolecular Triplet Energy Transfer in Pyrene-Metal Polypyridine Dyads: A Strategy for Extending the Triplet Lifetime of the Metal Complex. *Chem. Eur. J.* **1999**, *5*, 3366.

97. Danilov, E. O.; Pomestchenko, I. E.; Kinayyigit, S.; Gentili, P. L.; Hissler, M.; Ziessel, R.; Castellano, F. N. Ultrafast Energy Migration in Platinum(II) Diimine Complexes Bearing Phenylacetylide Chromophores. *J. Phys. Chem. A* **2005**, *109*, 2465.

98. Demas, J. N.; Crosby, G. A. Measurements of Photoluminescence Quantum Yields. Review. *J. Phys. Chem.* **1971**, *75*, 991.

99. Wang, Y.; Schanze, K. S. Photochemical Probes of Intramolecular Electron and Energy Transfer. *Chem. Phys.* **1993**, *176*, 305.

100. Wei, J.; Buriak, J.; Siuzdak, G. Desorption-Ionization Mass Spectrometry on Porous Silicon. *Nature* **1999**, *399*, 243.

101. Shen, Z.; Thomas, J. J.; Averbuj, C.; Broo, K. M.; Engelhard, M.; Crowell, J. E.; Finn, M. G.; Siuzdak, G. Porous Silicon as a Versatile Platform for Laser Desorption/Ionization Mass Spectrometry. *Anal. Chem.* **2001**, *73*, 612.

102. Kauffman, G. B.; Teter, L. A. *cis* and *trans*-Dichloro-bis-(tri-*n*-butylphosphine)platinum(II). *Inorganic Syntheses* **1963**, *7*, 245.

103. Greenham, N. C.; Moratti, S. C.; Bradley, D. D. C.; Friend, R. H.; Holmes, A. B. Efficient Light-Emitting Diodes Based on Polymers with High Electron Affinity. *Nature* **1993**, *365*, 628.

104. Pichler, K.; Jarrett, C. P.; Friend, R. H.; Ratier, B.; Moliton, A. Field-Effect Transistors Based on Poly(*p*-phenylene vinylene) Doped by Ion Implantation. *J. Appl. Phys.* **1995**, *77*, 3523.

105. Roichman, Y.; Tessler, N. Structures of Field-Effect Transistor: Experimental and Numerical Analyses. *Appl. Phys. Lett.* **2002**, *80*, 151.

106. Sariciftci, N. S.; Smilowitz, L.; Heeger, A. J.; Wudl, F. Photoinduced Electron Transfer from a Conducting Polymer to Buckminsterfullerene. *Science* **1992**, *258*, 1474.

107. Shaheen, S. E.; Radspinner, R.; Peyghambarian, N.; Jabbour, G. Fabrication of Bulk Heterojunction Plastic Solar Cells by Screen Printing. *Appl. Phys. Lett.* **2001**, *79*, 2996.

108. Scott, J. C.; Brock, P. J.; Salem, J. R.; Ramos, S.; Malliaras, G. G.; Carter, S. A.; Bozano, L. Charge Transport Processes in Organic Light-Emitting Devices. *Synth. Met.* **2000**, *111-112*, 289.

109. Su, W. P.; Schrieffer, J. R.; Heeger, A. J. Soliton Excitations in Polyacetylene. *Phys. Rev. B: Condens. Matter* **1980**, *22*, 2099.

110. Rice, M. J.; Phillpot, S. R.; Bishop, A. R.; Campbell, D. K. Solitons, Polarons and Phonons in the Infinite Polyyne Chain. *Phys. Rev. B: Condens. Matter* **1986**, *34*, 4139.

111. Yukihiro, S.; Shuji, A. Competition Between Polarons and Bipolarons in Nondegenerate Conjugated Polymers. *Phys. Rev. B: Condens. Matter* **1994**, *50*, 14781.

112. Furukawa, Y. Electronic Absorption and Vibrational Spectrocopies of Conjugated Conducting Polymers. *J. Phys. Chem.* **1996**, *100*, 15644.

113. Burrows, H. D.; Miguel, M. d. G.; Monkman, A. P.; Horsburgh, L. E.; Hamblett, I.; Navaratnam, S. Pulse Radiolysis Studies on Charge Carriers in Conjugated Polymers. *J. Chem. Phys.* **2000**, *112*, 3082.

114. Winokur, M. J.; Chunwachirasiri, W. Nanoscale Structure-Property Relationships in Conjugated Polymers: Implications for Present and Future Device Applications. *J. Polym. Sci., Part B: Polym. Phys.* **2003**, *41*, 2630.

115. Nguyen, T.-Q.; Kwong, R. C.; Thompson, M. E.; Schwartz, B. J. Improving the Performance of Conjugated Polymer-Based Devices by Control of Interchain Interactions and Polymer Film Morphology. *Appl. Phys. Lett.* **2000**, *76*, 2454.

116. Ho, P. K. H.; Kim, J.-S.; Burroughes, J. H.; Becker, H.; Li, S. F. Y.; Brown, T. M.; Cacialli, F.; Friend, R. H. Molecular-Scale Interface Engineering for Polymer Light-Emitting Diodes. *Nature* **2000**, *404*.

117. Cao, Y.; Parker, I. D.; Yu, G.; Zhang, C.; Heeger, A. J. Improved Quantum Efficiency for Electroluminescence in Semiconducting Polymers. *Nature* **1999**, *397*, 414.

118. Wohlgenannt, M.; Tandon, K.; Mazumdar, S.; Ramasesha, S.; Vardeny, Z. V. Formation Cross-Sections of Singlet and Triplet Excitons in π-Conjugated Polymers. *Nature* **2001**, *409*, 494.

119. Wilson, J. S.; Dhoot, A. S.; Seeley, A. J. A. B.; Khan, M. S.; Köhler, A.; Friend, R. H. Spin-Dependent Exciton Formation in π-Conjugated Compounds. *Nature* **2001**, *413*, 828.

120. Wohlgenannt, M.; Vardeny, Z. V. Spin-Dependent Exciton Formation Rates in π-Conjugated Materials. *J. Phys.: Condens. Matter* **2003**, *15*, R83.

121. Adachi, C.; Baldo, M. A.; Thompson, M. E.; Forrest, S. R. Nearly 100% Internal Phosphorescence Efficiency in an Organic Light Emitting Device. *J. Appl. Phys.* **2001**, *90*, 5048.

122. Anthopoulos, T.; Frampton, M. J.; Namdas, E. B.; Burns, P. L.; Samuel, I. D. W. Solution-Processable Red Phosphorescent Dendrimers for Light-Emitting Device Applications. *Adv. Mater.* **2004**, *16*, 557.

123. Holder, E.; Langeveld, B. M. W.; Schubert, U. New Trends in the Use of Transition Metal-Ligand Complexes for Applications in Electroluminescent Devices. *Adv. Mater.* **2005**, *17*, 1109.

124. Baldo, M. A.; O'Brien, D. F.; You, Y.; Shoustikov, A.; Sibley, S.; Thompson, M. E.; Forrest, S. R. Highly Efficient Phosphorescent Emission from Organic Electroluminescent Devices. *Nature* **1998**, *395*, 151.

125. Jabbour, G.; Wang, J.-F.; Peyghambarian, N. High-Efficiency Organic Electrophosphorescent Devices Through Balance of Charge Injection. *Appl. Phys. Lett.* **2002**, *80*, 2026.

126. Cocchi, M.; Fattori, V.; Virgili, D.; Sabatini, C.; Di Marco, P.; Maestri, M.; Kalinowski, J. Highly Efficient Organic Electrophosphorescent Light-Emitting Diodes with a Reduced Quantum Efficiency Roll Off at Large Current Densities. *Appl. Phys. Lett.* **2004**, *84*, 1052.

127. Grozema, F. C.; Hoofman, R. J. O. M.; Candeias, L. P.; De Haas, M. P.; Warman, J. M.; Siebbeles, L. D. A. The Formation and Recombination Kinetics of Positively Charged Poly(phenylene vinylene) Chains in Pulse-Irradiated Dilute Solutions. *J. Phys. Chem. A* **2003**, *107*, 5976.

128. Emmi, S. S.; D'Angelantino, M.; Beggiato, G.; Poggi, G.; geri, A.; Pietropaolo, D.; Zotti, G. Generation and Spectral Characterization of Oligothiophenes Radical Cations. A Pulse Radiolysis Investigation. *Radiat. Phys. Chem.* **1999**, *54*, 263.

129. Hertel, D.; Scherf, U.; Baessler, H. Charge Carrier Mobility in a Ladder-Type Conjugated Polymer. *Adv. Mater.* **1998**, *10*, 1119.

130. Lee, S. H.; Yasuda, T.; Tsutsui, T. Charge Carrier Mobility in Blue-Green Emitting Fluorenyl-Substituted Poly(*p*-phenylene vinylene)s. *J. Appl. Phys.* **2004**, *95*, 3825.

131. Tseng, H.-E.; Jen, T.-H.; Peng, K.-Y.; Chen, S.-A. Measurements of Charge Mobility and Diffusion Coefficient of Conjugated Electroluminescent Polymers by Time-of-Flight Method. *Appl. Phys. Lett.* **2004**, *84*, 1456.

132. Barth, M.; Guillerez, S.; Bidan, G.; Bras, G.; Lapkowski, M. Electrochemical Investigation of Regioregular Alkyl Substituted Oligothiophenes. *Electrochim. Acta* **2000**, *45*, 4409.

133. Domagala, W.; Lapkowski, M.; Guillerez, S.; Bidan, G. Electrochemical Studies of Selected Regioregular Oligooctylthiophenes in Solution and in Thin Film Solid State. *Electrochim. Acta* **2003**, *48*, 2379.

134. Frère, P.; Raimundo, J.-M.; Blanchard, P.; Delaunay, J.; Richomme, P.; Sauvajol, J.-L.; Orduna, J.; Garin, J.; Roncali, J. Effect of Local Molecular Structure on the Chain-Length Dependence of the Electronic Properties of Thiophene-Based π-Conjugated Systems. *J. Org. Chem.* **2003**, *68*, 7254.

135. Ferraris, J. P.; Eissa, M. M.; Brotherston, I. D.; Loveday, D. C.; Moxey, A. A. Preparation and Electrochemical Evaluation of Poly(3-phenylthiophene) Derivatives: Potential Materials for Electrochemical Capacitors. *J. Electronanal. Chem.* **1998**, *459*, 57.

136. Pappenfus, T. M.; Mann, K. R. Synthesis, Spectroscopy, and Electrochemical Studies of Binuclear Tris-Bipyridine Ruthenium(II) Complexes with Oligothiophene Bridges. *Inorg. Chem.* **2001**, *40*, 6301.

137. Jones, N. D.; Wolf, M. O.; Giaquinta, D. M. Synthesis of a Ferrocenyl-Capped Ruthenium(II) Bis(Acetylide) Complex: A Model for Organometallic Molecular Wire. *Organometallics* **1997**, *16*, 1352.

138. Clot, O.; Akahori, Y.; Moorlag, C.; Leznoff, D. B.; Wolf, M. O.; Batchelor, R. J.; Patrick, B. O.; Ishii, M. Model Complexes for Metalated Polythiophenes: Gold(I) and Palladium(II) Complexes of Bis(diphenylphosphino)oligothiophenes. *Inorg. Chem.* **2003**, *42*, 2704.

139. Encinas, S.; Flamigni, L.; Barigelletti, F.; Constable, E. C.; Housecroft, C. E.; Schofield, E. R.; Figgemeier, E.; Fenske, D.; Neuburger, M.; Vos, J. G.; Zehnder, M. Electronic Energy Transfer and Collection in Luminescent Molecular Rods Containing Ruthenium(II) and Osmium(II) 2,2:6,2-Terpyridine Complexes Linked by Thiophene-2,5-diyl Spacers. *Chem. Eur. J.* **2002**, *8*, 137.

140. Meerholz, K.; Heinze, J. Electrochemical Solution and Solid-State Investigations on Conjugated Oligomers and Polymers of the α-Thiophene and *p*-Phenylene Series. *Electrochim. Acta* **1996**, *41*, 1839.

141. Garcia, P.; Pernaut, J. M.; Hapiot, P.; Wintgens, V.; Valat, P.; Garnier, F.; Delabouglise, D. Effect of End Substitution on Electrochemical and Optical Properties of Oligothiophenes. *J. Phys. Chem.* **1993**, *97*, 513.

142. Cheng, L.; Yang, J.; Yao, Y.; Price, D. W.; Dirk, S. M.; Tour, J. M. Comparative Study of Electrochemically Directed Assembly Versus Conventional Self-Assembly of Thioacetyl-Terminated Oligo(phenylene ethynylene)s on Gold and Platinum Surfaces. *Langmuir* **2004**, *20*, 1335.

143. Benito, J.; Berenguer, J. R.; Forniés, J.; Gil, B.; Gómez, J.; Lalinde, E. Synthesis, Characterization and Luminescence Properties of Homoleptic Platinum(II) Acetylide Complexes. *J. Chem. Soc., Dalton Trans.* **2003**, 4331.

144. Yam, V. W.-W.; Tang, R. P.-L.; Wong, K. M.-C.; Cheung, K.-K. Synthesis, Luminescence, Electrochemistry, and Ion-Binding Studies of Platinum(II) Terpyridyl Acetylide Complexes. *Organometallics* **2001**, *20*, 4476.

145. Wohlgenannt, M.; Jiang, X. M.; Vardeny, Z. V. Confined and Delocalized Polarons in π-Conjugated Oligomers and Polymers: A Study of the Effective Conjugation Length. *Phys. Rev. B: Condens. Matter* **2004**, *69*, 241204.

146. Barlow, S.; O'Hare, D. Metal-Metal Interactions in Linked Metallocenes. *Chem. Rev.* **1997**, *97*, 637.

147. Bonvoisin, J.; Launay, J.-P.; Van der Auweraer, M.; De Schryver, F. C. Organic Mixed-Valence Systems.I. Intervalence Transition in Partly Oxidized Aromatic Polyamines. *J. Phys. Chem.* **1994**, *98*, 5052.

148. Bonvoisin, J.; Launay, J.-P.; Verbouwe, W.; Van der Auweraer, M.; De Schryver, F. C. Organic Mixed-Valence Systems. II. Two-Centers and Three-Centers Compounds with Meta Connections Around a Central Phenylene Ring. *J. Phys. Chem.* **1996**, *100*, 17079.

149. Lahlil, K.; Moradpour, A.; Bowlas, C.; Menou, F.; Cassoux, P.; Bonvoisin, J.; Launay, J.-P.; Dives, G.; Dehareng, D. Intervalence Transitions in Mixed Valence bis(Tetrathiafulvalene) Compounds. *J. Am. Chem. Soc.* **1995**, *117*, 9995.

150. Coropceanu, V.; Gruhn, N. E.; Barlow, S.; Lambert, C.; Durivage, J. C.; Bill, T. G.; Noell, G.; Marder, S. R.; Brédas, J.-L. Electronic Coupling in Organic Mixed-Valence Compounds: The Contribution of Photoelectron Spectroscopy. *J. Am. Chem. Soc.* **2004**, *126*, 2727.

151. Barlow, S.; Risko, C.; Coropceanu, V.; Tucker, N. M.; Jones, S. C.; Zerubba, L.; Khrustalev, V. N.; Antipin, M. Y.; Kinnibrugh, T. L.; Timofeeva, T.; Marder, S. R.; Brédas, J.-L. A Mixed-Valence bis(Diarylamino)stilbene: Crystal Structure and Comparison of Electronic Coupling with Biphenyl and Tolane Analogues. *Chem. Comm.* **2005**, 764.

152. Robin, M. B.; Day, P. In *Advances in Inorganic Chemistry and Radiochemistry*; Emeléus, H. J., Sharpe, A. G., Eds.; Academic Press, 1967; Vol. 10, p 247.

153. Hill, M. G.; Penneau, J. F.; Zinger, B.; Mann, K. R.; Miller, L. L. Oligothiophene Cation Radicals. π-Dimers as Alternatives to Bipolarons in Oxidized Polythiophenes. *Chem. Mater.* **1992**, *4*, 1106.

154. Frankevich, E.; Ishii, H.; Hamanaka, Y.; Yokoyama, T.; Fuji, A.; Li, S.; Yoshino, K.; Nakamura, A.; Seki, K. Formation of Polaron Pairs and Time-Resolved Photogeneration of Free Charge Carriers in π-Conjugated Polymers. *Phys. Rev. B: Condens. Matter* **2000**, *62*, 2505.

155. Hertel, D.; Bässler, H.; Scherf, U.; Horhold, H. H. Charge Carrier Transport in Conjugated Polymers. *J. Chem. Phys.* **1999**, *110*, 9214.

156. Emmi, S. S.; D'Angelantonio, M.; Poggi, G.; Beggiato, G.; Camaioni, N.; Geri, A.; Martelli, A.; Pietropaolo, D.; Zotti, G. Spectral Characterization of Thiophene Radical Cation Generated by Pulse Radiolysis. *Res. Chem. Intermed.* **1998**, *24*, 1.

157. Deussen, M.; Bässler, H. Anion and Cation Absorption Spectra of Conjugated Oligomers and Polymers. *Chem. Phys.* **1992**, *164*, 247.

158. Grozema, F. C.; Candeias, L. P.; Swart, M.; van Duijnen, P. T.; Wildeman, J.; Hadziioanou, G.; Siebbeles, L. D. A.; Warman, J. M. Theoritical and Experimental Studies of the Optoelectronic Properties of Positively Charged Oligo(phenylene vinylene)s: Effects of Chain Length and Alkoxy Substitution. *J. Chem. Phys.* **2002**, *117*, 11366.

159. Yu, Y.; Gunic, E.; Zinger, B.; Miller, L. L. Spectra and Reactivity of Methoxyoligothiophene Cation Radicals. *J. Am. Chem. Soc.* **1996**, *118*, 1013.

160. Bäuerle, P.; Segelbacher, U.; Maier, A.; Mehring, M. Electronic Structure of Mono- and Dimeric Cation Radicals in End-Capped Oligothiophenes. *J. Am. Chem. Soc.* **1993**, *115*, 10217.

161. Guay, J.; Diaz, A.; Wu, R.; Tour, J. M.; Dao, L. H. Electrooxidation of Soluble α,α'-Coupled Thiophene Oligomers. *Chem. Mater.* **1992**, *4*, 254.

162. Guay, J.; Kasai, P.; Diaz, A.; Wu, R.; Tour, J. M.; Dao, L. H. Chain-Length Dependence of Electrochemical and Electronic Properties of Neutral and Oxidized Soluble α,α'-Coupled Thiophene Oligomers. *Chem. Mater.* **1992**, *4*, 1097.

163. Jones, S. C.; Coropceanu, V.; Barlow, S.; Kinnibrugh, T.; Timofeeva, T.; Brédas, J.-L.; Marder, S. R. Delocalization in Platinum-Alkynyl Systems: A Metal-Bridged Organic Mixed-Valence Compound. *J. Am. Chem. Soc.* **2004**, *126*, 11782.

164. Hush, N. S. In *Progress in Inorganic Chemistry*; Cotton, F. A., Ed.; Interscience Publishers: New York, 1967; Vol. 8, p 391.

165. Lambert, C.; Nöll, G. Intervalence Charge-Transfer Bands in Triphenylamine-Based Polymers. *Synth. Met.* **2003**, *139*, 57.

166. Wishart, J. F. In *In Radiation Chemistry: Present Status and Future Trends*; Jonah, C. D., Rao, B. S. M., Ed.; Elsevier Science: Amsterdam, 2001; Vol. 87, pp 21.

167. Wishart, J. F.; Cook, A. R.; Miller, J. R. LEAF Picosecond Pulse Radiolysis Facility at Brookhaven National Laboratory. *Rev. Sci. Inst.* **2004**, *75*, 4359.

168. Ding, L.; Lu, Z.; Egbe, D. A. M.; Karasz, F. E. Structure-Morphology-Electroluminescence Relationship for Hybrid Conjugated Polymers. *Macromolecules* **2004**, *37*, 10031.

169. Kulkarni, A. P.; Jenekhe, S. A. Blue Light-Emitting Diodes with Good Spectral Stability Based in Blends of Poly(9,9-dioctylfluorene): Interplay between Morphology, Photophysics, and Device Performance. *Macromolecules* **2003**, *36*, 5285.

170. Corcoran, N.; Arias, A. C.; Kim, J. S.; MacKenzie, J. D.; Friend, R. H. Increased Efficiency in Vertically Segregated Thin-Film Conjugated Blends for Light-Emitting Diodes. *Appl. Phys. Lett.* **2003**, *82*, 299.

171. Müllen, K.; Wegner, G. *Electronic Materials: The Oligomer Approach*; Wiley-VCH: Weinheim, 1998.

172. Lehn, J.-M. Toward Self-Organization and Complex Matter. *Science* **2002**, *295*, 2400.

173. Ajayaghosh, A.; George, S. J. First Phenylenevinylene Based Organogels: Self-Assembled Nanostructures via Cooperative Hydrogen Bonding and π-Stacking. *J. Am. Chem. Soc.* **2001**, *123*, 5148.

174. Prince, R. B.; Moore, J. S.; Brunsveld, L.; Meijer, E. W. Cooperativity in the Folding of Helical *m*-Phenylene Ethynylene Oligomers Based Upon the "Sergeants-and-Soldiers" Principle. *Chem. Eur. J.* **2001**, *7*, 4150.

175. Goto, H.; Heemstra, J. M.; Hill, D. J.; Moore, J. S. Single-Site Modifications and Their Effect on the Folding Stability of *m*-Phenylene Ethynylene Oligomers. *Org. Lett.* **2004**, *6*, 889.

176. Cary, J. M.; Moore, J. S. Hydrogen Bond-Stabilized Helix Formation of a *m*-Phenylene Ethynylene Oligomer. *Org. Lett.* **2002**, *4*, 4663.

177. Schenning, A. P. H. J.; Jonkheijm, P.; Peeters, E.; Meijer, E. W. Hierarchical Order in Supramolecular Assemblies of Hydrogen-Bonded Oligo(*p*-phenylene vinylene)s. *J. Am. Chem. Soc.* **2001**, *123*, 409.

178. Würthner, F.; Chen, Z.; Hoeben, F. J. M.; Osswald, P.; You, C.-C.; Jonkheijm, P.; Herrikhuyzen, J. v.; Schenning, A. P. H. J.; van der Schoot, P. P. A. M.; Meijer, E. W.; Beckers, E. H. A.; Meskers, S. C. J.; Janssen, R. A. J. Supramolecular p–n-Heterojunctions by Co-Self-Organization of Oligo(*p*-phenylene vinylene) and Perylene Bisimide Dyes. *J. Am. Chem. Soc.* **2004**, *126*, 10611.

179. Hulvat, J. F.; Sofos, M.; Tajima, K.; Stupp, S. I. Self-Assembly and Luminescence of Oligo(*p*-phenylene vinylene) Amphiphiles. *J. Am. Chem. Soc.* **2005**, *127*, 366.

180. Hoeben, F. J. M.; Herz, L. M.; Daniel, C.; Jonkheijm, P.; Schenning, A. P. H. J.; Silva, C.; Meskers, S. C. J.; Beljonne, D.; Phillips, R. T.; Friend, R. H.; Meijer, E. W. Efficient Energy Transfer in Mixed Columnar Stacks of Hydrogen-Bonded Oligo(*p*-phenylenevinylene)s in Solution. *Angew. Chem., Int. Ed.* **2004**, *43*, 1976.

181. Daniel, C.; Herz, L. M.; Beljonne, D.; Hoeben, F. J. M.; Jonkheijm, P.; Schenning, A. P. H. J.; Meijer, E. W.; Phillips, R. T.; Silva, C. Resonance Energy Transfer Dynamics in Hydrogen-Bonded Oligo-*p*-Phenylenevinylene Nanostructures. *Synth. Met.* **2004**, *147*, 29.

182. Herz, L. M.; Daniel, C.; Silva, C.; Hoeben, F. J. M.; Schenning, A. P. H. J.; Meijer, E. W.; Friend, R. H.; Phillips, R. T. Fast Exciton Diffusion in Chiral Stacks of Conjugated *p*-Phenylene Vinylene Oligomers. *Phys. Rev. B: Condens. Matter* **2003**, *68*, 045203.

183. Beljonne, D.; Hennebicq, E.; Daniel, C.; Herz, L. M.; Silva, C.; Scholes, G. D.; Hoeben, F. J. M.; Jonkheijm, P.; Schenning, A. P. H. J.; Meskers, S. C. J.; Philips, R. T.; Friend, R. H.; Meijer, E. W. Excitation Migration Along Oligophenylenevinylene-Based Stacks: Delocalization Effects on Transport Dynamics. *J. Phys. Chem. B* **2005**, *109*, 10594.

184. Daniel, C.; Herz, L. M.; Silva, C. Exciton Bimolecular Annihilation Dynamics in Supramolecular Nanostructures of Conjugated Oligomers. *Phys. Rev. B: Condens. Matter* **2003**, *68*, 235212.

185. Yan, M.; Rothberg, L. J.; Kwock, E. W.; Miller, T. M. Interchain Excitation in Conjugated Polymers. *Phys. Rev. Lett.* **1995**, *75*, 1992.

186. Huang, W. Y.; Matsuoka, S.; Kwei, T. K.; Okamoto, Y. Aggregation and Gelation of Fully Conjugated Rigid-Rod Polymers. Poly(2,5-dialkyl-1,4-phenyleneethynylene)s. *Macromolecules* **2001**, *34*, 7166.

187. Wang, P.; Collison, C. J.; Rothberg, L. J. Origins of Aggregation Quenching in Luminescent Phenylenevinylene Polymers. *J. Photochem. Photobiol., A* **2001**, *144*, 63.

188. Wu, J.; Watson, M. D.; Zhang, L.; Wang, Z.; Müllen, K. Hexakis(4-iodophenyl)-*peri*-hexabenzocoronene - A Versatile Building Block for Highly Ordered Discotic Liquid Crystalline Materials. *J. Am. Chem. Soc.* **2004**, *126*, 177.

189. Hofmeier, H.; El-Ghayoury, A.; Schenning, A. P. H. J.; Schubert, U. S. Synthesis and Optical Properties of (A)chiral Terpyridine-Ruthenium Complexes. *Tetrahedron* **2004**, *60*, 6121.

190. Pieterse, K.; Lauritsen, A.; Schenning, A. P. H. J.; Vekemans, J. A. J. M.; Meijer, E. W. Symmetrical Electron-Deficient Materials Incorporating Azaheterocycles. *Chem. Eur. J.* **2003**, *9*, 5597.

191. Punna, S.; Meunier, S.; Finn, M. G. A Hierarchy of Aryloxide Deprotection by Boron Tribromide. *Org. Lett.* **2004**, *6*, 2777.

192. Terech, P.; Weiss, R. G. Low Molecular Mass Gelators of Organic Liquids and the Properties of Their Gels. *Chem. Rev.* **1997**, *97*, 3133.

193. Kishimura, A.; Yamashita, T.; Aida, T. Phosphorescent Organogels via "Metallophilic" Interactions for Reversible RGB-Color Switching. *J. Am. Chem. Soc.* **2005**, *127*, 179.

194. An, B.-K.; Lee, D.-S.; Lee, J.-S.; Park, Y.-S.; Song, H.-S.; Park, S. Y. Strongly Fluorescent Organogel System Comprising Fibrillar Self-Assembly of a Trifluoromethyl-Based Cyanostilbene Derivative. *J. Am. Chem. Soc.* **2004**, *126*, 10232.

195. Geiger, C.; Stanescu, M.; Chen, L.; Whitten, D. G. Organogels Resulting from Competing Self-Assembly Units in the Gelator: Structure, Dynamics, and Photophysical Behavior of Gels Formed from Cholesterol-Stilbene and Cholesterol-Squaraine Gelators. *Langmuir* **1999**, *15*, 2241.

196. Walters, K. A.; Ley, K. D.; Schanze, K. S. Photophysical Consequences of Conformation and Aggregation in Dilute Solutions of π-Conjugated Oligomers. *Langmuir* **1999**, *15*, 5676.

197. Chen, H.; Law, K.-Y.; Perlstein, J.; Whitten, D. G. Amphiphilic Squaraine Dye Aggregate: Evidence for a Cyclic Chiral Structure as a General Supramolecular Structure for Aggregates of Dyes and Aromatic Molecules. *J. Am. Chem. Soc.* **1995**, *117*, 7257.

198. Neuteboom, E. E.; Meskers, S. C. J.; Meijer, E. W.; Janssen, R. A. J. Photoluminescence of Self-Organized Perylene Bisimide Polymers. *Macromol. Chem. Phys.* **2004**, *205*, 217.

199. DiCésare, N.; Belletête, M.; Marrano, C.; Leclerc, M.; Durocher, G. Intermolecular Interactions in Conjugated Oligothiophenes. 1. Optical Spectra of Terthiophene and Substituted Terthiophenes Recorded in Various Environments. *J. Phys. Chem. A* **1999**, *103*, 795.

200. Billsten, H. H.; Sundström, V.; Polívka, T. Self-Assembled Aggregates of the Carotenoid Zeaxanthin: Time-Resolved Study of the Excited States. *J. Phys. Chem. A* **2005**, *109*, 1521.

201. Barazzouk, S.; Lee, H.; Hotchandani, S.; Kamat, P. V. Photosensitization Aspects of Pinacyanol H-Aggregates. Charge Injection from Singlet and Triplet Excited States into SnO_2 Nanocrystallites. *J. Phys. Chem. B* **2000**, *104*, 3616.

202. Davis, R.; Rath, N. P.; Das, S. Thermally Reversible Fluorescent Polymorphs of Alkoxy-cyano-substituted Diphenylbutadiene: Role of Crystal Packing in Solid State Fluorescence. *Chem. Comm.* **2004**, 74.

203. Xiang, J.; Yang, X.; Chen, C.; Tang, Y.; Yan, W.; Xu, G. Effects of NaCl on the J-Aggregation of Two Thiacarbocyanine Dyes in Aqueous Solutions. *J. Colloid Interface Sci.* **2003**, *258*, 198.

204. Miteva, T.; Palmer, L.; Kloppenburg, L.; Neher, D.; Bunz, U. H. F. Interplay of Thermochromocity and Liquid-Crystalline Behavior in Poly(*p*-phenyleneethynylene)s: π-π Interactions or Planarization of the Conjugated Backbone? *Macromolecules* **2000**, *33*, 652.

205. Li, K.; Wang, Q. Synthesis and Solution Aggregation of Polystyrene-Oligo(*p*-phenyleneethynylene)-Polystyrene Triblock Copolymer. *Macromolecules* **2004**, *37*, 1172.

206. Bunz, U. H. F. Poly(*p*-phenyleneethynylene)s by Alkyne Metathesis. *Acc. Chem. Res.* **2001**, *34*, 998.

207. Oelkrug, D.; Tomper, A.; Gierschner, J.; Egelhaaf, H.-J.; Hanack, M.; Hohloch, M.; Steinhuber, E. Tuning of Fluorescence in Films and Nanoparticles of Oligophenylenevinylenes. *J. Phys. Chem. B* **1998**, *102*, 1902.

208. Whitten, D. G.; Chen, L.; Geiger, H. C.; Perlstein, J.; Song, X. Self-Assembly of Aromatic-Functionalized Amphiphiles: The Role and Consequences of Aromatic-Aromatic Noncovalent Interactions in Building Supramolecular Aggregates and Novel Assemblies. *J. Phys. Chem. B* **1998**, *102*, 10098.

209. Song, X.; Geiger, C.; Leinhos, U.; Perlstein, J.; Whitten, D. G. *trans*-Stilbene Aggregates in Microheterogeneous Media: Evidence for a Chiral Cyclic Supramolecular Unit. *J. Am. Chem. Soc.* **1994**, *116*, 10340.

210. Deans, R.; Kim, J. S.; Machacek, M. R.; Swager, T. M. A Poly(*p*-phenyleneethynylene) with a Highly Emissive Aggregated Phase. *J. Am. Chem. Soc.* **2000**, *122*, 8565.

211. Luo, J.; Xie, Z.; Lam, J. W. Y.; Cheng, L.; Chen, H.; Qiu, C.; Kwok, H. S.; Zhan, X.; Liu, Y.; Zhu, D.; Tang, B. Z. Aggregation-Induced Emission of 1-Methyl-1,2,3,4,5-pentaphenylsilole. *Chem. Comm.* **2001**, 1740.

212. Belton, C.; O'Brien, D. F.; Blau, W. J.; Cadby, A. J.; Lane, P. A.; Bradley, D. D. C.; Byrne, H. J.; Stockmann, R.; Hörhold, H.-H. Excited-State Quenching of a Highly Luminescent Conjugated Polymer. *Appl. Phys. Lett.* **2001**, *78*, 1059.

213. Komatsu, T.; Moritake, M.; Nakagawa, A.; Tsuchida, E. Self-Organized Lipid-Porphyrin Bilayer Membranes in Vesicular Form: Nanostructures, Photophysical Properties, and Dioxygen Coordination. *Chem. Eur. J.* **2002**, *8*, 5469.

214. Kubát, P.; Lang, K.; Zelinger, Z.; Král, V. Aggregation and Photophysical Properties of Water-Soluble Sapphyrins. *Chem. Phys. Lett.* **2004**, *395*, 82.

215. Zhao, X.; Cardolaccia, T.; Farley, R.; Abboud, K. A.; Schanze, K. S. A Platinum Acetylide Polymer with Sterically Demanding Substituents: Effect of Aggregation on the Triplet Excited State. *Inorg. Chem.* **2005**, *44*, 2619.

216. Haskins-Glusac, K.; Ghiviriga, I.; Abboud, K. A.; Schanze, K. S. Photophysics and Photochemistry of Stilbene-Containing Platinum Acetylides. *J. Phys. Chem. B* **2004**, *108*, 4969.

217. Bruce, M. I.; Davy, J. R.; Hall, B. C.; Van Galen, Y. J.; Skelton, B. W.; White, A. H. Some Platinum(II) Complexes Derived from Aromatic Alkynes. *Appl. Organometal. Chem.* **2002**, *16*, 559.

218. van Asselt, R.; Rijnberg, E.; Elsevier, C. J. Stabilization of High Oxidation States by Rigid Bidentate Nitrogen Ligands: Synthesis and Characterization of Diorgano-and Triorganopalladium(IV) and Cationic Triorganoplatinum(IV) Complexes. *Organometallics* **1994**, *13*, 706.

219. Packett, D. L.; Jensen, C. M.; Cowan, R. L.; Strouse, C. E.; Trogler, W. C. Syntheses, Structures, and Mechanism of Formation of *trans*-Chlorohydrobis(trimethylphosphine)platinum(II) and *trans*-dihydrobis(trimethylphosphine)platinum(II). Energetics of Cis-Trans Isomerization. *Inorg. Chem.* **1985**, *24*, 3578.

BIOGRAPHICAL SKETCH

Thomas Cardolaccia was born on February 10th, 1976, in Clamart, France, in the south suburbs of Paris. He enjoyed a lively childhood living near Marseille and then in Bordeaux where his parents moved when he was nine years old. During high school, he liked biology but during his last year in high school realized that chemistry was far more fascinating. He graduated from Lycée Camille-Julian with "Mention Assez Bien" in 1994. He obtained his "Maîtrise de Chimie" from Université Bordeaux I in June 2000. During his time as an undergraduate, he spent one year at the University of Reading, England, as an ERASMUS student. During the summer of 1999, he also took part in the France-United States REU exchange program and worked for three months in Dr. Schanze's group at the University of Florida where he was first exposed to the field of conjugated polymers. After returning to France to finish his degree, Thomas came back to the University of Florida and joined Dr. Schanze's group as a graduate student to work toward his PhD. While there, he met his wife Joanne, who was teaching French in a high school in Gainesville and they got married in October 2003. After his PhD, Thomas will continue his education as a postdoctoral associate with Dr. Thomas J. Meyer at the University of North Carolina at Chapel Hill.